Contemporary Issues in Cancer Imaging

Carcinoma of the Kidney

Edited by
Uday Patel

Series Editors
Rodney Reznek
Janet Husband

CAMBRIDGE
Medicine

CAMBRIDGE www.cambridge.org/9780521878388

This page intentionally left blank

Carcinoma of the Kidney

Contemporary Issues in Cancer Imaging

A Multidisciplinary Approach

Series Editors

Rodney H. Reznek

Cancer Imaging, St. Bartholomew's Hospital, London

Janet E. Husband

Diagnostic Radiology, Royal Marsden Hospital, Surrey

Current titles in the series

Cancer of the Ovary
Lung Cancer
Colorectal Cancer
Carcinoma of the Esophagus

Forthcoming titles in the series

Carcinoma of the Bladder
Prostate Cancer
Squamous Cell Cancer of the Neck
Pancreatic Cancer
Interventional Radiological Treatment of Liver Tumours

Carcinoma of the Kidney

Edited by
Uday Patel

Series Editors
Rodney H. Reznek
Janet E. Husband

CAMBRIDGE
UNIVERSITY PRESS

CAMBRIDGE UNIVERSITY PRESS
Cambridge, New York, Melbourne, Madrid, Cape Town, Singapore, São Paulo

Cambridge University Press
The Edinburgh Building, Cambridge CB2 8RU, UK
Published in the United States of America by Cambridge University Press, New York
www.cambridge.org
Information on this title: www.cambridge.org/9780521878388

First published in print format 2007

ISBN-13 978-0-511-37731-0 eBook (EBL)

ISBN-13 978-0-521-87838-8 hardback

Contents

Contributors

Saroja Adusumilli, MD
Department of Radiology
University of Michigan Hospital
Ann Arbor, MI, USA

Ravi Barod, FRCS
Urology Fellow
Department of Urology
Guy's & St Thomas' Hospitals
London, UK

Tristan Barrett, MBBS
Molecular Imaging Program
National Cancer Institute
Bethesda, Maryland, USA

David J. Breen, MRCP, FRCR
Department of Radiology
Southampton University Hospitals
Southampton, UK

Colin P. Cantwell, MB BCH, FRCR, FFR
Division of Abdominal Imaging and
Interventional Radiology
Department of Radiology and Harvard
Medical School
Massachusetts General Hospital
Boston, USA

Peter L. Choyke, MD
Molecular Imaging Program
National Cancer Institute
Bethesda, Maryland, USA

Richard H. Cohan, MD
Professor, Department of Radiology
University of Michigan Hospital
Ann Arbor, MI, USA

Debra Gervais, MD
Division of Abdominal Imaging and
Interventional Radiology
Department of Radiology and Harvard
Medical School
Massachusetts General Hospital
Boston, USA

Patricia Harnden, MD, PHD, FRCPATH
Consultant Urological Pathologist
Cancer Research UK Clinical Centre
St James's University Hospital
Leeds, UK

Brian R. Herts, MD
Associate Professor of Radiology
Section of Abdominal Imaging
Division of Diagnostic Radiology and
The Glickman Urological and Kidney Institute
The Cleveland Clinic Foundation
Cleveland, OH, USA

Vincent Khoo, FRACR, FRCR, MD
Consultant in Clinical Oncology
Academic Urology Unit
Royal Marsden NHS Foundation Trust & Institute of Cancer Research
London, UK

Peter R. Mueller, MD
Division of Abdominal Imaging and Interventional Radiology
Department of Radiology and Harvard Medical School
Massachusetts General Hospital
Boston, USA

Tim O'Brien, FRCS
Consultant Urologist
Department of Urology
Guy's & St Thomas' Hospitals
London, UK

Parvati Ramchandani, MD
Department of Radiology
University of Pennsylvania Medical Centre
Philadelphia, USA

Sheila C. Rankin, FRCR
Consultant Radiologist
Radiology Department
Guy's and St. Thomas Foundation Trust
Guy's Hospital
London, UK

Erick M. Remer, MD
Associate Professor of Radiology
Division of Radiology
Cleveland Clinic Foundation
Cleveland, OH, USA

Rodney H. Reznek, FRANZCR (Hon) FRCP FRCR
Professor of Diagnostic Imaging
Cancer Imaging, Institute of Cancer
St Bartholomew's Hospital
West Smithfield
London, UK

Giles Rottenberg, MRCP, FRCR
Consultant Radiologist
Radiology Department
Guy's and St. Thomas Foundation Trust
Guy's Hospital
London, UK

Elizabeth E. Rutherford, MRCS, FRCR
Department of Radiology
Southampton University Hospitals
Southampton, UK

Anju Sahdev, MBBS, MRCP, FRCR
Consultant Radiologist
Department of Diagnostic Imaging
St. Bartholomew's Hospital
West Smithfield
London, UK

Series foreword

Imaging has become pivotal in all aspects of the management of patients with cancer. At the same time it is acknowledged that optimal patient care is best achieved by a multidisciplinary team approach. The explosion of technological developments in imaging over the past years has meant that all members of the multidisciplinary team should understand the potential applications, limitations, and advantages of all the evolving and exciting imaging techniques. Equally, to understand the significance of the imaging findings and to contribute actively to management decisions and to the development of new clinical applications for imaging, it is critical that the radiologist should have sufficient background knowledge of different tumors. Thus the radiologist should understand the pathology, the clinical background, the therapeutic options, and the prognostic indicators of malignancy.

Contemporary Issues in Cancer Imaging: *A Multidisciplinary Approach* aims to meet the growing requirement for radiologists to have detailed knowledge of the individual tumors in which they are involved in making management decisions. A series of single subject issues, each of which will be dedicated to a single tumor site, edited by recognized expert guest editors, will include contributions from basic scientists, pathologists, surgeons, oncologists, radiologists, and others.

While the series is written predominantly for the radiologist, it is hoped that individual issues will contain sufficient varied information so as to be of interest to all medical disciplines and to other health professionals managing patients with cancer. As with imaging, advances have occurred in all these disciplines related to cancer management and it is our fervent hope that this series, bringing together expertise from such a range of related specialties, will not only promote the understanding and rational application of modern imaging but also help to achieve the ultimate goal of improving outcomes of patients with cancer.

Rodney H. Reznek
London

Janet E. Husband
London

Preface to Carcinoma of the Kidney

The last two decades have seen ground-shifting advances in the epidemiology, genetics, diagnosis, and management of the renal cancer, particularly renal cell cancer. The most striking is that almost half are now diagnosed at an asymptomatic and earlier stage, and there have been parallel advances in the management of these early stage tumors. Nephron-sparing procedures are increasingly performed for these small tumors. Such procedures include radiologically guided ablative procedures, such as radiofrequency ablation and cryotherapy, as well as surgical options such as open or laparoscopic nephron-sparing surgery. More recently still, there have been encouraging advances in immunotherapy and the treatment of recurrent disease. There have also been sweeping advances in our understanding of the genetics of renal cancer.

However all these changes have also raised some contemporary dilemmas: for example, using imaging can we reliably resolve the nature of atypical renal masses; how to differentiate the indolent from the aggressive asymptomatic tumor; the recognition of residual or inadequately treated tumor post nephron-sparing procedures; and, finally, the follow-up of the accumulating cohort of patients treated by nephron-sparing procedures and those with familial or genetic renal cancer. These current predicaments are the focus of this issue of *Contemporary Issues in Cancer Imaging*. The authors are all recognized experts in their fields and I hope that this single volume should provide an up-to-date clinical and radiological summary of renal cell cancer for all those involved in the diagnosis and management of this challenging tumor.

Uday Patel

1

Renal cell cancer: overview and immunochemotherapy

Vincent Khoo

Introduction and epidemiology

Kidney cancer is a relatively common urological cancer, accounting for approximately 2% of all adult cancers. In the UK during 2003, 6683 new kidney cancer cases were registered [1]. Of these 4059 cases were male and 2624 cases were female making it approximately two times more common in males. In the USA, the American Cancer Society predicts that there will be approximately 51 200 new cases of kidney cancer (31 590 in men and 19 600 in women) in 2007 and some 12 890 people will die from this disease [2].

The incidence appears to be rising not only in Western societies owing to a variety of reasons, including the increased use of cross-sectional imaging [3], but also throughout the world [4]. Risk factors for kidney cancer include obesity, smoking, and hypertension [5]. Other implicated factors are environmental exposure to asbestos [6], end-stage renal disease, and hemodialysis. Long-term dialysis may result in acquired renal cystic disease, predisposing to the development of multifocal and bilateral renal cancers [7].

The histological subtypes of kidney cancers are listed in Table 1.1 and discussed in more detail in Chapter 2. This chapter, and indeed most of this book, will concentrate on adult renal cell carcinoma (RCC). Traditionally RCCs were often detected late as they can grow to a relatively large size because of their retroperitoneal location. Now, with the widespread use of computed tomography (CT) or ultrasound scanning, many more asymptomatic RCCs are being diagnosed, resulting in a downward stage migration of the disease, with smaller and earlier stage tumors. Renal cell carcinomas are usually unilateral but can occur in both kidneys in up to 5% of cases. Renal cell carcinomas also have the tendency to grow into the renal vein, and can further propagate along the inferior vena cava (IVC) into the right atrium in up to 10% of cases with venous invasion [8].

Carcinoma of the Kidney, ed. Uday Patel. Published by Cambridge University Press.

Table 1.1. WHO subtype classification of renal cell carcinoma (RCC)

RCC Subtype	Resected kidney cancers (%)	5-year DSS[a]	5-year PFS[b]
Clear cell	75	76	70
Papillary	10–12	86	88
Chromophobe	4–5	100	94
Oncocytoma	4–5	–	–
Collecting duct carcinomas	< 1	–	–
Sarcomatous carcinomas and other unclassified subtypes	< 1–2	24–35	18–27

[a] DSS – Disease-specific survival

[b] PFS – Progression-free survival

Source: Delahunt, 2005 [9]; Amin *et al.*, 2002 [12]

Renal cell carcinoma can also be inherited or be associated with familial syndromes. Up to 5% of RCCs fall into this category. This will only be briefly addressed here as it is discussed in detail in Chapter 3. The critical gene involved is located on the short arm of chromosome 3. This is the von Hippel–Lindau (VHL) gene and is involved in the organization of key proteins of cancer initiation and progression. The VHL gene targets the transcription factor hypoxia inducible factor-1 (HIF-1) gene for destruction. Under hypoxic conditions, the VHF gene is not expressed and thus HIF-1 levels increase. This in turn causes the production of several hypoxia response genes including pro-angiogenic factors such as vascular endothelial growth factor (VEGF) and erythropoietin (this process is discussed in greater detail in Chapter 3). The loss of the VHF tumor suppressor gene has been reported to occur in up to 50%–70% of sporadic RCCs [10,11]. This molecular etiology has led to an improved understanding of the development of RCC and the recent development of targeted agents and therapies, currently being clinically investigated.

Prognostic factors

Prognostic factors provide estimations of disease progression and survival, and help guide clinical management. For this, the TNM staging system is extensively used, based mainly on tumor size, nodal status, and presence of metastases

Table 1.2. A summary of the TNM classification of renal tumors

Kidney		Subdivisions	
T1	$\leq$ 7 cm; limited to the kidney	T1a	$\leq$ 4 cm
		T1b	$>$ 4 cm
T2	$>$ 7 cm; limited to the kidney		
T3	Adrenal or perinephric invasion; major veins	T3a	Adrenal or perinephric invasion
		T3b	Renal vein(s); vena cava below diaphragm
		T3c	Vena cava above diaphragm
T4	Beyond Gerota fascia		
N+	Positive nodes	N1	Single node
		N2	More than one node

(Table 1.2). It has limitations if used singularly. Methods used for staging, the TNM classification, and its issues are further discussed in Chapters 4 and 5.

Tumor histology

In a single institutional study of 405 consecutive cases, it was reported that routine light microscopic hematoxylin and eosin-based histological sub-typing using the contemporary classification scheme demonstrated prognostic utility [12]. This is summarized in Table 1.1. In this study with a median follow-up of 56 months, multivariate analysis revealed that histological type, Fuhrman's nuclear grade, TNM stage, vascular invasion, and necrosis were all significantly associated with disease-specific survival and progression-free survival rates. More recently, a larger multi-institutional center multivariate analysis of 4063 patients confirmed that TNM stage, Fuhrman grade and ECOG (Eastern Cooperative Oncology Group) performance status, but not histology, were independent prognostic factors [13].

Clinical risk stratification

Other disease characteristics often used to define patient prognosis and likelihood of therapeutic response are performance status, low tumor burden, absence of

paraneoplastic syndromes, and a long disease-free interval. In order to improve prognostic estimations, two systems have been devised by the University of California Los Angeles (UCLA) and Memorial Sloane Kettering Cancer Centre (MSKCC). Both systems include the use of clinical variables and are based on single institutional experience. The UCLA system was based on 670 patients from 24 trials and the MSKCC system used 814 patients in 11 trials. In the UCLA system, five stratification groups were proposed based on the 1997 TNM staging system, Fuhrman grade and ECOG performance status, with projected 5-year survivals of 94% for Group I, 67% for Group II, 39% for Group III, 23% for Group IV, and 0% for Group V [14]. This system was subsequently modified so as to group cases into three different risk groups according to localized or metastatic disease at presentation [15]. The validity of the UCLA system was subsequently assessed in an international multi-institutional analysis of 4202 patients [16]. This analysis revealed that the 5-year survival rates for localized RCC were 92%, 67%, and 44% for low, intermediate, and high risk groups, respectively. For the metastatic RCC group, the 3-year survival rates were 37%, 23%, and 12% for low, intermediate, and high risk groups, respectively. There was an observed trend toward a higher risk of death with increasing risk category. This study confirmed the good concordance of the UCLA system with other institutional databases and that it was an accurate predictor for patients with localized RCC. However, for the metastatic disease group it was less accurate because of patient heterogeneity and variability of treatments.

The MSKCC system for advanced RCC identified five negative prognostic factors by multivariate analysis: Karnofsky performance status $< 80\%$, lactate dehydrogenase levels > 1.5 times normal limits, serum hemoglobin below the normal range, elevated corrected serum calcium levels, and the absence of prior nephrectomy [17]. These factors were used to categorize cases into one of three risk groups, with the best-outcome group having no risk factors; the intermediate risk group having 1–2 risk factors; and the poor risk group having > 2 risk factors. The median survival times for the favorable, intermediate, and poor risk groups were 22, 11.9, and 5.4 months, respectively [18]. In addition, the use of cytokine therapy appeared to double the median survival time regardless of risk category compared to the use of chemotherapy or hormonal therapy [19].

A more recent report of localized non-metastatic RCC reviewed four prognostic models: the Kattan model, the UCLA integrated staging system model, the Yaycioglu model, and the Cindolo model [20]. This study of 2404 patients from six European centers reported that all four models discriminated well for overall survival, cancer-specific survival, and disease recurrence free survival ($P < 0.0001$)

with postoperative models discriminating better than preoperative ones, and the Kattan model being consistently the most accurate. In addition, the Kattan model was also noted to be useful in identifying the intermediate-risk patients described by the UCLA system.

Prognostic biomarkers

Whilst clinical systems are useful, another potential avenue for prognostication and response assessment is the identification of reliable predictive biomarkers. Several biochemical and molecular markers have been proposed including p53, CD-44, CD-95, B7-H4, pAkt, adipose differentiation-related protein, gamma-enolase, IMP3, Ki67, and G250/CAIX. The carbonic anhydrase isoenzyme (CAIX) appears to have a role in cellular adhesion and proliferation via growth factor receptor dependent pathways and has been suggested to be an independent prognostic marker for survival in metastatic RCC, when assessed in a cohort of 321 cases [21]. The predictive value of CAIX could be further enhanced using Ki67 for sub-stratification [22] since an inverse relationship exists between these two factors [22]. Multivariate analysis of 224 cases suggested that the combined use of CAIX and Ki67 can stratify cases in low, intermediate, and high risk groups with median survival times of $>$ 101, 31, and 9 months, respectively ($p < 0.001$). These biomarkers appear promising but need to be validated in clinical trials.

Management of RCC

The median age of patients presenting with RCC is 60 years. At diagnosis, only 30%–40% have localized disease whilst 25%–30% will have metastatic cancer [23]. A further 30%–40% of patients are likely to develop metastatic disease during follow-up and the clinical course can be extremely variable [24]. Metastatic disease can be resistant to conventional forms of systemic therapy such as chemotherapy but spontaneous remissions are possible. These patients can experience substantial morbidity from their metastatic disease. Mortality is approximately 30%–50% and the median survival time of patients with metastatic disease is only about 12 months [25].

Localized RCC: the role of surgery

The gold standard for localized RCC is surgery. Traditionally a radical nephrectomy was the standard procedure and was performed through a variety of surgical

approaches; but in recent times laparoscopic techniques and minimally invasive ablative approaches have radically changed the surgical arena for RCCs. The open surgical approaches are now usually reserved for larger tumors (>7–8 cm) or tumors that are locally extensive, or have invaded the renal vein or IVC. Following complete resection in a single center series of 1737 T1–3N0M0 cases, the incidence of renal bed recurrence was $<2\%$; aggressive surgical management of these cases results in long-term disease-free survival [26].

For patients with smaller lesions, laparoscopic nephrectomy or partial (nephron sparing) nephrectomy is becoming the standard of care. It is anticipated that laparoscopic procedures can reduce the length of in-hospital stay, with better recovery for comparable local control and complication rates. Robotic technology is now being used in laparoscopic approaches and its relative value is being assessed. In addition, when surgical approaches are not feasible, minimally invasive ablative methods such as cryotherapy and radiofrequency ablation may be used. The clinical criteria for considering these procedures with their relative merits are discussed in Chapters 8 and 9.

Localized RCC: the role of radiotherapy

Radiotherapy has a limited role in the primary management of RCC. However, it has been considered as either a preoperative or adjuvant measure to reduce the risk of local recurrence following the resection of large and advanced RCCs. Early retrospective studies suggested a survival benefit [27,28,29,30] and two randomized trials have addressed the value of preoperative radiotherapy, and two more randomized trials have assessed adjuvant radiotherapy.

For preoperative radiotherapy, both studies did not demonstrate any difference in 5-year overall survival rates [31,32]. Criticisms of these trials include the small number of patients, the sub-therapeutic radiation dose used, and the inclusion of T1N0 cases where additional local therapy is unlikely to be beneficial. The two randomized trials of adjuvant radiotherapy used more appropriate radiation doses but did not demonstrate any survival benefit [33,34]. At 5 years, the overall survival rate in the UK trial of 100 cases was 36% for the combined therapy arm, compared to 47% with surgery alone [33]; whilst the Danish trial of 65 cases reported a 5-year survival rate of 38% with the combined treatment arm compared to 64% after surgery alone [34]. Other issues with these two trials include the inclusion of early stage cancers, inconsistent reporting, and protocol violations.

It is clear that all these four randomized trials were small – too small to detect any clinically meaningful difference in overall survival. More importantly, there is some concern that the combined therapy arms were associated with a lower survival rate with substantial radiation-related toxicity. Excess toxicity may be caused by the outdated radiotherapy methods, now recognized to be unsuitable for high dose regimes, as well as the little regard paid to bowel irradiation.

Although there are no randomized data to support the use of radiotherapy for unresectable primary disease, postoperative residual disease, or local recurrence following surgery, it is reasonable to consider its use when there are no other treatment options. Radiotherapy may be used as a primary therapy for palliation, or to prevent disease progression or infiltration into surrounding normal tissues or critical adjacent structures. Radiotherapy may also be considered for cases of local recurrence that are unresectable; recurrences that have occurred following a second resection; or those not amenable to other local treatments, with the same intention of preventing severe or troublesome local symptoms from local tumor invasion.

Furthermore, modern radiotherapy techniques can now deliver higher doses with a more acceptable side-effect profile. These new techniques involve the 3D-shaping of the treatment beam (conformal radiotherapy [CFRT]) which tailors the radiotherapy fields to the patient and can substantially reduce the dose to surrounding structures (Figure 1.1). In addition, further advances in radiotherapy technique such as intensity modulation of radiotherapy (IMRT) beams can permit high doses to be "painted" to selected regions of the tumor target. Thus IMRT can better conform the prescribed radiation dose to very irregular or concave shapes compared to CFRT techniques. Other recent advances in radiotherapy include charged particle therapy using protons and light-ions. Particle therapy may provide an improved dose distribution and light-ion therapy may confer a higher biologically effective dose for a better therapeutic ratio. These new techniques are currently being evaluated. Together with the use of image-guided radiotherapy (IGRT), these new techniques may change the place of radiotherapy for the treatment of RCCs, which is otherwise limited.

Metastatic RCC: the role of surgery

The value of nephrectomy in the metastatic setting also continues to generate debate. Two prospective trials randomizing patients to receive immunotherapy alone or post-nephrectomy have been undertaken. Both trials were relatively small.

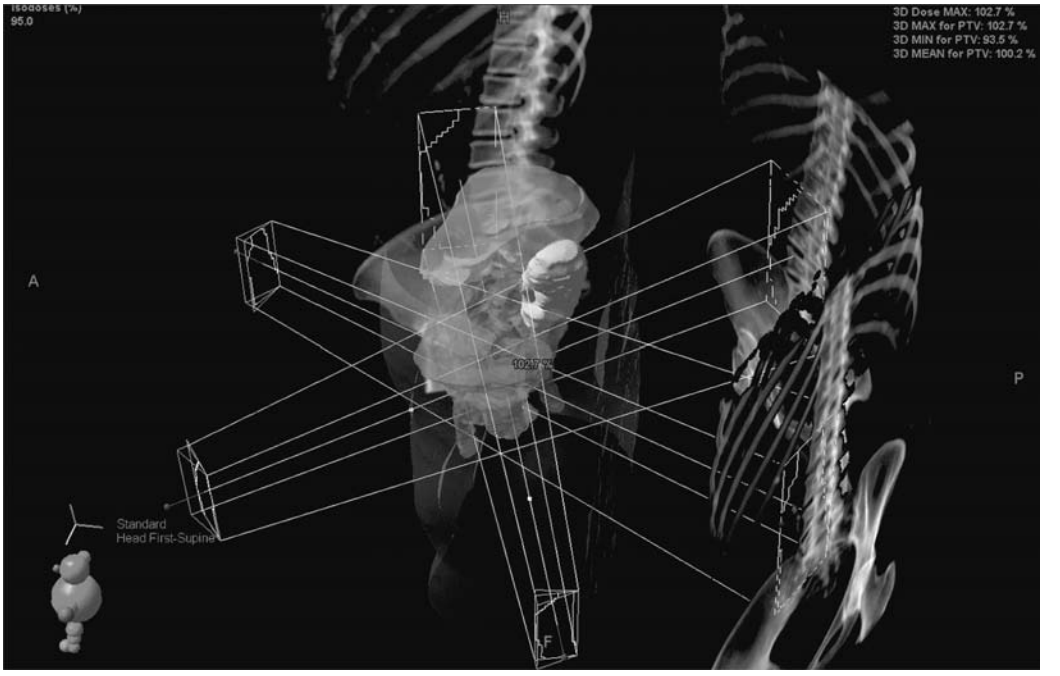

Figure 1.1 Conformal radiotherapy treatment for a postoperative renal bed recurrence. Each treatment beam has been shaped to the profile of the tumor volume within the orientation of the projected treatment beam. This shaped treatment field is then projected onto the outline of the patient's axial skeleton for further illustration of the conformal field shapes. The target volume (near cylindrical shape) is located centrally and is denoted by the pink outline (see also color plate section).

A European trial of 83 patients reported that nephrectomy followed by interferon-alfa-based immunotherapy improved the time to disease progression (5 versus 3 months, hazard ratio 0.60) with better median survival (17 versus 7 months, hazard ratio 0.54) compared to those treated with interferon-alfa alone [35]. In the larger American Southwest Oncology Group (SWOG) study of 241 patients, the median survival time of those undergoing surgery, followed by interferon-alfa therapy, was 11.1 months compared to 8.1 months in those receiving immunotherapy alone ($p = 0.05$) [36]. In this study, the difference in survival was independent of performance status and metastatic site but the median survival times were relatively poor in both study arms, making interpretation more difficult compared to the European study. However, it is generally accepted that a debulking nephrectomy should be considered when the operative risks are acceptable, when palliation from unrestricted growth of the primary tumor is necessary, and if subsequent

immunotherapy is feasible. What is currently uncertain is whether debulking nephrectomy remains of additional benefit in those treated with the novel targeted therapies (discussed below).

Metastatic RCC: the role of radiotherapy

Conventionally, RCC has been considered a relatively radio-resistant tumor but clinical experience and retrospective data have demonstrated that a proportion of renal tumors can be radio-responsive. It is particularly effective in the palliation of symptomatic metastatic disease and the prevention of progressive disease in critical sites, such as in the spinal cord and brain. For example, radiotherapy can provide palliation in 67%–77% of patients suffering from symptomatic bony metastases [37,38]. Radiotherapy can be used alone or in combination with surgery.

Metastatic RCC: the role of chemotherapy and hormonal therapies

Renal cell carcinoma remains relatively resistant to both chemotherapy and hormonal therapies. Conventional chemotherapy agents have proved disappointing, with response rates ranging between 6% and 15%. A recent review of over 4000 patients in 83 trials treated with a variety of cytotoxic regimes revealed an overall response rate of only up to 6% [39]. Whilst some durable responses have been reported, in general the median survival times remain unchanged.

Metastatic RCC: the role of immunotherapy

Immunotherapy has been used with more success than conventional cytotoxics but the results are also disappointing. The use of interferon-alfa and high-dose interleukin-2 have been analyzed in a Cochrane review, with a more recent update, in 2007, that identified 58 randomized controlled trials with 6880 patients, comparing immunotherapy with non-immunotherapy controls [40,41]. There are no reported survival data published from randomized studies of high-dose interleukin-2 versus a non-immunotherapy control or interferon-alfa. This issue is currently under evaluation in the UK-led trial RE-04, comparing interferon-alfa alone versus interferon-alfa, interleukin-2 and 5-fluorouracil. This study has just completed recruitment with 1106 patients, and will be reported in the future [42].

The Cochrane reviews outline that immunotherapies provided an overall remission rate of 12.4% compared to only 2.4% in the non-immunotherapy controls,

and 4.3% in the placebo arms [40,41]. Of the remissions, approximately 28% were complete; but the remission did not independently predict for survival. However, the use of interferon-alfa is superior to non-immunotherapy controls, with a pooled hazard ratio (HR) of 0.74 (0.63–0.88), resulting in a weighted average median improvement in survival of 2.6 months. The median survival time was 13 months (range 6–28 months) and the 2-year survival averaged 22% (8%–41%). The Cochrane reviews also noted that the use of either low dose intravenous or subcutaneous interleukin-2 with interferon-alfa did not improve survival compared to interferon-alfa alone. The optimal duration and dose of interferon-alfa remain to be determined.

Metastatic RCC: the role of targeted therapies

Given the modest improvement in survival from immunotherapy, newer approaches have now been directed to potential molecular targets, following the example of the anti-vascular endothelial growth factor (VEGF), bevacizumab, in colorectal cancer [43].

The process of tumor growth and dissemination is reliant on new vascular growth or angiogenesis, and VEGF has an established role as one of the key regulators of this pathway. It has been previously outlined that the HIF-1/VEGF axis is over-expressed in subsets of RCC, particularly in sporadic clear cell RCCs. Thus inhibiting VEGF receptors via their tyrosine kinases has recently been shown to provide substantial anti-tumor activity. One of the first randomized double-blind phase 2 trials comparing bevacizumab versus placebo was stopped early when the trial termination rules were met [44]. This study used two different doses in the active arms of bevacizumab at 3 mg/kg and 10 mg/kg, with the higher dose arm significantly prolonging the time to progression of disease (HR 2.55, $p = < 0.001$). Progression-free survival at 8 months was 30%, 14%, and 5% for the high dose, low dose, and placebo arms respectively, but overall survival was similar between the groups.

Sorafenib (BAY 43–9006) is a small molecule targeted at tyrosine kinase receptor domains including VEGF-2, VEGF-3, FLT3, PDGF, and c-KIT [45]. A recent double-blind, placebo-controlled trial of 903 patients who failed standard therapy, randomized patients to either sorafenib (oral dose of 400 mg twice-daily) or placebo [46]. The first planned interim analysis revealed that sorafenib provided improved median progression-free survival of 5.5 months versus 2.8 months in the placebo group (HR 0.44; CI 0.35 to 0.55; $p < 0.01$) and reduced the risk of death (HR 0.72; CI 0.54 to 0.94; $p = 0.02$). The best responses were partial responses in 10% of

patients receiving sorafenib and in 2% of those receiving placebo ($p < 0.001$). The common side effects of sorafenib were diarrhea, rash, fatigue, and hand–foot skin reactions, with rare serious complications being hypertension and cardiac ischemia.

Sunitinib maleate (SU 11248) is another oral multitargeted tyrosine kinase inhibitor. In a phase 2 study of 63 metastatic RCC patients who had progressed on first-line immunotherapy, 40% (25/63 cases) achieved partial responses and 27% (17/63 cases) had disease stabilization lasting > 3 months [47]. The median time to progression was 8.7 months with a median survival time of 16.4 months, and treatment-related toxicity was acceptable. This agent has now been tested in a phase III trial of 750 patients as first-line treatment of metastatic RCC [48]. Patients were randomized to repeated 6-week cycles of sunitinib using a 50 mg oral dose daily for 4 weeks, followed by 2 weeks without treatment or interferon-alfa given as a 9 MU subcutaneous dose three times weekly. In patients receiving sunitinib, the median progression-free survival was significantly longer (11 months versus 5 months, HR 0.42; CI 0.32 to 0.54; $p < 0.001$), the objective response rate was higher (31% versus 6%, $p < 0.001$), and there was a significantly better quality of life compared to patients treated with interferon–alfa ($p < 0.001$). Table 1.3 shows the profile of response rates and Figure 1.2 reveals the progression-free survival within the subgroups. Grade 3 or 4 treatment-related fatigue was a feature of patients receiving interferon-alfa (12% versus 7% with sunitinib), compared to diarrhea in patients treated with sunitinib (5% versus 0% with interferon-alfa).

Table 1.3. Best tumor response in the randomized sunitinib versus interferon-alfa trial

Response[a] (%)	Sunitinib (ICR)	Interferon (ICR)	Sunitinib (IA)	Interferon (IA)
	($N = 335$)	($N = 327$)	($N = 374$)	($N = 373$)
Overall response	31	6	37	9
Complete response	0	0	< 1	0
Partial response	31	6	36	9
Stable disease	48	49	47	57
Progressive disease/DNE	21	45	16	34

[a] tumor response was assessed according to RECIST (Response Evaluation Criteria in Solid Tumors)

ICR – Independent central review, IA – investigator assessment, DNE – disease could not be evaluated.

Modified from Motzer *et al.* [48]

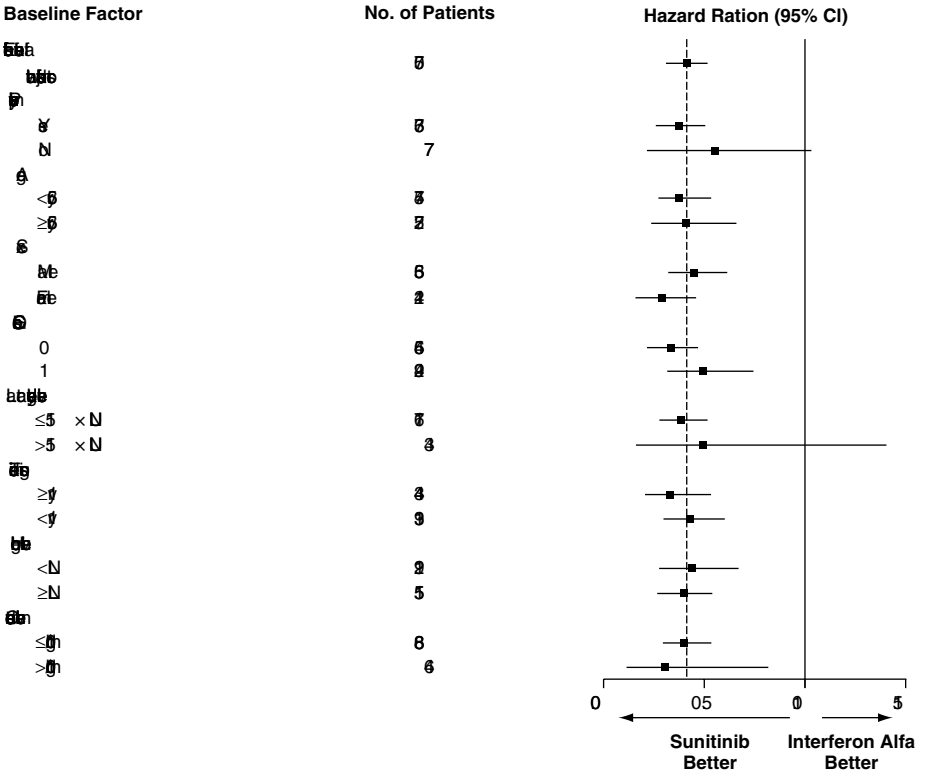

Figure 1.2 The progression-free survival in subgroups according to baseline factors in the sunitinib versus interferon-alfa trial [48].

This agent has now received Food and Drug Administration's (FDA) approval as first-line therapy for metastatic RCC.

Other targeted agents are also being actively investigated; for example Temsirolimus (CCI-779), a mammalian target of rapamycin inhibitor. In a multidose phase II trial, 111 patients with refractory RCC achieved an objective response rate of 7% (7 partial responses and 1 complete response) whilst a further 26% were classified as having a minor response. The median time to tumor progression was 5.8 months and median survival was 15 months. The dose levels did not appear to influence efficacy or toxicity. Common side effects included maculopapular rash (76%), mucositis (70%), asthenia (50%), and nausea (43%), whilst grade 3/4 toxicity involved hyperglycemia (17%), hypophosphatemia (13%), anemia (9%), and hypertriglyceridemia (6%).

Thus, the tyrosine kinase inhibitors have emerged as important agents in the treatment of metastatic RCC. Sorafenib has significant disease-stabilizing activity in metastatic RCC, with acceptable toxicity. Sunitinib has demonstrated effective

antitumor activity as second-line therapy in immunotherapy refractory metastatic RCC and as first-line therapy for metastatic RCC with improved patient outcomes, progression-free survival, and quality of life.

Conclusion

The clinical course of advanced and metastatic renal cancer remains limited, with substantial patient morbidity. The contribution from adjuvant radiotherapy is of minimal benefit but opportunities exist, with emerging new radiotherapy technology, for the palliation of advanced local disease and metastatic disease. The response to both conventional cytotoxic chemotherapy and hormonal treatments in metastatic disease has been poor. The use of immunotherapies has only provided a modest improvement in median survival times. New understanding of the molecular etiology of renal cancer has led to the development of potent angiogenesis inhibitors and targeted agents that may provide greater efficacy with less treatment-related toxicity. The treatment of advanced and metastatic RCC has undergone a radical change with the development of angiogenesis inhibitors and targeted agents.

Several multitargeted tyrosine kinase inhibitors, for example sunitinib and sorafenib, have already been approved for the treatment of metastatic RCC, following clinical results that support the hypothesis that VEGF and PDGF receptor-mediated signaling is an effective therapeutic target in RCC. Nevertheless, these targeted agents rarely induce sustained or complete responses and currently all patients will develop resistance and progressive disease. Evaluation of new strategies is needed with studies underway of combined targeted agents for adjuvant therapy and in combination with immunotherapy. These combinations may allow resistance that develops with single-agent therapy to be overcome by dealing with several targets at the same time. All these strategies will need careful evaluation in phase I/II studies to better evaluate issues regarding optimal dose, scheduling, treatment duration, and treatment-related morbidity. Ultimately randomized trials are needed to determine appropriate patient outcomes for the management of advanced and metastatic RCC.

REFERENCES

1. http://www.cancerhelp.org.uk. *Kidney Cancer*. 2007.
2. http://www.cancer.org/docroot/CRI/CRI_2x.asp?sitearea=&dt=22.

3. W. H. Chow, S. S. Devesa, J. L. Warren *et al.*, Rising incidence of renal cell cancer in the United States. *JAMA*, **281**:17 (1999), 1628–31.
4. A. Mathew, S. S. Devesa, J. F. Fraumeni, Jr. *et al.*, Global increases in kidney cancer incidence, 1973–1992. *Eur J Cancer Prev*, **11**:2 (2002), 171–8.
5. W. H. Chow, G. Gridley, J. F. Fraumeni, Jr. *et al.*, Obesity, hypertension, and the risk of kidney cancer in men. *N Engl J Med*, **343**:18 (2000), 1305–11.
6. A. H. Smith, V. I. Shearn, and R. Wood, Asbestos and kidney cancer: the evidence supports a causal association. *Am J Ind Med*, **16**:2 (1989), 159–66.
7. P. N. Bretan, Jr., M. P. Busch, H. Hricak *et al.*,. Chronic renal failure: a significant risk factor in the development of acquired renal cysts and renal cell carcinoma. Case reports and review of the literature. *Cancer*, **57**:9 (1986), 1871–9.
8. D. G. Skinner, T. R. Pritchett, G. Lieskovsky *et al.*, Vena caval involvement by renal cell carcinoma. Surgical resection provides meaningful long-term survival. *Ann Surg*, **210**:3 (1989), 387–92, discussion 392–4.
9. B. Delahunt, and J. N. Eble, History of the development of the classification of renal cell neoplasia. *Clin Lab Med*, **25**:2 (2005), 231–46.
10. N. Barnabas, M. B. Amin, K. Pindolia *et al.*, Mutations in the von Hippel–Lindau (VHL) gene refine differential diagnostic criteria in renal cell carcinoma. *J Surg Oncol*, **80**:1 (2002), 52–60.
11. R. E. Banks, P. Tirukonda, C. Taylor *et al.*, Genetic and epigenetic analysis of von Hippel–Lindau (VHL) gene alterations and relationship with clinical variables in sporadic renal cancer. *Cancer Res*, **66**:4 (2006), 2000–11.
12. M. B. Amin, P. Tamboli, J. Javidan *et al.*, Prognostic impact of histologic subtyping of adult renal epithelial neoplasms: an experience of 405 cases. *Am J Surg Pathol*, **26**:3 (2002), 281–91.
13. J. J. Patard, E. Leray, N. Rioux-Leclercq *et al.*, Prognostic value of histologic subtypes in renal cell carcinoma: a multicenter experience. *J Clin Oncol*, **23**:12 (2005), 2763–71.
14. A. Zisman, A. J. Pantuck, F. Dorey *et al.*, Improved prognostication of renal cell carcinoma using an integrated staging system. *J Clin Oncol*, **19**:6 (2001), 1649–57.
15. A. Zisman, A. J. Pantuck, R. A. Figlin *et al.*, Validation of the Ucla integrated staging system for patients with renal cell carcinoma. *J Clin Oncol*, **19**:17 (2001), 3792–3.
16. J. J. Patard, H. L. Kim, J. S. Lam *et al.*, Use of the University of California Los Angeles integrated staging system to predict survival in renal cell carcinoma: an international multicenter study. *J Clin Oncol*, **22**:16 (2004), 3316–22.
17. R. J. Motzer, M. Mazumdar, J. Bacik *et al.*, Survival and prognostic stratification of 670 patients with advanced renal cell carcinoma. *J Clin Oncol*, **17**:8 (1999), 2530–40.
18. R. J. Motzer, J. Bacik, L. H. Schwartz *et al.*, Prognostic factors for survival in previously treated patients with metastatic renal cell carcinoma. *J Clin Oncol*, **22**:3 (2004), 454–63.
19. R. J. Motzer, M. Mazumdar, J. Bacik *et al.*, Effect of cytokine therapy on survival for patients with advanced renal cell carcinoma. *J Clin Oncol*, **18**:9 (2000),1928–35.

20. L. Cindolo, J. J. Patard, P. Chiodini *et al.*, Comparison of predictive accuracy of four prognostic models for nonmetastatic renal cell carcinoma after nephrectomy: a multicenter European study. *Cancer*, **104**:7 (2005), 1362–71.
21. M. H. Bui, D. Seligson, K. R. Han *et al.*, Carbonic anhydrase IX is an independent predictor of survival in advanced renal clear cell carcinoma: implications for prognosis and therapy. *Clin Cancer Res*, **9**:2 (2003), 802–11.
22. M. H. Bui, H. Visapaa, D. Seligson *et al.*, Prognostic value of carbonic anhydrase IX and KI67 as predictors of survival for renal clear cell carcinoma. *J Urol*, **171**:6 (Pt 1) (2004), 2461–6.
23. R. J. Motzer, N. H. Bander, and D. M. Nanus, Renal-cell carcinoma. *N Engl J Med*, **335**:12 (1996), 865–75.
24. J. S. Lam, O. Shvarts, J. T. Leppert R. A. Figlin, and A. S. Belldegrun, Renal cell carcinoma 2005: new frontiers in staging, prognostication and targeted molecular therapy. *J Urol*, **173**:6 (2005), 1853–62.
25. C. Coppin, F. Porzsolt, J. Kumpf *et al.*, Immunotherapy for advanced renal cell cancer. *Cochrane Database Syst Rev* **3** (2000), CD001425.
26. N. B. Itano, M. L. Blute, B. Spotts *et al.*, Outcome of isolated renal cell carcinoma fossa recurrence after nephrectomy. *J Urol*, **164**:2 (2000), 322–5.
27. E. W. Riches, I. H. Griffiths, and A. C. Thackray, New growths of the kidney and ureter. *Br J Urol*, **23**:4 (1951), 297–356.
28. R. H. Flocks and M. C. Kadesky, Malignant neoplasms of the kidney; an analysis of 353 patients for followed five years or more. *J Urol*, **79**:2 (1958), 196–201.
29. D. G. Bratherton, The place of radiotherapy in the treatment of hypernephroma. *Br J Radiol*, **42**:504 (1969), 949.
30. W. B. Peeling, B. S. Mantell, and B. G. Shepheard, Post-operative irradiation in the treatment of renal cell carcinoma. *Br J Urol*, **41**:1 (1969), 23–31.
31. B. van der Werf-Messing, Proceedings: Carcinoma of the kidney. *Cancer*, **32**:5 (1973), 1056–61.
32. H. Juusela, K. Malmio, O. Alfthan *et al.*, Preoperative irradiation in the treatment of renal adenocarcinoma. *Scand J Urol Nephrol*, **11**:3 (1977), 277–81.
33. R. Finney, The value of radiotherapy in the treatment of hypernephroma – a clinical trial. *Br J Urol*, **45**:3 (1973), 258–69.
34. M. Kjaer, P. L. Frederiksen, and S. A. Engelholm , Postoperative radiotherapy in stage II and III renal adenocarcinoma. A randomized trial by the Copenhagen Renal Cancer Study Group. *Int J Radiat Oncol Biol Phys*, **13**:5 (1987), 665–72.
35. G. H. Mickisch, A. Garin, H. van Poppel *et al.*, Radical nephrectomy plus interferon-alfa-based immunotherapy compared with interferon alfa alone in metastatic renal-cell carcinoma: a randomised trial. *Lancet*, **358**:9286 (2001), 966–70.
36. R. C. Flanigan, S. E. Salmon, B. A. Blumenstein *et al.*, Nephrectomy followed by interferon alfa-2b compared with interferon alfa-2b alone for metastatic renal-cell cancer. *N Engl J Med*, **345**:23 (2001), 1655–9.

37. E. C. Halperin and L. Harisiadis, The role of radiation therapy in the management of metastatic renal cell carcinoma. *Cancer*, **51**:4 (1983), 614–17.
38. V. Onufrey and M. Mohiuddin, Radiation therapy in the treatment of metastatic renal cell carcinoma. *Int J Radiat Oncol Biol Phys*, **11**:11 (1985), 2007–9.
39. A. Yagoda, B. Abi-Rached, and D. Petrylak, Chemotherapy for advanced renal-cell carcinoma: 1983–1993. *Semin Oncol*, **22**:1 (1995), 42–60.
40. C. Coppin, F. Porzsolt, A. Awa *et al.*, Immunotherapy for advanced renal cell cancer. *Cochrane Database Syst Rev*, 1 (2005), CD001425.
41. C. Coppin, F. Porzsolt, M. Autenrieth *et al.*, Immunotherapy for advanced renal cell cancer. *Cochrane Database Syst Rev* (2007) 1 (2007).
42. J. M. Larkin and M. E. Gore, The MRC randomised-controlled trial of interferon-alpha, interleukin-2 and 5-fluorouracil vs. interferon-alpha alone in patients with advanced renal cell carcinoma (RE04): rationale and progress. *Clin Oncol (R Coll Radiol)*, **17**:5 (2005), 319–21.
43. D. J. Hicklin and L.M, Ellis. Role of the vascular endothelial growth factor pathway in tumor growth and angiogenesis. *J Clin Oncol*, **23**:5 (2005), 1011–27.
44. J. C. Yang, R. M. Sherry, S. M. Steinberg *et al.*, Randomized study of high-dose and low-dose interleukin-2 in patients with metastatic renal cancer. *J Clin Oncol*, **21**:16 (2003), 3127–32.
45. S. Wilhelm, C. Carter, M. Lynch *et al.*, Discovery and development of sorafenib: a multikinase inhibitor for treating cancer. *Nat Rev Drug Discov* , **5**:10 (2006), 835–44.
46. B. Escudier, T. Eisen, W. M. Stadler *et al.*, Sorafenib in advanced clear-cell renal-cell carcinoma. *N Engl J Med*, **356**:2 (2007), 125–34.
47. R. J. Motzer, M. D. Michaelson, B. G. Redman *et al.*, Activity of SU11248, a multitargeted inhibitor of vascular endothelial growth factor receptor and platelet-derived growth factor receptor, in patients with metastatic renal cell carcinoma. *J Clin Oncol*, **24**:1 (2006), 16–24.
48. R. J. Motzer, T. E. Hutson, P. Tomczak *et al.*, Sunitinib versus interferon alfa in metastatic renal-cell carcinoma. *N Engl J Med*, **356**:2 (2007), 115–24.

2

Pathology of adult renal parenchymal cancers

Patricia Harnden

Introduction

There have been a number of recent advances in our understanding of the pathology of renal cancer. This has not only resulted in some re-classification of cancer types but also improved our ability to pathologically characterize tumors allowing improved prognostication. All these aspects are reviewed here. Additionally the role of modern immunohistochemistry in the characterization of tumors from samples obtained by image-guided core biopsy is discussed.

Pathological classification of malignant renal tumors

Previous classifications

Previous classifications of renal tumors were based on their morphology [1], resulting in numerous subtypes and practical difficulties because of overlapping appearances. Subsequently, greater understanding of the genetic alterations underlying different subtypes and their morphological correlates led to a simplified and more relevant classification – the Heidelberg consensus classification [2,3]. Whereas the original World Health Organization (WHO) classification [1] separated clear cell from granular cell renal carcinomas, cytogenetic analyses revealed that these were different manifestations of the same abnormality involving the von Hippel–Lindau (VHL) gene on the short arm of chromosome 3, giving rise to the most common type of renal carcinoma. These "conventional" carcinomas have variable proportions of clear or granular cells (Figure 2.1) depending on the cytoplasmic content of fat (which "clears" during histological processing) or mitochondria (responsible for the granular or oncocytic appearance of cells). Spindle cell or sarcomatoid change has long been recognized as an indication of poor differentiation rather than an

Carcinoma of the Kidney, ed. Uday Patel. Published by Cambridge University Press.

Table 2.1. 2004 WHO classification of malignant renal cell tumors

Clear cell renal cell carcinoma
Multilocular clear cell renal cell carcinoma
Papillary renal cell carcinoma
Chromophobe renal cell carcinoma
Carcinoma of the collecting ducts of Bellini
Renal medullary carcinoma
Unclassified renal carcinoma
Xp11 translocation carcinoma
Carcinoma associated with neuroblastoma
Mucinous tubular and spindle cell carcinoma

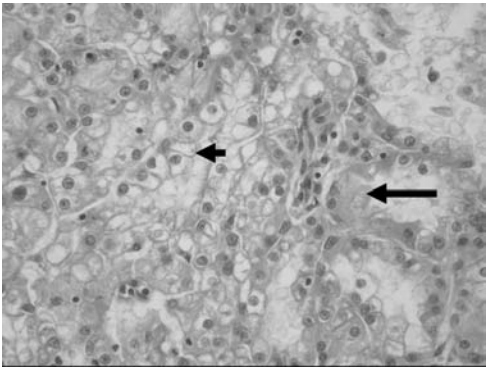

Figure 2.1 Conventional renal carcinoma showing a mixture of clear (short arrow) and granular (long arrow) cells (see also color plate section).

indication of cell lineage [4], and tumors within the WHO spindle cell category [1] could often be classified by cytogenetic analysis [2,3]. In the absence of residual morphological evidence of the original subtype, they should be considered as "unclassified" pending refinements in ancillary techniques.

World Health Organization classification 2004

The more recent 2004 WHO classification [5] was modeled to an extent on the consensus classification, with some important differences (Table 2.1). The term "clear cell" rather than conventional carcinoma was retained, leading to conceptual difficulties when granular cells predominate. Medullary carcinomas continued to be separated from collecting duct carcinomas, rather than considered as a variant in

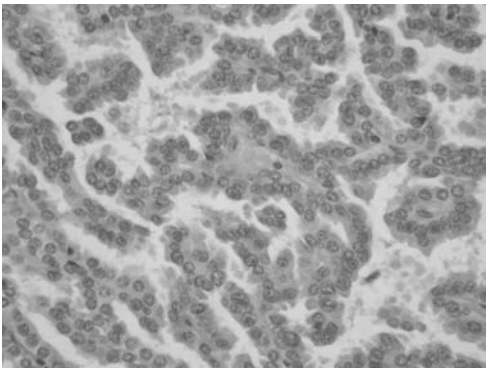

Figure 2.2 Papillary renal carcinoma composed of fibrovascular stalks and fairly uniform cells (see also color plate section).

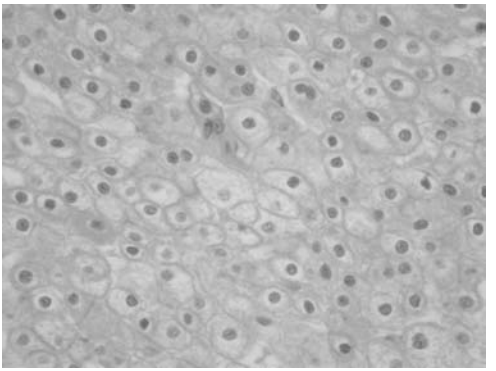

Figure 2.3 Chromophobe renal carcinoma with perinuclear haloes, slightly flocculent cytoplasm and accentuated cell membranes (see also color plate section).

patients with sickle-cell disease or trait, with minor histological differences attributable to local ischemia and inflammation caused by sickling. Finally, the rare, new entities described since the development of the consensus classification were included.

Conventional (clear cell) carcinomas are the most common subtype of renal carcinoma representing 89% of cases in a population-based study [6] and between 83% and 88% of large hospital-based series [7,8,9]. Only two other types occur with some frequency: papillary carcinomas (Figure 2.2) representing between 8% [6] and 11% [7] of tumors and chromophobe carcinomas (Figure 2.3) between 2% [6] and 5% [8].

Diagnostic difficulties: distinction between benign and malignant renal tumors

Renal adenoma versus carcinoma

There are no histological features that reliably distinguish between adenomas and carcinomas. Size was initially used as the only criterion, based largely on autopsy series showing that the risk of metastases increased with increasing tumor size. Only 4.6% of tumors less than 30 mm were associated with metastases in a series reported in 1950 [10]. The reliance on size alone to define an adenoma was further questioned by more recent surgical series, demonstrating metastatic behavior in a high proportion of small tumors [11]. The diagnosis of adenoma was then refined to exclude any tumor with a clear cell component [1]. However, papillary proliferations are common in older patients (40% of patients aged over 70) [12,13]

and they are morphologically indistinguishable from tumors that are known to have metastasized. Cytogenetic studies have shown abnormalities common to both well-differentiated papillary tumors, as small as 2–5 mm, and carcinomas (trisomies of chromosome 7 and 17 and loss of Y in males), with additional abnormalities in carcinomas [2,14]. This suggests that gains of chromosome 7 and 17 are early events in the development of papillary neoplasms, with additional events accumulating during growth leading to malignant behavior. Cytogenetic analysis may therefore not be definitive if performed early in the evolution of the tumor. A size limit of 5 mm for the diagnosis of adenoma has been suggested, as there are no published reports of metastases arising from tumor of that size [2]. In practice, these tumors will only be detected in nephrectomies, but may cause problems if found in kidneys harvested for transplantation.

Granular variants of renal carcinoma versus oncocytoma

Oncocytomas (Figure 2.4) are benign tumors with variable, sometimes irregular nuclei but entirely composed of cells with eosinophilic, granular cytoplasm. This is because of the presence of large numbers of cytoplasmic mitochondria, also found in the granular variant of conventional renal carcinoma and the eosinophilic variant of chromophobe carcinoma. These tumors can often, but not always, be distinguished by cytogenetic analysis [2,15], but this is not yet routinely available. Extensive tumor sampling may reveal an admixture of clear cells, which is sufficient for the diagnosis of conventional carcinoma. Similarly, the characteristic accentuated cytoplasmic borders and perinuclear haloes of chromophobe carcinoma may be focally present in the eosinophilic variant. More commonly, however, ancillary tests are required.

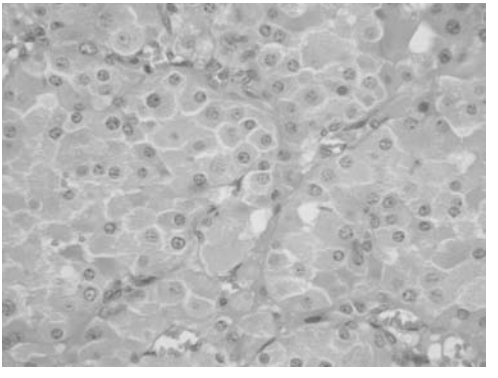

Figure 2.4 Oncocytoma composes of cells with eosinophilic, granular cytoplasm (see also color plate section).

Electron microscopy

This is the gold standard for diagnosis as the ultrastructural appearances of each tumor are distinctive. In oncocytomas, mitochondria are tightly packed to the virtual exclusion of any other organelle. Organelles, and sometimes small lipid droplets, separate the mitochondria in conventional renal carcinomas. Chromophobe carcinomas are characterized by the presence of membrane bound 150–300 nm cytoplasmic vesicles. However, electron microscopy requires good tissue preservation and is labor intensive and costly.

Histochemical stains

Hale's colloidal iron staining has been put forward as a marker of chromophobe carcinomas but can be difficult to interpret and lacks specificity as it is positive in a proportion of oncocytomas [16,17,18].

Immunohistochemistry

There is a vast literature on the use of antibodies to distinguish between different types of renal oncocytic tumors. CD-10 is commonly used to identify conventional renal carcinomas but is found in a high proportion of oncocytomas and chromophobe carcinomas [18,19]. The so-called RCC antibody, which was in fact raised against the proximal tubule brush border, is not only negative in oncocytomas and chromophobe carcinomas but also negative in a proportion of conventional renal carcinomas [18,20]. Although the distribution of keratins 7, 8, 18, and 19 may vary, they are present in all tumor subtypes [21]. Typical examples of new markers showing initial promise include the proto-oncogene product Ron, the receptor for macrophage stimulating protein, first reported as a specific marker for oncocytomas [22], later described in over 90% of chromophobe carcinomas in a separate series [23]. Similarly kidney-specific cadherin, first heralded as specific for chromophobe carcinomas [24], was subsequently demonstrated in a high proportion of oncocytomas [20,25].

Why do these markers repeatedly fail independent validation? One reason may be the diagnostic standard against which the antibodies are being tested. Most studies use pathological opinion based on light microscopy to initially discriminate between tumors, yet diagnostic agreement is known to be slight (kappa statistic = 0.3) even among experienced pathologists [16]. Also, the biotin-avidin/streptavidin system is often used as an amplification step in the immunohistochemical

technique to increase the sensitivity of detection. However, mitochondria contain large amounts of endogenous biotin leading to "non-specific" positivity in cells with large numbers of mitochondria [26,27]. Finally, although the marker of interest may be more frequently observed in a specific subtype [23,25,28] or show variations in the extent of positivity or antibody localization [28,29,30], these differences are open to subjective interpretation.

Pathological prognostic factors

Pathological stage

The 1960s Robson classification [31] has largely been superseded by the tumor, nodes, and metastases system (TNM classification), first developed by the Union Internationale Contre le Cancer (UICC) in the 1970s. Subsequent close collaboration with the American Joint Committee for Cancer (AJCC) resulted in identical classifications and therefore a single international standard [32]. The TNM classification uses tumor size to subdivide intrarenal tumors and is also more precise than the Robson system in the categorization of the extent of spread. Both systems have shown correlations with patient outcome although there are relatively large variations within each stage (Table 2.2).

The TNM pathological staging system is almost entirely dependent on gross findings, which are then confirmed microscopically. This can lead to variations in staging depending on the experience and meticulousness of the pathologist performing the dissection. Unlike a histological diagnosis, macroscopic observations cannot generally be reviewed or corrected and study populations cannot be restaged to standardize the TNM version. The TNM system was historically derived from expert consensus, and a continuous improvement process has been introduced in a move toward evidence-based medicine [33]. However, this is at the cost of hindering comparison of studies using different editions. This applies particularly to the distinction between stages pT1 and pT2, for which the cut-off was raised from 25 mm to 70 mm in 1997 [34]. Stage pT1 was subsequently divided using the cut-off of 40 mm, considered the upper limit for eligibility for nephron-sparing surgery (Table 2.2) [35]. Another modification introduced in 2002 removed the need to demonstrate residual normal nodal tissue in order to diagnose lymph involvement. As long as the tumor nodule had the form and smooth contour of a lymph node and was anatomically situated in the lymph drainage area, it was diagnosed as an involved node. This could result in more patients being classified as node positive.

Table 2.2. Comparison of the Robson and TNM staging systems

Robson [31]	Disease extent	2002 TNM [35]	Range of 5-year overall survival [89]
I	Tumor confined within the kidney	pT1 $\leq$ 7 cm in greatest dimension (pT1a $\leq$ 4 cm, pT1b > 4 cm) pT2 tumor > 7 cm in greatest dimension	74%–96%
II	Tumor spread to adrenal gland or perinephric tissues but within Gerota's fascia	pT3a	65%–80%
IIIA	Grossly visible extension into renal vein or vena cava	pT3b below the diaphragm pT3c above the diaphragm	0%–20%
IV	Invasion of adjacent organs (except adrenal)	pT4	0%–20%

Tumor size

Although the prognostic significance of using a 7 cm limit to divide organ confined tumors has been validated [8,36,37], other larger studies found that the main transition in risk was at 5 rather than 7 cm [38,39,40] and a further transition was found at 10 cm [41]. Tumor size was also significantly associated with survival when analyzed as a continuous variable [37,42]. Large size remains significantly associated with recurrence for carcinomas extending beyond the kidney, at least for the conventional/clear cell subtype [43,44]. In fact, in a registry-based review of patients with renal tumors, but with tumor measurements recorded in only 61.5% of cases, the correlation between tumor size and 5-year survival was only observed if the tumor had spread beyond the kidney [45]. It is important to bear in mind that small tumors are not necessarily associated with good prognosis: long-term follow- up of a surgical series of patients with tumors 30 mm or less showed 19% cancer-specific mortality at 5 years and 28% at 10 years [11].

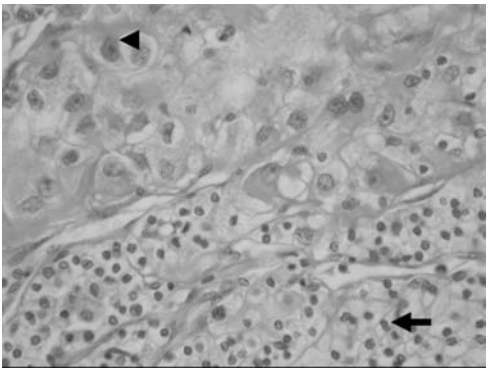

Figure 2.5 Grade heterogeneity within conventional renal carcinoma contrasting Fuhrman grade 3 cells with prominent nucleoli (arrowhead) with small grade 1 cells (arrow) (see also color plate section).

Tumor grade

The grading system in most common use is the Fuhrman system, which consists of four nuclear grades in order of increasing nuclear size, irregularity, and nucleolar prominence [4], and its independent prognostic value has been confirmed in large studies both for organ confined and metastatic disease [6,9,38,46,47]. Sarcomatoid change, although included in Fuhrman grade 4, is an independent prognostic factor even within this group of patients [48], regardless of the subtype of renal carcinoma [8,48,49]. The other major grading system, developed at the Mayo Clinic, uses similar criteria to define grades 3 and 4 but grade 1 is equivalent to Fuhrman grade 2, and grade 2 is intermediate between Fuhrman grades 2 and 3 [43]. In practice grade is often heterogeneous (Figure 2.5), and in the Fuhrman system, the overall grade is the highest regardless of extent whereas in the Mayo system, it is the highest grade occupying at least one high-power microscopic field. The Mayo clinic system has only been used and validated for conventional (clear cell) carcinomas [43,50] but the Fuhrman system is also prognostically useful for papillary and chromophobe carcinomas [6,7,9].

Histological subtype

Given the low frequency of non-conventional subtypes, only a large series can reliably assess the relationship between histological subtype and survival. Series including at least 500 patients (range 588–4063) have generally only compared conventional (clear cell), papillary, and chromophobe carcinomas and, in univariate analysis, have reported poorer disease-specific survival for conventional carcinomas [6,7,8,9]. However, when multivariate analysis was performed to adjust for stage and grade [6,7,9], histological subtyping was only of prognostic significance in one study [7].

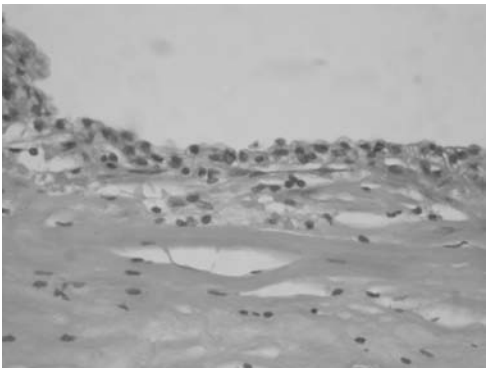

Figure 2.6 Multilocular cystic renal carcinoma with clear cells lining the cysts and a small number of clear cells in the stroma of the septa (see also color plate section).

Data regarding the rarer subtypes of carcinoma are scant, but patients with unclassifiable tumors appear to have the worst prognosis [46,51], possibly because many are unclassifiable because of sarcomatoid change, which itself is associated with a dismal prognosis [8,48,49]. Patients with collecting-duct carcinomas often present at an advanced stage and prognosis is poor [52]. At the other end of the spectrum, multilocular cystic renal carcinoma (Figure 2.6), which is composed entirely of cysts with small numbers of carcinoma cells, is associated with an excellent prognosis with no reported cases of spread beyond the kidney [53].

Tumor necrosis

Tumor necrosis is a well-established independent poor prognostic indicator particularly for clinically localized disease, whether it is seen at gross examination [54] or microscopically [40,43,44,55,56,57,58]. When subtyping has been performed, the association was significant only for conventional and chromophobe, but not papillary, carcinomas [7]. From a practical point of view, caution should be used when assessing tumor necrosis in cases of preoperative embolization, although if performed shortly before surgery, it does not generally cause tumor infarction.

Vascular invasion

Macroscopic invasion into the renal vein or its segmental tributaries defines stage pT3b in the TNM system (Table 2.2). However, the identification of vascular invasion microscopically in patients with clinically localized carcinoma has also been identified as a risk factor for recurrence [44,59,60,61].

Invasion of the collecting system

Invasion of the calyces or renal pelvis is relatively rare but it appears to confer a worse prognosis particularly in lower-stage disease [62,63,64].

Prognostic algorithms

Several groups have sought to build prognostic algorithms by combining multiple prognostic factors. These may provide superior predictive information for individual patients and identify those at low risk for whom follow-up, including imaging, can safely be reduced and select those at high risk for adjuvant therapies.

All renal cancer subtypes grouped

The UCLA Integrated Staging System (UISS) uses stage (1997 TNM), Fuhrman grade, and the Eastern Cooperative Oncology Group (ECOG) performance status to stratify patients into low-, intermediate-, and high-risk groups [65]. The 5-year disease-specific survival for patients with clinically localized carcinoma is 91.1% ($\pm$3.6), 80.4% ($\pm$4.0), and 54.7% ($\pm$5.4) for the low-, intermediate-, and high-risk groups, respectively. The corresponding figures for patients presenting with metastatic disease are 32.0% ($\pm$8.7), 19.5% ($\pm$3.2), and 0%. The use of the 1997 rather than 2002 TNM system impacts only on the assessment of nodal status as the diagnosis of node positivity can only be made in the earlier system if there is residual, identifiable nodal tissue.

Systems for conventional (clear cell), clinically localized carcinoma only

The Memorial Sloan Kettering Cancer Centre (MSKCC) nomogram [44] includes clinical presentation (incidental or symptomatic). This was of prognostic significance in cohort surgical studies [66,67,68] but not in a population-based study [69], suggesting that the apparent improvement in survival in cohort studies is because of lead time bias. Other factors in the nomogram are tumor size, pathological stage (2002 TNM), Fuhrman grade, the presence of necrosis, and/or vascular invasion. The nomogram of a 5-year predicted probability of freedom from recurrence is available at nomograms@mskcc.org.

The Mayo Clinic algorithm [43] is based on pathological tumor stage (2002 TNM), nodal status, tumor size (10 cm cut-off), nuclear grade (Mayo system), and

histological tumor necrosis. Although there was a potential selection bias toward good performance status, this large study (1671 patients) showed good discrimination for the 5-year risk of recurrence between low- (97.1%, ±0.7), intermediate- (73.8%, ±2.0), and high-risk (31.2%, ±2.7) groups and it has been independently validated [50].

Molecular markers

The last decades have seen an explosion of studies on the prognostic value of differences in gene and protein expression in different tumor types. However, few markers have been translated into clinical practice, a failure that has been attributed to poor study design, execution, and reporting [70], prompting the National Cancer Institute (NCI) and the European Organization for Research and Treatment of Cancer (EORTC) to develop guidance to remedy the situation [71]. As in other areas, most published studies in renal cancer are retrospective and based on a relatively small series of selected patients without a validation arm. An example of a possible exception, based on the exploitation of our understanding of relevant pathways in renal cancer, illustrates the potential of these markers to deliver patient benefits. The VHL gene product normally induces the proteolysis of hypoxia induced factors (HIF), so that inactivation of the VHL gene, as seen in the majority of conventional renal carcinomas, leads to constitutive upregulation of HIF (the process is explained in detail in Chapter 3) and consequently multiple targets including angiogenic and other factors such as the tumor-associated carbonic anhydrases (CAs) [72]. CA9 in particular is not expressed in normal tissues. The association between over-expression and favorable prognosis and response to interleukin-2 (IL-2) therapy in patients with advanced conventional carcinomas was demonstrated [73] and confirmed [74]. The development of monoclonal antibodies to CA9 has opened the possibility of predicting treatment response non-invasively by immunoscintigraphy [75] and developing new, less toxic treatments [76].

The role of biopsy in the characterization of renal masses

Fine needle aspiration cytology was initially used for the characterization of renal masses, but specificity, even in experienced hands, is low compared to histology [77], so that percutaneous core biopsy is now the more common approach. The technical details of renal mass biopsy are covered in Chapter 6.

Established indications for biopsy

Biopsy is useful if the imaging is equivocal and the diagnosis of a non-renal parenchymal neoplasm would lead to a change in treatment, such as systemic therapy. In patients with multiple sites of disease, renal biopsy may be the safest approach or the best option for obtaining viable tissue. Liaison with the histopathology laboratory is essential to optimize tissue handling as marker studies may require fresh tissue. Tumor biopsies must be clearly distinguished from medical renal biopsies, otherwise precious tissue may be wasted on special stains which would not be useful. It is usually best to take only an initial shallow section for diagnosis to maximize the amount of tissue available for immunohistochemistry.

Patients with extrarenal cancer

In addition to lymphoma, the most common primaries to involve the kidney are lung and breast cancer and malignant melanoma [78]. However, biopsy may reveal a new renal primary in up to 50% of cases [79]. Providing adequate tissue is available, the diagnosis of lymphoma can readily be achieved by morphology and immunohistochemistry. Comparison of the morphological appearances of the primary carcinoma or melanoma and the renal mass biopsy should be performed wherever possible as a definitive diagnosis can often be made. Retroperitoneal sarcomas may secondarily involve the kidney but primary tumors may also arise from mesenchymal elements in or immediately around the kidney. Although surgery may still represent the best treatment, modifications to the surgical technique may be required. The distinction between benign and malignant soft tissue tumors, particularly leiomyoma versus low grade leiomyosarcoma, may not be possible on biopsy as extensive tumor sampling is often required to demonstrate focal mitotic activity or nuclear pleomorphism in malignant tumors. The distinction between sarcomatoid carcinomas and sarcomas is generally only made with the benefit of molecular markers.

Patients with advanced tumors

Characterization of the tumor can be important to offer the best choice of systemic therapy, such as chemotherapy for transitional cell carcinomas or biological therapies for conventional renal carcinoma. A tissue diagnosis may also be required for trial eligibility.

Patients with possible infections

This is a rare indication because most infections are diagnosed through a combination of careful history supplemented by laboratory investigations. However, xanthogranulomatous pyelonephritis, an uncommon reaction to infection, can present as a mass. Biopsy reveals large numbers of foamy macrophages but infiltration by foamy macrophages is a common occurrence in renal carcinomas, so that continued surveillance and re-biopsy if necessary are required when findings are initially negative.

Potential new indications for biopsy

Patients with benign tumors

Benign tumors, if small and asymptomatic, could reasonably be left untreated, particularly in patients with co-morbidities. Size was previously a criterion for their diagnosis (as commentated above), but at least 85% of tumors less than 7 cm [80] and 72% of tumors less than 2 cm [81] are histologically malignant.

As discussed earlier in this chapter, oncocytomas cannot be diagnosed reliably on biopsy since extensive tumor sampling and ancillary tests are required, unless special techniques such as interphase fluorescent *in situ* hybridization (FISH) for the chromosomal loci involved in different tumor subtypes are available. Accuracies of up to 86% have been reported with this method, although 6% of tumors were incorrectly classified and 8% of tests failed because of inadequate material [15]. The only type of (usually) benign tumor that can currently be routinely diagnosed on biopsy is angiomyolipoma (Figure 2.7), which occurs either sporadically or

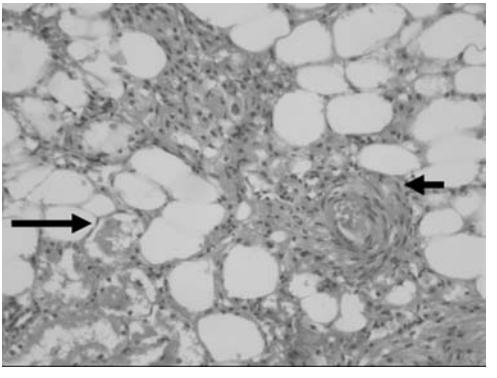

Figure 2.7 Intrarenal angiomyolipoma with abnormal vessels and proliferation of pericytes (short arrow), fat and adjacent normal renal parenchyma (long arrow) (see also color plate section).

in patients with Tuberous Sclerosis. These tumors belong to a family of tumors characterized by a clonal proliferation of perivascular epithelioid cells (PEComas) with a polyclonal proliferation of adipose tissue, the extent of which varies [82]. Associations with malignant epithelial tumors are well described and a small proportion of these tumors can themselves metastasize [83]. Reliable diagnostic criteria to distinguish benign from malignant forms have not been established: even invasion of the vascular system or regional lymph nodes can be an indication of multifocal growth pattern rather than metastasis [84].

Although an absolute diagnosis of benign versus malignant may not be possible, histological factors may help in the assessment of risk, balancing those of tumor progression against treatment associated risks for individual patients, taking their biological age and co-morbidities into account. Macroscopic necrosis, which can be demonstrated radiologically, is a poor prognostic factor but this is also the case for histological tumor necrosis on biopsy (section 3.5). The accuracy of Fuhrman grade is relatively low on biopsy material [85,86], but can be improved by grouping grades 1 and 2 into low and 3 and 4 into high grades [85]. As even small foci of poor differentiation are associated with poorer outcomes [4,43], the finding of high grade on biopsy is likely to be a strong indicator of high risk of progression, but low grade on biopsy could result from sampling error.

Patients undergoing radio-frequency ablation

Biopsies should be performed prior to treatment to make the diagnosis of a benign tumor if possible, but just as importantly, for audit purposes. Correlation with outcomes should determine whether any histological parameters are predictive of treatment response or failure.

Patients with indeterminate masses

Cystic angiomyolipomas have been described but are rare [87]. The main differential diagnoses are renal carcinoma with cysts including multilocular cystic carcinoma (Figure 2.6) versus benign complex cysts, including cystic nephroma (Figure 2.8). A diagnosis of carcinoma can be made if there are clear cells in the septa between cysts, but this may be difficult to demonstrate in biopsy material. Similarly, if the cells lining the cysts have clear or granular abundant cytoplasm, carcinoma is more likely, particularly if there is multilayering. However, histological examination of resected specimens has shown that both these features may be

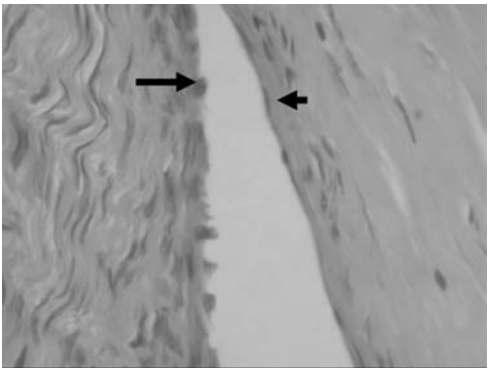

Figure 2.8 Cystic nephroma with cysts lined by hobnail cells with underlying cellular stroma (long arrow) or attenuated cells and paucicellular stroma (short arrow) (see also color plate section).

present only focally so that their absence on biopsy may result from sampling error and biopsy does not exclude malignancy, so that biopsy may be unhelpful in up to 30% of patients [88].

Conclusion

Marked progress has been made in the characterization of renal tumors but robust, externally validated, studies are needed to develop biomarkers for the diagnosis of these tumors, for more accurate assessment of risk to enable individually tailored follow-up and treatment, and for the prediction of response to specific therapies.

REFERENCES

1. F. K. Mostofi, and C. J. Davis, *Histological Typing of Kidney Tumours*, 2nd edn (Berlin, Heidelberg, New York: Springer, 1998).
2. G. Kovacs, M. Akhtar, B. J. Beckwith *et al.*, The Heidelberg classification of renal cell tumours. *J Pathol*, **183** (1997), 131–3.
3. S. Storkel, J. N. Eble, K. Adlakha *et al.*, Classification of renal cell carcinoma: Workgroup No. 1. Union Internationale Contre le Cancer (UICC) and the American Joint Committee on Cancer (AJCC). *Cancer*, **80** (1997), 987–9.
4. S. A. Fuhrman, L. C. Lasky, and C. Limas, Prognostic significance of morphologic parameters in renal cell carcinoma. *Am J Surg Pathol*, **6** (1982), 655–63.
5. J. Eble, G. Sauter, J. Epstein *et al.*, *Pathology and Genetics of Tumours of the Urinary System and Male Genital Organs* (Lyon: IARC Press, 2004).

6. T. Gudbjartsson, S. Hardarson, V. Petursdottir *et al.*, Histological subtyping and nuclear grading of renal cell carcinoma and their implications for survival: a retrospective nation-wide study of 629 patients. *Eur Urol*, **48** (2005), 593–600.
7. J. C. Cheville, C. M. Lohse, H. Zincke *et al.*, Comparisons of outcome and prognostic features among histologic subtypes of renal cell carcinoma. *Am J Surg Pathol*, **27** (2003), 612–24.
8. H. Moch, T. Gasser, M. B. Amin *et al.*, Prognostic utility of the recently recommended histologic classification and revised TNM staging system of renal cell carcinoma: a Swiss experience with 588 tumors. *Cancer*, **89** (2000), 604–14.
9. J. J. Patard, E. Leray, N. Rioux-Leclercq *et al.*, Prognostic value of histologic subtypes in renal cell carcinoma: a multicenter experience. *J Clin Oncol*, **23** (2005), 2763–71.
10. E. T. Bell, *Renal Diseases* (Philadelphia: Lea & Febiger, 1950).
11. P. Eschwege, C. Saussine, G. Steichen *et al.*, Radical nephrectomy for renal cell carcinoma 30 mm. or less: long-term follow results. *J Urol*, **155** (1996), 1196–9.
12. M. Reis, V. Faria, J. Lindoro *et al.*, The small cystic and noncystic noninflammatory renal nodules: a postmortem study. *J Urol*, **140** (1988), 721–4.
13. J. M. Xipell, The incidence of benign renal nodules (a clinicopathologic study). *J Urol*, **106** (1971), 503–6.
14. G. Kovacs, L. Fuzesi, A. Emanual *et al.*, Cytogenetics of papillary renal cell tumors. *Genes Chromosomes Cancer*, **3** (1991), 249–55.
15. D. A. Barocas, S. Mathew, J. J. DelPizzo *et al.*, Renal cell carcinoma sub-typing by histopathology and fluorescence in situ hybridization on a needle-biopsy specimen. *BJU Int*, **99** (2007), 290–5.
16. N. A. Abrahams, G. T. MacLennan, J. D. Khoury *et al.*, Chromophobe renal cell carcinoma: a comparative study of histological, immunohistochemical and ultrastructural features using high throughput tissue microarray. *Histopathology*, **45** (2004), 593–602.
17. N. Kuroda, M. Toi, M. Yamamoto *et al.*, Immunohistochemical identification of intracytoplasmic lumens by cytokeratin typing may differentiate renal oncocytomas from chromophobe renal cell carcinomas. *Histol Histopathol*, **19** (2004), 23–8.
18. H. Y. Wang and S. E. Mills, KIT and RCC are useful in distinguishing chromophobe renal cell carcinoma from the granular variant of clear cell renal cell carcinoma. *Am J Surg Pathol*, **29** (2005), 640–6.
19. P. R. Mazal, M. Stichenwirth, A. Koller *et al.*, Expression of aquaporins and PAX-2 compared to CD10 and cytokeratin 7 in renal neoplasms: a tissue microarray study. *Mod Pathol*, **18** (2005), 535–40.
20. S. S. Shen, B. Krishna, R. Chirala *et al.*, Kidney-specific cadherin, a specific marker for the distal portion of the nephron and related renal neoplasms. *Mod Pathol*, **18** (2005), 933–40.
21. C. Langner, B. J. Wegscheider, M. Ratschek *et al.*, Keratin immunohistochemistry in renal cell carcinoma subtypes and renal oncocytomas: a systematic analysis of 233 tumors. *Virchows Arch*, **444** (2004), 127–34.

22. T. Rampino, M. Gregorini, G. Soccio *et al.*, The Ron proto-oncogene product is a phenotypic marker of renal oncocytoma. *Am J Surg Pathol*, **27** (2003), 779–85.
23. K. T. Patton, M. S. Tretiakova, J. L. Yao *et al.*, Expression of RON Proto-oncogene in Renal Oncocytoma and Chromophobe Renal Cell Carcinoma. *Am J Surg Pathol*, **28** (2004), 1045–50.
24. P. R. Mazal, M. Exner, A. Haitel *et al.*, Expression of kidney-specific cadherin distinguishes chromophobe renal cell carcinoma from renal oncocytoma. *Hum Pathol*, **36** (2005), 22–8.
25. B. P. Adley, A. Gupta, F. Lin *et al.*, Expression of kidney-specific cadherin in chromophobe renal cell carcinoma and renal oncocytoma. *Am J Clin Pathol*, **126** (2006), 79–85.
26. R. E. Banks, R. A. Craven, P. A. Harnden *et al.*, Use of a sensitive EnVision +-based detection system for Western blotting: avoidance of streptavidin binding to endogenous biotin and biotin-containing proteins in kidney and other tissues. *Proteomics*, **3** (2003), 558–61.
27. J. Southgate, P. Harnden, and J. Holt, Which proliferation markers for routine immunohistology? *J Clin Pathol*, **49** (1996), 270.
28. B. P. Adley, V. Papavero, J. Sugimura *et al.*, Diagnostic value of cytokeratin 7 and parvalbumin in differentiating chromophobe renal cell carcinoma from renal oncocytoma. *Anal Quant Cytol Histol*, **28** (2006), 228–36.
29. P. G. Chu and L. M. Weiss, Cytokeratin 14 immunoreactivity distinguishes oncocytic tumour from its renal mimics: an immunohistochemical study of 63 cases. *Histopathology*, **39** (2001), 455–62.
30. O. Mete, I. Kilicaslan, M. G. Gulluoglu *et al.*, Can renal oncocytoma be differentiated from its renal mimics? The utility of anti-mitochondrial, caveolin 1, CD63 and cytokeratin 14 antibodies in the differential diagnosis. *Virchows Arch*, **447** (2005), 938–46.
31. C. J. Robson, B. M. Churchill, and W. Anderson, The results of radical nephrectomy for renal cell carcinoma. *J Urol*, **101** (1969), 297–301.
32. P. Guinan, L. H. Sobin, F. Algaba *et al.*, TNM staging of renal cell carcinoma: Workgroup No. 3. Union International Contre le Cancer (UICC) and the American Joint Committee on Cancer (AJCC). *Cancer*, **80** (1997), 992–3.
33. M. K. Gospodarowicz, D. Miller, P. A. Groome *et al.*, The process for continuous improvement of the TNM classification. *Cancer*, **100**:1 (2004), 1–5.
34. L. H. Sobin and C. Wittekind, *TNM Classification of Malignant Tumours*, 5th edn (New York: John Wiley, 1997).
35. L. H. Sobin and C. Wittekind, *TNM Classification of Malignant Tumours*, 6th edn (New York: Wiley-Liss, 2002).
36. R. Minervini, A. Minervini, N. Fontana *et al.*, Evaluation of the 1997 tumour, nodes and metastases classification of renal cell carcinoma: experience in 172 patients. *BJU Int*, **86** (2000), 199–202.
37. B. Delahunt, J. M. Kittelson, M. R. McCredie *et al.*, Prognostic importance of tumor size for localized conventional (clear cell) renal cell carcinoma: assessment of TNM T1 and T2

tumor categories and comparison with other prognostic parameters. *Cancer*, **94** (2002), 658–64.

38. W. K. Lau, J. C. Cheville, M. L. Blute *et al.*, Prognostic features of pathologic stage T1 renal cell carcinoma after radical nephrectomy. *Urology*, **59** (2002), 532–7.
39. M. Kuczyk, G. Wegener, A. S. Merseburger *et al.*, Impact of tumor size on the long-term survival of patients with early stage renal cell cancer. *World J Urol*, **23** (2005), 50–4.
40. I. Frank, M. L. Blute, J. C. Cheville *et al.*, An outcome prediction model for patients with clear cell renal cell carcinoma treated with radical nephrectomy based on tumor stage, size, grade and necrosis: the SSIGN score. *J Urol*, **168** (2002), 2395–400.
41. I. Frank, M. L. Blute, B. C. Leibovich *et al.*, pT2 classification for renal cell carcinoma. Can its accuracy be improved? *J Urol*, **173** (2005), 380–4.
42. F. Di Silverio, P. Casale, D. Colella *et al.*, Independent value of tumor size and DNA ploidy for the prediction of disease progression in patients with organ-confined renal cell carcinoma. *Cancer*, **88** (2000), 835–43.
43. B. C. Leibovich, M. L. Blute, J. C. Cheville *et al.*, Prediction of progression after radical nephrectomy for patients with clear cell renal cell carcinoma: a stratification tool for prospective clinical trials. *Cancer*, **97** (2003), 1663–71.
44. M. Sorbellini, M. W. Kattan, M. E. Snyder *et al.*, A postoperative prognostic nomogram predicting recurrence for patients with conventional clear cell renal cell carcinoma. *J Urol*, **173** (2005), 48–51.
45. P. D. Guinan, N. J. Vogelzang, A. M. Fremgen *et al.*, Renal cell carcinoma: tumor size, stage and survival. Members of the Cancer Incidence and End Results Committee. *J Urol*, **153** (1995), 901–3.
46. M. B. Amin, M. B. Amin, P. Tamboli *et al.*, Prognostic impact of histologic subtyping of adult renal epithelial neoplasms: an experience of 405 cases. *Am J Surg Pathol*, **26** (2002), 281–91.
47. V. Ficarra, R. Righetti, S. Pilloni *et al.*, Prognostic factors in patients with renal cell carcinoma: retrospective analysis of 675 cases. *Eur Urol*, **41** (2002), 190–8.
48. J. C. Cheville, C. M. Lohse, H. Zincke *et al.*, Sarcomatoid renal cell carcinoma: an examination of underlying histologic subtype and an analysis of associations with patient outcome. *Am J Surg Pathol*, **28** (2004), 435–41.
49. B. C. Leibovich, K. R. Han, M. H. Bui *et al.*, Scoring algorithm to predict survival after nephrectomy and immunotherapy in patients with metastatic renal cell carcinoma: a stratification tool for prospective clinical trials. *Cancer*, **98** (2003), 2566–75.
50. V. Ficarra, G. Martignoni, C. Lohse *et al.*, External validation of the Mayo Clinic Stage, Size, Grade and Necrosis (SSIGN) score to predict cancer specific survival using a European series of conventional renal cell carcinoma. *J Urol*, **175** (2006), 1235–9.
51. A. Zisman, D. H. Chao, A. J. Pantuck *et al.*, Unclassified renal cell carcinoma: clinical features and prognostic impact of a new histological subtype. *J Urol*, **168** (2002), 950–5.

52. N. Tokuda, S. Naito, O. Matsuzaki *et al.*, Collecting duct (Bellini duct) renal cell carcinoma: a nationwide survey in Japan. *J Urol*, **176** (2006), 40–3; discussion 43.
53. S. Suzigan, A. Lopez-Beltran, R. Montironi *et al.*, Multilocular cystic renal cell carcinoma: a report of 45 cases of a kidney tumor of low malignant potential. *Am J Clin Pathol*, **125** (2006), 217–22.
54. S. E. Lee, S. S. Byun, J. K. Oh *et al.*, Significance of macroscopic tumor necrosis as a prognostic indicator for renal cell carcinoma. *J Urol*, **176** (2006), 1332–7.
55. S. Sengupta, C. M. Lohse, B. C. Leibovich *et al.*, Histologic coagulative tumor necrosis as a prognostic indicator of renal cell carcinoma aggressiveness. *Cancer*, **104** (2005), 511–20.
56. J. S. Lam, O. Shvarts, J. W. Said *et al.*, Clinicopathologic and molecular correlations of necrosis in the primary tumor of patients with renal cell carcinoma. *Cancer*, **103** (2005), 2517–25.
57. I. Frank, M. L. Blute, J. C. Cheville *et al.*, A multifactorial postoperative surveillance model for patients with surgically treated clear cell renal cell carcinoma. *J Urol*, **170** (2003), 2225–32.
58. E. Sabo, A. Boltenko, Y. Sova *et al.*, Microscopic analysis and significance of vascular architectural complexity in renal cell carcinoma. *Clin Cancer Res*, **7** (2001), 533–7.
59. P. D. Goncalves, M. Srougi, M. F. Dall'lio *et al.*, Low clinical stage renal cell carcinoma: relevance of microvascular tumor invasion as a prognostic parameter. *J Urol*, **172** (2004), 470–4.
60. D. F. Griffiths, A. Verghese, A. Golash *et al.*, Contribution of grade, vascular invasion and age to outcome in clinically localized renal cell carcinoma. *BJU Int*, **90** (2002), 26–31.
61. M. Sevinc, Z. Kirkali, K. Yorukoglu *et al.*, Prognostic significance of microvascular invasion in localized renal cell carcinoma. *Eur Urol*, **38** (2000), 728–33.
62. G. S. Palapattu, A. J. Pantuck, F. Dorey *et al.*, Collecting system invasion in renal cell carcinoma: impact on prognosis and future staging strategies. *J Urol*, **170** (2003), 768–72.
63. C. Terrone, C. Cracco, S. Guercio *et al.*, Prognostic value of the involvement of the urinary collecting system in renal cell carcinoma. *Eur Urol*, **46** (2004), 472–6.
64. R. G. Uzzo, E. E. Cherullo, J. Myles *et al.*, Renal cell carcinoma invading the urinary collecting system: implications for staging. *J Urol*, **167** (2002), 2392–6.
65. A. Zisman, A. J. Pantuck, J. Wieder *et al.*, Risk group assessment and clinical outcome algorithm to predict the natural history of patients with surgically resected renal cell carcinoma. *J Clin Oncol*, **20** (2002), 4559–66.
66. V. Ficarra, T. Prayer-Galetti, G. Novella *et al.*, Incidental detection beyond pathological factors as prognostic predictor of renal cell carcinoma. *Eur Urol*, **43** (2003), 663–9.
67. C. T. Lee, J. Katz, P. A. Fearn *et al.*, Mode of presentation of renal cell carcinoma provides prognostic information. *Urol Oncol*, **7** (2002), 135–40.
68. J. J. Patard, A. Rodriguez, N. Rioux-Leclercq *et al.*, Prognostic significance of the mode of detection in renal tumours. *BJU Int*, **90** (2002), 358–63.
69. T. Gudbjartsson, A. Thoroddsen, V. Petursdottir *et al.*, Effect of incidental detection for survival of patients with renal cell carcinoma: results of population-based study of 701 patients. *Urology*, **66** (2005), 1186–91.

70. L. M. McShane, D. G. Altman, and W. Sauerbrei. Identification of clinically useful cancer prognostic factors: what are we missing? *J Natl Cancer Inst*, **97**:14 (2005), 1023–5.
71. L. M. McShane, D. G. Altman, W. Sauerbrei *et al.*, Reporting recommendations for tumor marker prognostic studies. *J Clin Oncol*, **23** (2005), 9067–72.
72. C. C. Wykoff, N. J. Beasley, P. H. Watson *et al.*, Hypoxia-inducible expression of tumor-associated carbonic anhydrases. *Cancer Res*, **60** (2000), 7075–83.
73. M. H. Bui, D. Seligson, K. R. Han *et al.*, Carbonic anhydrase IX is an independent predictor of survival in advanced renal clear cell carcinoma: implications for prognosis and therapy. *Clin Cancer Res*, **9** (2003), 802–11.
74. M. Atkins, M. Regan, D. McDermott *et al.*, Carbonic anhydrase IX expression predicts outcome of interleukin 2 therapy for renal cancer. *Clin Cancer Res*, **11** (2005), 3714–21.
75. A. H. Brouwers, U. Dorr, O. Lang *et al.*, 131 I-cG250 monoclonal antibody immunoscintigraphy versus [18 F]FDG-PET imaging in patients with metastatic renal cell carcinoma: a comparative study. *Nucl Med Commun*, **23** (2002), 229–36.
76. I. Bleumer, E. Oosterwijk, J. C. Oosterwijk-Wakka *et al.*, A clinical trial with chimeric monoclonal antibody WX-G250 and low dose interleukin-2 pulsing scheme for advanced renal cell carcinoma. *J Urol*, **175** (2006), 57–62.
77. S. Torp-Pedersen, N. Juul, T. Larsen *et al.*, US-guided fine needle biopsy of solid renal masses – comparison of histology and cytology. *Scand J Urol Nephrol Suppl*, **137** (1991), 41–3.
78. R. B. Bracken, G. Chica, D. E. Johnson *et al.*, Secondary renal neoplasms: an autopsy study. *South Med J*, **72** (1979), 806–7.
79. F. J. Rybicki, K. M. Shu, E. S. Cibas *et al.*, Percutaneous biopsy of renal masses: sensitivity and negative predictive value stratified by clinical setting and size of masses. *AJR Am J Roentgenol*, **180** (2003), 1281–7.
80. M. E. Snyder, A. Bach, M. W. Kattan *et al.*, Incidence of benign lesions for clinically localized renal masses smaller than 7 cm in radiological diameter: influence of sex. *J Urol*, **176** (2006), 2391–5.
81. B. Schlomer, R. S. Figenshau, Y. Yan *et al.*, Pathological features of renal neoplasms classified by size and symptomatology. *J Urol*, **176**:4 (Pt 1) (2006), 1317–20; discussion 1320.
82. A. Saxena, E. C. Alport, S. Custead *et al.*, Molecular analysis of clonality of sporadic angiomyolipoma. *J Pathol*, **189** (1999), 79–84.
83. H. L'Hostis, C. Deminiere, J. M. Ferriere *et al.*, Renal angiomyolipoma: a clinicopathologic, immunohistochemical, and follow-up study of 46 cases. *Am J Surg Pathol*, **23** (1999), 1011–20.
84. C. Tallarigo, R. Baldassarre, G. Bianchi *et al.*, Diagnostic and therapeutic problems in multicentric renal angiomyolipoma. *J Urol*, **148** (1992), 1880–4.
85. L. Daniel, D. Barriol, E. Lechevallier *et al.*, Diagnostic value of percutaneous biopsy of the renal masses. 73 cases. *Ann Pathol*, **20** (2000), 119–23.
86. Y. Neuzillet, E. Lechevallier, M. Andre *et al.*, Accuracy and clinical role of fine needle percutaneous biopsy with computerized tomography guidance of small (less than 4.0 cm) renal masses. *J Urol*, **171** (2004), 1802–5.

87. C. J. Davis, J. H. Barton, and I. A. Sesterhenn, Cystic angiomyolipoma of the kidney: a clinicopathologic description of 11 cases. *Mod Pathol*, **19** (2006), 669–74.
88. E. K. Lang, R. J. Macchia, B. Gayle *et al.*, CT-guided biopsy of indeterminate renal cystic masses (Bosniak 3 and 2F): accuracy and impact on clinical management. *Eur Radiol*, **12** (2002), 2518–24.
89. B. J. Drucker, Renal cell carcinoma: current status and future prospects. *Cancer Treat Rev*, **31** (2005), 536–45.

3

Familial and inherited renal cancers

Tristan Barrett and Peter L. Choyke

Introduction

Although familial and inherited renal cancers account for only 1%–4% of all renal tumors [1], they have had a disproportionate impact on our understanding of renal cancer biology. Unlike sporadic renal cancer, hereditary forms tend to be multiple, bilateral, develop earlier in life, and occur with similar frequency between the sexes. The discovery of the von Hippel–Lindau (VHL) tumor suppressor gene in 1993 was the first definitive genetic evidence for hereditary renal cancer and it has subsequently been shown to be important in the formation of sporadic clear cell carcinomas of the kidney [1,2]. The advance of genomics over the last 15 years has led to the discovery of a number of new genes and new inherited renal cancer syndromes. Inheritable diseases with an increased risk of developing renal cancer in adults include VHL (von Hippel–Lindau), BHD (Birt–Hogg–Dubé), HPRC (hereditary papillary renal carcinoma), HLRCC (hereditary leiomyomatosis renal cell cancer), TS (tuberous sclerosis), and FRO (familial renal oncocytoma). The proportion of renal tumors attributed to inherited disease may well increase as the understanding of these syndromes improves [3]. Knowledge of these syndromes is of practical importance to the radiologist, who may be the first to suggest a hereditary basis on typical imaging findings.

The diagnosis of a genetic predisposition to cancer can lead to screening of close family members, the early detection of cancer in these individuals, and earlier, potentially more successful, treatment. Furthermore, new treatments, such as localized, organ-sparing surgery, percutaneous ablation therapy, or novel drug therapies, which are often tested in this population, may be of benefit to patients with the more common, sporadic forms of renal cancer.

Carcinoma of the Kidney, ed. Uday Patel. Published by Cambridge University Press.

Basic genetics

The human genome contains 23 chromosome pairs of alleles, each allele inherited from one parent. The Human Genome Project set out to map and sequence the estimated 3 billion nucleotides contained within the genome, and the results indicate that there are approximately 30 000 genes in the human genome [4]. Most genes encode one or more proteins, although some produce non-coding RNA molecules, important for protein biosynthesis and gene regulation. Alterations in the nucleotide sequence of genes coding for critical proteins can lead to disease states. Proto-oncogenes are normally responsible for promoting cell development: a mutation in one copy may lead to an uncontrolled overgrowth of cells. Tumor suppressor genes are normally responsible for regulating cell growth, and mutations in these genes may also result in overgrowth of cells. Unlike proto-oncogenes, tumor suppressor genes require the loss of both alleles for tumor formation, a phenomenon summarized by the "two-hit" hypothesis, proposed by Knudson [5]. In the Knudson hypothesis, hereditary cancers occur if a particular tumor suppressor gene inherited from one parent is defective (first "hit"), and a subsequent non-inherited "hit" is acquired on the corresponding allelic pair, causing tumor formation. Thus, whilst not inevitable, tumor growth is highly likely in this patient population.

Another potential mechanism by which genetic diseases can occur is by chromosomal translocation during mitosis, when the "break point" occurs across a tumor suppressor gene locus. This mechanism is seen when there are defective mismatch-repair genes, which fail to correct mitotic errors. Additionally, not all mutations are inherited, and may occur spontaneously within an individual. If a "germline" mutation occurs (during embryogenesis), the patient will have the potential to pass the gene on to future generations. All of these genetic mechanisms can be found in the inherited renal syndromes (Table 3.1).

Advances in diagnostic testing and improved understanding of genetic diseases mean that genetic screening can be offered to family members of affected individuals. Pre-natal diagnosis can even be performed on fetal DNA within the maternal plasma [6], or in the placenta, or amniotic fluid. Screening and accurate diagnosis of a genetic disease is straightforward if the familial mutation is known. Screening "at risk" patients may be more complicated if the familial gene is unknown and several potential mutations may lead to the disease phenotype. Nevertheless, advances in microarray techniques mean that a panel of known genetic mutations can be checked simultaneously [7]. Screened

Table 3.1. Hereditary renal cancer syndromes

Syndrome	Gene, Chr location	Inheritance	Prevalence	Renal manifestations	Cancer prevalence (%)	Other manifestations
von Hippel–Lindau	VHL, 3p25	AD	1/40 000	Clear cell RCC, renal cysts	28–45	CNS, retinal hemangiomas, PNET, pancreatic cysts, pheochromocytoma, inner ear tumors, epididymal cystadenomas
Birt–Hogg–Dubé	BHD, 17p11.2	AD with variable expressivity	1/200 000	Chromophobe RCC, clear cell RCC, papillary RCC, oncocytoma	8–15	Lung cysts, spontaneous pneumothoraces, fibrofolliculomas, multiple lipomas
Hereditary papillary renal carcinoma	MET, 7p31	AD	Unknown	Papillary type 1 RCC	19	None
Hereditary leiomyomatosis renal cell carcinoma	FH, 1q42–43	AD	Unknown	Papillary type 2 RCC	20	Cutaneous and uterine leiomyomas, uterine leiomyosarcomas
Tuberous sclerosis	9q34 (TSC1), or 16p13 (TSC2)	AD with variable expressivity	1 in 6 000	Clear cell RCC, Papillary RCC, Chromophobe RCC, oncocytoma, renal cysts	1–2	CNS tubers, cardiac rhabdomyomas, angiofibromas of the skin
Familial renal oncocytoma	Unknown	AD	Unknown	Oncocytoma RCC	Unknown	None
Chr 3 translocation	From Chr 3 to Chr 2,6,8, or 11	–	–	Clear cell RCC	Unknown	None

RCC = renal cell carcinoma, CNS = central nervous system, PNET = pancreatic neuroendocrine tumors, FH = fumarate hydratase, Chr = chromosome, p = short arm of chromosome, q = long arm of chromosome

individuals typically receive pre-test counseling regarding the procedure, its accuracy, and their future management based on the test outcome.

Hereditary renal cancer syndromes

von Hippel–Lindau syndrome

Genetics

The VHL gene is a tumor suppressor gene. The inheritance of one defective gene is sufficient to cause VHL (although the manifestations require a second "hit" on the normal allele), hence the disease is considered to follow an autosomal-dominant pattern of inheritance [8]. The gene product is the protein "pVHL" which is important for the regulation of a number of growth factors and hypoxia. pVHL binds the cellular proteins elongin B and C and forms a complex with Cullin-2, which in turn recruits Rbx1 [9]. The resulting complex, termed the E3 ubiquitin ligase complex, is able to bind to hypoxia inducible factor-α (HIF-α), a key oxygen regulator of the cell, targeting it for destruction by proteosomes [10]. This process is normally oxygen-dependent; thus under conditions of physiological hypoxia, the HIF-α protein remains intact. Free HIF-α is able to move into the nucleus of the cell and act as a transcription factor for activation of a number of hypoxia-inducible genes (>60 identified to date) [11]. These include vascular endothelial growth factor (VEGF), platelet derived growth factor-β (PDGF-β), transforming growth factor-α (TGF-α), and erythropoietin, which help lead to new blood vessel formation. Loss of the regulatory protein pVHL leads to up-regulation of HIF-α even in normoxic conditions [12]. Even more importantly, mutations in the VHL gene are also found in nearly 75% of sporadic clear cell renal tumors [13].

Clinical features

Von Hippel–Lindau renal tumors are of the clear cell type. Up to 28%–45% of VHL patients will develop renal tumors at some point during their life, with peak incidence occurring between the second and fourth decades [14]. Von Hippel–Lindau syndrome can lead to a number of other tumors, including benign hemangioblastomas of the cerebellum and spinal cord, retinal angiomas, pancreatic neuroendocrine tumors (PNET), pancreatic cystic tumors, pheochromocytomas, and epididymal cystadenomas. The VHL syndrome is divided into type 1 (without pheochromocytoma) and type 2 (with pheochromocytoma), and can be further subdivided into type 2 A (without RCC) and type 2B (with RCC). An additional class,

type 2 C, is also known to exist, in which the syndrome is limited almost exclusively to pheochromocytomas. The majority of type 1 families have deletions or premature termination mutations that cause total loss of VHL function. Most type 2 families are affected by mis-sense mutations that reduce, but do not eliminate, VHL function [15]. The subtypes predisposing to renal cancer (types 1 and 2B) are thought to have a complete loss of HIF-1α regulation, whereas non-cancer predisposing types have mutations causing an incomplete defect in HIF-1α regulation [16].

Imaging

Renal VHL typically consists of bilateral, multifocal cystic tumors of varying sizes, which can range from entirely cystic to entirely solid in nature. In a minority of cases, a cystic lesion may convert to a solid tumor over time (Figure 3.1). Histological examination of apparently normal renal tissue reveals that numerous additional microscopic tumors ("tumorlets") exist, below the imaging resolution threshold. In keeping with the angiogenic nature of the tumors, the solid areas of tumors enhance rapidly and distinctly (50–200 HU) on CT following contrast media administration (Figure 3.2). Whole body images will reveal other manifestations of the disease, for example in the pancreas (Figure 3.3), central nervous system (Figure 3.4), adrenals (Figure 3.5), and retina. Pancreatic neuroendocrine tumors (PNET) tend to be small, located in the pancreatic head, and enhance homogeneously following CT contrast (Figure 3.3). As PNET tumors enlarge they become more prone to metastasize, usually to the liver [17]. Management of VHL-associated renal cancers is a balance between the risk of metastases and the risks associated with overly

(a)

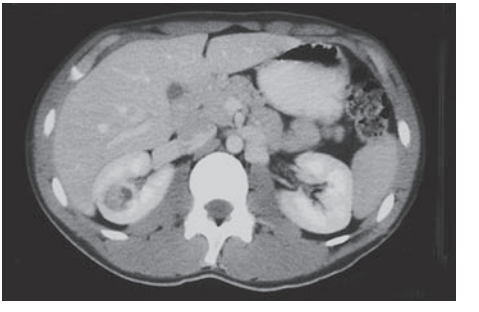

(b)

Figure 3.1 Von Hippel–Lindau syndrome. Post-contrast CT abdominal scans from the same patient taken in January 2001 (a) and January 2003 (b). Right central renal lesion demonstrates a change from predominantly cystic to predominantly solid over this time interval.

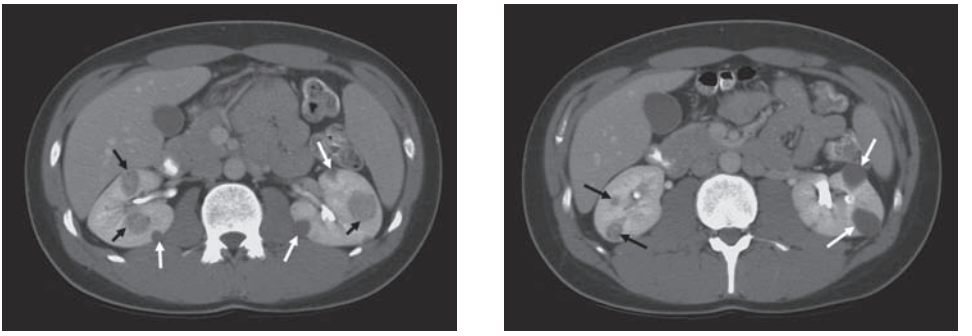

(a) (b)

Figure 3.2 Contrast-enhanced CT Abdomen in a patient with von Hippel–Lindau syndrome (images (a) and (b) taken from the same series). Kidneys show bilateral, multifocal disease, with both cystic (white arrows) and solid lesions (black arrows).

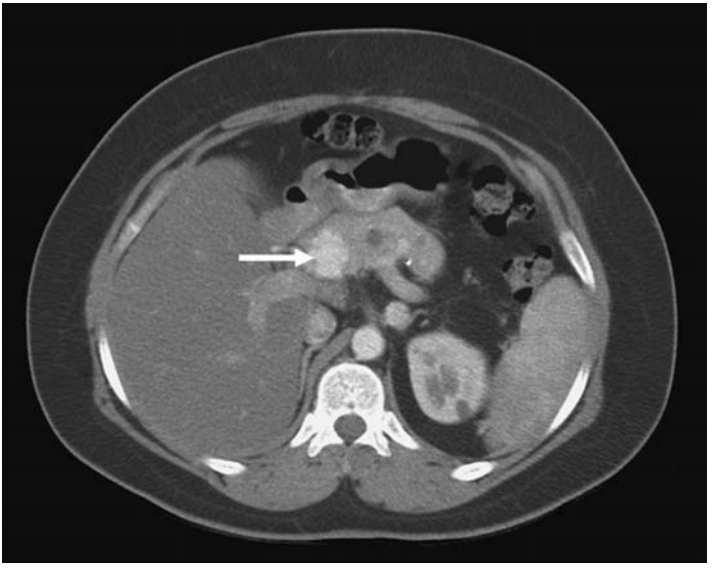

Figure 3.3 CT Abdomen in a patient with von Hippel–Lindau syndrome showing a pancreatic neuroendocrine tumor (arrow) in the head of the pancreas, enhancing intensely after contrast media administration.

aggressive surgical resection resulting in renal failure. Renal tumors < 3 cm in size are statistically unlikely to metastasize [3]. Whilst the risk of additional tumor occurrence is high in VHL, there are also risks and disadvantages associated with renal replacement therapies (dialysis or transplantation). Thus, in order to preserve renal function, radiological surveillance is continued and surgery is often delayed until tumors reach a 3 cm diameter, whereupon nephron-sparing procedures or radiofrequency ablations are undertaken [18]. Patients are frequently scanned at 6 month to 1-year intervals to monitor the progress of renal

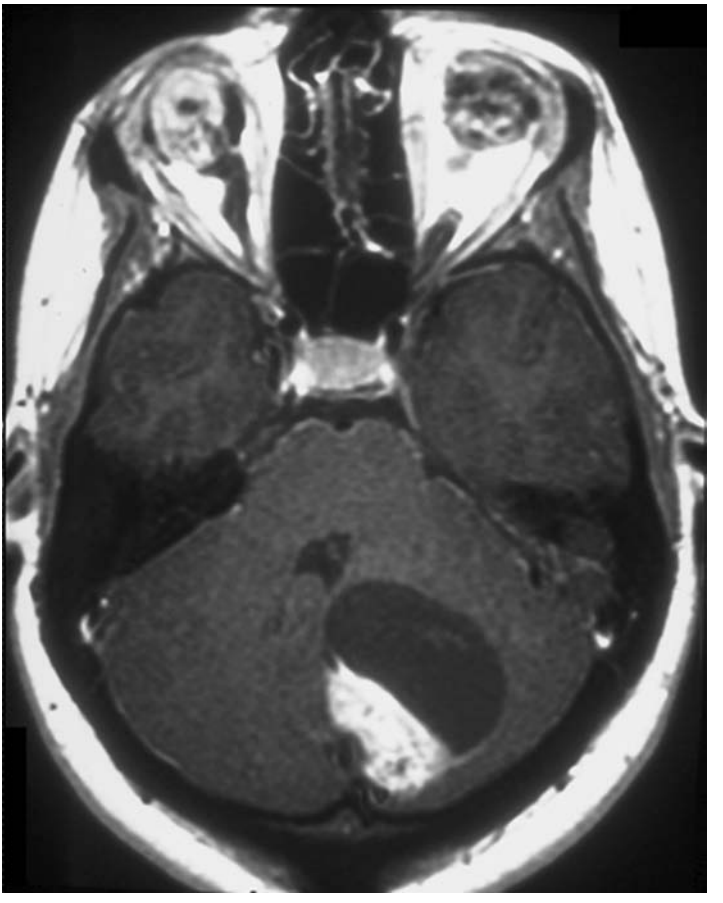

Figure 3.4 MRI in a patient with von Hippel–Lindau syndrome who is clinically blind. Scan demonstrates a left-sided hemangioblastoma with both cystic and solid components. Note that bilateral retinal angiomas are present in both eyes, a further manifestation of VHL.

tumors. Lesions that are deep within the renal parenchyma are often treated at an earlier stage than peripheral lesions because the complexity of the procedure increases with increasing size. This strategy can be successful in minimizing the number of surgeries a VHL patient will have over the course of their life and thus prolong their native renal function.

Birt–Hogg–Dubé syndrome

Genetics

The BHD gene encodes for folliculin, a protein that is highly conserved across animal species. Although the exact function of folliculin is yet to be established, it is believed to act as a tumor suppressor. Birt–Hogg–Dubé mutations include

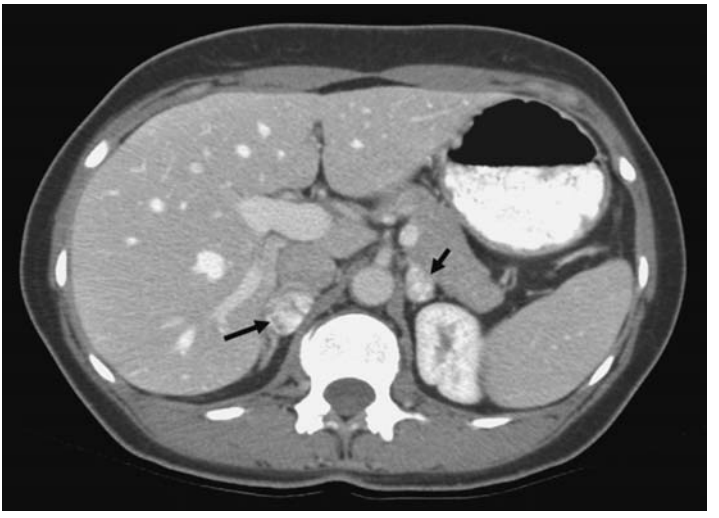

Figure 3.5 Bilateral pheochromocytomas in a patient with von Hippel–Lindau syndrome, which enhance rapidly following administration of CT contrast media.

insertions, deletions, somatic frameshifts, or mis-sense mutations that produce a truncated, non-functional version of this protein. Animal models have demonstrated that loss of the folliculin protein leads to renal cell cancer formation, predominantly of the clear cell type [19]. Unlike the VHL gene, mutations in the BHD gene are rarely found in cases of non-familial, sporadic renal cancers [20].

Clinical features

Birt–Hogg–Dubé syndrome is unusual among hereditary renal cancer syndromes in that patients can develop tumors with a variety of different histologies. The most common form of renal tumor seen in BHD is an oncocytic hybrid tumor (~50% of all tumors), with areas reminiscent of both chromophobe RCC and renal oncocytoma [21]. Other tumor types, in descending order of frequency, are chromophobe RCC, clear cell RCC, oncocytoma, and papillary RCC [22]. Tumors may develop either unilaterally, with a single focus, or bilaterally, with multiple foci. Patients with BHD develop fibrofolliculomas of the face and neck, typically in the third to fourth decade. Lung cysts are often found on CT (Figure 3.6), and may be associated with spontaneous pneumothoraces. Patients may also develop lipomas, but an association with colonic polyps and/or colon cancer remains controversial [23].

Imaging

Renal tumors in BHD tend to be solid; they enhance rapidly and homogeneously on CT following contrast injection, in comparison to VHL where there are usually

Figure 3.6 High resolution CT Chest obtained with the patient prone demonstrates pneumothorax (black arrows) and multiple pulmonary cysts (white arrows) in a patient with Birt–Hogg–Dubé syndrome.

cystic components (Figure 3.7). Metastases from renal cancers in BHD are less common than in VHL, and lesions tend to be relatively slow growing. Renal cysts may also be seen, but they are usually separate from the tumors and it is unclear whether there is a true increased risk of renal cysts in BHD or whether these are incidental to the process. Lung cysts are an important manifestation and are more commonly found in the lower lobes, and are typically small, round, and well circumscribed. Lung cysts are responsible for the increased risk of spontaneous pneumothorax in this syndrome, and may even be the presenting symptom. The presence of multiple lung cysts helps to differentiate BHD from other inherited renal cancer syndromes and should point the differential diagnosis to either BHD, or TS. The respective differences in clinical features can then help distinguish between BHD and TS.

Hereditary papillary renal carcinoma

Genetics

HPRC patients inherit defects in the MET proto-oncogene. This gene encodes for c-MET, a transmembrane receptor tyrosine kinase. The hepatocyte growth factor (HGF) binds to this receptor and then acts in a paracrine manner on a variety of cell types, for instance epithelial, endothelial, and hematopoietic cells [24]. Hepatocyte growth factor can induce a number of physiological

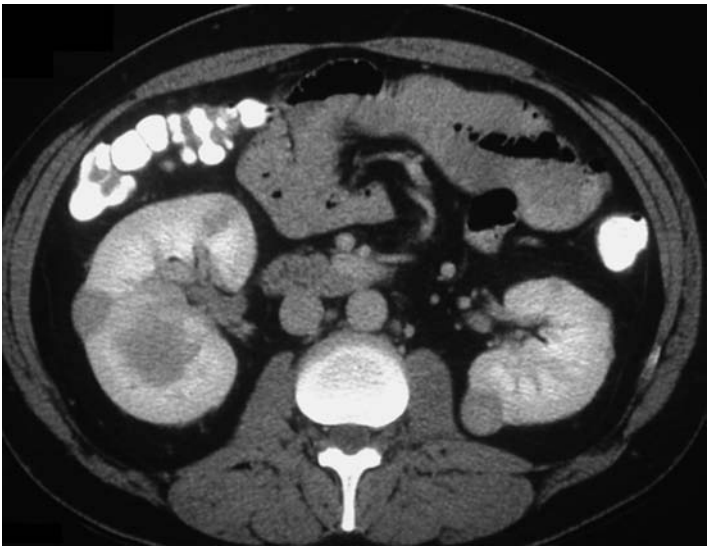

Figure 3.7 Multiple, bilateral solid renal tumors in a patient diagnosed with Birt–Hogg–Dubé; no cystic lesions are seen. These lesions proved to be chromophobe carcinomas of low grade.

processes, including cell migration, proliferation, and tissue repair and regeneration. A number of different mis-sense mutations have been identified within the MET gene in HPRC families. The majority of these mutations allow autophosphorylation of the c-MET protein, leading to over-activity, and thus tumor growth [25].

Clinical features

The HPRC syndrome produces a specific cell type of renal tumour, the papillary type 1 RCC. Typically papillary type 1 renal tumors are bilateral and multifocal and both microscopic and macroscopic in nature. To date, no additional systemic manifestations of the disease have been discovered. The macroscopic lesions tend to be slow growing, and patients typically present later in life, often in the 5th–6th decades. Diagnosis can be established by detecting the familial c-MET germline mutation, and may allow earlier diagnosis and treatment within families.

Imaging

The HPRC tumor are hypovascular, thus they show minimal enhancement (10–30 HU) upon CT contrast administration (Figure 3.8). Relative hypovascularity of the lesions means that care needs to be taken to differentiate tumors

(a)

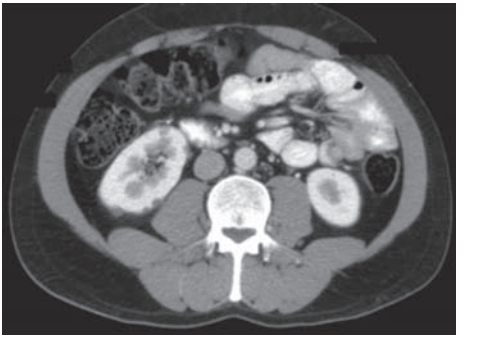

(b)

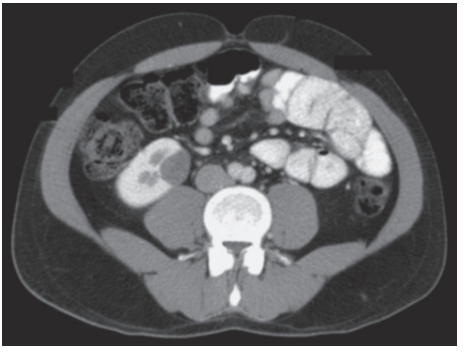

(c)

Figure 3.8 Patient diagnosed with Hereditary Papillary Renal Cancer (HPRC). Post-contrast CT images (a, b, and c) taken from the same series show hypo-enhancing tumors, with multifocal, bilateral disease. The tumors associated with HPRC are typically slow-growing and poorly enhancing.

from simple cysts, which are common in the aging population. Thus, it is vital to obtain accurate measurements of attenuation changes following contrast injection. Metastatic disease is unusual but local recurrence following resection can be seen. Ultrasound scans should be interpreted with caution, because HPRC lesions may appear isoechoic to normal renal parenchyma, especially when they are small.

Hereditary leiomyomatosis renal cell carcinoma

Genetics

Mutations in the fumarate hydratase (FH) gene lead to the clinical syndrome HLRCC. The FH gene encodes the mitochondrial enzyme fumarate hydratase, which functions within the Krebs cycle to convert fumarate to malate [26]. A number of different mutations within this gene have been reported including insertions, deletions, mis-sense mutations, or splice mutations, and lead to a truncated version of the protein and a significant reduction in enzyme activity [1]. Apart

from its role in the Kreb's cycle, FH is thought to function as a tumor suppressor gene. Studies have demonstrated FH deficiency causes an over-expression of HIF-α in cells, possibly via inhibition of HIF prolyl hydroxylase, thus preventing binding of the pVHL complex and downstream inactivation of HIF-α [27]. Thus, FH gene mutations may ultimately lead to tumor formation through activation of the HIF pathway, analogous to the VHL gene mutations. However, unlike VHL, only a small percentage of sporadic RCCs demonstrate FH mutations ($< 2\%$) [28].

Clinical features

Renal tumors develop in approximately 20% [26] of patients with HLRCC; histologically they fall into the category of papillary type 2 cancers, but a complete description of their cellular features is still under investigation. The tumors are typically solitary in nature, an unusual feature amongst the hereditary renal cancer syndromes. Tumours tend to be highly aggressive and metastasize early which is also at variance with the other hereditary renal cancer syndromes. Additional clinical features include cutaneous and uterine leiomyomas, often before the age of 30.

Imaging

In their early stages the tumors associated with HLRCC are hypovascular or cystic in nature, a fact reflected by imaging studies. Unlike the other syndromes, tumors are less frequently bilateral and multiple, although multiplicity can certainly be present. As the tumours grow they become more vascularized and distinction from other renal syndrome tumors becomes more difficult. Metastases may also be prominent, especially lymphatic metastases that occur early in the course of the disease while the lesions are still small (Figure 3.9). Excess fumarate drives glycolysis via Glut-1, thus HLRCC tumors and their metastases have intense uptake on FDG-PET scans. Small cysts are commonly found in patients with HLRCC but their relation to the disease and to HLRCC-related tumors is still uncertain.

Tuberous sclerosis complex

Genetics

Although tuberous sclerosis complex (TSC) is a genetic disease with autosomal dominant inheritance, approximately two-thirds of cases result from spontaneous mutations. Two separate genes, located on different chromosomes, are responsible for the majority of cases of TSC. The first is TSC1, which encodes for the protein

Figure 3.9 A patient with the Hereditary Leimyoma and Renal Cell Carcinoma (HLRCC) syndrome demonstrates a large right renal tumor measuring up to 8 cm in antero-posterior dimension, causing compression of normal right renal parenchyma. An enlarged perihilar lymph node is seen (white arrow). HLRCC tumors often metastasize to the regional lymphatics. The tumor is unilateral, rapidly growing, and aggressive; lung metastases were also present.

hamartin; the second is TSC2, which encodes for the protein tuberin. The two proteins form a dimeric complex, hamartin/tuberin, which appears to play a key role in regulating protein synthesis and cell growth via inhibition of the kinase mTOR [29]. In TSC, inactivation of either of the genes encoding these proteins results in a loss of this growth regulation. Sporadic cases of TSC caused by TSC2 mutations tend to have a more severe phenotype [30]. This may explain why there is equal prevalence of TSC1 and TSC2 mutations in familial cases of TSC, despite mutations of TSC2 accounting for the majority (80%) of sporadic cases. The TSC2 gene locus is adjacent to the PKD1 gene, mutations of which produce the most common form of the syndrome autosomal dominant polycystic kidney disease (ADPKD). Contiguous deletion of both genes results in a syndrome with manifestations of both syndromes (i.e. cystic disease and angiomyolipomas of the kidneys) and, typically, early onset, severe renal impairment [31].

Clinical features

Tuberous sclerosis complex has a number of systemic and clinical manifestations which are used to aid the diagnosis of the condition. These include

angiofibromas, ungual fibromas, subependymal and renal angiomyolipomas, cerebral sclerosis, Shagreen patches, pulmonary lymphangiolyomyomatosis, cardiac rhabdomyomas, subependymal giant cell astrocytoma, and retinal nodular hamartomas [29]. Cerebral involvement may lead to epilepsy; mental retardation may be present, but patients are often of average or above-average intelligence. Benign renal angiomyolipomas are a frequent manifestation and are often bilateral. Very large AMLs can bleed, requiring angioembolization for control. Although AMLs can be locally aggressive they generally do not metastasize. Some cases labeled as RCC may instead represent a monotypic, epithelioid variant of AML that does not contain fat. Malignant renal tumors develop in 1%–2% of TSC patients, and can be one of various histological types. Tuberous sclerosis complex is associated with, in decreasing order of frequency, clear cell RCC, papillary RCC, chromophobe RCC, and oncocytoma. The issue of TSC as a risk factor for, rather than an association with, renal cell carcinoma remains controversial [32].

Imaging

Renal cysts (non-enhancing) in TSC can be readily differentiated on CT from AMLs and renal cancers – which both enhance dramatically, following contrast administration. Angiomyolipomas can often be diagnosed because of the presence of low attenuating fat within the lesions (Figure 3.10). However, non-fatty AMLs are difficult to distinguish from renal cell carcinoma (Figure 3.11). Such AMLs tend to be hyperdense relative to normal renal parenchyma on non-contrast-enhanced studies and enhance homogenously after contrast media attenuation. Renal cancers tend to grow faster than AMLs and calcifications are more likely in malignancy [3]. However, biopsy is usually necessary for diagnosis.

Hyperparathyroidism-jaw tumor syndrome

Genetics

Hyperparathyroidism-jaw tumor (HPT-JT) is a rare autosomal dominant condition. The condition is caused by mutations in the HRPT2 gene, located on the long arm of chromosome 1, which encodes parafibromin [33]. The exact function of the gene is yet to be determined, although it is likely to function as a tumor suppressor [34].

Clinical features

Affected individuals have a propensity to develop multiple parathyroid adenoma, fibro-osseous tumors of the maxilla and mandible, and renal disease. Renal lesions

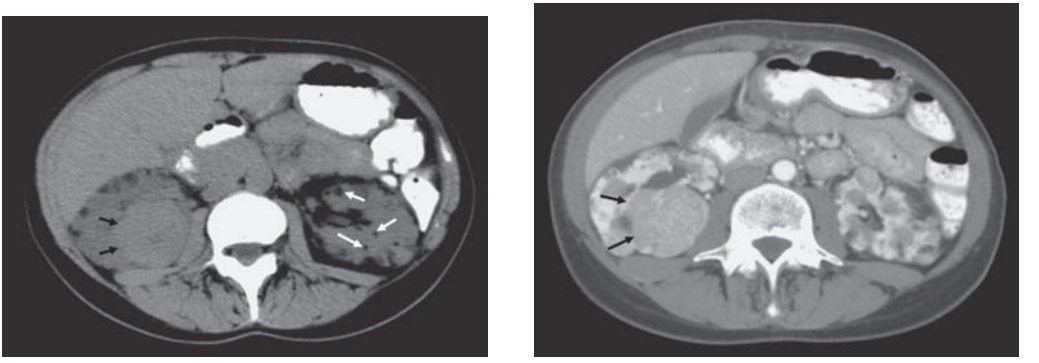

(a) (b)

Figure 3.10 CT scans taken before (a) and after (b) contrast administration in a patient with Tuberous Sclerosis Complex. Small fatty angiomyolipomas (AML) are seen (white arrows). Large, non-fatty AML is seen in the right kidney (black arrow); this lesion is hyper-attenuating relative to the normal renal parenchyma prior to contrast, and enhances homogenously with contrast.

Figure 3.11 Renal cancer in Tuberous Sclerosis Complex. Solid lesion (arrow) enhances heterogeneously upon contrast administration. Biopsy confirmed clear cell carcinoma which was subsequently surgically removed.

described in the literature include hamartomas, cystic disease, papillary RCC, mixed epithelial and stromal tumors, late onset Wilms' tumours, and mesoblastic nephromas [35,36]. The fibro-osseous bone tumors are distinct from the "brown tumors" seen in hyperparathyroidism; they appear and enlarge even upon correction of hypercalcemia [37]. Histologically they are distinct fibro-osseous lesions without the giant cells seen in "brown tumors" and have a vascular fibroblast-rich

stroma admixed with the bone trabeculae – some of which show osteoblast-like rimming and occasional osteoclasts [38].

Imaging

Computed tomography of the bone tumors demonstrates well-demarcated lesions, and the vascular nature of the tumors means they enhance rapidly on contrast-enhanced CT or MRI. Patients typically present with hyperparathyroidism. In such cases, the radiological work-up includes high resolution ultrasound (US) of the neck to locate parathyroid adenomas. A Technetium-Sestimibi scan may lead to the detection of additional lesions in the jaw; these can be characterized by plain radiography and CT, and additional lesions are sought with radionuclide bone scans. When this condition is suspected, CT or MRI of the abdomen should also be undertaken to check for renal lesions – the imaging characteristics of renal lesions will depend on their underlying pathology. Patients should be periodically evaluated for the development of potentially lethal renal tumors.

Inherited renal cancer syndromes without a known genetic defect

There are a number of familial diseases of the kidney for which a gene has not yet been identified. Efforts are underway to identify the genes; however, the rarity of these conditions combined with their clinical heterogeneity make the genetic study of these diseases very challenging.

Familial renal oncocytoma

Genetics

Familial renal oncocytoma is a rare syndrome, and only a few cases have been described [39]. It is inherited in an autosomal dominant manner, but the causative gene is yet to be identified.

Clinical features

Renal oncocytomas are often multiple and bilateral, but metastatic disease has not been observed [40]. Phenotypes can range from multiple oncocytomas to milder manifestations of disease, or even renal dysfunction alone [3]. Familial renal oncocytoma may overlap with BHD; three families classified with FRO were

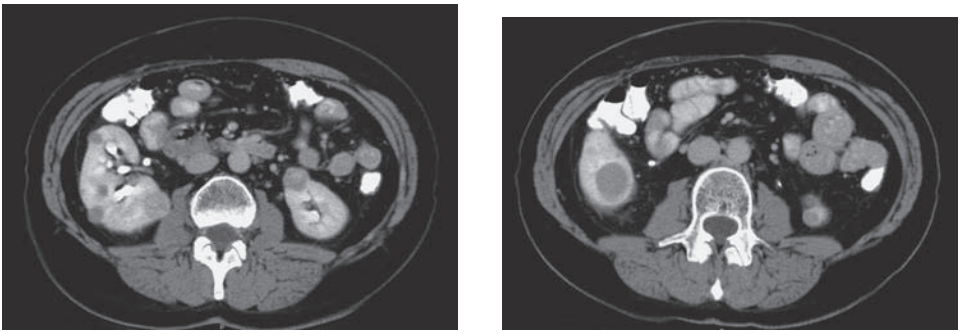

(a) (b)

Figure 3.12 CT Abdomen of a patient diagnosed with Familial Renal Oncocytoma. Multiple bilateral solid tumors are seen (images (a) and (b) are taken from the same series). Prior resection had revealed multiple oncocytomas.

identified as having BHD mutations, which represents the first disease gene associated with this rare hereditary syndrome [41]. However, not all cases of FRO overlap with BHD; so there is likely to be another, additional genetic cause.

Imaging

Oncocytomas appear as solid lesions on CT (Figure 3.12). They may be multiple and bilateral, or even diffusely infiltrate the kidneys – a process termed "renal oncocytomatosis" [42]. The lesions are indistinguishable from other solid tumors and biopsy is required for confirmation. Diagnosis is established when renal oncocytomas are demonstrated within multiple family members.

Translocation of chromosome 3

Genetics

The "break point" of the translocation may occur across a critical gene locus, effectively resulting in a mutation. In the case of germline translocations, the defect may be passed on to subsequent generations. In 1979 Cohen *et al.* described a small number of families with chromosome 3 translocations that developed renal cancer [43]. These all involved the short arm of chromosome 3 translocated to a number of other chromosomes, including 2, 6, 8, and 11.

Clinical features

Patients are predisposed to develop clear cell RCC, which is often multiple and bilateral, akin to the VHL syndrome. The VHL gene is also located on the short arm

of chromosome 3 (3p21), and mutations within the VHL gene locus have been demonstrated in two-thirds of the members of one affected family [44]. However, the VHL gene is not always affected in this disorder and, moreover, patients with chromosome 3 translocation do not demonstrate the other characteristic features of VHL.

Imaging

Computed tomography demonstrates intensely enhancing non-cystic clear cell carcinomas, which may be multiple and bilateral. However, these lesions can be distinguished from those seen in VHL, because such patients will not display the typical extra-renal features of the VHL syndrome.

Medullary carcinoma of the kidney

Genetics and clinical features

Medullary carcinoma of the kidney is a rare, recently described aggressive neoplasm, associated with the sickle cell (SC) hemoglobinopathies, predominantly sickle cell trait and hemoglobin SC disease [45,46]. At the time of diagnosis most patients have widespread metastatic disease, and the median survival is 15 weeks. Patients tend to be young, and diagnosis may be delayed if hematuria is dismissed simply as a micro-hematuria associated with sickle-cell disorders. A genetic predisposition is proposed owing to the strong association with sickle cell trait, an autosomal recessive disorder. However, an exact gene locus is yet to be established [47].

Imaging

Tumors are located centrally within the kidney, grow in an infiltrative pattern, and often invade the renal sinus and retroperitoneum [48]. In addition, the tumors tend to be hypovascular in nature. They are associated with retroperitoneal adenopathy, caliectasis, and often distal metastases [49].

Management of hereditary renal cancers

Diagnosis, screening, and genetic counseling

There are no firm guidelines for the screening and diagnosis of the hereditary renal cancer syndromes. However, the pattern of disease can provide clues to the

diagnosis and greatly accelerate the diagnostic process. A hereditary renal syndrome should be suspected if the patient presents at an early age with bilateral or multifocal lesions, and/or a first-degree relative is also diagnosed with renal cancer. The nature of the lesions on imaging is key to establishing the diagnosis: cystic renal tumors are suggestive of VHL, solid enhancing lesions imply BHD or FRO, and poorly enhancing solid lesions are suspicious for HPRC. An aggressive phenotype should raise the spectre of HLRCC. Investigations should include a careful family history, and a thorough physical examination, paying particular attention to the skin; BHD, HLRCC, and TS all have characteristic dermatological lesions. Cystic disease in the lungs can suggest BHD or TSC. FRO, HPRC, and chromosome-3 translocation families will not have any extra-renal manifestations.

Computed tomography is the radiological investigation of choice for hereditary renal cancer syndromes in adults. The high resolution of CT and the use of iodine contrast agents enable a more accurate diagnosis of lesions, which must be weighed against the risks of repeated radiation exposure [50]. MRI can be used if CT is contraindicated, or it may be useful as an adjunct to CT in cases of diagnostic difficulty. MRI is also suitable for follow-up in many cases either alone or in alternation with CT. Ultrasound has an established role in the intra-operative assessment of renal lesions (discussed below). However, it should be noted that routine US in the context of renal cancer syndromes is highly operator-dependent and may lead to a high false-negative diagnosis rate, particularly for smaller lesions [51]. In cases where diagnosis of an inherited syndrome is difficult to establish, the histological findings may be helpful. The syndromes of VHL, HPRC, HLRCC, and chromosome-3 translocations develop one specific RCC subtype. Conversely, the discovery of multiple tumors demonstrating different histological subtypes in a particular patient is suggestive of BHD.

The discovery of the responsible gene in the majority of these syndromes has made genetic testing within families a possibility. There are currently diagnostic tests available for germline mutations in the causative genes for VHL, MET (for Hereditary Papillary Renal Carcinoma), FH (for Hereditary Leiomyomatosis RCC), TSC1, TSC2 (both for Tuberous Sclerosis), and HRPT2 (for Hyperparathyroidism-jaw tumor syndrome) [52]. When diagnosis of an inheritable renal syndrome has been established, it is recommended that the respective germline gene is analyzed for the causative mutation. Once the familial mutation has been discovered, and appropriate genetic counseling takes place, other family members can be screened for the mutation. A positive genetic test, however, does not confer information about the aggressiveness of the disease in a particular patient, thus

imaging is a necessary adjunct to the management of all patients with hereditary renal cancers.

The frequency of radiological surveillance will vary according to disease severity, for example the tumor growth rate and the patient or family history. Unless otherwise indicated, the follow-up investigation of choice is either MRI or CT – depending on the availability of the former. An adequate CT can usually be performed and interpreted anywhere, but machines capable of dynamic renal MRI are less available and there is less expertise for interpretation. Family members who are known to carry a germline mutation predisposing to renal cancer but who have not yet developed a tumor, or patients with a relatively mild phenotype, can be safely imaged every 2–3 years, except in the case of HLRCC where an aggressive screening approach is warranted. Of course, this strategy may change within an individual if, for example, a patient with small lesions develops larger, more aggressive tumors.

Treatment options

Large tumors often necessitate radical nephrectomy, regardless of their genetic status. However, the recent increase in awareness of inherited renal cancer syndromes, along with the use of imaging, and the improved screening of affected families have meant that tumors can be diagnosed at an earlier stage. The diagnosis of tumors at a smaller diameter makes nephron-sparing treatment a viable option. Nephron-sparing procedures include surgery (partial nephrectomy), radiofrequency (heat) ablation, and cryotherapy. This approach is rarely curative, because the risk of subsequent additional lesions appearing later is high; nevertheless it has the advantage of preserving renal function and postponing the requirement of renal-replacement therapy with its associated quality-of-life issues, mortality, and morbidity. A number of studies of VHL patients have shown that lesions less than 3 cm are usually of a low grade and have a very low risk of metastasizing [53,54]. Thus, it is recommended that patients undergo follow-up imaging until one lesion reaches approximately 3 cm in diameter, whereupon nephron-sparing procedures are undertaken. This management strategy has also been shown to be successful for BHD patients [55]. Although yet to be validated in the other hereditary conditions, it is logical to adopt a similar treatment policy for these syndromes. The only exception to this rule is the syndrome of HLRCC, in which renal tumors tend to be highly aggressive and are prone to metastasize. Therefore, surgery is recommended for HLRCC lesions of any size, provided that metastases have not occurred.

Surgery

Surgeons now have considerable experience in renal parenchymal sparing techniques. Renal function can be preserved, metastases rates are low, recurrence rates acceptable, and survival rates excellent [53]. Patients with peripheral tumors may be candidates for minimally invasive, laparoscopic partial nephrectomy procedures, which help reduce recovery time. When nephron-sparing surgery is undertaken, it is usual to remove all other lesions within the same kidney in order to minimize the number of surgical procedures the individual will receive during their lifetime [1]. Intra-operative US (Figure 3.13) is often used as an adjunct both to define the target lesion and identify other lesions requiring removal. Intra-operative US has been shown to identify lesions that were undetectable by visualization or palpation in up to 25% of patients [56]. The 3 cm tumor size criterion is merely a guideline and the clinical context should always be taken into account. Some lesions greater than 3 cm may be appropriate for nephron-sparing surgery, whereas some smaller lesions may not, for example because of their central location, or papillary type 2 RCC subtype. In some cases, recurrent disease may also be amenable to nephron-sparing surgery, but it is likely that such patients will eventually require completion nephrectomy.

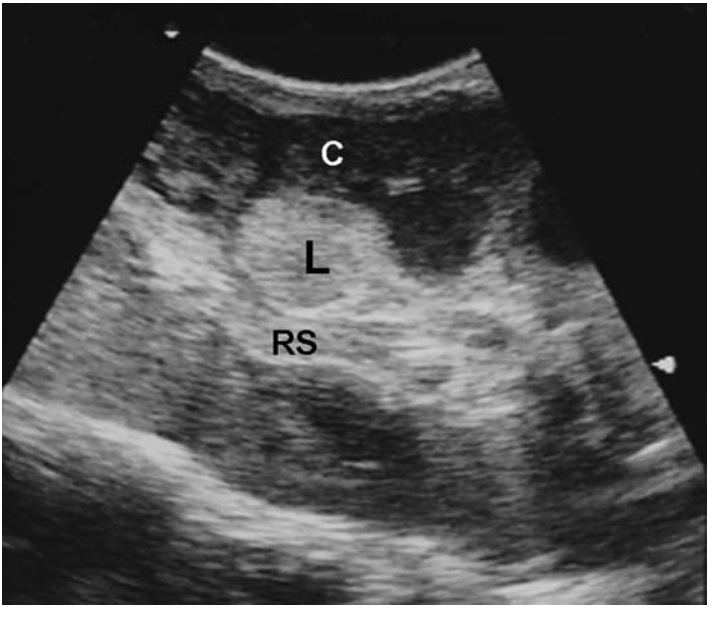

Figure 3.13 Intra-operative ultrasound of a patient with von Hippel–Lindau syndrome demonstrates a solid renal lesion (L) deep to the surface of the kidney and not visible to the surgeon. RS = renal sinus, C = renal cortex.

Minimally invasive treatments

Radiofrequency ablation and cryotherapy are less invasive alternatives to surgery. Complication rates from these procedures are low. Indications are currently limited to tumors that are exophytic in nature, less than 4 cm in diameter, and situated away from hilar structures [57]. They are often performed when surgery is contraindicated, but increasingly they are desired by patients because of the very short recovery time. Lesions that have been managed in this way require continued surveillance of the treated site. The treated lesion may take several years to scar to the point where it is no longer visible; however, in the intervening time it may be difficult to assess whether the treatment was complete.

Medical treatment

In patients with distant metastases, medical treatment can be undertaken. The downstream pathways of the affected gene provide attractive targets for novel anti-tumor therapy. The HIF-induced angiogenesis pathway is known to be responsible for tumor formation in VHL; furthermore it has also been implicated in BHD and HLRCC disease, as well as approximately 75% of sporadic clear cell RCCs. This pathway has been targeted in drug trials of anti-angiogenesis agents, including SU5416 (an inhibitor of the VEGF-2 receptor) [58] and bevacizumab (anti-VEGF antibody) [59] for patients with sporadic clear cell RCC. The genetic nature of the inherited renal cancer syndromes may eventually allow gene therapy for these conditions; wherein the mutated gene is replaced with a normal, functional copy.

Conclusion

In recent years there has been an increasing understanding of hereditary renal cancer syndromes. The list includes VHL, BHD, HPRCC, HLRCC, TSC, FRO, HPT-JT, and medullary carcinoma of the kidney. Hereditary syndromes account for approximately 4% of all renal tumors; they tend to be multifocal and bilateral, present at an earlier age than sporadic tumors, and are often amenable to nephron-sparing treatments. Radiologists may be the first to suggest a hereditary basis for renal disease based on typical imaging findings; therefore an awareness of the clinical features and radiological findings of these conditions is of importance. Radiology has a role to play in the diagnosis of these syndromes, screening of family members, and the follow-up of affected patients. In the vast majority of cases abdominal CT or MRI are the

investigations of choice. Understanding the underlying genetic basis of disease and the molecular pathways involved will enable better treatment of these syndromes. Furthermore, novel treatments that are effective in these renal cancer syndromes are likely to prove of benefit in the management of the more common, sporadic forms of renal cancer.

REFERENCES

1. C. P. Pavlovich and L. S. Schmidt, Searching for the hereditary causes of renal-cell carcinoma. *Nat Rev Cancer*, **4**:5 (2004), 381–93.
2. F. Latif, K. Tory, J. Gnarra *et al.*, Identification of the von Hippel–Lindau disease tumour suppressor gene. *Science*, **260** (1993), 1317–20.
3. P. L. Choyke, G. M. Glenn, M. M. Walther *et al.*, Hereditary renal cancers. *Radiology*, **226**:1 (2003), 33–46.
4. International Human Genome Sequencing Consortium. Finishing the euchromatic sequence of the human genome. *Nature*, **431** (2004), 931–45.
5. A. G. Knudson, Jr., Genetics of human cancer. *Genetics*, **79**:Suppl (1975), 305–16.
6. L. Jackson, Fetal cells and DNA in maternal blood. *Prenat Diagn*, **23** (2003), 837–46.
7. T. K. Lau and T. N. Leung,. Genetic screening and diagnosis. *Curr Opin Obstet Gynecol*, **17**:2 (2005), 163–9.
8. M. Ohh and W. G. Kaelin, Jr., VHL and kidney cancer. *Methods Mol Biol*, **222** (2003), 167–83.
9. S. C. Clifford, D. Astuti, L. Hooper *et al.*, The pVHL-associated SCF ubiquitin ligase complex: molecular genetic analysis of elongin B and C, Rbx1 and HIF-1alpha in renal cell carcinoma. *Oncogene*, **20**:36 (2001), 5067–74.
10. M. Ohh, C. W. Park, M. Ivan *et al.*, Ubiquitination of hypoxia-inducible factor requires direct binding to the beta-domain of the von Hippel–Lindau protein. *Nat Cell Biol*, **2**:7 (2000), 423–7.
11. M. Ohh, Ubiquitin pathway in VHL cancer syndrome. *Neoplasia*, **8**:8 (2006), 623–9.
12. O. Iliopoulos, A. P. Levy, C. Jiang *et al.*, Negative regulation of hypoxia-inducible genes by the von Hippel–Lindau protein. *Proc Natl Acad Sci*, **93**:20 (1996), 10595–9.
13. R. E. Banks, P. Tirukonda, C. Taylor *et al.*, Genetic and epigenetic analysis of von Hippel–Lindau (VHL) gene alterations and relationship with clinical variables in sporadic renal cancer. *Cancer Res*, **66**:4 (2006), 2000–11.
14. P. L. Choyke, G. M. Glenn, M. M. Walther *et al.*, von Hippel–Lindau disease: genetic, clinical, and imaging features. *Radiology*, **194**:3 (1995), 629–42.
15. B. Zbar, T. Kishida, F. Chen *et al.*, Germline mutations in the von Hippel–Lindau disease (VHL) gene in families from North America, Europe, and Japan. *Hum Mutat*, **8**:4 (1996), 348–57.

16. S. C. Clifford, M. E. Cockman, A. C. Smallwood *et al.*, Contrasting effects on HIF-1alpha regulation by disease-causing pVHL mutations correlate with patterns of tumourigenesis in von Hippel–Lindau disease. *Hum Mol Genet*, **10**:10 (2001), 1029–38.
17. H. B. Marcos, S. K. Libutti, H. R. Alexander *et al.*, Neuroendocrine tumours of the pancreas in von Hippel–Lindau disease: spectrum of appearances at CT and MR imaging with histopathologic comparison. *Radiology*, **225**:3 (2002), 751–8.
18. R. L. Grubb, 3rd, P. L. Choyke, P. A. Pinto *et al.*, Management of von Hippel–Lindau-associated kidney cancer. *Nat Clin Pract Urol*, **2**:5, (2005, May), 248–55.
19. K. Okimoto, J. Sakurai, T. Kobayashi *et al.*, A germ-line insertion in the Birt–Hogg–Dubé (BHD) gene gives rise to the Nihon rat model of inherited renal cancer. *Proc Natl Acad Sci*, **101**:7 (2004), 2023–7.
20. N. F. da Silva, D. Gentle, L. B. Hesson *et al.*, Analysis of the Birt–Hogg–Dubé (BHD) tumour suppressor gene in sporadic renal cell carcinoma and colorectal cancer. *J Med Genet*, **40**:11 (2003), 820–4.
21. S. K. Tickoo, V. E. Reuter, M. B. Amin *et al.*, Renal oncocytosis: a morphological study of fourteen cases. *Am J Surg Pathol*, **23** (1999), 1094–101.
22. C. P. Pavlovich, R. L. Grubb 3rd, K. Hurley *et al.*, Evaluation and management of renal tumours in the Birt–Hogg–Dubé syndrome. *J Urol*, **173** (2005), 1482–6.
23. B. Zbar, W. G. Alvord, G. Glenn *et al.*, Risk of renal and colonic neoplasms and spontaneous pneumothorax in the Birt–Hogg–Dubé syndrome. *Cancer Epidemiol Biomarkers Prev*, **11**:4 (2002), 393–400.
24. P. G. Dharmawardana, A. Giubellino, and D. P. Bottaro, Hereditary papillary renal carcinoma type I. *Curr Mol Med*, **4**:8 (2004), 855–68.
25. M. Jeffers, L. Schmidt, N. Nakaigawa *et al.*, Activating mutations for the met tyrosine kinase receptor in human cancer. *Proc Natl Acad Sci*, **94**:21 (1997), 11445–50.
26. I. P. Tomlinson, N. A. Alam, A. J. Rowan *et al.*, Multiple Leiomyoma Consortium. Germline mutations in FH predispose to dominantly inherited uterine fibroids, skin leiomyomata and papillary renal cell cancer. *Nat Genet*, **30**:4 (2002), 406–10.
27. P. J. Pollard, J. J. Briere, N. A. Alam *et al.*, Accumulation of Krebs cycle intermediates and overexpression of HIF1alpha in tumours which result from germline FH and SDH mutations. *Hum Mol Genet*, **14**:15 (2005), 2231–9.
28. M. Kiuru, R. Lehtonen, J. Arola *et al.*, Few FH mutations in sporadic counterparts of tumour types observed in hereditary leiomyomatosis and renal cell cancer families. *Cancer Res*, **62**:16 (2002), 4554–7.
29. J. R. Yates, Tuberous sclerosis. *Eur J Hum Genet*, **14**:10 (2006), 1065–73.
30. S. L. Dabora, S. Jozwiak, D. N. Franz *et al.*, Mutational analysis in a cohort of 224 tuberous sclerosis patients indicates increased severity of TSC2, compared with TSC1, disease in multiple organs. *Am J Hum Genet*, **68** (2001), 64–80.
31. J. R. Sampson, M. M. Maheshwar, R. Aspinwall *et al.*, Renal cystic disease in tuberous sclerosis: role of the polycystic kidney disease 1 gene. *Am J Hum Genet*, **61** (1997), 843–51.

32. M. Pea, F. Bonetti, G. Martignoni *et al.*, Apparent renal cell carcinomas in tuberous sclerosis are heterogeneous: the identification of malignant epithelioid angiomyolipoma. *Am J Surg Pathol*, **22**:2 (1998), 180–7.
33. J. D. Carpten, C. M. Robbins, A. Villablanca *et al.*, HRPT2, encoding parafibromin, is mutated in hyperparathyroidism-jaw tumour syndrome. *Nat Genet*, **32**:4 (2002), 676–80.
34. V. M. Howell, C. J. Haven, K. Kahnoski *et al.*, HRPT2 mutations are associated with malignancy in sporadic parathyroid tumours. *J Med Genet*, **40**:9 (2003), 657–63.
35. J. D. Chen, C. Morrison, C. Zhang *et al.*, Hyperparathyroidism-jaw tumour syndrome. *J Intern Med*, **253**:6 (2003), 634–42.
36. B. T. Teh, F. Farnebo, U. Kristoffersson *et al.*, Autosomal dominant primary hyperparathyroidism and jaw tumour syndrome associated with renal hamartomas and cystic kidney disease: linkage to 1q21-q32 and loss of the wild type allele in renal hamartomas. *J Clin Endocrinol Metab*, **81**:12 (1996), 4204–11.
37. C. E. Jackson, R. A. Norum, S. B. Boyd *et al.*, Hereditary hyperparathyroidism and multiple ossifying jaw fibromas: a clinically and genetically distinct syndrome. *Surgery*, **108**:6 (1990), 1006–12; discussion 1012–13.
38. R. A. DeLellis, Parathyroid carcinoma: an overview. *Adv Anat Pathol*, **12**:2 (2005), 53–61.
39. G. Weirich, G. Glenn, K. Junker *et al.*, Familial renal oncocytoma: clinicopathological study of 5 families. *J Urol*, **160** (1998), 335–40.
40. D. Bodmer, W. van den Hurk, J. J. M. van Groningen *et al.*, Understanding familial and non-familial renal cell cancer. *Human Molecular Genetics*, **11**:20 (2002), 2489–98.
41. L. S. Schmidt, M. L. Nickerson, M. B. Warren *et al.*, Germline BHD-mutation spectrum and phenotype analysis of a large Cohort of families with Birt–Hogg–Dubé syndrome. *Am J Hum Genet*, **76**:6 (2005), 1023–33.
42. D. S. Katz, A. M. Gharagozloo, T. R. Peebles *et al.*, Renal oncocytomatosis. *Am J Kidney Dis*, **27**:4 (1996), 579–82.
43. A. J. Cohen, F. P. Li, S. Berg *et al.*, Hereditary renal-cell carcinoma associated with a chromosomal translocation. *N Engl J Med*, **301**:11 (1979), 592–5.
44. L. Valle, A. Cascon, L. Melchor *et al.*, About the origin and development of hereditary conventional renal cell carcinoma in a four-generation t(3;8)(p14.1;q24.23) family. *Eur J Hum Genet*, **13**:5 (2005), 570–8.
45. C. J. Davis, F. K. Mostofi, and I. A. Sesterhenn, Renal medullary carcinoma: the seventh sickle cell nephropathy. *Am J Surg Pathol*, **19** (1995), 1–11.
46. H. Dimashkieh, J. Choe, and G. Mutema, Renal medullary carcinoma: a report of 2 cases and review of the literature. *Arch of Pathol and Lab Med*, **127**:3, 135–8.
47. X. J. Yang, J. Sugimura, M. S. Tretiakova *et al.*, Gene expression profiling of renal medullary carcinoma: potential clinical relevance. *Cancer*, **100**:5 (2004), 976–85.
48. A. J. Davidson, P. L. Choyke, D. S. Hartman *et al.*, Renal medullary carcinoma associated with sickle cell trait: radiologic findings. *Radiology*, **195**:1 (1995), 83–5.

49. N. M. Blitman, R. G. Berkenblit, A. M. Rozenblit *et al.*, Renal medullary carcinoma: CT and MRI features. *AJR Am J Roentgenol*, **185**:1 (2005), 268–72.
50. P. L. Choyke, Imaging of hereditary renal cancer. *Radiol Clin North Am*, **41**:5 (2003), 1037–51.
51. C. A. Jamis-Dow, P. L. Choyke, S. B. Jennings *et al.*, Small (< or = 3-cm) renal masses: detection with CT versus US and pathologic correlation. *Radiology*, **198**:3 (1996, March), 785–8.
52. http://www.genetests.org (accessed December 2006).
53. J. C. Herring, E. G. Enquist, A. Chernoff *et al.*, Parenchymal sparing surgery in patients with hereditary renal cell carcinoma: 10-year experience. *J Urol*, **165**:3 (2001), 777–81.
54. B. G. Duffey, P. L. Choyke, G. Glenn *et al.*, The relationship between renal tumour size and metastases in patients with von Hippel–Lindau disease. *J Urol*, **172**:1 (2004), 63–5.
55. C. P. Pavlovich, R. L. Grubb, 3rd, K. Hurley *et al.*, Evaluation and management of renal tumours in the Birt–Hogg–Dubé syndrome. *J Urol*, **173**:5 (2005), 1482–6.
56. P. L. Choyke, C. P. Pavlovich, K. D. Daryanani *et al.*, Intraoperative ultrasound during renal parenchymal sparing surgery for hereditary renal cancers: a 10-year experience. *J Urol*, **165**:2 (2001), 397–400.
57. A. Mejean, J. M. Correas, N. Thiounn *et al.*, Conservative treatment of kidney cancer by cryoablation and radiofrequency. *Prog Urol*, **16**:2 (2006), 101–4.
58. J. C. Yang, L. Haworth, R. M. Sherry *et al.*, A randomized trial of bevacizumab, an anti-vascular endothelial growth factor antibody, for metastatic renal cancer. *N Engl J Med*, **349**:5 (2003), 427–34.
59. P. N. Lara, Jr, D. I. Quinn, K. Margolin *et al.*, California Cancer Consortium. SU5416 plus interferon alpha in advanced renal cell carcinoma: a phase II California Cancer Consortium Study with biological and imaging correlates of angiogenesis inhibition. *Clin Cancer Res*, **9**:13 (2003), 4772–81.

4

Radiological diagnosis of renal cancer

Richard H. Cohan and Saroja Adusumilli

Introduction

Multi-detector CT (Computed tomography) and MRI (Magnetic resonance imaging) can detect and characterize most renal cancers, often differentiating them from non-surgical renal masses with a high degree of accuracy [1]. In the paragraphs that follow, use of CT and MRI in detecting and appropriately characterizing renal cancers will be reviewed. There will be an emphasis on recent developments in the use of imaging to differentiate cancers from benign renal lesions. Suggested CT and MRI protocols also will be provided.

Recommended CT and MRI technique

Computed tomography performed in patients with suspected or known renal masses should include a series of thin section non-contrast images (obtained using an image thickness of no more than 3–5 mm and with images reconstructed at no more than 3–5 mm intervals). At least one series of contrast-enhanced images should be acquired (usually after intravenous injection of 100–150 ml of a 300–370 mg I/ml concentration of non-ionic contrast material, infused at a rate of 2–4 ml/s) during or after the nephrographic phase (at or after 100 seconds). Image thickness and reconstruction interval should be the same as that employed for the non-contrast images.

Magnetic resonance imaging examinations performed to evaluate patients with known or suspected renal masses should include T1-weighted sequences obtained before and after gadolinium administration. While some feel that T2-weighted sequences are not as helpful and may even be omitted, we believe that they should be obtained, as they can help identify small renal cysts (by their high signal

Carcinoma of the Kidney, ed. Uday Patel. Published by Cambridge University Press.

intensity). At the present time, our MRI technique for evaluating patients with suspected or known renal masses includes the following six sequences. (1) Coronal single-shot fast spin-echo (SSFSE) images are obtained using a TE of about 180 ms as a localizer sequence. (2) Axial in- and out-of-phase T1-weighted gradient-echo sequence images are performed for detecting fat, lipid, or blood in a renal mass. (3) T1-weighted in-phase gradient-echo sequences with water suppression are used to detect small angiomyolipomas (AMLs), which will be of high signal intensity against a background of low signal intensity renal parenchyma, since the water protons of the kidney are suppressed. (4) Axial T2-weighted fast spin-echo are then obtained as a respiratory triggered sequence, using a TE of 120 ms and covering the abdomen from the liver dome through the kidneys, so that hepatic abnormalities will not be missed. (5) Coronal 3D T1-weighted gradient-echo sequences are acquired pre-contrast and dynamically post-contrast. Axial or sagittal plane images can be acquired as well, as lesion location dictates. It is critical that the pre-contrast data set be identical to the contrast-enhanced images in case subtraction images are needed (such as in the case of hemorrhagic lesions). (6) Finally, delayed contrast-enhanced axial 2D T1-weighted fast spoiled gradient-echo images are obtained through the kidneys.

Phases of renal enhancement

With the advent of multi-detector CT and with rapid MRI image acquisition, it is now possible to image the kidneys entirely in each or all of the four phases of renal enhancement after intravenous contrast material administration. These include the vascular phase (VP), the corticomedullary phase (CMP), the nephrographic phase (NP), and the excretory phase (EP) [2,3]. The VP occurs 20–40 seconds after initiation of a bolus contrast injection (performed at a rate of 2–4 ml/s) [3]. During the VP, the aorta and renal arteries enhance briskly, the renal cortex has just begun to enhance, and there is little renal medullary enhancement. The CMP usually occurs 25–80 seconds after initiation of contrast injection. During the CMP, the renal cortex enhances briskly, but the medulla enhances only minimally [4,5,6]. On CT, attenuation differences between cortex and medulla are pronounced and approach 100 HU [4,5,6]. The NP begins at about 85–120 seconds. In the NP, renal medullary enhancement has increased, so that its attenuation is similar to that of renal cortex [4,6]. The EP occurs when contrast material is first excreted into the renal collecting systems, usually beginning at 3–5 minutes [2]. Nephrograms remain homogeneous during the EP; however, renal parenchymal

attenuation is lower than that encountered during the NP. Variation in the timing for each of these phases may occur as a result of differences in the rate of contrast material injection (with more rapid injection rates resulting in more rapid appearance of each phase) and cardiac output (with reduced cardiac output resulting in a more delayed appearance of each phase).

Detection of renal cancers

Most published studies have found that NP or EP images are more sensitive than CMP or VP images in detecting renal masses, including cancers, since it is difficult to distinguish some hypovascular masses from normal hypoenhancing renal medulla and some hypervascular cortical masses from briskly enhancing normal renal cortex on VP and CMP images (Figure 4.1) [4,7,8,9]. Of the two delayed phases (NP and EP), neither one appears to be superior to the other [10]. While Sussman and colleagues observed extensive artifact by excreted contrast material in the renal calyces and pelvis [11], and suggested that such artifact might interfere with evaluation of the kidneys on EP images, with current scanners and injection techniques this has not proved to be a problem [10].

In contrast, CMP images appear to be more sensitive than NP images in detecting solid renal masses in patients with end-stage renal disease. In these patients, the background renal parenchyma demonstrates little early enhancement, while solid renal masses enhance briskly [12]. In comparison, by the time NP or EP images are acquired, renal cancers frequently have the same attenuation as renal parenchyma, with both demonstrating similar and only mild enhancement.

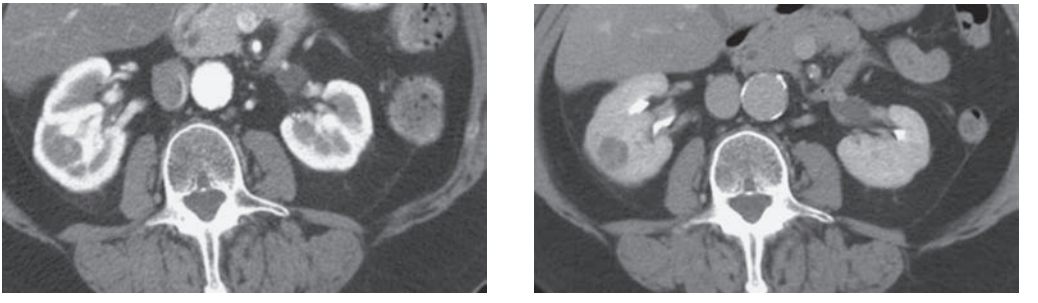

(a) (b)

Figure 4.1 Renal cancer not visible on vascular phase images. (a) A vascular phase CT image fails to demonstrate any evidence of a renal mass. (b) In comparison, the right renal cancer is easily identified as a low attenuation lesion on an excretory phase image obtained at 5 minutes.

Characterization of renal cancers

Differentiating a mass from another abnormality

Differentiating a renal mass from another renal abnormality is usually easy. Masses tend to be round and project outside the expected margins of the renal cortex; however, on occasion, they can be infiltrative or centrally located, in which case distinction from an inflammatory abnormality may be difficult. Also, a prominent column of Bertin or a localized inflammatory process, such as focal acute pyelonephritis or focal xanthogranulomatous pyelonephritis, can mimic a mass (Figures 4.2 and 4.3). Fortunately, in most cases of infection, patient presentation (flank pain, pyuria, fever, and leukocytosis) often facilitates a correct diagnosis.

Absolute attenuation measurements

Most renal cancers contain solid tissue components which can be seen on non-contrast and contrast-enhanced CT or MR images. Region-of-interest measurements are more variable on multi-detector CT than those that are obtained on older non-helical scanners. As a result, many abdominal radiologists now accept a fairly wide range of attenuation measurements from –5 to 20 HU on both pre-contrast and enhanced CT images as indicating that a mass contains fluid. Only unenhanced measurements exceeding 20 HU can be considered to indicate soft

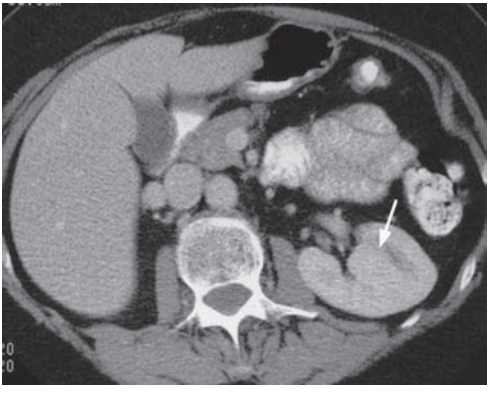

(a)

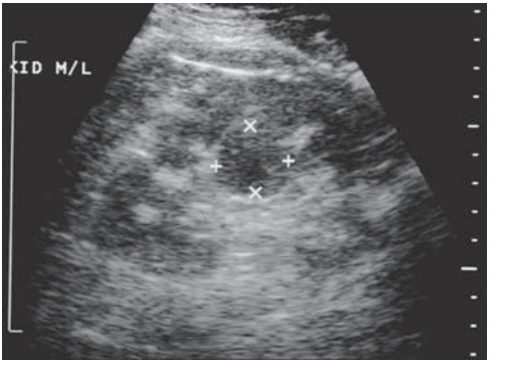

(b)

Figure 4.2 Renal abnormality mimicking a renal mass. This elderly patient with hematuria was referred for an ultrasound examination. (a) The ultrasound revealed a suspicious isoechoic area in the mid left kidney that was believed to represent a mass. A follow-up CT (b) did not demonstrate a mass, but instead showed that the suspicious area seen on the ultrasound was merely a prominent column of Bertin.

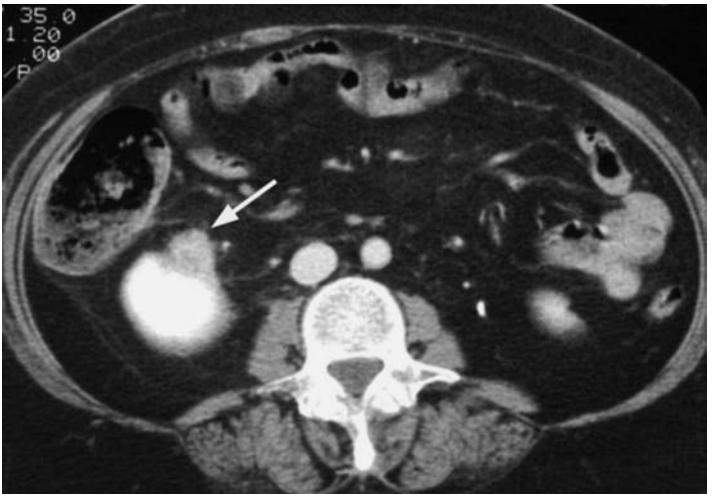

Figure 4.3 Focal xanthogranulomatous pyelonephritis. A heterogeneous solid mass is identified in the anterior aspect of the lower pole of the right kidney (arrow) in this patient with low grade fevers. Final pathology, obtained after partial nephrectomy, revealed that this mass represented a focus of xanthogranulomatous pyelonephritis.

tissue with certainty. On MRI, soft tissue often can be distinguished from fluid, since the latter usually has high signal intensity on T2-weighted images and low signal intensity on T1-weighted images. When fluid contains blood products or proteinaceous material, it may not demonstrate these features, however. This fluid, present in hyperdense cysts, often has high attenuation (of up to 80 HU) on CT and high signal intensity on T1-weighted MRI sequences.

Mass heterogeneity

Renal cancers often have areas of necrosis and occasionally contain calcification (in up to 11% of cases) [13], while benign, simple and hyperdense cysts are homogeneous.

Assessing masses for enhancement

With the emergence of multi-detector CT, the determination of what constitutes enhancement on CT has changed. As previously mentioned, HU measurements vary more widely on multi-detector helical than on non-helical scanners, and, as a result, it has been suggested that while attenuation differences < 10 HU between unenhanced and enhanced images still indicate absence of enhancement, a change in attenuation of 10–20 HU now should be considered indeterminate, with many masses demonstrating this limited increase in attenuation needing

additional evaluation (with immediate repeat CT, MRI, ultrasonography, or follow-up imaging) [14]. Only increases in attenuation of > 20 HU should be considered to indicate definite enhancement [14]. On MRI, enhancement is identified by an increase in signal intensity after contrast material has been administered; however, qualitative assessment of enhancement on MRI is more difficult. In comparison to the properties of iodinated contrast material and CT, the relationship of gadolinium concentration to signal intensity is not linear. As a result, absolute signal intensity measurements cannot be used. Instead, determination of relative signal intensity change or use of subtraction images can be very helpful [15].

When renal masses are assessed for enhancement, it is important that NP or EP images be utilized in addition to or rather than CMP images. This is because enhancement of some renal cancers does not occur until the NP [4,5]. In one series of 31 indeterminate renal masses, all 16 renal neoplasms demonstrated enhancement on NP images; however, only 11 of these tumors demonstrated enhancement on the CMP images [5]. While both benign and malignant lesions may have varying degrees of vascularity [16], two small studies have shown that early brisk enhancement (in the VP or early CMP) of a solid renal mass in excess of that of normal renal parenchyma [17] or such that its attenuation exceeds 100 HU strongly suggests that the mass is malignant [18].

De-enhancement

Renal mass de-enhancement can demonstrate the solid nature of a renal mass just as well as enhancement can [19,20]. After contrast-enhancement peaks, solid masses lose attenuation on CT or T1-weighted signal on MRI examinations. While most researchers wait 10–15 minutes to detect this change, perceptible de-enhancement can be seen earlier in many instances (Figure 4.4). This feature is useful when patients undergoing contrast-enhanced CT or MRI for other reasons are found to have renal masses unexpectedly.

Limitations in the use of enhancement

It is important not to rely on attenuation measurements to diagnose enhancement in subcentimeter renal masses, even on thin section images. On CT, attenuation measurements of these lesions are often erroneous, owing to volume averaging and pseudoenhancement. Volume averaging occurs when a small lesion

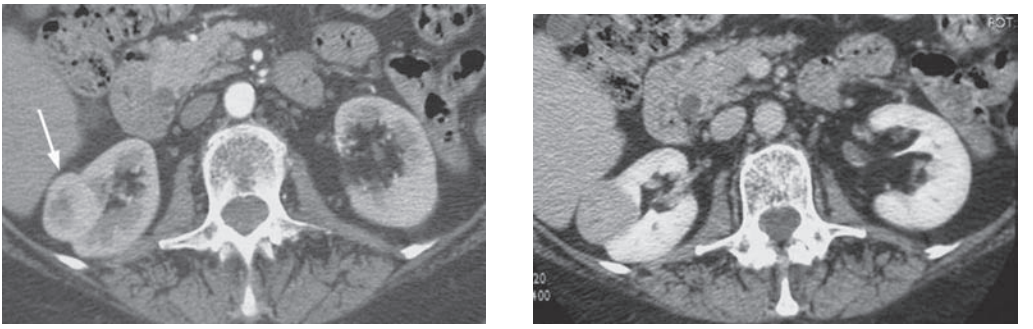

(a) (b)

Figure 4.4 De-enhancement of a solid renal mass. (a) Soft tissue in the periphery of a right renal mass (arrow) seen on a CMP image in this patient measured 127 Hounsfield units (HU). (b) Three minutes later, the same area measured only 94 HU.

does not occupy the entire thickness of an image. On CT, its measured attenuation, accordingly, will be affected by included adjacent normal renal parenchyma when a region of interest is applied, a feature that can lead to the incorrect identification of some small renal cysts as enhancing solid masses. Computed tomography pseudoenhancement results from beam hardening artifact that occurs when a low attenuation area (such as a renal mass) is surrounded by a very high attenuation area (such as briskly enhancing normal renal parenchyma). Pseudoenhancement is more likely and more dramatic when the renal mass being evaluated is small, when background renal parenchymal enhancement is great, and when narrow image collimation is not utilized [21,22]. Fortunately, pseudoenhancement exceeding 10 HU is rarely a problem for masses 2 cm or more in diameter imaged at a thickness of 5 mm or less [23].

Differentiating renal cancers from other renal masses on imaging

When a detected renal mass is of a sufficient size (usually 1.5 cm or larger in diameter), it is often possible to further characterize the lesion if thin section CT or MR images are obtained. The next step in characterization relates to differentiating a renal cancer from a simple cyst, a benign complex cyst, or a benign solid neoplasm. This is done primarily by determining whether or not the entire mass is of fluid attenuation on CT or fluid signal intensity on MRI, whether it contains any macroscopic fat, and whether it demonstrates any enhancement after contrast material administration.

Simple renal cysts

Simple cysts are easily distinguished from cancers. These benign lesions have a diagnostic appearance on cross-sectional imaging studies and require no additional imaging or follow-up. Criteria for diagnosing simple renal cysts vary for each imaging modality. On CT, simple cysts should measure water attenuation (0–20 HU), fail to enhance (ideally demonstrating an increase in attenuation between unenhanced and enhanced images of less than 10 HU), be homogeneous, and have no complicating features such as septations, wall thickening, nodularity, or calcification. On MRI, simple cysts should have uniform low signal intensity on T1-weighted imaging, uniform high signal intensity on T2-weighted imaging, fail to enhance, and have no complicating features such as septations, wall thickening, or nodularity. Any cystic masses that do not demonstrate all of these features must be considered complex renal cysts.

Complex renal cysts

Complex renal cysts can be problematic on cross-sectional imaging studies, as some of these lesions are cystic cancers, while others are benign. The imager is often asked to make management recommendations based upon his or her impression of the likelihood that the mass will contain malignant cells. In 1986, Bosniak first described his cyst classification system [24], categorizing renal cysts according to their likelihood of being malignant. This system has undergone a number of revisions, with the most recent version published in 2005 [14], summarized in Table 4.1 and illustrated in Figure 4.5. According to Bosniak's system, Category I or II cysts are always benign and do not require any further imaging or treatment. Category IIF lesions require imaging follow-up, sometimes for as long as 5 years, since a few of these are malignant. Category III and IV cysts are generally treated surgically or with percutaneous ablation, since about half of all Category III lesions and all Category IV lesions are cystic renal cancers.

Several studies have confirmed that the Bosniak cyst classification system is accurate [25,26,27]. For example, in one of the largest series [27], which included 109 patients from two institutions, all 15 surgically removed Category I and II lesions were benign, while 29 of 49 Category III lesions and all 18 Category IV lesions were malignant. Some have recommended slight modifications of the Bosniak system. For example, in one series of 32 Bosniak Category II and III

Table 4.1. The Bosniak cyst classification system (from Ref. 14)

Category	Features	Likelihood of malignancy
Category I	1. Hairline-thin wall 2. Water attenuation (−5 to +20 HU) 3. No enhancement	0%
Category II	1. Few hairline-thin septa which may enhance (not measurably) 2. Fine or short segment of thickened calcification in wall or septa 3. Uniformly high attenuation and < 3 cm with sharp margins and no enhancement (hyperdense cysts)	0%
Category IIF	1. Multiple hairline-thin septa which may enhance (but not measurably) 2. Minimal thickening of wall or septa 3. Thick or nodular calcification in wall or septa 4. Totally intrarenal or large ($\geq$ 3 cm) high attenuation lesions that do not enhance (large hyperdense cysts)	few
Category III	Thickened irregular or smooth walls and/or septa that demonstrate measurable enhancement	50%
Category IV	Distinct enhancing soft-tissue components independent of the wall or septa	100%

renal masses, all 21 cystic cancers had enhancing septa or nodules, while no malignancy demonstrated only an enhancing wall [28]. As a result, the reviewers concluded that cystic masses with only mural enhancement should be classified as Bosniak IIF rather than III lesions.

Regardless of the exact definitions used for the Bosniak or any other complex cyst classification system, occasionally, problems are encountered owing to rare exceptions [29,30] and interobserver disagreement [26]. Since CT cannot image microscopically, renal cysts that contain only small foci of tumor will be classified erroneously as Category I or Category II lesions [29]. To further complicate the issue, even expert radiologists, with extensive experience in abdominal CT interpretation, will disagree with one another about some lesions. In the series

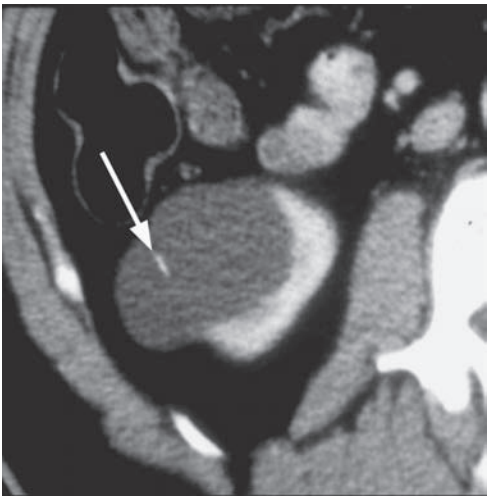

(a)

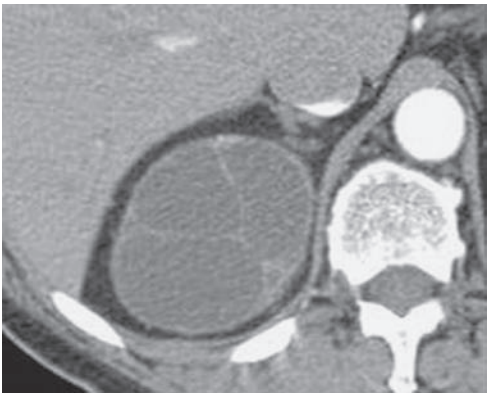

(b)

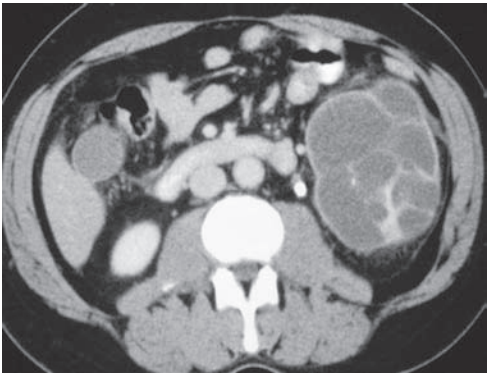

(c)

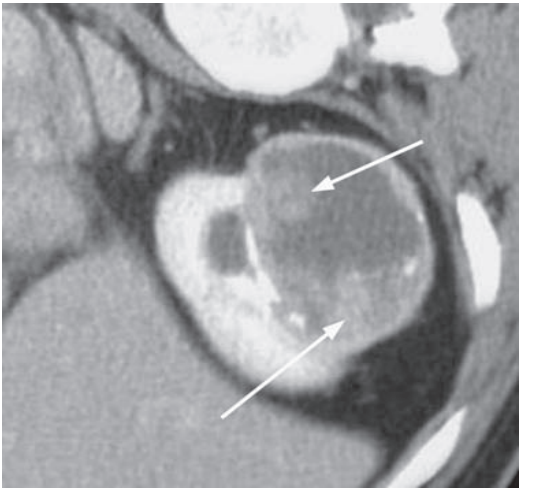

(d)

Figure 4.5 Complex renal cysts. (a) This right renal mass contains a single thin septation and, therefore, would be categorized as a Bosniak Type II cyst. This is most likely a benign lesion. (b) The Category III cystic right renal mass illustrated here is a cystic cancer. (c) In comparison, this similar appearing Category III lesion is a multilocular cystic nephroma. (d) A right renal cancer in another patient contains multiple enhancing nodular areas (arrows), a Category IV feature.

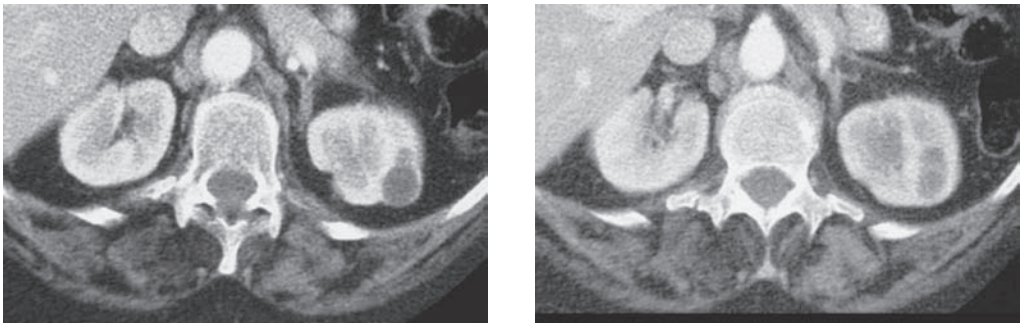

(a) (b)

Figure 4.6 Interobserver variability in evaluating cystic renal masses. (a) On this CMP image, a small renal mass in the posterolateral aspect of the upper pole of the left kidney demonstrates an apparent thin enhancing wall along its lateral aspect. (b) On a slightly more caudal image, the renal parenchyma appears normal. The apparent wall thickening could be construed as true wall thickening (a Bosniak Category III cyst) by some radiologists or merely as compressed adjacent normal parenchyma (a Bosniak Category I cyst) by others.

reported by Siegel and colleagues [26], 11 (16%) of 70 lesions classified as Category I or II lesions by one expert reader were classified as Category III or IV lesions by at least one of two other expert readers. One of the commonly encountered problems concerned confusion about whether enhancing tissue adjacent to a low attenuation mass represented adjacent normal parenchyma or an enhancing cyst wall (Figure 4.6).

On MRI, some cystic masses demonstrate similar complexity as seen on CT or ultrasound (Figure 4.7), while others demonstrate additional internal septations, septal or wall thickening, or enhancement [31]. The increased complexity of some lesions is due to the higher sensitivity of MRI in detecting some complicating internal cyst features (in comparison with CT). However, MRI also is prone to more artifacts than is CT, and some simple cysts will occasionally demonstrate spurious wall thickening and internal pseudo-septations (Figure 4.8). In a recent study of 69 cystic renal masses categorized with both CT and MRI [31], seven lesions were upgraded on MRI, with the upgrades having the potential of changing patient management in five of the seven cases. Subsequent follow-up suggested that CT had been more accurate in three instances (including one lesion upgraded to Category III by MRI), while MRI was more accurate in three (including one lesion upgraded to Category III by MRI). The nature of the seventh lesion was not determined.

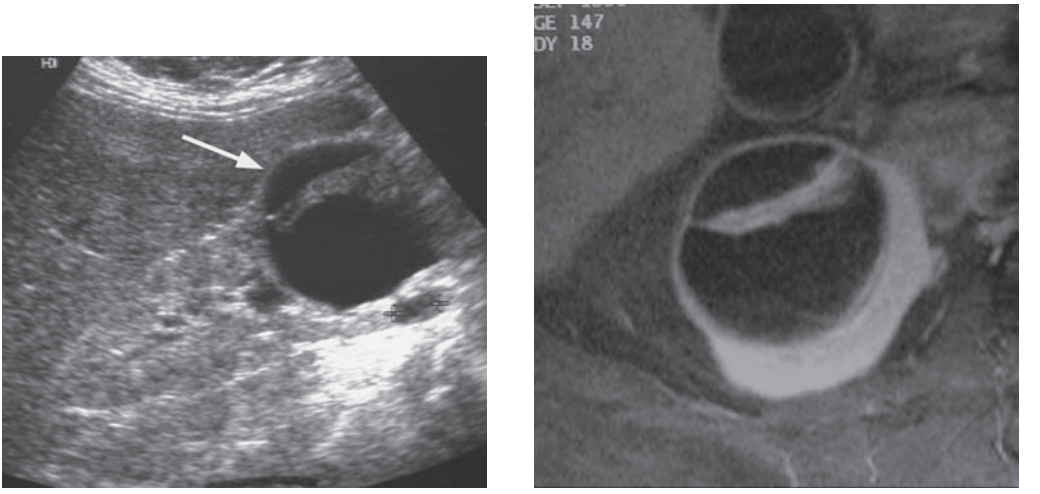

(a) (b)

Figure 4.7 MRI diagnosis of a Category III cyst. An ultrasound examination (a) shows a mass (arrow) containing thick lobulated internal septations. The same feature is well visualized on an axial fat-saturated gadolinium-enhanced T1-weighted image (b).

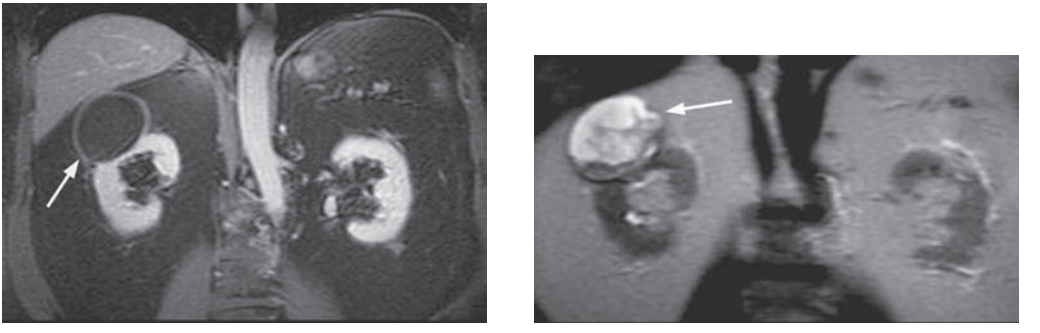

(a) (b)

Figure 4.8 MRI of a benign renal cyst. MRI demonstrates more renal cyst complexity than CT in some patients, owing to a greater number of artifacts. In the case illustrated here, a coronal T1-weighted gadolinium-enhanced fat saturated image (a) reveals artifactual wall thickening, while a coronal T2-weighted unenhanced image (b) shows artifactual internal components, the latter probably occurring because of fluid movement.

Macroscopic fat-containing angiomyolipomas

The only solid renal masses that can be differentiated from renal cancers on CT or MRI with certainty are AMLs. This is because the macroscopic fat present in most AMLs has a characteristic CT and MRI appearance. On CT, identification of

even small areas measuring −10 HU or less in a renal mass is considered diagnostic of AML [32,33,34]. These regions of fatty attenuation may be so small that they will be seen only if thinly collimated unenhanced images are obtained [33]. On MRI, most AMLs have high signal intensity on T1- and T2-weighted imaging and lose signal intensity when fat-suppressed images are obtained. AMLs demonstrate a characteristic "India ink" artifact at the interface of the mass and adjacent renal parenchyma but not between the AML and adjacent perinephric fat on opposed-phase chemical-shift MRI images. In contrast, renal cancers demonstrate this artifact at interfaces with perinephric fat, but not at interfaces with adjacent renal parenchyma [35].

Although identification of fat within a renal mass generally should be considered diagnostic of AML, there are case reports of macroscopic fat detected by CT in renal cancers. This occurs as a result of osseous metaplasia [36,37], engulfed renal sinus fat, extensive lipid vacuoles, and cholesterol clefts in clear cell carcinomas [38]. In some cases in which fat is seen in a renal cancer, so too is calcification. Since calcification is exceedingly rare in AMLs, the presence of fat and calcification together in a renal mass should preferentially suggest the diagnosis of renal cancer, particularly if there are only small foci of macroscopic fat present [39].

Solid renal masses that do not contain recognizable fat

Unfortunately, no consistent cross-sectional imaging characteristics have yet been identified that allow for differentiation of benign from malignant solid renal masses that do not contain identifiable fat. Although, most non-fat containing solid renal masses are carcinomas (Figure 4.9), many other renal masses, including rare unusual neoplasms (Figure 4.10), can have this appearance [40,41,42,43,44]. While, in the past, this lack of specificity was not felt to be very important, as it was believed that the vast majority of these solid masses were renal cancers, a number of recent publications have suggested otherwise.

Several studies have shown that a large minority of solid renal masses that do not contain identifiable fat, particularly those that are small, are benign lesions. For example, one recent study found that 10 of 27 renal masses measuring 1.0 to 4.6 cm that were referred for cryotherapy were benign [45]. In another series, 18 of 90 solid renal masses measuring 4 cm or less in diameter were benign [46]. In comparison, all masses exceeding 7 cm in diameter were malignant. Finally, in a much larger study of 2770 patients with renal masses referred for surgery [47], the percentage of benign, resected renal masses measuring <1 cm, 1–1.9 cm, 2–2.9 cm, 3–3.9 cm,

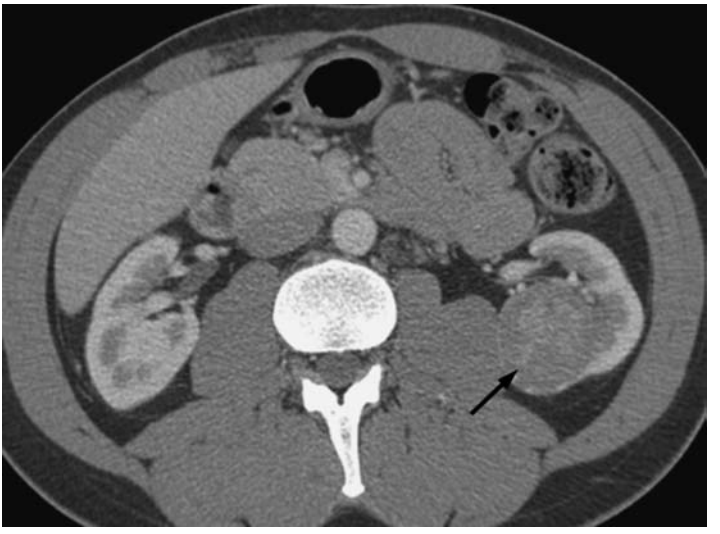

Figure 4.9 Chromophobe renal cancer. A large solid mass in the mid left kidney (arrow) does not contain any recognizable fat. The most likely diagnosis is renal cancer; however, benign renal masses can have this appearance.

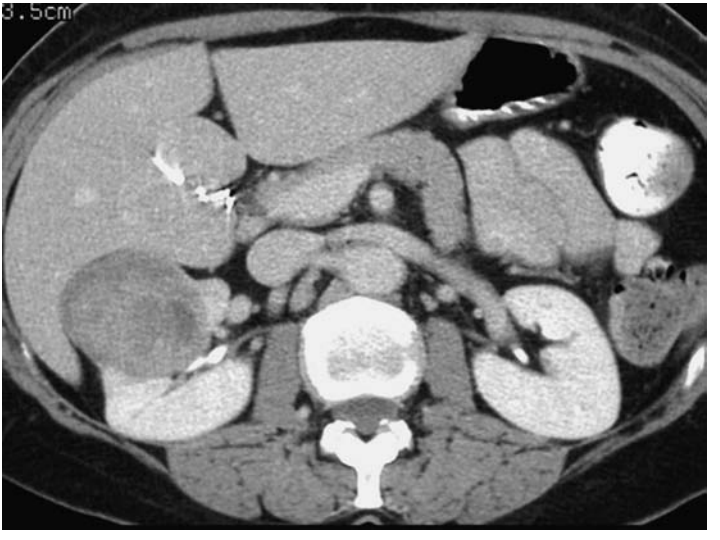

Figure 4.10 Juxtaglomerular tumor. Solid renal masses that do not contain fat cannot be distinguished from one another reliably. This young woman has a heterogeneous mass that could have been a renal cancer; however, a juxtaglomerular tumor was identified at surgery.

4–4.9 cm, 5–5.9 cm, 6–6.9 cm, and 7 cm or greater was 46%, 22%, 22%, 20%, 10%, 13%, 4%, and 6%, respectively. Given these results, a strong argument can be made for performing pre-treatment biopsies on all small solid renal masses (measuring 4 cm or less). In comparison, large solid renal masses probably need not be biopsied routinely, since they are overwhelmingly likely to be malignant.

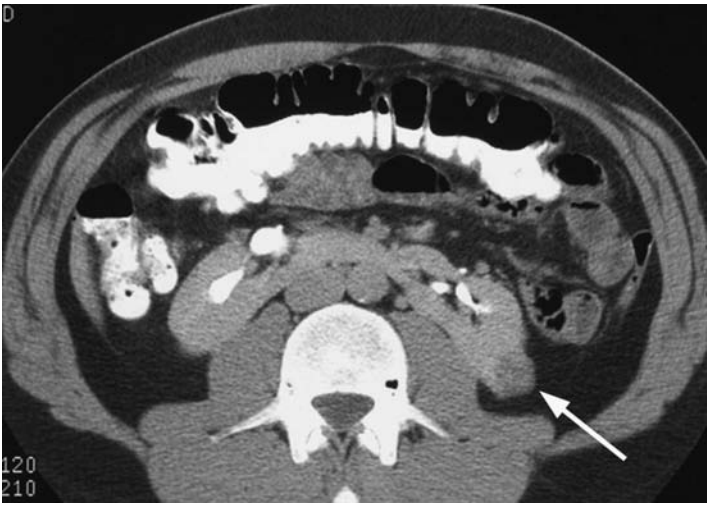

Figure 4.11 Minimal fat-containing AML. Angiomyolipomas that do not contain identifiable fat cannot be distinguished from renal cancers on cross-sectional imaging studies, as seen in this patient with a horseshoe kidney who has small soft tissue attenuation AML on the left.

Renal cancer versus the minimal fat containing AML

Unfortunately, some AMLs contain such small amounts of fat that no fatty areas can be identified on CT or MRI (Figure 4.11). These variants have been referred to as "renal angiomyolipomas with minimal fat." Unlike typical AMLs, these tumors can be mischaracterized as probable malignant neoplasms on CT and MRI; however, several other suggestive imaging characteristics have been identified. On CT, AMLs with minimal fat are more likely to have higher attenuation than normal renal parenchyma on unenhanced images, to enhance homogeneously and to enhance in a prolonged fashion (neither losing nor gaining attenuation values exceeding 20 HU between 30 second CMP and 120–150 second EP images) [48,49,50]. Unfortunately, these features are not completely specific or sensitive. A minority of renal cancers will demonstrate both of these characteristics, and some AMLs will not. While special MRI techniques have been designed that allow for detection of tiny amounts of fat in some minimal fat-containing AMLs [51], these are not completely sensitive.

Renal cancer versus oncocytoma

When they are large, oncocytomas (benign renal neoplasms derived from proximal renal tubular cells) often have central scars that can be detected on imaging studies [52,53,54]. While visualization of a possible scar in a renal mass imaged with CT or MRI may suggest that it is an oncocytoma, scars cannot be differentiated reliably

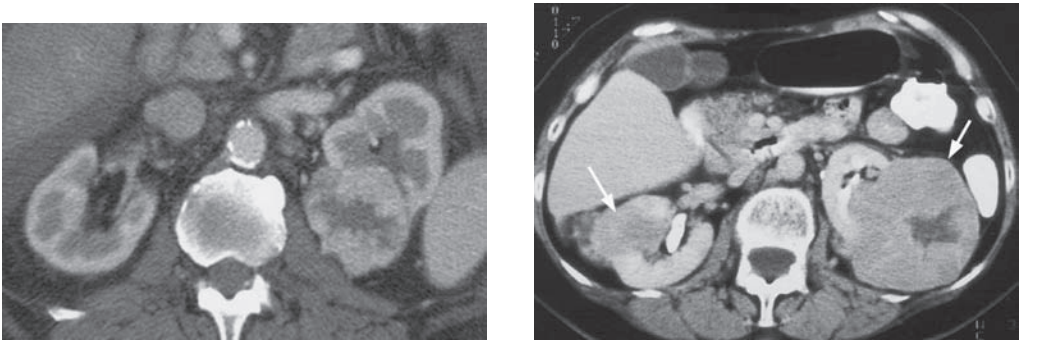

(a) (b)

Figure 4.12 Oncocytoma. (a) A central stellate scar is identified easily in this patient with a large left renal oncocytoma. (b) The central necrosis in a left renal cancer in another patient with bilateral renal cell carcinomas (arrows) has a very similar appearance.

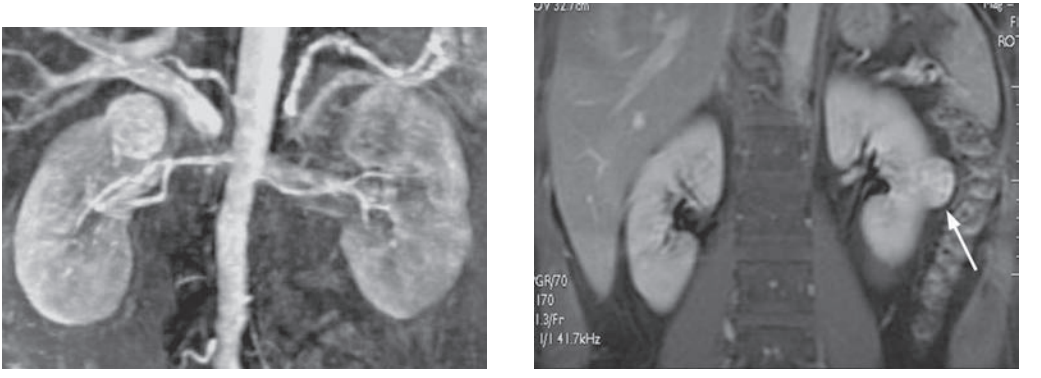

(a) (b)

Figure 4.13 Some renal cancers and some oncocytomas enhance briskly and homogeneously and are indistinguishable from one another. (a) This elderly patient has an enhancing RCC in the upper pole of the right kidney, easily seen on this T1-weighted gadolinium-enhanced coronal image. (b) Another patient has a very similar appearing oncocytoma in the lower pole of the left kidney (arrow).

from necrosis in renal cancers (Figure 4.12). Furthermore, many oncocytomas do not contain scars (Figure 4.13). Oncocytomas also frequently demonstrate a spoke-wheel vascular pattern on conventional CT or MR arteriography, but these features are also not distinctive. Many renal cancers demonstrate a spoke-wheel arterial pattern and since renal cancer is much more common, most tumors that have this appearance are cancers. Finally, both renal cancers and oncocytomas have been observed to enhance briskly on early CMP images and to demonstrate prompt washout [18].

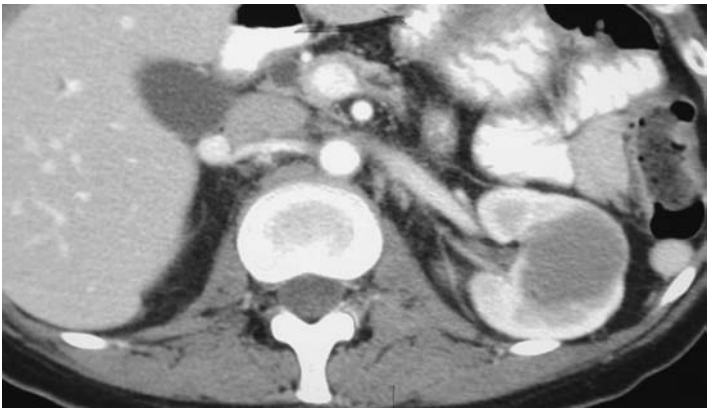

Figure 4.14 Renal lymphoma. This patient with known lymphoma has developed a solitary homogeneous enhancing mass in his mid left kidney, which was subsequently determined to represent lymphoma.

Renal cancer versus renal lymphoma

While the most common renal manifestation of lymphoma is multiple bilateral renal masses [55], in some patients a single solid renal mass may be present [56]. In yet other patients, lymphomatous masses in the retroperitoneum may secondarily invade the kidney, while other patients develop perinephric masses [55,56]. Lymphomatous renal masses tend to be homogeneous and do not distort the renal outline as much as many renal cancers do (Figure 4.14); however, there is overlap. When multiple renal masses or perinephric masses are encountered in a patient with known lymphoma, the diagnosis of renal lymphoma is usually obvious. In comparison, when a solitary renal mass develops in a lymphoma patient, there is no distinctive imaging characteristic that allows one to distinguish a renal cancer from renal lymphoma with certainty, and biopsy may be required for diagnosis.

Differentiation of subtypes of renal cancer from one another

Several studies have focused on the ability of imaging studies to distinguish papillary from other types of renal cancer. While most of these appeared before a recent decision to sub-classify papillary tumors into two types [54], it is likely that previous reports included mostly or only the more common Type I papillary cancers. Type I papillary cancers tend to be small [57], to enhance homogeneously [58], and to enhance to a lesser extent [59,60] than other types of renal cancer. On MRI, these tumors are almost always homogeneous and of low signal intensity on T2-weighted images, while clear cell tumors have high signal intensity and are

heterogeneous on T2-weighted images [60]. In comparison, the more aggressive Type II papillary renal cancers demonstrate a greater degree of heterogeneity and enhancement and, therefore, cannot be distinguished from other renal cancer cell types [59].

Clear cell carcinomas possess several distinctive imaging characteristics. They tend to enhance more quickly and intensely than the majority of other renal cancers. In a small series, Jinzaki and associates found that all 29 clear cell cancers had attenuation values of > 100 HU on enhanced images obtained at 35 seconds and all also demonstrated de-enhancement between the 35- and 180-second images [18]. Only one other neoplasm in the series (one of two included oncocytomas) demonstrated similar early enhancement. On MRI, clear cell cancers often lose signal intensity on opposed-phase chemical-shift MR images, while other renal cancer types do not [61].

There is another suggestive feature of some renal cancer types. Collecting duct carcinomas originate within medullary pyramids and for this reason are centrally located [62]. On CT, they also tend to enhance poorly after contrast material administration [62]. Renal medullary carcinoma is a rapidly growing, centrally located, high-grade neoplasm that almost always occurs in young black males with sickle cell trait [63]. Metastases occur early, so that enlarged lymph nodes and distant metastases are often present on initial imaging. Other more common renal neoplasms also may be centrally located however, including the other renal cancer cell types (Figure 4.15), urothelial malignancies, and renal lymphoma.

Figure 4.15 Centrally located renal cancer. A centrally located solid renal mass can represent a renal cancer, as in the mass illustrated here (arrow), a urothelial malignancy, or lymphoma. Certain types of renal cancers, such as collecting duct and renal medullary cancers, tend to be centrally located.

Differentiating renal cancers from other masses based on growth and metabolism

Since the imaging appearance of the different types of non-fat containing solid renal masses is not definitive, researchers have also evaluated tumor behaviour and metabolism, in an attempt to predict the likelihood of a renal mass being malignant.

Growth

A number of studies have assessed solid renal masses for growth as a potential means of distinguishing benign from malignant lesions. Unfortunately, reliance upon renal mass growth has limited utility because many small renal cancers grow slowly (Figure 4.16). Even if a solid renal mass is stable in size for a year or more, it could still be a cancer. For example, Bosniak and colleagues reported on 40 renal tumors measuring ≤ 3.5 cm in diameter that were followed for a mean of over 3 years [64]. The diameters of these small tumors increased at a rate of 0.1–1 cm/year, and together they demonstrated mean growth of only 3.6 mm/year. Volpe and colleagues reported a series of 32 renal masses (25 solid and 7 cystic) measuring < 4 cm in greatest dimension, followed for a median of 27.9 months [65]. Overall, there was no significant increase in the mean diameters of these masses. As was the case in Bosniak *et al.*'s series, no patient in this report eventually developed metastatic disease. Both groups concluded that small renal cancers generally grow slowly and that most small renal masses can be followed safely for years, without concern for worsening patient prognosis.

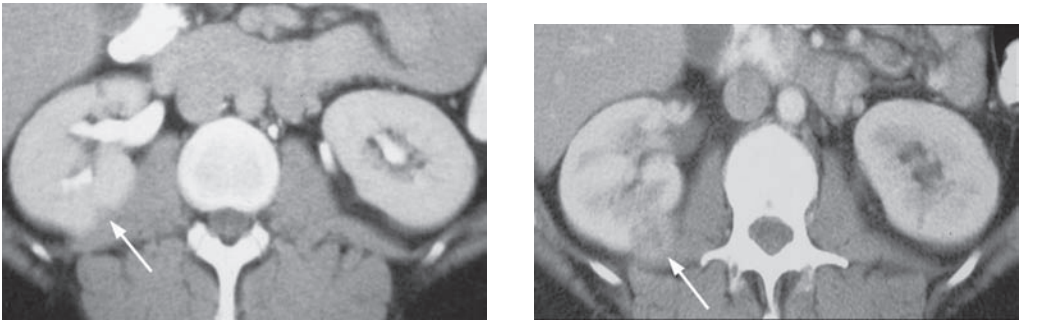

(a) (b)

Figure 4.16 Slow growth of small renal cancers. (a) A CT performed for abdominal pain demonstrates a small indeterminate low attenuation lesion in the posteromedial aspect of the mid right kidney (arrow). The patient was lost to follow-up and then returned four-and-a-half years later, at which time another CT was performed (b). The mass has increased in size, but still represents a T1N0M0 cancer.

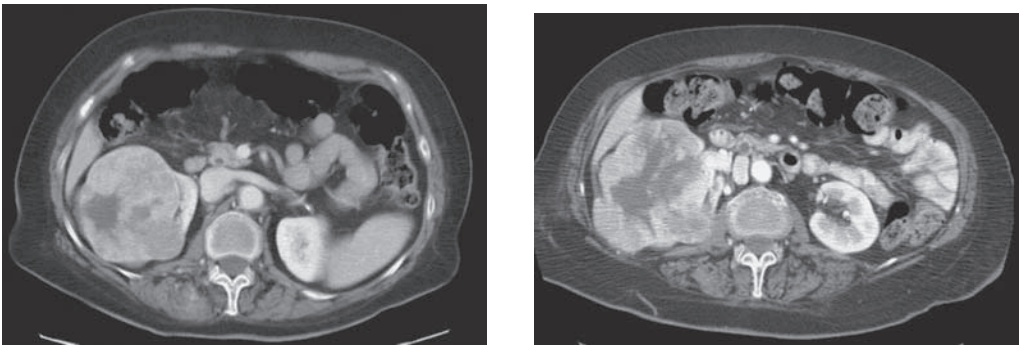

(a) (b)

Figure 4.17 Slow growth of a large renal cancer. (a) A large heterogeneous renal cancer was identified in this patient. The patient was not an operative candidate because of co-morbidity, so the patient was observed. (b) A follow-up CT performed more than 2 years later shows that the mass has increased in size, although the interval change has not been dramatic.

Some large renal cancers can grow slowly as well (Figure 4.17). In one series, 36 patients with a median tumor size of 6 cm who did not have nephrectomy (usually because they were poor operative candidates) were followed for 3 to 36 months [66]. The mean tumor growth rate, which was available for 20 patients, was only 3.9 mm/year. Thirteen patients died during the follow-up period; however, death was caused by an unrelated illness in eight patients, and in five others, who had no evidence of disease progression, the cause of death was unknown. No patient in this series (including three patients with renal vein and inferior vena cava invasion) was known to have died as a result of metastatic disease.

It is important to note, however, that some renal cancers, even small ones, can grow and spread rapidly. In other studies, 7%–17% of patients with small renal masses were observed to have lymph node or distant metastases at the time of initial diagnosis [67]. This is why initial imaging follow-up should be performed within a relatively short interval of 6 months. Another problem is that benign lesions, including cysts, can also demonstrate slow increases in size over time.

18-Fluorine-2-deoxy glucose (FDG) positron emission tomography activity

While many renal cancers are FDG-avid and, therefore, theoretically, can be identified on PET (Positron Emission Tomography) examinations [68], there are exceptions [69]. In comparison, some benign renal tumours are not FDG-avid.

In one small study, neither of two AMLs demonstrated increased uptake, while 13 of 15 renal cancers did [70]. Of course, FDG merely measures metabolic activity, a feature that also can be seen in benign disease. In the previously cited series [70], increased uptake was noted in one patient with xanthogranulomatous pyelonephritis. Unfortunately, the kidney normally excretes FDG, making renal cancer detection difficult, given the high background of normally accumulated FDG. At the present time, the most common role of FDG-PET in renal cancer patients is to evaluate those in whom the primary tumor is known to be FDG-avid for locally recurrent or distant metastatic disease.

Lesions that are too small to characterize

Many renal masses detected with CT and MRI cannot be characterized as cystic or solid because of their small size. In general, this is true for renal masses that have a *z*-axis diameter less than twice the CT slice thickness. While the vast majority of these masses are cysts, a few are cancers. Because tiny renal masses are so common, further imaging assessment of all tiny lesions is not feasible. Follow-up studies to assess these lesions for stability are only recommended in the following circumstances: (1) when imaging characteristics suggest a small lesion may not be a simple cyst (such as mild heterogeneity or a thickened rim) (Figure 4.18); (2) when a small indeterminate mass is seen in a patient under the age of 40; or (3) when a new small mass is seen in a patient who is at risk for developing a renal malignancy, such as in a patient with von Hippel–Lindau disease or hereditary papillary renal cell cancer [71,72]. We now recommend follow-up CT in these patients at regular intervals,

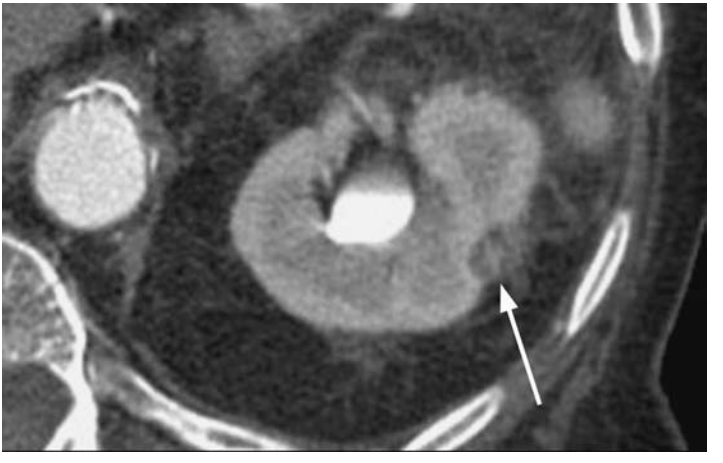

Figure 4.18 Suspicious tiny renal mass. A tiny sub centimeter left renal lesion (arrow) is suspicious for a cancer, because it contains a central area of high attenuation, which may represent enhancement. Follow-up is warranted.

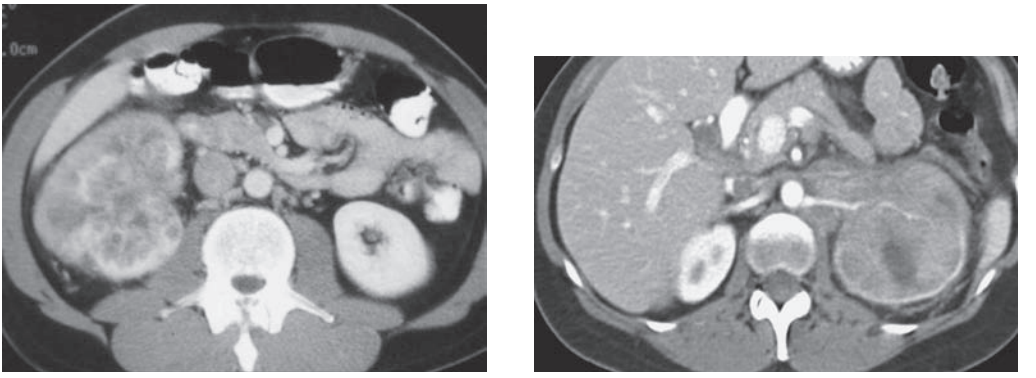

(a) (b)

Figure 4.19 Infiltrative renal masses. (a) Renal cancer can occasionally diffusely infiltrate the kidney, as in the case illustrated here, where the entire right kidney demonstrates abnormal heterogeneous enhancement. Other neoplasms can produce the same appearance, including lymphoma, as in the left kidney illustrated in (b) and urothelial malignancies.

doubling the time between the current and the next scan, if no growth is shown on the first follow-up study. In most patients, this works out to be a follow up of 6, 18, and 36 months, as needed. Long-term follow-up of suspicious indeterminate lesions is necessary because, as has been seen, most small renal cancers grow slowly. As previously noted, such follow-up can be performed safely in most cases without concern for a change in tumor stage, even should the mass being followed up be a small cancer.

Infiltrative renal masses

A variety of malignant tumors can diffusely infiltrate the kidney. These include renal cell cancers, lymphoma, urothelial carcinomas, and metastases (Figure 4.19) [14]. Infiltrative renal cancer can often be distinguished from infiltrative transitional cell carcinoma since the latter produces intrinsic renal collecting system abnormalities. The former usually merely distorts or compresses the intrarenal collecting system, but usually does not grow into it.

Conclusion

CT and MRI are the imaging studies of choice for evaluation of patients with suspected or known solid renal masses. Nephrographic and excretory phase

images are similar to one another, but superior to CMP phase images in their ability to detect solid renal masses and to differentiate them from cysts, although, in some instances, the addition of CMP images may improve diagnostic accuracy. CT and MRI can be used to identify simple renal cysts and to classify complex cysts so that the likelihood of a complex cyst being malignant can be predicted accurately. With the exception of AMLs that contain identifiable fat, CT and MRI still cannot differentiate the various types of solid renal lesions from one another reliably.

REFERENCES

1. A. J. Beer, A. J. Dobritz, N. Zantl *et al.*, Comparison of 16-MDCT and MRI for characterization of kidney lesions. *AJR Am J Roentgenol*, **186** (2006), 1639–50.
2. B. I. Yuh and R. H. Cohan, Different phases of renal enhancement: role on detecting and characterizing renal masses during helical CT. *AJR Am J Roentgenol*, **173** (1999), 747–55.
3. B. R. Herts, D. M. Coll, M. L. Lieber *et al.*, Triphasic helical CT of the kidneys: contribution of vascular phase scanning in patients before urologic surgery. *AJR Am J Roentgenol*, **173** (1999), 1273–7.
4. R. H. Cohan, L. S. Sherman, M. Korobkin *et al.*, Renal masses: assessment of corticomedullary-phase and nephrographic-phase CT scans. *Radiology*, **196** (1995), 445–51.
5. B. A. Birnbaum and J. E. Jacobs, Multiphasic renal CT: comparison of renal mass enhancement during the corticomedullary and nephrographic phases. *Radiology*, **200** (1996), 753–8.
6. D. H. Szolar, F. Kammerhuber, S. Altziebler *et al.*, Multiphasic helical CT of the kidney: increased conspicuity for detection and characterization of small ($<$ 3-cm) renal masses. *Radiology*, **202** (1997), 211–17.
7. B. R. Herts, D. M. Einstein, and D. M. Paushter, Spiral CT of the abdomen: artifacts and potential pitfalls. *AJR Am J Roentgenol*, **161** (1993), 1185–90.
8. R. K. Zeman, Z. Zeiberg, W. S. Hayes *et al.*, Helical CT of renal masses: the value of delayed scans. *AJR Am J Roentgenol*, **167** (1996), 771–6.
9. L. Kopka, U. Fischer, G. Zoeller *et al.*, Dual-phase helical CT of the kidney: value of the corticomedullary and nephrographic phase for evaluation of renal lesions and preoperative staging of renal cell carcinoma. *AJR Am J Roentgenol*, **169** (1997), 1573–8.
10. B. I. Yuh, R. H. Cohan, I. R. Francis *et al.*, Comparison of nephrographic and excretory phase renal helical CT. *Canad Assoc Radiol J*, **51** (2000), 170–6.
11. S. K. Sussman, F. F. Illescas, J. P. Opalacz *et al.*, Renal streak artifact during contrast enhanced CT: comparison of high versus low osmolality contrast media. *Abdom Imaging*, **18** (1993), 180–5.
12. S. Takebayashi, H. Hidai, T. Chiba *et al.*, Using helical CT to evaluate renal cell carcinoma in patients undergoing hemodialysis: value of early enhanced images. *AJR Am J Roentgenol*, **172** (1999), 429–33.

13. K. A. Kim, J. W. Choi, C. M. Park *et al.*, Unusual renal cell carcinomas: a pictorial essay. *Abdom Imag*, **31** (2006), 154–63.
14. G. M. Israel and M. A. Bosniak, How I do it: evaluating renal masses. *Radiology*, **236** (2005), 441–50.
15. E. M. Hecht, G. M. Israel, G. A. Krinsky *et al.*, Renal masses: quantitative analysis of enhancement with signal intensity measurements versus qualitative analysis of enhancement with image subtraction for diagnosing malignancy at MR imaging. *Radiology*, **232** (2004), 373–8.
16. J. H. Wang, P. Q. Min, P. J. Wang *et al.*, Dynamic CT evaluation of tumor vascularity in renal cell carcinoma. *AJR Am J Roentgenol*, **186**:5 (2006), 1423–30.
17. M. Garant, M. Bonaldi, P. Taourel *et al.*, Enhancement patterns of renal masses during multiphase helical CT acquisitions. *Abd Imag*, **23** (1998), 431–6.
18. M. Jinzaki, A. Tanimoto, M. Mukau *et al.*, Double-phase helical CT of small renal parenchymal neoplasms: correlation with pathologic findings and tumor angiogenesis. *J Comput Assist Tomogr*, **26** (2000), 835–42.
19. M. Macari and M. A. Bosniak, Delayed CT to evaluated renal masses incidentally discovered at contrast-enhanced CT: demonstration of vascularity with deenhancement. *Radiology*, **213** (1999), 674–80.
20. S. L. Voci, R. H. Gottlieb, P. J. Fultz *et al.*, Delayed computed tomographic characterization of renal masses: preliminary experience. *Abdom Imag*, **25** (2000), 317–21.
21. D. D. Maki, B. A. Birnbaum, D. P. Chakraborty *et al.*, Renal cyst pseudoenhancement: beam hardening effects on CT numbers. *Radiology*, **213** (1999), 468–72.
22. C. H. Coulam, D. H. Sheafor, R. A. Leder *et al.*, Evaluation of pseudoenhancement of renal cysts during contrast-enhanced CT. *AJR Am J Roentgenol*, **174** (2000), 493–8.
23. B. A. Birnbaum, D. D. Maki, D. P. Chakraborty *et al.*, Renal cyst pseudoenhancement: evaluation with an anthropomorphic body CT phantom. *Radiology*, **225** (2002), 83–90.
24. M. A. Bosniak. The current radiological approach to renal cysts. *Radiology*, **158** (1986), 1–10.
25. S. Ronson, H. A. Frazier, J. D. Baluch *et al.*, Cystic renal masses: usefulness of the Bosniak classification. *Urol Radiol*, **13** (1991), 83–90.
26. C. L. Siegel, E. G. McFarland, J. A. Brink *et al.*, CT of cystic renal masses: analysis of diagnostic performance and interobserver variation. *AJR Am J Roentgenol*, **169** (1997), 813–18.
27. N. S. Curry, S. T. R. Cochran, and N. K. Bissada, Cystic renal masses: accurate Bosniak classification requires adequate renal CT. *AJR Am J Roentgenol*, **175** (2000), 339–42.
28. O. Benjaminov, M. Atri, M. O'Malley *et al.*, Enhancing component on CT to predict malignancy in cystic renal masses and interobserver agreement of different CT features. *AJR Am J Roentgenol*, **186** (2006), 665–72.
29. D. S. Hartman, W. Ellsworth, W. B. Laskin *et al.*, Cystic renal cell carcinoma: CT findings mimicking a benign hyperdense cyst. *AJR Am J Roentgenol*, **159** (1992), 1235–6.
30. T. E. Wilson, E. A. Doelle, R. H. Cohan *et al.*, Cystic renal masses: a re-evaluation of the usefulness of the Bosniak system *Acad Radiol*, **3** (1996), 564–70.

31. G. M. Israel, N. Hindman, and M. A. Bosniak, Evaluation of cystic renal masses: comparison of CT and MR imaging by using the Bosniak classification system. *Radiology*, **231** (2004), 365–71.
32. M. A. Bosniak, A. J. Megibow, D. H. Hulnick *et al.*, CT diagnosis of renal angiomyolipoma: the importance of detecting small amounts of fat. *AJR Am J Roentgenol*, **151** (1988), 497–501.
33. S. G. Silverman, G. D. N. Pearson, and S. E. Seltzer, Small (< 3 cm) hyperechoic renal masses: comparison of helical and conventional CT for diagnosing angiomyolipoma. *AJR Am J Roentgenol*, **167** (1996), 877–81.
34. E. Simpson and U. Patel, Diagnosis of angiomyolipoma using computed tomography-region of interest $<$ or $=$ –10 HU or 4 adjacent pixels $<$ or $=$ –10 HU are recommended as the diagnostic thresholds *Clin Radiol*, **61** (2006), 410–16.
35. G. M. Israel, N. Hindman, E. Hecht *et al.*, The use of opposed-phase chemical shift MRI in the diagnosis of renal angiomyolipomas. *AJR Am J Roentgenol*, **194** (2005), 1868–72.
36. O. Helenon, Y. Chretien, F. Paraf *et al.*, Renal cell carcinoma containing fat: demonstration with CT. *Radiology*, **188** (1993), 429–30.
37. M. Strotzer, K. B. Lehner, and K. Becker, Detection of fat in a renal cell carcinoma mimicking angiomyolipoma. *Radiology*, **188** (1993), 427–8.
38. D. R. Radin and P. Chandrasoma, CT demonstration of fat density in renal cell carcinoma. *Acta Radiologica*, **33** (1992), 365–7.
39. S. Merran, A. Vieillefond, M. Peyromaure *et al.*, Case report: renal angiomyolipoma with calcification: CT-pathology correlation. *Br J Radiol*, **77** (2004), 782–3.
40. T. Akkad, A. Tsankov, A. Pelzer *et al.*, Case report: early diagnosis and straight forward surgery of an asymptomatic primary angiosarcoma of the kidney led to long-term survival. *Int J Urol*, **13** (2006), 1112–14.
41. H. J. Kim, C. H. Kim, Y. J. Choi *et al.*, Juxtaglomerular cell tumor of kidney with CD34 and CD117 immunoreactivity: report of five cases. *Arch Pathol Lab Med*, **130** (2006), 707–11.
42. C. W. Mak, C. K. Chou, and W. S. Tzeng, Renal capsular leiomyoma: report of a case with unusual CT appearance. *Acta Radiol*, **47** (2006), 752–4.
43. Y. Owari, R. Konda, S. Omori *et al.*, Case report: myxoma of the kidney. *Int J Urol*, **13** (2006), 987–9.
44. E. E. Rutherford, J. L. Manners, J. M. Smart *et al.*, Renal haemangioma: a diagnostic challenge. *Clin Radiol*, **61** (2006), 370–3.
45. K. Tuncali, E. vanSonnenberg, S. Shankar *et al.*, Evaluation of patients referred for percutaneous ablation of renal tumors: importance of a preprocedural diagnosis. *AJR Am J Roentgenol*, **183** (2004), 575–82.
46. D. A. Duchene, Y. Lotan, J. A. Cadeddu *et al.*, Histopathology of surgically managed renal tumors: analysis of a contemporary series. *Urology*, **62** (2003), 827–30.
47. I. Frank, M. L. Blute, J. C. Cheville *et al.*, Solid renal tumors: an analysis of pathological features related to tumor size. *J Urol*, **170**:6 (part 1) (2003), 2217–20.
48. J. Hafron, J. D. Fogarty, D. M. Hoenig *et al.*, Imaging characteristics of minimal fat renal angiomyolipoma with histologic correlations. *Urology*, **66** (2005), 1155–9.

49. J. K. Kim, S. U. Park, J. H. Shon *et al.*, Angiomyolipoma with minimal fat: differentiation from renal cell carcinoma at biphasic helical CT. *Radiology*, **230** (2004), 677–84.
50. M. Jinzaki, S. G. Silverman, A. Tanimoto *et al.*, Angiomyolipomas that do not contain fat attenuation at unenhanced CT. *Radiology*, **234** (2005), 311–12.
51. J. K. Kim, S. H. Kim, Y. J. Jang *et al.*, Renal angiomyolipoma with minimal fat: differentiation from other neoplasms at double-echo chemical shift FLASH MR imaging. *Radiology*, **239** (2006), 174–80.
52. R. H. Cohan, N. R. Dunnick, G. E. Degesys *et al.*, Computed tomography of renal oncocytoma. *J Comput Asst Tomogr*, **8** (1984), 284–7.
53. T. Gudbjartsson, H. Hardarson, V. Petursdottir *et al.*, Renal oncocytoma: a clinicopathological analysis of 45 consecutive cases. *BJU Int*, **96** (2005), 1275–9.
54. A. Lopez-Beltran, M. Scarpelli, R. Montironi *et al.*, 2004 WHO classification of the renal tumors of the adults. *Eur Urol*, **49** (2006), 798–805.
55. R. H. Cohan, N. R. Dunnick, R. A. Leder *et al.*, Computed tomography of renal lymphoma. *J Comput Asst Tomogr*, **14** (1990), 933–8.
56. S. Seth, S. Ali, and E. Fishman, Imaging of renal lymphoma: patterns of disease with pathologic correlation. *Radiographics*, **26** (2006), 1151–68.
57. P. L. Choyke, M. M. Walther, G. M. Glenn *et al.*, Imaging features of hereditary papillary renal cancers. *J Comput Assist Tomogr*, **21** (1997), 737–41.
58. B. R. Herts, D. M. Coll, A. C. Novick *et al.*, Enhancement characteristics of papillary renal neoplasms revealed on triphasic helical CT of the kidneys. *AJR Am J Roentgenol*, **178** (2002), 367–72.
59. J. H. Mydlo, R. Weinstein, R. Misseri *et al.*, Radiologic, pathologic, and molecular attributes of two types of papillary renal adenocarcinomas. *Scand J Urol Nephrol*, **35** (2001), 262–9.
60. C. Roy, B. Sauer, V. Lindner *et al.*, MR imaging of papillary renal neoplasms: potential application for characterization of small renal masses. *Eur Radiol*, **17** (2007), 193–200.
61. E. K. Outwater, M. Bhatia, E. S. Siegelman *et al.*, Lipid in clear cell carcinoma: detection on opposed-phase gradient-echo MR images. *Radiology*, **205** (1997), 39–40.
62. S. K. Yoon, K. J. Nam, S. H. Rha *et al.*, Collecting duct carcinoma of the kidney: CT and pathologic correlation. *Eur J Radiol*, **57**:3 (2006), 453–60.
63. A. J. Davidson, P. L. Choyke, D. S. Hartman *et al.*, Renal medullary carcinoma associated with sickle cell trait: radiologic findings. *Radiology*, **195** (1995), 83–5.
64. M. A. Bosniak, B. A. Birnbaum, G. A. Krinsky *et al.*, Small renal parenchymal neoplasms: further obervations on growth. *Radiology*, **197** (1995), 589–97.
65. A. Volpe, T. Panzarella, R. A. Rendon *et al.*, The natural history of incidentally detected renal masses. *Cancer*, **100** (2004), 738–45.
66. G. W. A. Lamb, E. J. Bromwich, P. Vasey *et al.*, Management of renal masses in patients medically unsuitable for nephrectomy – natural history, complications, and outcome. *Urology*, **64** (2004), 909–13.

67. N. S. Curry, Imaging the small solid renal mass. *Abd Imag*, **27** (2002), 629–636.
68. S. F. Hain and M. N. Maisey, Positron emission tomography for urological tumors. *BJU Int*, **92** (2003), 159–64.
69. S. C. Cherng, C. Y. Chang, Y. M. Fan *et al.*, CT with anatomic delineation identifying renal cell carcinoma with normal metabolic activity on F-18 FDG PET imaging. *Clin Nuc Med*, **31** (2006), 490–1.
70. J. Ak and C. Can, F-18 FDG PET in detecting renal cell carcinoma. *Acta Radiol*, **46** (2005), 895–9.
71. M. A. Bosniak and N. M. Rofsky, Problems in the detection and characterization of small renal masses. *Radiology*, **198** (1996), 638–41.
72. B. A. Birnbaum, M. A. Bosniak, A. J. Megibow *et al.*, Observations on the growth of renal neoplasms. *Radiology*, **176** (1990), 695–701.

5

Staging of renal cancer

Giles Rottenberg and Sheila C. Rankin

Introduction: Why stage disease?

The staging of renal tumors is important as it divides them into groups that enable a logical framework for treatment planning, entry into clinical trials, and prognostication. With the increasing use of techniques such as nephron-sparing surgery and laparoscopic surgery the radiological staging information will determine the type of surgical approach. Also, unlike surgery which provides tissue for pathological staging, ablative therapies such as cryotherapy or radiofrequency ablation rely solely on radiological staging, with the occasional benefit of renal biopsy.

History of staging

The first staging system for renal tumors was introduced by Flocks and Kadesky in 1958 and subsequently modified by Robson in 1963 [1]. The TNM criteria was introduced in 1978 and revised in 1987, 1997, and most recently in 2002 (Table 5.1). These modifications reflected a change in surgical approach and better understanding of the survival characteristics of the different groups.

The 1997 AJCC (American Joint Committee on Cancer) revision resulted in reclassification of T1 lesions from confined tumors less than or equal to 2.5 cm to those lesions 7 cm or less. Confined tumors measuring greater than 7 cm were classified as T2. A subsequent study demonstrated an 83% 5-year survival for T1 tumors with a 57% 5-year survival for T2 tumors [2]. This major difference in prognosis underlies the rationale for the division between T1 and T2 tumors. The classification of T1 tumors was revised in 2002, as a result of the increased use of partial nephrectomy, and to allow further stratification of prognostic information. T1 stage tumors were divided into T1a tumors that were 4 cm or less in maximal

Carcinoma of the Kidney, ed. Uday Patel. Published by Cambridge University Press.

Table 5.1. The 2002 AJCC TNM staging system for renal cell carcinoma

TX	Primary tumor cannot be assessed
T0	No evidence of primary tumor
T1	Tumor 7 cm or less in greater dimensions and limited to the kidney
T1a	Tumor 4 cm or less and limited to the kidney
T1b	Tumor more than 4 cm but not more than 7 cm in greatest diameter
T2	Tumor more than 7 cm in greatest diameter and limited to the kidney
T3	Tumor extends into the major veins, adrenal gland, or outside the kidney
T3a	Tumor directly invades adrenal gland or perirenal and/or renal sinus fat but not beyond Gerota's fascia
T3b	Tumor grossly extends into the renal vein, or the vena cava below the diaphragm
T3c	Tumor grossly extends into the vena cava above the diaphragm
T4	Tumor invades beyond Gerota's fascia
Nx	Regional nodes cannot be assessed
N0	No regional lymph node metastases
N1	Metastasis in single regional lymph node
N2	Metastasis in more than one regional lymph node
MX	Distant metastases cannot be assessed
M0	No distant metastasis
M1	Distant metastasis
AJCC stage groupings	
Stage 1	T1 N0 M0
Stage 2	T2 N0 M0
Stage 3	T1 N1 M0, T2 N1 M0, T3 N0 M0, T3 N1 M0
Stage 4	Any T4, Any T N2, Any T Any N M1

diameter, and T1b tumors that were greater than 4 cm but less than 7 cm. The 2002 sub-classification has been validated as providing excellent stratification of patients according to cancer-specific survival [3]. Subdivision of T2 stage tumors into T2a and T2b with a cut-off size of 10 cm has been recently suggested to further improve the prognostic accuracy, but has not yet been adopted [4].

Techniques for staging

Techniques for diagnostic imaging of renal cell carcinoma (RCC) are discussed in detail in Chapter 4 of this book but it should be stressed that meticulous

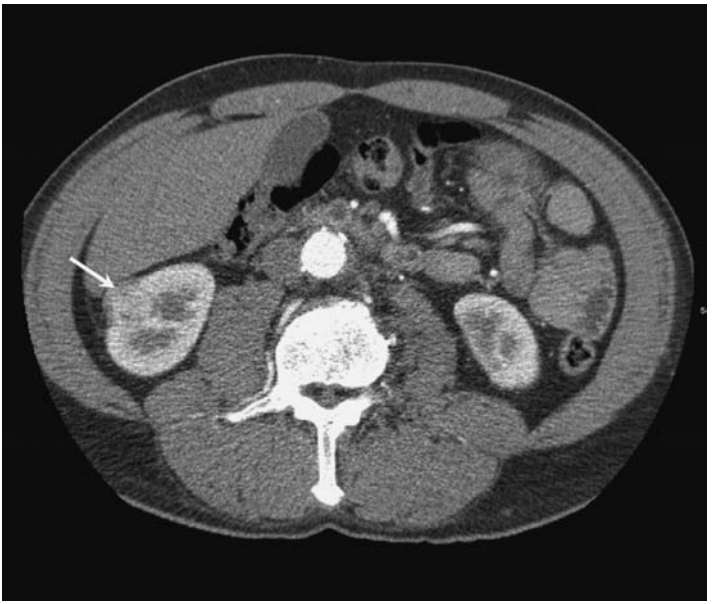

Figure 5.1 T1a N0 Renal cell carcinoma. There is a small renal tumor arising from the lateral aspect of the right kidney (arrow). This is a typical example of the sort of tumor that is an incidental finding on CT or ultrasound and ideal for a nephron-sparing procedure.

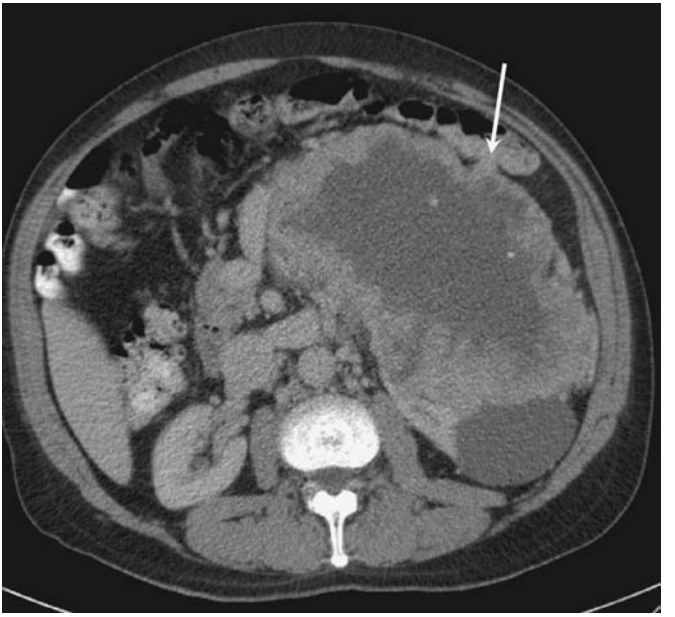

Figure 5.2 T2 Renal cell carcinoma. A 30-year-old man presented with hematuria and was discovered to have a large centrally necrotic left-sided renal tumor. The mass crosses the mid-line and extends up to loops of small bowel (arrow). Surgery confirmed the presence of a large tumor but contrary to the preoperative imaging, which suggested invasion of adjacent organs, the tumor was found to be pT2.

technique is vital for the optimal staging of tumors as well and is illustrated in Figures 5.1, 5.2, and 5.3. Either computed tomography (CT) or magnetic resonance imaging (MRI) can be used for abdominal staging, but overall CT is preferred as the thorax can also be imaged. Ultrasound and positron

Figure 5.3 T2 N0 Renal cell carcinoma. Contrast-enhanced CT demonstrates an enhancing right renal mass which extends up to the right psoas muscle. There is loss of the fat plane (arrow) which was thought to suggest invasion. Surgery demonstrated an intact renal capsule with no infiltration of surrounding structures and pathological analysis confirmed the presence of T2 disease.

emission tomography (PET) have limited trouble-shooting roles as further discussed below.

For renal tumor staging all the phases of renal enhancement discussed in the last chapter have a role. Imaging at 30–40 seconds post-contrast provides optimal enhancement of the renal vein for assessment of venous invasion. Later phase (nephrographic) studies are also crucially important for staging as the kidneys and the other organs are seen more uniformly enhanced. Local, perinephric infiltration as well as invasion or metastasis to the other abdominal organs can be assessed. It is worth stressing that in addition to staging the tumor, a careful examination of the contralateral kidney should be performed, as up to 2% of patients may have a synchronous tumor [5]. The nephrographic phase is the best for identification of synchronous tumours (whether contralateral or on the same side). This may prompt the surgeon to consider partial nephrectomy as an alternative to radical surgery (Figure 5.1).

Staging

T Staging

Differentiating T1/T2 disease

This is dependent on tumor size (Table 5.1). Measurement of renal tumors should be made in their maximum transverse diameter for staging. The size measured at

CT correlates very well with size at pathological analysis although the pathological measurements may be slightly smaller because of blood volume losses and fixation. The widespread use of cross-sectional imaging has resulted in increasingly large numbers of early stage tumors which are often felt to be of low grade potential. However a recent study of over 200 tumors demonstrated a 28% incidence of high nuclear grade tumors and a 38% incidence of T3 disease in tumors less than 3 cm in size. Tumors that were between 3 and 5 cm in size did not have a significantly worse T stage than the smaller lesions although the tumors that exceeded 5 cm had a higher incidence of T3 stage (65% versus 38%) [6].

Differentiating T2/T3 disease

Differentiating T1 and T2 tumors from T3 disease is difficult even with good technique and equipment and is responsible for 50% of staging errors [7]; as illustrated by Figures 5.4 and 5.5. The presence of perinephric stranding is an unreliable indicator of T3 disease as it can be seen in 50% of T1 and T2 tumors. Stranding may be caused by edema, vascular engorgement, or fibrosis because of previous infection. The presence of an enhancing nodule of tumor is the most reliable indicator of extra-capsular extension but has a sensitivity of only 46% and a specificity of 98% [8]. It will always be difficult to exclude microscopic

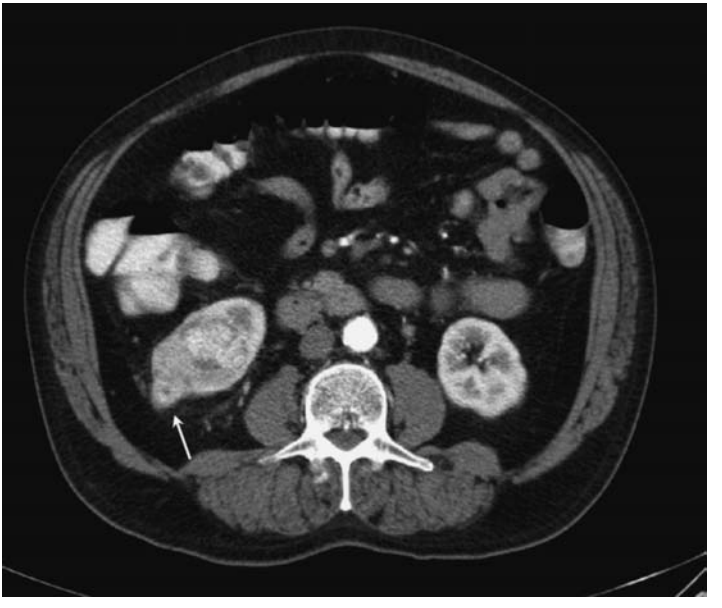

Figure 5.4 T3a Renal cancer. Contrast-enhanced CT demonstrates a right-sided lower pole renal tumor. Although small, it has an irregular lobulated contour extending into the perinephric fat (arrow). This was confirmed at surgery to be a T3a tumor.

Figure 5.5 Axial CT demonstrates an exophytic mass arising from the right kidney. Pathological analysis following radical nephrectomy confirmed the presence of T3 disease.

capsular penetration with conventional imaging techniques, but it is reassuring to note that a recent retrospective study demonstrated that tumors initially classified as T1 but upgraded on pathological analysis to T3a showed the same recurrence-free survival rate as patients with pathologically confirmed T1 lesions [9].

Magnetic resonance imaging offers little advantage over CT in the T staging with the correct T stage in 81%–86% [10], but with overstaging of T2 tumors especially if the tumor surface is nodular. Narumi *et al*. reported 62%–81% accuracy for MRI in assessing local extension into the perinephric fat, with an overall sensitivity of 60%–70% and a specificity of 94% [11]. Although extension into the perinephric fat may not be significant if a nephrectomy is performed it may preclude nephron-sparing surgery. The identification of an intact pseudocapsule on MRI is a sign of lack of perinephric invasion with a reported sensitivity 86%, specificity 95%, positive predictive value (PPV) 95%, and negative predictive value (NPV) 88% [12]. Most tumors are slightly hyperintense on T2 W and hypointense on T1 W sequences compared to normal renal cortex and demonstrate intense enhancement on early post-contrast studies with washout in the interstitial phase. Smaller tumors may be better seen on the interstitial phase. Hemorrhage occurs quite commonly in tumors in patients with renal failure and will be high signal

on non-contrast T1 W and overall MRI may be better than CT for identifying renal cancers in the presence of renal failure.

Identifying T3b/c disease

Renal cell carcinomas have a tendency to demonstrate vascular invasion and renal vein disease can be seen in 23% of patients, with disease in the IVC identified in 4%–10% [13]. Accurate delineation of the extent of thrombus in the IVC is a crucial part of staging tumours as it radically alters the surgical approach and also can reduce the risk of tumour thrombus during surgery. Extension of thrombus into the chest or right atrium may require cardiac bypass to allow complete resection of disease.

Computed tomography for assessment of venous invasion

Magnetic resonance imaging has historically been used for this purpose owing to its multiplanar demonstration although most cases can be more than adequately displayed on good quality CT examination (Figures 5.6a and b), assuming the contrast delivery and timing are adequate. Recent studies comparing MDCT (multi-detector computed tomography) and MRI for staging patients with suspected caval disease have demonstrated similar staging results [14]. A recent study, albeit with small numbers, has even suggested that CT can outperform MRI in

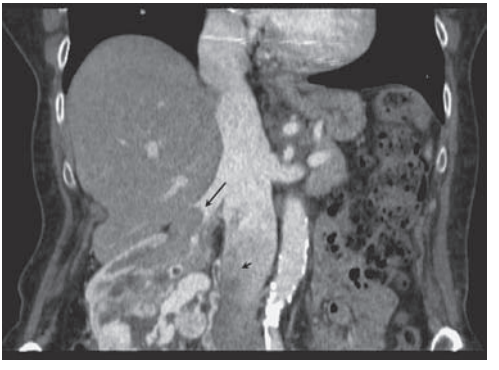

(a)

Figure 5.6a Coronal CT demonstrates thrombus in the right renal vein (long arrow) but not extending into the vena cava. There is unopacified blood from the lower limbs in the vena cava below the renal vein (short arrow).

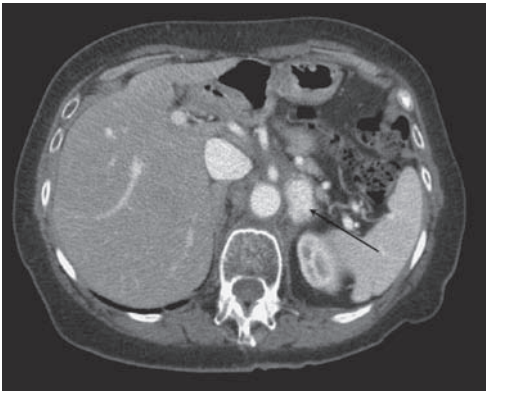

(b)

Figure 5.6b This image demonstrates an enlarged, richly enhancing left para-aortic lymph node (arrow) secondary to metastatic renal cancer.

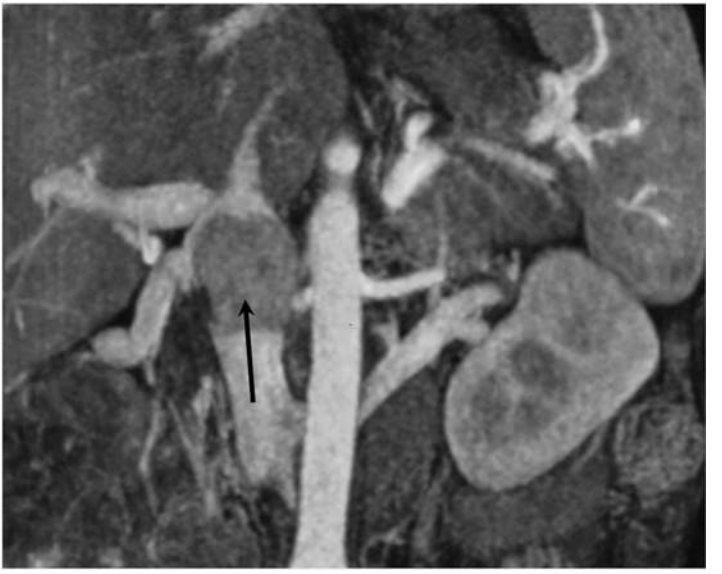

Figure 5.7 Coronal MR angiogram demonstrates a large thrombus in the inferior vena cava (arrow). Magnetic resonance imaging has been shown to be more accurate than CT in differentiating bland from tumor thrombus and for demonstration of venous wall invasion.

assessing the upper level of tumor invasion. [15]. MDCT is accurate at detecting renal vein thrombus with a PPV of 92% and a NPV of 97% [16]. The optimal timing for assessment of venous invasion is the late corticomedullary phase (around 60 seconds) of enhancement. The presence of a filling defect in an otherwise well-opacified vein is the most reliable direct sign of thrombus. Enlargement of the vessel and the presence of venous collaterals may also be useful surrogate indicators, although these features can also be seen in patients with large vascular tumors. It is possible to differentiate bland thrombus from tumor thrombus by the presence of thrombus enhancement although it has been demonstrated that MRI is more accurate than CT for this [17]. If the thrombus is in direct continuity with the tumor this may suggest that the thrombus is not bland (Figure 5.7).

But there are potential pitfalls. False-positive diagnosis of clot can be caused by artifact from the infra-renal unopacified blood mixing with the opacified blood from the renal veins. It is important not to diagnose thrombus in the IVC when the renal veins are well opacified and appear normal. If there is doubt following CT examination of the renal vein, a Doppler ultrasound examination of the IVC can be considered and occasionally a repeat CT with bolus tracking of contrast in the IVC can be undertaken. Patients with IVC thrombus, but without IVC wall invasion or metastases, have an encouraging prognosis if the tumor is completely resected

(32%–64% 5-year survival). The extent of IVC disease, in the absence of invasion, has little impact on long-term survival apart from the perioperative mortality from surgery in these cases.

Magnetic resonance imaging for assessment of venous invasion

MRI is very good for the detection of venous thrombus and for distinguishing blood (bland) clot from tumor thrombus using gadolinium-enhanced spoiled gradient echo or fat-suppressed sequences. Tumor thrombus enhances whereas bland clot does not. Subacute thrombus may be high signal on pre-contrast images so signal intensity measurements before and after contrast may be required to identify enhancement. MRI is superior to CT for the identification of tumor thrombus (MRI 90%, CT 79%) [17]. Although differentiation between the two may not change surgical management, it may change technique as tumor thrombus may be adherent to the wall, requiring resection of the wall and vascular reconstruction. Invasion of the wall of the IVC is diagnosed if there is enhancement of the wall or tumor seen on either side of the wall [18].

Ultrasound for assessment of venous invasion

The role of US in assessing venous invasion has reduced over the years with the increased availability of high quality CT and MRI. A recent study of 44 patients with renal carcinoma demonstrated an 87% accuracy of US for detecting renal vein tumor and 100% accuracy for the five patients with IVC tumor [19]. Ultrasound should generally be reserved for patients who are unwilling or unable to undertake MRI or contrast-enhanced CT. It may occasionally be of use for problem-solving when the contrast opacification of the vessels on MRI/CT is suboptimal.

T4 disease

T4 disease is present in only 3% of patients at diagnosis and may be difficult to diagnose in the absence of clear soft tissue mass extending into the adjacent organs. The loss of a fat plane, or the presence of an irregular tumor edge are not reliable signs of tumor extension as these are seen in up to 15% of patients. Nevertheless, the presence of such change should be communicated to the surgeon so that the possibility of local invasion is expected. Multiplanar reformatted CT is often helpful for the detection and display of T4 disease and provides a useful aid for

surgical planning. An accuracy of 97%–100% for adjacent organ invasion has been reported with overstaging caused by the absence of a fat plane [20].

N Staging

Lymphovascular invasion

The regional nodes of the kidney include renal hilar, abdominal para-aortic and paracaval regions. The presence of lymph node disease confers a very poor prognosis with reported 5-year survival of between 5% and 30% [21]. The diagnostic accuracy of lymph node disease with CT or MRI is equivalent as it is solely dependent upon the size of the node (Figure 5.8). Assuming a cut-off of 10 mm (short axis), studies have shown a 4% false-negative rate but a false-positive rate of up to 50% because of benign reactive change in the nodes [22]. Other studies have demonstrated better results with a 83% sensitivity and 88% specificity [8].

Benign enlargement of lymph nodes may be caused by venous thrombosis or extensive tumoral necrosis. Nodes that are greater than 2 cm usually contain tumor. Florid nodal enhancement which mirrors the pattern of the primary tumor makes the probability of lymph node disease much higher. Underestimation of lymph node disease may occur when the tumor forms a large conglomerate mass and the individual lymph nodes cannot be separated out from the primary tumor. Lymph node disease that is out of proportion to the size of the primary tumor may indicate

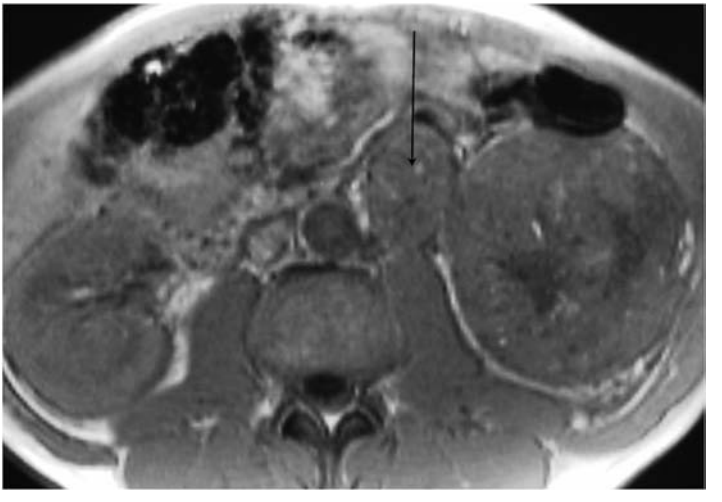

Figure 5.8 Magnetic resonance imaging demonstrates a large left-sided para-aortic lymph node mass (arrow). Magnetic resonance imaging was performed in preference to CT in this patient because of a previous reaction to iodinated contrast but in general MRI does not provide any supplementary information to CT for most cases of renal cancer.

renal lymphoma, and biopsy should be considered. Although ultrasmall iron oxide particles have been used for MR lymphangiography with very good results in bladder cancer [23], there have been no large studies undertaken in RCC [24].

The presence of lymphadenopathy does not necessarily alter management as patients will usually still proceed to nephrectomy and local lymph node clearance. Thus, the presence of nodal disease may alter surgical planning. The role of radical lymph node dissection is highly contentious and is not supported by a randomized trial [25]. It is suggested that lymph node disease is usually associated with the presence of distant metastases although there may be a small group of patients in whom radical lymph node dissection has a beneficial effect on survival.

M Staging

Metastases

Thirty percent of patients with RCC have metastatic disease at presentation [26]. Metastatic disease usually occurs within 2–4 years of surgery [27] but can be seen in up to 11% of patients by 10 years [28]. The incidence of metastases is higher with larger tumors and in those with vascular or local invasion (Figure 5.9). The

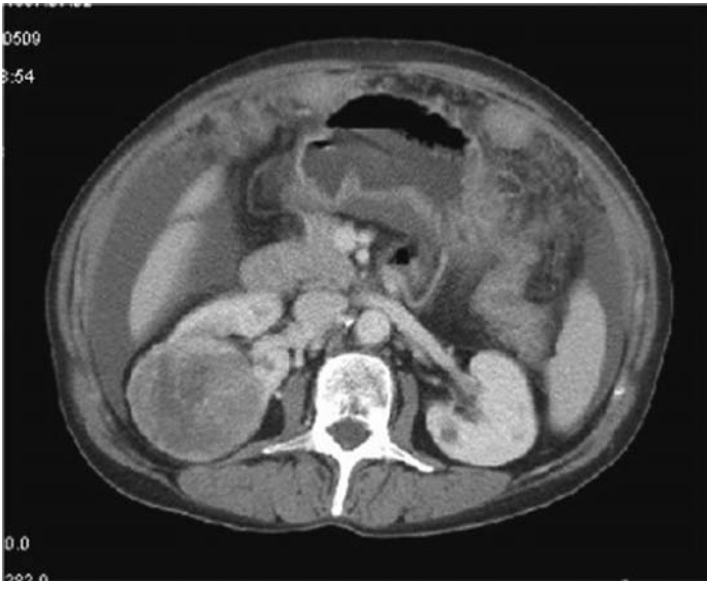

Figure 5.9 Computed tomography demonstrates a large right-side renal mass associated with abundant ascites and peritoneal disease. Although peritoneal metastases can be seen in advanced renal cell tumor, on this occasion the renal tumor was an incidental finding on a staging CT for the patients' known ovarian cancer. Nephrectomy confirmed the diagnosis of renal cell cancer.

common sites of metastases include the lung, mediastinum, bones, and liver. Other sites include the brain, pancreas, mesentery, contralateral kidney or adrenal gland, and the abdominal wall. The radiological appearance of metastatic disease may mimic the primary tumor and hypervascular bone, liver, or cutaneous lesions are not infrequently seen. Detection of hypervascular liver lesions is improved by performing CT of the liver in the arterial phase.

Adrenal invasion

The incidence of adrenal metastases at diagnosis has been reported as 4.3% [29]. It is more common with large upper pole tumors and in those with associated vascular invasion. A large study of patients with renal cancer demonstrated that the presence of a normal adrenal gland on CT prior to surgery was associated with a 100% NPV for tumor. But conversely, an abnormal adrenal gland on CT criteria does not necessarily imply invasion. The incidence of malignancy was only 24% in those patients who had enlargement, displacement, or non-visualization of the adrenal gland [30]. A more recent study of over 200 patients with renal cancer demonstrated similar results with a 99% NPV for adrenal metastasis and a 37% PPV. There was a strong correlation between tumor stage and the probability of adrenal metastatic disease [31] as demonstrated by the example shown in Figure 5.10. The poor PPV is because adrenal adenomas are a common incidental finding (10% of patients over 60). Adenomas can be differentiated from metastases using in- and out-of-phase MRI. A recent study [32] found MRI

Figure 5.10 Metastatic cancer spread to the contralateral adrenal gland. A 55-year-old man with a 10-year history of renal cancer with multiple local recurrences presents with a new enhancing metastasis in the left adrenal gland (long arrow). Note the previous right nephrectomy for cancer, with a caval graft (short arrow) performed for caval invasion.

Figure 5.11 Incidental pulmonary nodule (circled) discovered on staging a new renal cancer. This lesion is too small to classify as a definite metastasis and is too small for PET. A follow-up CT chest was performed at 6 months and 1 year post-surgery, and confirmed an absence of growth of the lesion, which was assumed to be benign (see also color plate section).

(a)

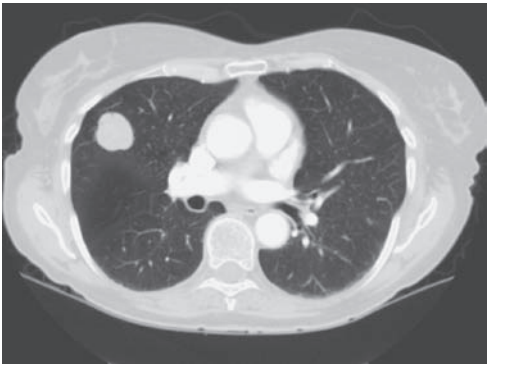

(b)

Figure 5.12 Computed tomography of the chest in a patient with known renal cancer demonstrates a solid lung nodule in the right mid zone which had increased in size over a 3-month period of observation in keeping with a metastasis. If there is a solitary lung lesion, a primary lung carcinoma should be excluded.

was 89% sensitive, 99% specific, and 93.9% accurate in identifying adrenal metastases.

Pulmonary nodules

Pulmonary metastases are common in RCC and can be found at initial diagnosis in up to 20% of individuals and at autopsy in 50%–75% of patients (Figures 5.11 and 5.12). Lung deposits are usually multiple and spherical, and more frequent in the lower and outer third of the lungs. They may all be of a similar size because of a shower of tumor. Chest radiography may demonstrate a

solitary nodule, but CT will normally demonstrate many more unsuspected masses. Although calcification and cavitation is uncommon in RCC, hemorrhagic metastases can be seen which produce areas of ground glass density surrounding the nodules.

With the expansion in the use of MDCT, chest CT is now becoming routine for tumor staging, leading to an increased detection of small pulmonary nodules. When large the diagnosis is not usually in doubt, but with tiny nodules (< 1 cm) it can be difficult to confidently diagnose metastasis. Benign lesions such as hamartoma, granuloma, sarcoidosis, and infarcts may mimic metastases and it is important to consider these particularly in the patient with the smaller primary tumor. A synchronous primary lung carcinoma should also be considered particularly with a spiculated lesion. Incidental nodules are an especial problem in areas where histoplasmosis and tuberculosis are endemic. Positron emission tomography may be useful if the lesions are 1 cm or greater in size but smaller lesions may not demonstrate significant PET uptake.

The presence of multiple tiny nodules should not alter the primary management of RCC as debulking surgical nephrectomy is usually the initial treatment of choice. If there is a solitary pulmonary nodule which is highly suspicious of a metastasis, surgical metastatectomy may be indicated although a period of observation or biopsy can be considered, which will prevent unnecessary surgery on benign lesions.

Positron emission tomography for staging of renal cancer

Positron emission tomography is an imaging technique that can map functional and metabolic activity before structural changes have taken place and is well established for the staging of many malignancies. PET scanning using 2-^{18}fluoro-2-deoxy-D-glucose (^{18}FDG) can differentiate malignant from normal tissue based on enhanced glycolysis by tumor cells and increased expression of glucose transporters (GLUT-1) at its surface. Renal tumors exhibit these features but as FDG is excreted via the renal tract the perception is that the accuracy may be less than in other tumors.

Primary tumor

The original study by Wahl *et al.* identified five out of five tumors [33] but results of later studies were more variable and are shown in Table 5.2 [33,34,35,36,37,38]. In a study of 29 patients [34] PET identified 20 of the 26 renal cell cancers with 6

Table 5.2. Summary of studies of renal cell cancer with FDG-PET

Authors	Number of tumors	Sensitivity FDG-PET(%)
Wahl *et al.* [33]	5	100
Bachor *et al.* [34]	26	77
Ramdave *et al.* [35]	16	94
Kang *et al.* [36]	15	60
Kumar *et al.* [39]	8	89
Miyakita *et al.* [37]	19	31
Aide *et al.* [42]	35	47

false-negatives and 3 false-positives including an angiomyolipoma. In a more recent study [35] FDG-PET identified 15 of 16 renal cancers with no false-positives. In six patients (35%) PET altered the management with renal vein thrombus excluded in one, distant metastases found in two, and three being considered eligible for partial nephrectomy; and PET had a similar accuracy (94%) as CT. This high sensitivity has not been matched in other studies with only 9 of 15 tumors appearing hypermetabolic on the study by Kang *et al.*, giving a sensitivity of 60% and a specificity of 100%, compared to 92% and 100% for CT [36]. The detection of the primary tumor is related to size with larger lesions more easily visualized than smaller lesions. The histological type and grading may also be significant [38], although Kumar *et al.* found no difference in uptake between primary renal tumors and metastases to the kidney [39]. The GLUT-1 receptor expression has also been studied. Miyakita *et al.* identified only 6 of 19 (31.5%) renal cancers using FDG-PET and found no correlation between GLUT-1 immunoreactivity and FDG positivity, whereas Miyauchi *et al.* found a positive correlation between GLUT-1 expression and FDG uptake [40].

Metastatic disease

The results of FDG-PET in assessing metastatic disease are also variable. Ramdave *et al.* studied eight patients with metastatic or recurrent disease. PET identified all correctly with a diagnostic accuracy of 100% (CT was 88% accurate) with PET altering management in four cases [35]. However Majhail *et al.* in a study of 21 patients with proven metastases in 33 sites found the sensitivity and specificity of PET was 64% and 100% respectively with a PPV of 100% [41]. The mean size of the positive metastases was 2.2 cm compared to the false-negative size of 1 cm, and

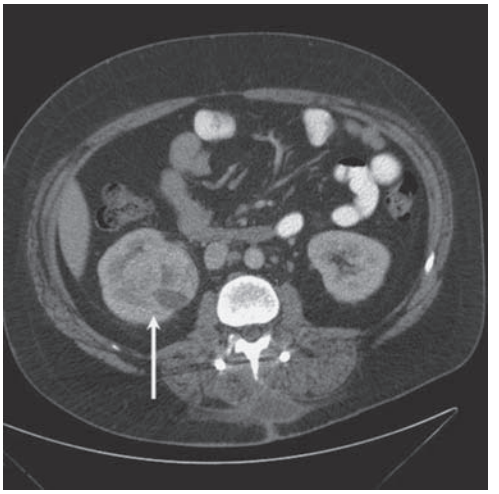

(a)

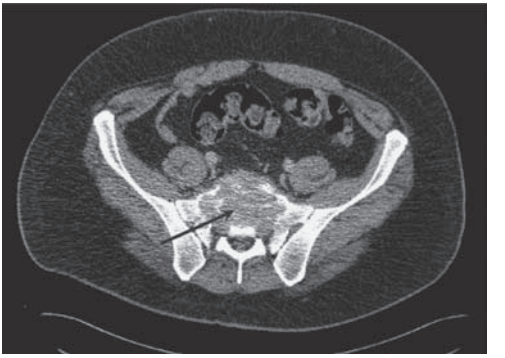

(b)

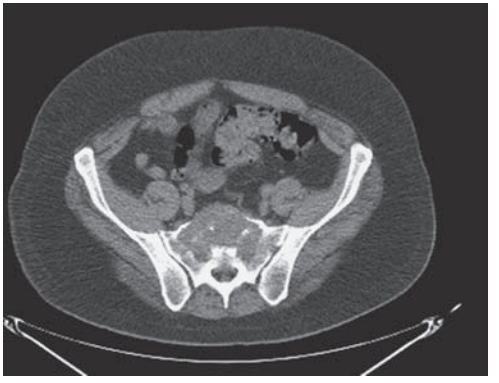

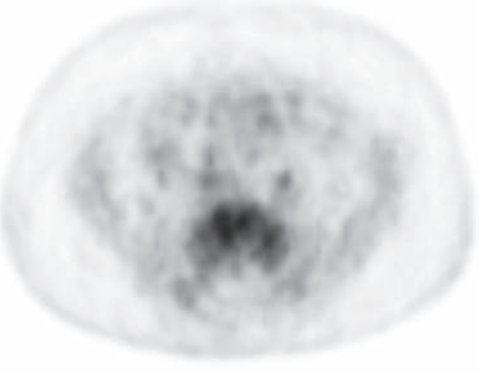

(c)

Figure 5.13 A 25-year-old man presented with back pain. Computed tomography of the abdomen demonstrated a right-sided renal tumor (a) with a large destructive lesion in the sacrum (b, c). CT did not demonstrate any other metastatic disease. A FDG-PET scan was performed (c) prior to palliative sacral surgery for intractable bone pain. FDG-PET did not demonstrate activity in the primary tumor but uptake was demonstrated in the metastatic sacral deposit (see also color plate section).

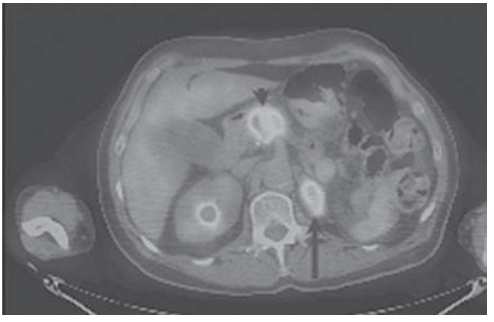

Figure 5.14 A FDG-PET scan in a 55-year-old man with a previous history of renal cell cancer demonstrates marked increased uptake in metastatic deposits in the adrenal gland (long arrow) and pancreas (short arrow) (see also color plate section).

none of the lesion identified on PET were missed by conventional imaging. Aide *et al*. found PET had a sensitivity of 47% for the primary tumor, compared to 97% for CT; but was superior to CT for metastatic disease (accuracy 94%, CT 89%) with PET identifying eight additional sites not seen on CT [32]. Kang *et al*. in a large series found PET was 64% sensitive for soft tissue metastases and 78% sensitive for bone metastases (CT and bone scans gave a combined sensitive of 94%) and found CT more sensitive than PET for lung nodules (91% for CT, 75% for PET). In this study multiple lesions within a patient exhibited different levels of uptake and in 12% PET failed to detect any metastases; however the specificity of PET was higher than CT and bone scans [36]. Some clinical examples are shown in Figures 5.13, 5.14, and 5.15, demonstrating the value of PET in some, but not all, cases of metastatic renal cancer.

Conclusion

Computed tomoraphy will continue to be the investigation of choice for the primary tumor. PET has limited sensitivity for small metastases and a negative

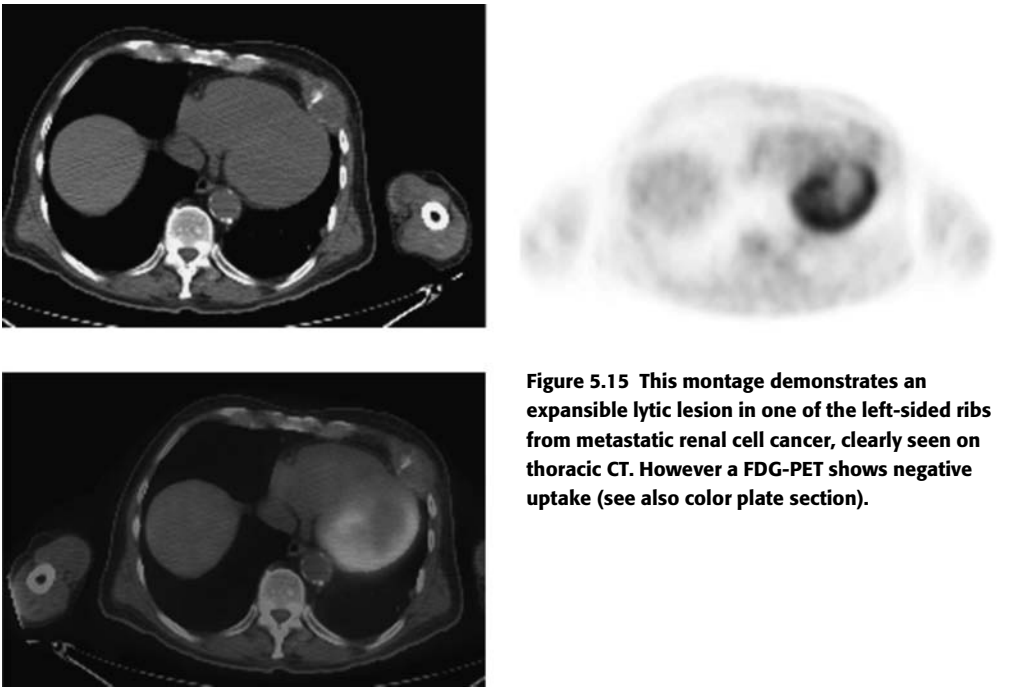

Figure 5.15 This montage demonstrates an expansible lytic lesion in one of the left-sided ribs from metastatic renal cell cancer, clearly seen on thoracic CT. However a FDG-PET shows negative uptake (see also color plate section).

PET does not rule out malignancy but a positive PET should be considered strongly suspicious for metastatic disease and PET may be helpful when equivocal lesions are seen on CT. The use of PET and CT, combining the sensitivity of CT with the specificity of PET, may overcome many of the difficulties.

REFERENCES

1. C. J. Robson, B. M. Churchill, and W. Anderson, The results of radical nephrectomy for renal cell carcinoma. *AJCC*, **101** (1969), 297–301.
2. K. H. Tsui, O. Shvarts, R. B. Smith *et al.*, Prognostic indicators for renal cell carcinoma: a multivariate analysis of 643 patients using the revised TNM staging criteria. *J Urol*, **163** (2000), 1090–5.
3. I. Frank, M. L. Blute, B. C. Leibovich *et al.*, Independent validation of the 2002 American Joint Committee on cancer primary tumour classification for renal cell carcinoma using a large, single institution cohort. *J Urol*, **173**:6 (2005), 1889–992.
4. I. Frank, M. L. Blute, B. C. Leibovich *et al.*, pT2 classification for renal cell carcinoma. Can its accuracy be improved? *J Urol*, **173**:2 (2005), 380–4.
5. F. F. Marshall, A. K. Stewart, and H. R. Menck, National Cancer data base. *Cancer*, **80** (1997), 2167–74.

6. R. M. Hsu, D. Y. Chan, and S. S. Siegelman, Small renal carcinomas: correlation of size with tumour stage, nuclear grade and histological subtype. *AJR Am J Roentgenol*, **182**:3 (2004), 551–7.
7. R. E. Bechtold and R. J. Zagoria, Imaging approach to staging of renal cell carcinoma. *Urol Clin North Am*, **24** (1997), 507–22.
8. C. D. Johnson, N. R. Dunnick, and R. H. Cohan, Renal adenocarcinoma: CT staging of 100 tumours. *AJR Am J Roentgenol*, **148** (1987), 59–63.
9. W. W. Roberts, S. B. Bhayani, M. E. Allaf *et al.*, Pathological stage does not alter the prognosis for renal lesions determined to be stage T1 by computerized tomography. *J Urol*, **173** (2005), 713–15.
10. F. B. Ergin, H. K. Hussain, E. M. Caoili *et al.*, MRI for preoperative staging of renal cell carcinoma using the 1997 TNM classification: comparison with surgical and pathological staging. *AJR Am J Roentgenol*, **182** (2004), 217–25.
11. Y. Narumi, H. Hricak, J. C. Presti, Jr. *et al.*, MR imaging evaluation of renal cell carcinoma. *Abdom Imag*, **22**:2 (1997), 216–25.
12. C. Roy, Sr., S. El Ghali, X. Buy *et al.*, Significance of the pseudocapsule on MRI of renal neoplasms and its potential application for local staging: a retrospective study. *AJR Am J Roentgenol*, **184** (2005), 113–20.
13. D. A. Kallman, B. F. King, R. R. Hatery *et al.*, Renal vein and inferior vena cava tumour thrombus in renal cell carcinoma: CT, US MRI and venacavography. *J Comput Assist Tomogr*, **16**:2 (1992), 240–7.
14. P. J. Hallscheidt, C. Fink, A. Haferkamp *et al.*, Preoperative staging of renal cell carcinoma with inferior vena cava thrombus using multidetector CT and MRI: prospective study with histopathological correlation. *JCAT*, **29**:1 (2005), 64–8.
15. N. Lawretschuk, J. Gani, R. Riordan, S. Esler, and D. M. Bolton, Multidetector computed tomography vs magnetic resonance imaging for defining the upper limit of renal cell carcinoma: a study and review. *BJU Intl*, **96** (2005), 291–5.
16. T. J. Welch and A. J. Le Roy, Helical and electron beam CT scanning in the evaluation of renal vein involvement in patients with renal cell carcinoma. *J Comput Assist Tomogr*, **21** (1997), 467–71.
17. A. Oto, B. R. Herts, E. M. Remer *et al.*, Inferior vena cava tumor thrombus in renal cell carcinoma: staging by MR imaging and impact on surgical treatment. *AJR Am J Roentgenol*, **171** (1998), 1619–24.
18. S. A. Sohaib, J. Teh, V. H. Nargund *et al.*, Assessment of tumour invasion of the vena caval wall in renal cell carcinoma cases by magnetic resonance imaging. *J Urol*, **167** (2002), 1271–5.
19. H. K. Habboub, M. M. Abu-Yousef, R. D. Williams *et al.*, Accuracy of colour Doppler sonography in assessing venous thrombus extension in renal cell carcinoma. *AJR Am J Roentgenol*, **168** (1997), 267–71.
20. H. Hricak, R. F. Thoeni, P. Carroll *et al.*, Adrenalectomy: defining its role in the surgical treatment of renal cell carcinoma. *Urol Int*, **71** (2003), 361–7.
21. J. B. Thrasher and D. F. Paulson, Prognostic factors in renal cancer. *Urol Clin North Am*, **20** (1993), 247–61.

22. E. E. Struder, S. Scherz, and J. Scheidegger, Enlargement of regional lymph nodes in renal cell carcinoma is often not due to metastases. *J Urol*, **1** (1990), 243–5.
23. W. M. Deserno, M. G. Harisinghani, M. Taupitz *et al.*, Urinary bladder cancer: preoperative nodal staging with ferumoxtran-10-enhanced MR imaging. *Radiology*, **233**:2 (2004), 449–56.
24. M. G. Harisinghani, M. A. Saksena, P. F. Hahn *et al.*, Ferumoxtran-10-enhanced MR lymphangiography: does contrast-enhanced imaging alone suffice for accurate lymph node characterization? *AJR Am J Roentgenol*, **186**:1 (2006), 144–8.
25. C. K. Phillips and S. S. Taneja, The role of lymphadenopathy in the surgical management of renal cell carcinoma. *Urol Oncol*, **22**:3 (2004), 214–23.
26. R. J. Motzer, N. H. Bander, and D. M. Nanus, Medical progress: renal cell carcinoma. *N Engl J Med*, **335** (1996), 865–75.
27. E. J. Chae, J. K. Kim, S. H. Kim *et al.*, Renal cell carcinoma: analysis of postoperative recurrence patterns. *Radiology*, **234**:1 (2005), 189–96.
28. J. R. Newmark, G. M. Newmark, J. I. Epstein *et al.*, Solitary late recurrence of renal cell carcinoma. *Urology*, **43** (1994), 725–8.
29. A. I. Sagalowsky, K. T. Kadesky, D. M. Ewalt *et al.*, Factors influencing adrenal metastasis in renal cell carcinoma. *J Urol*, **151** (1994), 1181–4.
30. I. S. Gill, B. L. McClennnan, K. Kerbl *et al.*, Adrenal involvement from renal cell carcinoma: predictive value of computerised tomography. *J Urol*, **152** (1994), 1082–5.
31. M. De Sio, R. Autorino, G. Di Lorenzo *et al.*, Adrenalectomy: defining its role in the surgical treatment of renal cell carcinoma. *Urol Int*, **71** (2003), 361–7.
32. S. Honigschnabl, S. Gallo, B. Niederle *et al.*, How accurate is MR imaging in characterisation of adrenal masses: update of a long-term study. *Eur J Radiol*, **41** (2002), 113–22.
33. R. L. Wahl, J. Harney, G. Hutchins *et al.*, Imaging of renal cancer using positron emission tomography with 2-deoxy-2-(18F)-fluoro-D-glucose: pilot animal and human studies. *J Urol*, **146** (1991), 1470–4.
34. R. Bachor, J. Kotzerke, H. W. Gottfried *et al.*, Positron emission tomography in diagnosis of renal cell carcinoma. *Urologe A*, **35**:2 (1996), 146–50.
35. S. Ramdave, G. W. Thomas, S. U. Berlangieri *et al.*, Clinical role of F-18 fluorodeoxyglucose positron emission tomography for detection and management of renal cell carcinoma. *J Urol*, **166** (2001), 825–30.
36. D. E. Kang, R. L. White, Jr., J. H. Zuger *et al.*, Clinical use of fluorodeoxyglucose F 18 positron emission tomography for detection of renal cell carcinoma. *J Urol*, **171** (2004), 1806–9.
37. H. Miyakita, M. Tokunaga, H. Onda *et al.*, Significance of 18F-fluorodeoxyglucose positron emission tomography (FDG-PET) for detection of renal cell carcinoma and immunohistochemical glucose transporter 1 (GLUT-1) expression in the cancer. *Int J Urol*, **9** (2002), 15–18.
38. F. Montravers, D. Grahek, K. Kerrou *et al.*, Evaluation of FDG uptake by renal malignancies (primary tumor or metastases) using a coincidence detection gamma camera. *J Nucl Med*, **41** (2000), 78–84.

39. R. Kumar, A. Chauhan, P. Lakhani *et al.*, 2-deoxy-2-(F-18)-fluoro-D-glucose positron emission tomography in characterization of solid renal masses. *Mol Imaging Biol*, **7** (2005), 431–9.
40. T. Miyauchi, R. S. Brown, and H. B. Grossman, Correlation between visualization of primary renal cancer by F18-FDG-PET and histopathological findings. *J Nucl Med*, **37**:Suppl (1996), 64P[abstract].
41. N. S. Majhail, J. L. Urbain, J. M. Albani *et al.*, F-18 fluorodeoxyglucose positron emission tomography in the evaluation of distant metastases from renal cell carcinoma. *J Clin Oncol*, **21**:21 (2003), 3995–4000.
42. N. Aide, O. Cappele, P. Bottet *et al.*, Efficiency of [(18)F]FDG PET in characterising renal cancer and detecting distant metastases: a comparison with CT. *Eur J Nucl Med Mol Imaging*, **30**:9 (2003), 1236–45.

6

The case for biopsy in the modern management of renal cancer

Colin P. Cantwell, Debra Gervais, and Peter R. Mueller

Introduction

In the past, focal renal biopsy had a limited role in the management of renal masses. Potential complications and an overestimated risk of seeding the biopsy tract dissuaded operators from biopsy, and when performed definitive results were uncommon. Hence, urologists presumed that solid renal lesions over 3 cm and complex cysts were predominantly renal cell carcinomas (RCC) and rarely performed biopsy before surgical procedures.

Attitudes have changed to renal biopsy for a number of reasons, firstly, histological techniques have become more reliable. The morphology, immunocytochemical, and genetic profiles of RCC and its subtypes have been better described. Immunohistochemistry and special stains and genetic test are available to help differentiate tumor subtypes. Oncocytoma, oncocytic cancers, RCC and fat poor angiomyolipomas (AML) can now be differentiated histologically. There has also been a downward-stage migration of renal tumors at diagnosis and a substantial fraction of contemporary solid renal masses are benign [1,2,3,4,5,6,7,8]. In one study, 12.8% of solid renal masses were found to be benign. When stratified by size, the proportion of benign masses was 25% for masses smaller than 3 cm, 30% for masses smaller than 2 cm, and 44% for masses smaller than 1 cm [5]. Furthermore, small solid benign renal masses cannot be reliably distinguished from malignant masses by means of imaging findings alone. For example, Tuncali *et al.* described 27 patients referred for thermal ablation techniques who had enhancing renal masses from 1 to 4.2 cm in size that were presumed to be RCC but benign lesions were found in 10 (37%) patients [9]. Hyper-attenuating, homogeneously enhancing renal masses may represent other benign tumors, including metanephric adenoma,

Carcinoma of the Kidney, ed. Uday Patel. Published by Cambridge University Press.

oncocytoma, and leiomyoma. Lastly biopsy results can alter patient management. Wood *et al.* found that biopsy altered the management in 41% of cases [10].

Since 1950, there has been a 126% increase in the incidence of RCC in the USA [11]. The number of patients with incidentally diagnosed asymptomatic renal lesions is growing because of the expansion in abdominal imaging. The incidental detection rate was 7%–13% in the early 1970s, but this percentage has increased to 48%–66% [12,13,14,15,16,17,18,19,20]. The increasing incidence has occurred in all clinical stages, but the greatest increase has been observed in patients with localized tumours, suggesting downward-stage migration as a result of earlier detection in a manner similar to breast cancer [21,22]. The increased incidence of RCC, accompanied by a higher fraction of benign or indolent masses, has led to a need for biopsy to triage patients. Lastly, biopsy of abdominal masses is cost-effective, relative to open surgical biopsy, on average saving $3000 per-patient [23]. Surgical biopsy with frozen section is only 75% accurate and has been outperformed by image-guided biopsy [24].

Technique

Before considering biopsy, review all contrast-enhanced CT or MRI images for biopsy appropriateness. If a benign diagnosis is suspected and could be diagnosed non-invasively, then an additional imaging test is performed (for example a non-contrast scan for angiomyolipoma to demonstrate fat), or follow-up imaging suggested after an appropriate interval. Table 6.1 lists the contemporary indications for biopsy of a focal renal mass.

Our preference is CT guidance for biopsy to ensure deployment of the biopsy needle in the appropriate tissue and to record the site for future reference if a

Table 6.1. Contemporary indications for focal renal biopsy

1. Indeterminate focal renal lesion
2. Bosniak IIF and III renal cyst
3. History of metastatic disease and a new renal mass
4. Widespread metastatic disease and the kidney lesion is the most accessible lesion
5. Confirmation of recurrence of RCC in the renal ablation bed on imaging follow-up
6. Prior to thermal ablation

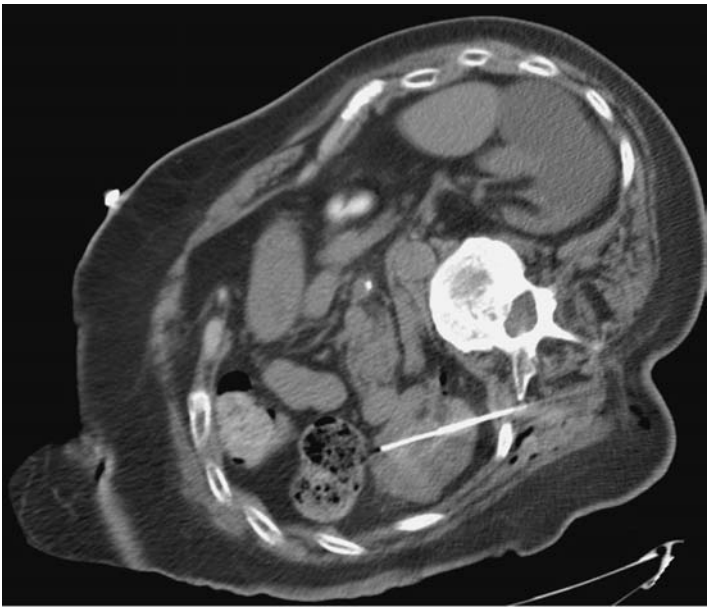

Figure 6.1 Percutaneous biopsy in a 77-year-old woman. Axial non-contrast CT with the patient positioned right side down confirms that the 22-gauge Chiba needle coaxially placed through the 17-gauge access needle is in the solid right renal lesion. The 17-gauge needle was placed inferior to the 12th rib to reduce the risk of pneumothorax.

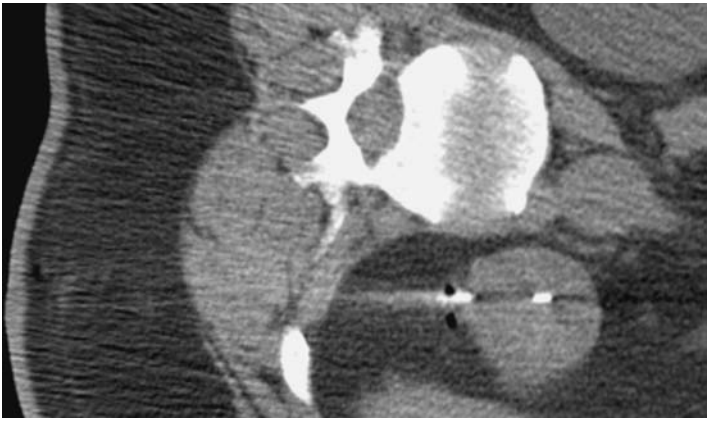

Figure 6.2 Percutaneous biopsy in a 41-year-old woman with Von Hippel–Lindau syndrome. CT confirms positioning of the18-gauge cutting needle in a solid renal mass.

negative biopsy result is obtained (Figures 6.1 and 6.2). Contrast may be administered during the procedure to identify the site or confirm adequate biopsy position. If a mass is large and easily visualized on ultrasound, we may consider ultrasound (Figure 6.3). The biopsy is usually performed as an outpatient procedure with moderate sedation. The patient lies in the lateral decubitus or prone position. The gantry can be angled to avoid organs and the intercostal space (Figures 6.4a, b, and c). The patient's body is centered in the gantry so that any biopsy tool may be

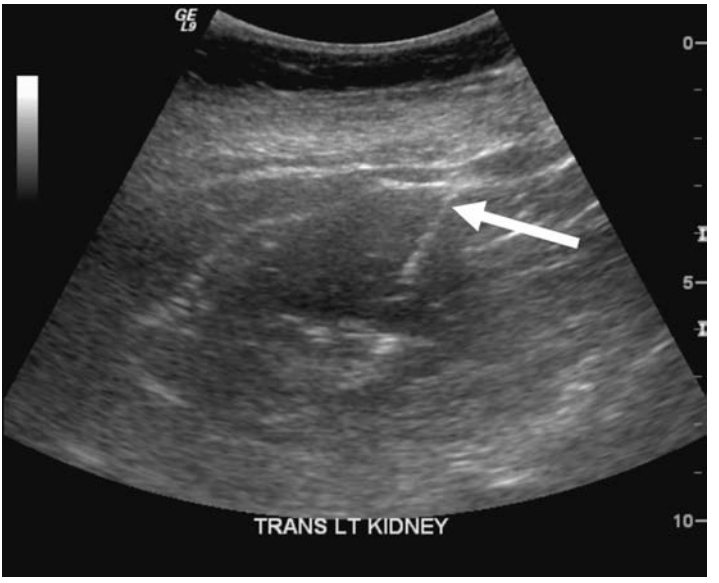

Figure 6.3 Percutaneous biopsy in a 44-year-old woman. US-guided biopsy of an inter-polar left renal mass. The 17-gauge cannula (arrow) is in the mass.

scanned while in the patient. The biopsy approach is selected to avoid adjacent organs, the renal sinus fat, and transgressing the peritoneum or pleura. If an intercostal approach is used, the lowest intercostal space accessible should be used to reduce the risk of pneumothorax (Figures 6.5a and b).

After administration of local anesthesia to the skin, a 1.5 cm 22-gauge needle is placed. This confirms our marked position and angulation. A 17-gauge coaxial system (Temno, Cardinal Health, McGaw Park, IL) is advanced to the lesion or through the lesion with image guidance. The central trocar of the biopsy device is removed to reduce the streak artifact and allow visualization of the mass and landmarks on the non-contrast CT scan. The needle end is covered with an intravenous cap to prevent air from entering the pleural space or a venous structure when scanning. The trocar is replaced before further manipulation.

Through the 17-gauge guiding needle, four to five 18-gauge cutting needle, three 22-gauge Chiba needle passes (fine-needle aspiration biopsy [FNAB]) without the central trocar and a single aspirate through the 22-gauge needle are obtained (Figure 6.6). The 17-gauge needle can be manipulated to guide the core and Chiba needle caudally, cranially, medially, and laterally in the lesion. If the lesion is a cyst, the biopsies are targeted onto solid areas of the cyst wall, thickened septa, or calcification (Figures 6.7a and b). If the lesion is infiltrative

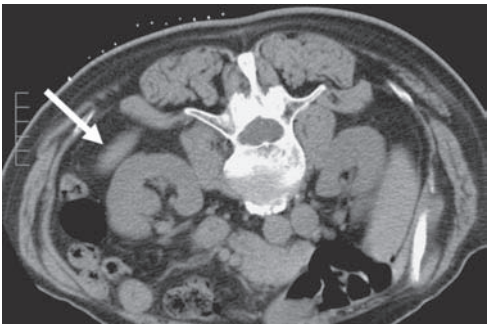

(a)

Figure 6.4a Percutaneous biopsy in a 73-year-old man. Axial CT in a prone patient demonstrates the spleen posterior to the hilar left renal mass.

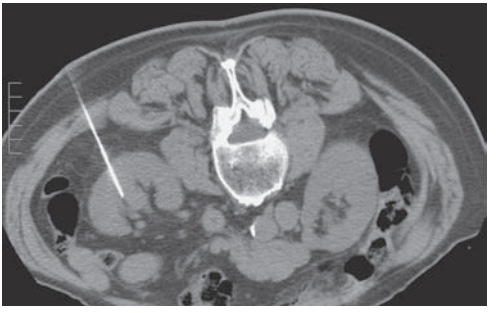

(b)

Figure 6.4b Percutaneous biopsy in a 73-year-old man. Non-contrast CT with caudal–cranial gantry angulation. Biopsy of the mass is possible without traversing the spleen. The 17-gauge biopsy cannula (without the trocar) is positioned lateral to the hilar left renal mass. There is minimal streak artifact owing to removal of the trocar, aiding visualization of landmarks and the mass outline.

(c)

Figure 6.4c Percutaneous biopsy in a 73-year-old man. Non-contrast CT with caudal–cranial gantry angulation. CT confirms 22-gauge Chiba needle deployment through the redirected 17-gauge biopsy cannula in the hilar left renal mass. Note the streak artifact has increased, particularly emanating from the biopsy device tip.

with surrounding soft tissue involvement we preferentially take a core from the renal abnormality which may include some normal renal tissue. This is because biopsy of the periphery of lesions may merely sample surrounding fibrous tissue or reaction.

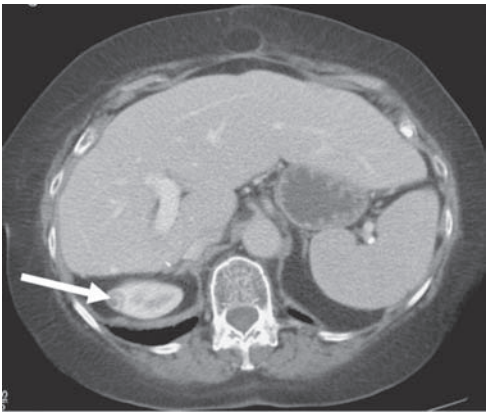

(a)

Figure 6.5a Percutaneous biopsy in a 55-year-old man. Axial contrast-enhanced CT in a patient with a previous partial right hepatectomy and cranial displacement of the right kidney. An enhancing small solid renal mass is seen laterally. An intercostal trans-pleural approach was necessary (arrow).

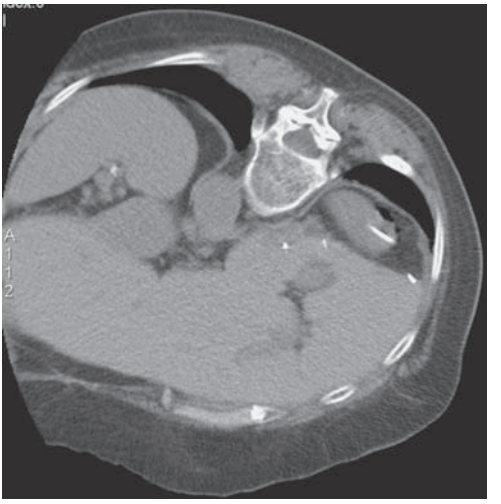

(b)

Figure 6.5b Axial non-contrast CT. Computed tomography confirms 17-gauge access cannula traversing the solid right renal mass. The 17-gauge needle was withdrawn for the biopsy.

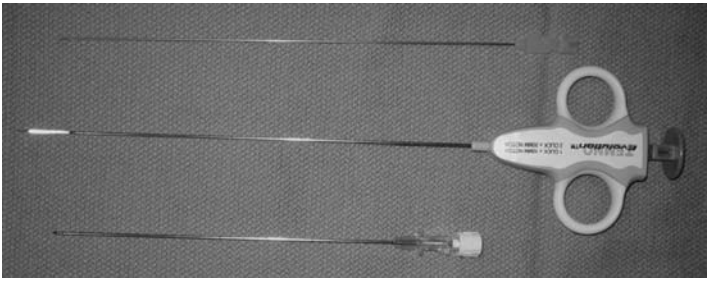

Figure 6.6 Biopsy access and sampling equipment. From top to bottom, 20 cm long, 22-gauge Chiba needle, 20 cm long, 18-gauge cutting needle and 15 cm long, 17-gauge access cannula and trocar.

The cores are examined visually to ensure adequate specimens are obtained. The core specimens are sent for histology in 0.9% saline. The three 22-gauge needle specimens are flushed onto slides using a 10 cc syringe containing 5 cc of room air and smeared with another slide and placed in 95% ethanol. The 22-gauge needle is flushed into a specimen tube on three occasions after slide preparation using 5 cc of air and 1 cc of saline – this material is used to generate a cell block after spinning. A further aspirate with the 22-gauge needle

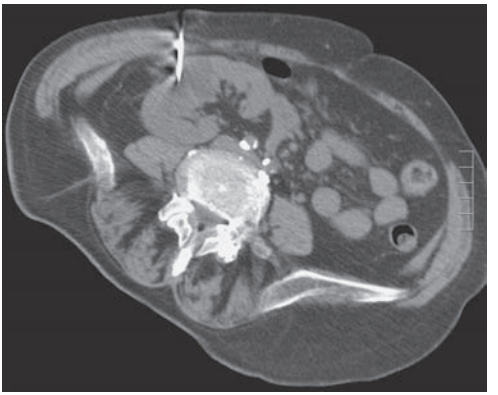

(a)

Figure 6.7a Percutaneous biopsy in an 83-year-old woman. A non-contrast CT scan demonstrates the biopsy cannula positioned in the approximate position of the high density solid component of a complex cystic right renal mass.

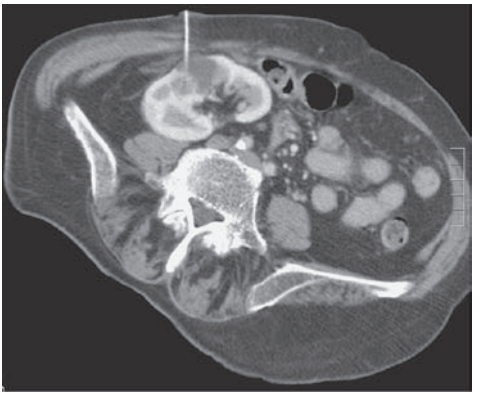

(b)

Figure 6.7b Percutaneous biopsy in an 83-year-old woman. Contrast-enhanced CT at the same table position confirms the biopsy cannula position in the enhancing solid component of a complex cystic right renal mass.

is sent in a separate container for flow cytometry. In the case of a cystic renal mass, the cyst contents are also aspirated and sent for cytological examination. If infection is suspected a sample is sent for gram stain, culture, and sensitivity. A post-procedure CT is performed to exclude an immediate complication (Figure 6.8) and includes the chest if the pleura is traversed. The patient is discharged if well after recovery from the sedation. We have a low index of suspicion before performing a follow-up CT scan if the patient has pain after lesion biopsy.

Diagnostic performance of focal solid renal biopsy

The results of 779 biopsies for focal renal lesions in eight studies performed between 1999 and 2004 show that image-guided biopsies provide sufficient tissue for diagnosis in 90.4% of cases [10,25,26,27,28,29,30,31,32]. A review of 393 renal mass biopsies found false diagnosis in only seven (1.2%). The sensitivity for malignancy ranged from 76% to 93% [32]. The performance of renal biopsy is dependant on the size of the mass. The sensitivity for malignancy was 84%, 97%, and 87% for masses ≤ 3 cm, between 4 and 6 cm, and masses greater than 6 cm, respectively [25]. Negative predictive values were 60%, 89%, and 44% for masses

Figure 6.8 Percutaneous biopsy in a 65-year-old man. Non-contrast axial CT demonstrates pockets of air in the biopsy tracts and a minor degree of perinephric stranding after sampling of a small left renal mass using landmarks for guidance.

≤ 3 cm, between 4 and 6 cm, and those > 6 cm, respectively [25]. False-positive diagnoses of malignancy are rare but have been reported after biopsy of a calcified cyst [33], multilocular cystic nephroma [34,35], angiomyolipoma [36,37], and chronic pyelonephritis [36,38].

Core biopsy versus fine needle ablation

There are no randomized series of patients to define the optimum gauge of the biopsy device. Some authors believe that needle size does not affect biopsy performance [39]. It is our practice to perform both 18-gauge core biopsy and FNAB with a 22-gauge needle owing to the increased diagnostic yield. We consider the potential for additional complication small as we obtain access with a single guiding 17-gauge needle. A number of limitations exist with FNAB. False-negative rates with FNAB can range from 8% to 36%. In a large retrospective analysis of over 300 biopsies, false-negative results occurred in the 20- or 22-gauge FNAB specimens and not in the larger gauge core biopsy [32]. Atypical cellular specimens occur frequently: FNAB yielded atypical suspicious cells in 36% of one series [40]. Suspicious or atypical results cannot be used alone to conclude that the sampled mass is malignant. When FNAB of an AML is performed the technique can lead to a diagnosis of cellular atypia and pleomorphism [41].

Johnson *et al.* described a group of 44 patients who had FNAB of focal renal masses with initially 22- to 18-gauge spinal needles. If the initial cytological evaluation findings were non-diagnostic, core biopsies were then performed with 20- to 18-gauge core biopsy guns. FNAB smears were diagnostic in 67%. The diagnosis made on the basis of cell block alone generated by the FNAB in an additional 6%. A definitive diagnosis came from core biopsy alone in 28%. Their group found 18-gauge core needle yielded diagnostic results more reliably than the 20-gauge core needle [42]. A non-diagnostic specimen is more likely if only a single 18-gauge core is obtained [43].

Renal cell carcinomas subtype analysis also appears to be superior with 18-gauge core biopsy when compared to FNAB. In a study of 38 primary tumors, FNAB specimens were compared with resected specimens – 74% were correctly subtyped. Two sarcomatoid RCC and three papillary renal cancers were misclassified as clear cell type [44]. In a second study of 27 primary tumors biopsied with an 18-gauge core needle, 89% were correctly subtyped. Two clear cell and one papillary RCC subtype tumor were miscategorized [26]. A 70% to 78% accuracy of determination of the Fuhrman grade has been reported with 18-gauge core needles [26,42,43].

Diagnostic performance of focal cystic tumour renal biopsy

Harisinghani *et al.* found CT-guided biopsy with multiple 18-gauge core needles and FNAB of the complex component of Bosniak IIF and III renal cysts to be 100% sensitive and specific [45]. Surgical resection is recommended for category III and IV lesions; however the evidence for surgery is not clear-cut for category III lesions [47]. In his study, unnecessary surgery could be avoided in 39% of patients. Of the 28 biopsied category IIF and III lesions, 17 (60.7%) were malignant (16 renal cell carcinomas and one lymphoma), and 11 (39.3%) were benign (six hemorrhagic cysts, three inflammatory cysts, one metanephric adenoma, and one cystic oncocytoma). Seventeen of the twenty-eight lesions (16 renal cell carcinomas and one inflammatory cyst) had surgical resection after the biopsy. All resected lesions had pathologic diagnoses identical to the percutaneous imaging-guided biopsy results. The remaining 11 patients who had undergone non-surgical biopsies had radiological follow-up for 1 year to ensure stability [45]. However, as sampling error may lead to a false-negative biopsy result, most authors maintain imaging surveillance for 2–5 years to document a satisfactory outcome in all those with a benign biopsy result. Aspiration of cysts for cytological examination has a low sensitivity.

Hemorrhagic aspirates have been considered indicative of malignancy but only 15%–20% of bloody cysts are malignant at resection [46].

Complications after biopsy of focal renal masses

Minor complications with renal biopsy are common. Major complications such as hemorrhage requiring transfusion, admission, and death are rare. Nevertheless, bleeding complications are the most common minor complications, including hematuria, perinephric, subcapsular, and retroperitoneal haemorrhage. Computed tomography detects a small perinephric hematoma in 91% of patients after biopsy [48]. Hematuria is rare (5%–7%) and usually self-limiting. An arteriovenous fistula may be present if hematuria persists after 3 days. Arterial pseudoaneurysm has been reported in patients after biopsy and can be managed percutaneously with embolization [49].

There is some evidence that larger gauge renal biopsy causes more bleeding complications, but this has not been corroborated with a randomized comparison. Subcapsular hemorrhage can lead to renal compression and hypertension. Renal biopsy is a clean procedure (infection rate $< 1\%$) and antibiotic prophylaxis is not indicated. Skin infection and renal abscess formation are rarely encountered or reported. Pneumothorax is also rarely encountered and more common with the cephalic intercostal route. Seeding of the biopsy tract is very rare, occurring in 0.01% of cases [50]. Only six cases of needle-track seeding associated with renal mass biopsy, primarily involving RCC and transitional cell carcinoma, have been reported in the literature [10,51,52,53,54,55,56]. Intestinal perforation, hemothorax, and disseminated intravascular coagulation are reported but are rare. Overall, the mortality and morbidity associated with a biopsy is small and the potential benefit is large if surgery or inappropriate therapy can be avoided.

Conclusion

Nephron sparing surgical techniques, laparoscopic partial nephrectomy and thermal ablation has developed and are being evaluated for smaller renal masses. More patients with co-morbidities can receive potentially curative or cytoreductive therapy and minimize renal function loss with these techniques. Therapy for RCC includes minimally invasive techniques such as thermal ablation techniques that do not yield tissue for histology. Documentation of maliganancy in these lesions is necessary before embarking on therapy and extensive imaging

follow-up. Genetic and cytological markers may help to improve the sensitivity and specificity of renal biopsy and sub-select RCC cases with a worse prognosis. Characterization of RCC and the relationship of tumour growth to apoptosis may determine prognosis and improve selection of candidates for surgery, ablation and medical therapy.

REFERENCES

1. D. A. Duchene, Y. Lotan, J. A. Cadeddu *et al.*, Histopathology of surgically managed renal tumors: analysis of a contemporary series. *Urology*, **62** (2003), 827–30.
2. H. Ozen, A. Colowick, and F. S. Freiha, Incidentally discovered solid renal masses: what are they? *Br J Urol*, **72** (1993), 274–6.
3. C. B. Dechet, D. G. Bostwick, M. L. Blute *et al.*, Renal oncocytoma: multifocality, bilateralism, metachronous tumor development and coexistent renal cell carcinoma. *J Urol*, **162** (1999), 40–2.
4. D. Filipas, J. Fichtner, C. Spix *et al.*, Nephron-sparing surgery of renal cell carcinoma with a normal opposite kidney: long-term outcome in 180 patients. *Urology*, **56** (2000), 387–92.
5. I. Frank, M. L. Blute, J. C. Cheville *et al.*, Solid renal tumors: an analysis of pathological features related to tumor size. *J Urol*, **170** (2003), 2217–20.
6. G. Li, M. Cuilleron, A. Gentil-Perret *et al.*, Characteristics of image-detected solid renal masses: implication for optimal treatment. *Int J Urol*, **11** (2004), 63–7.
7. J. McKiernan, O. Yossepowitch, M. W. Kattan *et al.*, Partial nephrectomy for renal cortical tumors: pathologic findings and impact on outcome. *Urology*, **60** (2002), 1003–9.
8. D. A. Silver, C. Morash, P. Brenner *et al.*, Pathologic findings at the time of nephrectomy for renal mass. *Ann Surg Oncol*, **4** (1997), 570–4.
9. K. Tuncali, E. vanSonnenberg, S. Shankar *et al.*, Evaluation of patients referred for percutaneous ablation of renal tumors: importance of a preprocedural diagnosis. *AJR Am J Roentgenol*, **183** (2004), 575–82.
10. B. J. Wood, M. A. Khan, F. McGovern *et al.*, Imaging guided biopsy of renal masses: indications, accuracy and impact on clinical management. *J Urol*, **161** (1999), 1470–4.
11. M. A. Bosniak, The small (less than or equal to 3.0 cm) renal parenchymal tumor: detection, diagnosis, and controversies. *Radiology*, **179** (1991), 307–17.
12. D. G. Skinner, R. B. Colvin, C. D. Vermillion *et al.*, Diagnosis and management of renal cell carcinoma. A clinical and pathologic study of 309 cases. *Cancer*, **28** (1971), 1165–77.
13. J. W. Konnak and H. B. Grossman, Renal cell carcinoma as an incidental finding. *J Urol*, **134** (1985), 1094–6.
14. I. Shintaku, Y. Suzuki, K. Uchi *et al.*, Characteristics of incidentally detected renal cell carcinoma by ultrasonography at health check-up. *Nippon Hinyokika Gakkai Zasshi*, **91** (2000), 43–8.

15. P. Russo, Localized renal cell carcinoma. *Curr Treat Options Oncol*, **2** (2001), 447–55.
16. L. G. Luciani, R. Cestari, and C. Tallarigo, Incidental renal cell carcinoma-age and stage characterization and clinical implications: study of 1092 patients (1982–1997). *Urology*, **56** (2000), 58–62.
17. Y. Homma, K. Kawabe, T. Kitamura *et al.*, Increased incidental detection and reduced mortality in renal cancer – recent retrospective analysis at eight institutions. *Int J Urol*, **2** (1995), 77–80.
18. S. D. Bos, C. T. Mellema, and H. J. Mensink, Increase in incidental renal cell carcinoma in the northern part of the Netherlands. *Eur Urol*, **37** (2000), 267–70.
19. M. Jayson and H. Sanders, Increased incidence of serendipitously discovered renal cell carcinoma. *Urology*, **51** (1998), 203–5.
20. D. Bretheau, E. Lechevallier, C. Eghazarian *et al.*, Prognostic significance of incidental renal cell carcinoma. *Eur Urol*, **27** (1995), 319–23.
21. W. H. Chow, S. S. Devesa, J. L. Warren *et al.*, Rising incidence of renal cell cancer in the United States. *JAMA*, **281** (1999), 1628–31.
22. L. M. Hock, J. Lynch, and K. C. Balaji, Increasing incidence of all stages of kidney cancer in the last 2 decades in the United States: an analysis of surveillance, epidemiology and end results program data. *J Urol*, **167** (2002), 57–60.
23. S. G. Silverman, T. E. Deuson, N. Kane *et al.*, Percutaneous abdominal biopsy: cost-identification analysis. *Radiology*, **206** (1998), 429–35.
24. C. B. Dechet, T. Sebo, G. Farrow *et al.*, Prospective analysis of intraoperative frozen needle biopsy of solid renal masses in adults. *J Urol*, **162** (1999), 1282–4.
25. F. J. Rybicki, K. M. Shu, E. S. Cibas *et al.*, Percutaneous biopsy of renal masses: sensitivity and negative predictive value stratified by clinical setting and size of masses. *AJR Am J Roentgenol*, **180** (2003), 1281–7.
26. E. Lechevallier, M. Andre, D. Barriol *et al.*, Fine-needle percutaneous biopsy of renal masses with helical CT guidance. *Radiology*, **216** (2000), 506–10.
27. D. Barriol, E. Lechevallier, M. Andre *et al.*, CT-guided percutaneous fine needle biopsy of solid tumors of the kidney. *Prog Urol*, **10** (2000), 1145–51.
28. E. M. Caoili, R. O. Bude, E. J. Higgins *et al.*, Evaluation of sonographically guided percutaneous core biopsy of renal masses. *AJR Am J Roentgenol*, **179** (2002), 373–8.
29. I. Eshed, S. Elias, and A. A. Sidi, Diagnostic value of CT-guided biopsy of indeterminate renal masses. *Clin Radiol*, **59** (2004), 262–7.
30. I. Hara, H. Miyake, S. Hara S *et al.*, Role of percutaneous image-guided biopsy in the evaluation of renal masses. *Urol Int*, **67** (2001), 199–202.
31. F. Mignon, B. Mesurolle, M. Ariche-Cohen *et al.*, Value of CT-guided renal biopsies: retrospective review of 67 cases. *J Radiol*, **82** (2001), 907–11.
32. F. Richter, N. G. Kasabian, R. J. Irwin, Jr. *et al.*, Accuracy of diagnosis by guided biopsy of renal mass lesions classified indeterminate by imaging studies. *Urology*, **55** (2000), 348–52.
33. C. A. Horwitz, J. C. Manivel, S. Inampudi *et al.*, Diagnostic difficulties in the interpretation of needle aspiration material from large renal cysts. *Diagn Cytopathol*, **11** (1994), 380–3.

34. S. P. Clark, I. T. Kung, and S. K. Tang, Fine-needle aspiration of cystic nephroma (multilocular cyst of the kidney). *Diagn Cytopathol*, **8** (1992), 349–51.
35. S. Pilotti, F. Rilke, L. Alasio *et al.*, The role of fine needle aspiration in the assessment of renal masses. *Acta Cytol*, **32** (1988), 1–10.
36. G. Leiman, Audit of fine needle aspiration cytology of 120 renal lesions. *Cytopathology*, **1** (1990), 65–72.
37. S. R. Orell, S. L. Langlois, and V. R. Marshall, Fine needle aspiration cytology in the diagnosis of solid renal and adrenal masses. *Scand J Urol Nephrol*, **19** (1985), 211–16.
38. C. W. Helm, R. J. Burwood, N. W. Harrison *et al.*, Aspiration cytology of solid renal tumours. *Br J Urol*, **55** (1983), 249–53.
39. B. R. Herts and M. E. Baker, The current role of percutaneous biopsy in the evaluation of renal masses. *Semin Urol Oncol*, **13** (1995), 254–61.
40. S. C. Campbell, A. C. Novick, B. Herts *et al.*, Prospective evaluation of fine needle aspiration of small, solid renal masses: accuracy and morbidity. *Urology*, **50** (1997), 25–9.
41. N. Tallada, S. Martinez, and A. Raventos, Cytologic study of renal angiomyolipoma by fine-needle aspiration biopsy: report of four cases. *Diagn Cytopathol*, **10** (1994), 37–40.
42. P. T. Johnson, L. N. Nazarian, R. I. Feld *et al.*, Sonographically guided renal mass biopsy: indications and efficacy. *J Ultrasound Med*, **20** (2001), 749–53.
43. A. Jaff, V. Molinie, F. Mellot *et al.*, Evaluation of imaging-guided fine-needle percutaneous biopsy of renal masses. *Eur Radiol*, **15** (2005), 1721–6.
44. A. A. Renshaw, K. R. Lee, R. Madge *et al.*, Accuracy of fine needle aspiration in distinguishing subtypes of renal cell carcinoma. *Acta Cytol*, **41** (1997), 987–94.
45. M. G. Harisinghani, M. M. Maher, D. A. Gervais *et al.*, Incidence of malignancy in complex cystic renal masses (Bosniak Category III): should imaging-guided biopsy precede surgery? *AJR Am J Roentgenol*, **180** (2003), 755–8.
46. A. A. Renshaw, S. R. Granter, and E. S. Cibas,. Fine-needle aspiration of the adult kidney. *Cancer*, **81** (1997), 71–88.
47. M. A. Bosniak, The current radiological approach to renal cysts. *Radiology*, **158** (1986), 1–10.
48. P. W. Ralls, J. A. Barakos, E. M. Kaptein *et al.*, Renal biopsy-related haemorrhage: frequency and comparison of CT and sonography. *J Comput Assist Tomogr*, **11** (1987), 1031–4.
49. V. G. Vassiliades and M. E. Bernardino, Percutaneous renal and adrenal biopsies. *Cardiovasc Intervent Radiol*, **14** (1991), 50–4.
50. E. H. Smith, Complications of percutaneous abdominal fine-needle biopsy: review. *Radiology*, **178** (1991), 253–8.
51. M. Abe and M. Saitoh, Selective renal tumour biopsy under ultrasonic guidance. *Br J Urol*, **70** (1992), 7–11.
52. J. Auvert, C. C. Abbou, and V. Lavarenne, Needle tract seeding following puncture of renal oncocytoma. *Prog Clin Biol Res*, **100** (1982), 597–8.
53. R. P. Gibbons, W. H. Bush, Jr., and L. L. Burnett,. Needle tract seeding following aspiration of renal cell carcinoma. *J Urol*, **118** (1977), 865–7.

54. G. C. Kiser, M. Totonchy, and J. M. Barry, Needle tract seeding after percutaneous renal adenocarcinoma aspiration. *J Urol*, **136** (1986), 1292–3.
55. P. D. Shenoy, B. N. Lakhkar, M. K. Ghosh *et al.*, Cutaneous seeding of renal carcinoma by Chiba needle aspiration biopsy: case report. *Acta Radiol*, **32** (1991), 50–2.
56. M. J. Wehle and H. Grabstald, Contraindications to needle aspiration of a solid renal mass: tumor dissemination by renal needle aspiration. *J Urol*, **136** (1986), 446–8.

7

Imaging characteristics of unusual renal cancers

Anju Sahdev and Rodney H. Reznek

Introduction

A wide variety of malignant neoplasms have been described in the kidney, but 90% of primary renal cancers are classified as renal cell carcinomas (RCC). Transitional cell carcinomas (TCC) account for about 5%–8% of renal cancers; and nephroblastomas, sarcomas, lymphoma, and metastases commonly from breast, bronchus, and malignant melanoma account for a further 5% of renal cancers [1].

The increased use of ever-evolving cross-sectional imaging has resulted in early and incidental diagnosis of renal cancers. Up to 40% of renal tumors are now incidentally detected and at an earlier stage. For example, 82% of incidentally detected tumors are below stage pT3 compared with only 35% of symptomatic tumors and the disease-free and 5-year survival time is significantly better in lower stage tumors [1,2]. These favorable prognostic features allow recent developments in localized lesion therapies such as ablation techniques, embolization and nephron-sparing surgery to be offered as practical treatment options to conventional nephrectomy. However, histological subtypes with a poor prognosis such as collecting duct carcinomas, sarcomas and TCCs are not suitable for these nephron-sparing treatment options. Lymphoma and metastatic lesions require systemic chemotherapy. Furthermore, although localized treatment may be offered to patients with locally advanced renal cancer and intractable hematuria in a palliative setting, recent developments in targeted chemotherapy may alter the approach to these patients (as discussed in Chapter 1). It is also important to know the histological subtype of the renal cancer prior to embarking on localized treatment options. To this purpose, and to separate benign from malignant disease, there has been an increasing trend toward performing

Carcinoma of the Kidney, ed. Uday Patel. Published by Cambridge University Press.

diagnostic renal biopsies in renal masses [3,4] and the current role of renal biopsy is examined in Chapter 6. The increased interest in renal biopsy is because the cross-sectional imaging appearances of many malignant tumors overlap such that preoperative histological characterization is seldom possible. However, some unusual renal cancers have sufficiently unique features to suggest the histology of the renal tumor. The aim of this review is not to provide an exhaustive list of unusual renal cancers but to describe unusual malignant tumors that may have characteristic imaging features. Pre-procedural diagnosis of these histological subtypes could alter the management of the patient or allow conservative management.

Unusual renal cancers of renal cell origin

The 2004 World Health Organization (WHO) classification recognizes several distinct histological subtypes of RCC (listed in Table 7.1) [5]. Clear cell renal cell carcinoma (CCRCC) is the commonest subset and accounts for more than 70% of all RCCs. Different RCC subtypes are associated with specific and distinct genetic abnormalities which explain the diverse biological behavior of the various subtypes (Table 7.1) [5,6].

Papillary (chromophile) carcinoma

Papillary renal cell carcinomas (PRCC) account for 10%–15% of RCC with a male to female ratio of 8:1. Multiple and bilateral tumors are common. They usually present early with Stage T1–T2 tumors and have a better 5-year survival rate (87%–100%) than does clear cell carcinoma of equivalent stage (65%–75%). The overall 5-year survival rate for PRCC (82%–90%) is also higher than CCRCC (44%–54%) [7]. This indicates that PRCC have a lower malignant potential than CCRCC. However, this tumor has the potential for progression and aggressive behavior and one recent study showed very poor response to systemic therapy once metastatic disease is present, with a median survival time of only 8 months [8].

Macroscopically, PRCC are often heterogeneous, hypovascular tumors with areas of hemorrhage, necrosis, and cystic degeneration. Microscopically, the tumor has a papillary growth pattern with variable amounts of foam cell macrophages and central fibro-vascular stroma. The foamy macrophages infiltrate

Table 7.1. WHO classification of renal cell cancer

Histological subtype	Prevalence (%)	Cell of origin	Cytogenetic findings
Clear cell RCC	70	Epithelium of proximal tubule	3p deletions, von Hippel–Lindau gene mutations
Papillary (Chromophile) RCC	10	Epithelium of proximal tubule	Trisomy of chromosomes 7 and 17, loss of Y chromosome, 7q34 chromosome abnormality
Chromophobe RCC	5	Intercalated cell of collecting duct	Loss of multiple chromosomes: 1,2,6,10,13,17,21
Hereditary cancer syndromes	5	variable	
Multilocular cystic RCC	< 1	variable	
Collecting duct RCC	< 1	Medullary collecting duct	Loss of multiple chromosomes: 1,6,14,15,22, and gain of chromosome: 3
Medullary carcinoma	< 1	Medullary collecting duct	Extracellular matrix gene loss
Mucinous tubular and spindle cell carcinoma	< 1	Loop of Henle	Loss of multiple chromosomes: 1,4,6,8,13,14
Neuroblastoma-associated RCC	< 1		Multiple gene loss
Xp11.2 translocation-TFE3 carcinoma	< 1		Translocations involving Xp11.2
Unclassified	4		

the interstitium which is also laden with hemosiderin and fat. There are two distinct types of PRCC: type 1 and type 2. Type 1 tumors are characterized by a single layer of small cells with scanty cytoplasm, whilst type 2 tumors have high nuclear grade cells with abundant cytoplasm. PRCC type 1 is associated with hereditary papillary cancer and has a good long-term prognosis. PRCC type 2 is associated with hereditary leiomyoma RCC syndrome and is more aggressive [5].

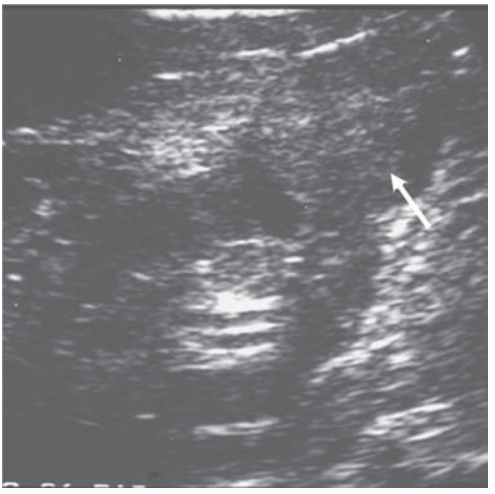

(a)

Figure 7.1a Longitudinal ultrasound image of the left kidney showing a complex hyperechoic solid mass (arrowed).

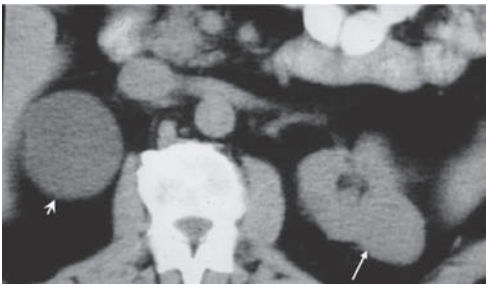

(b)

Figure 7.1b Non-contrast-enhanced CT demonstrating a soft tissue attenuation mass in the mid pole of the left kidney (arrow) with an attenuation value of 45 HU. A simple cyst is demonstrated in the right kidney (arrow head).

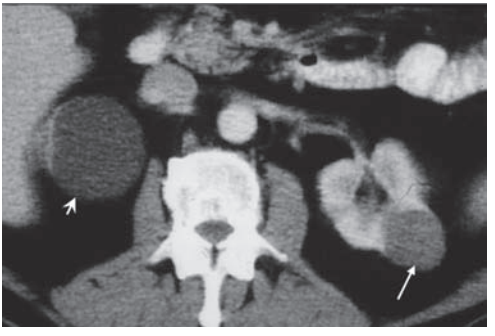

(c)

Figure 7.1c Contrast-enhanced CT in the nephrographic phase showing the left-sided mass is poorly enhancing with an attenuation value of 60 HU. These features are characteristic of papillary cell carcinoma.

On ultrasound the typical appearances of a PRCC are of a well-defined hyperechoic, almost cystic, usually cortical lesion with complex features such as solid nodules, hemorrhage, and septa. Complexity increases with the size of the tumor. On computed tomography (CT), the pre-contrast attenuation value ranges from 30–45 HU. Calcification is present in up to 30% of tumors. Contrast enhancement is heterogeneous, mainly peripheral and poor in 74% of tumors and homogenous in up to 30%. Nephrographic or excretory phase

Figure 7.2 Contrast-enhanced CT showing a large right-sided papillary carcinoma with multiple intra-lesional pockets of fat. Correlation with the pathological specimen showed lipid producing necrosis within the papillary carcinoma.

images appear to be similar to one another and superior to corticomedullary phase images in the ability to detect enhancement. In both corticomedullary and nephrographic or excretory phase CT, PRCC demonstrate enhancement of between 23 and 60 HU when compared to CCRCC which enhance between 37 and 154 HU (Figures 7.1a, b, and c). When compared to the enhancement of the abdominal aorta and normal renal cortex, a low tumor-to-aorta and a low tumor-to-normal renal parenchyma enhancement ratio on the vascular phase scans are typical of PRCC [9]. This is a reflection of the hypovascular nature of this tumor. Strong contrast enhancement (around 84 HU in corticomedullary phase and 44 HU in excretory phase) equivalent to renal cortex is a feature of CCRCC [10,11]. Venous invasion and lymphadenopathy is present in up to 11% of patients at presentation [10]. More recently, atypical features of fat within PRCC mimicking benign angiomyolipoma have been reported. This may be either because of intra-tumoral cholesterol necrosis or because of the presence of mature adipose tissue [12] (Figure 7.2). On MR imaging PRCC have low signal intensity on both T1- and T2-weighted images whilst CCRCC are hyperintense on both. The post-Gadolinium enhancement characteristics are similar to the CT patterns [13,14].

Chromophobe carcinoma

Chromophobe RCC (CHRCC) account for 4%–6% of all RCC, originating from type B intercalated cells of the collecting tubules and appear to have a more indolent behavior than clear cell or papillary RCC. Intercalated cells are also present in oncocytomas and case reports of composite oncocytoma/CHRCC have been described, leading to the suggestion that oncocytomas and CHRCC are related [15]. Oncocytomas are benign, but some cases may be difficult to distinguish from eosinophilic variants of CHRCC (CHRCC with increased cellular mitochondria). The tumors are slow growing compared to other RCC, mean age of incidence is in the 6th decade and there is an equal sex distribution. Most tumors present as Robson stage 1 or 2 tumors and renal vein invasion is rare ($< 5\%$) [16]. Patients with pure CHRCC have a good prognosis but those with mixed cell types, including sarcomatoid changes or collecting duct carcinoma, show a poor clinical course [17].

Macroscopically CHRCC are well circumscribed, solid lobulated brown tumors. Microscopically the tumors are composed of large polygonal eosinophilic tumor cells with abundant cytoplasmic microvesicles and prominent cell membranes. The key to diagnosis is the cytoplasmic diffuse blue staining with Hale colloidal iron stain. There are few descriptions regarding the radiological features of CHRCC. On ultrasound they are typically hyperechoic. On CT, 28% of tumors contain calcification and are isodense to the renal medulla. After contrast enhancement 69% of tumors are hypovascular with poor homogenous enhancement. In the corticomedullary and excretory phases the enhancement is between 27 and 71 HU and 18 and 38 HU respectively [9]. Up to 27% demonstrate spoke-wheel-like enhancement with a central scar similar to oncocytomas (Figures 7.3a, b, and c). A minority ($< 30\%$) have features indistinguishable from CCRCC [9]. On MRI, CHRCC have a low signal intensity on T2-weighted sequences, and on chemical shift imaging there is a diffuse distribution of intratumoral fat and hemosiderin [18]. Venous invasion and lymphadenopathy are rare at presentation (Figures 7.4a and b).

Collecting duct carcinoma

Collecting duct carcinomas (CDRCC) are rare, highly aggressive variants of RCC, accounting for less than 1% of RCC. They arise from the epithelium of Bellini's ducts, in the distal portion of the nephron. They occur in the 5th decade and have

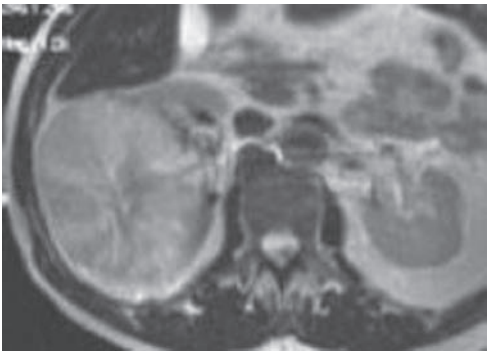

(a)

Figure 7.3a T2-weighted MRI image showing a large right-sided chromophobe RCC with a high signal intensity and a "spoke wheel" appearance mimicking an oncocytoma.

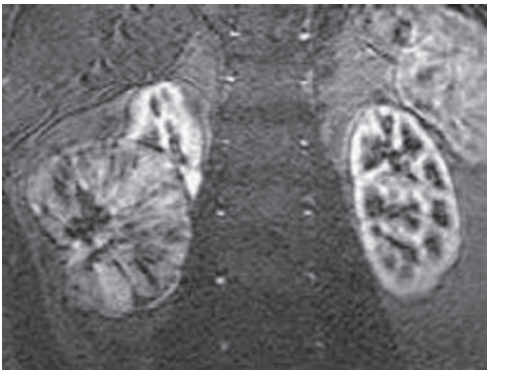

(b)

Figure 7.3b Coronal T1-weighted image with fat saturation following Gadolinium enhancement. The chromophobe RCC is a solid homogenous mass with spoke wheel enhancement again mimicking an oncocytoma.

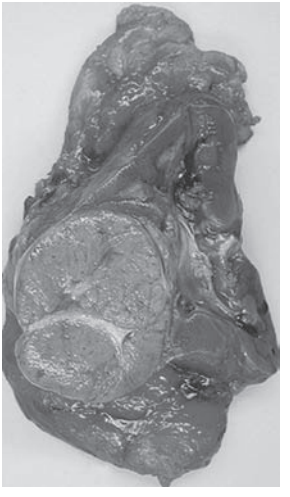

(c)

Figure 7.3c The histological specimen showing the macroscopic appearances of the chromophobe RCC as a solid, lobulated brown tumor (see also color plate section).

a strong male predominance (72%). At presentation the tumor is organ-confined in less than 40% of patients and between 30% and 35% have distant or regional lymph node metastases with few effective treatment options and a very poor prognosis, with a 5-year survival rate of less than 5% [19]. Macroscopically these tumors are infiltrative tumors with their epicenter in the pelvicalyceal system. They are composed of densely packed tubular or tubulo-papillary tumor cells producing mucin

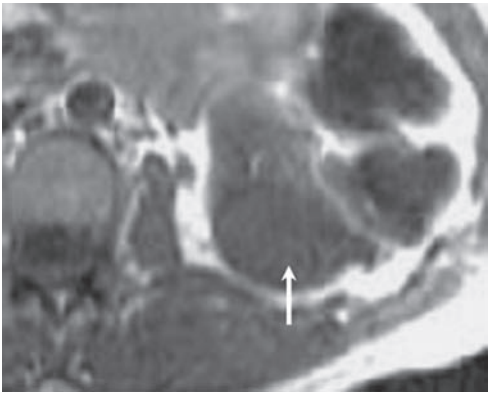

(a)

Figure 7.4a T1-weighted MRI image showing a left-sided chromophobe carcinoma (arrow) as a solid mass with intermediate to low signal intensity.

(b)

Figure 7.4b T2-weighted MRI image showing the mass as a solid homogenous lesion with a low signal intensity caused by the intra-tumoral hemosiderin.

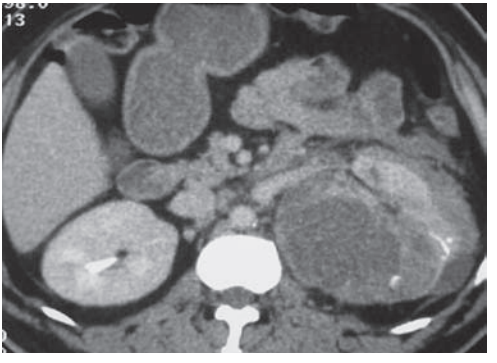

(a)

Figure 7.5a Contrast-enhanced CT showing a large left-sided collecting duct carcinoma involving the renal medulla and renal parenchyma.

(b)

Figure 7.5b Coronal T2-weighted image showing the high T2 signal intensity heterogeneous collecting duct carcinoma in the left, mid, and lower pole with close approximation to the renal medulla.

with surrounding desmoplastic stroma and tubular epithelial dysplasia. On imaging, smaller tumors lie in the medulla whilst the larger tumors are indistinguishable from typical CCRCC (Figures 7.5a and b). They are heterogeneous, hypervascular with necrosis, hemorrhage, and calcification. Renal vein invasion and regional nodal metastases are common, seen in up to 50% of patients at presentation [9].

Multilocular cystic renal cell carcinoma

Multilocular cystic renal cell carcinoma (MCRCC) is a recently described variant of cystic RCC with characteristic pathological and clinical features [20]. These tumors are unusual, comprising 1%–4% of all RCC. Five to ten percent of all RCCs are cystic and, amongst these, MCRCC is the commonest histological subtype (up to 40%) [20,21]. MCRCC occurs more frequently in males and the majority occurs in the 4th–6th decades. The adult tumors have a very good prognosis as the majority present as stage 1 tumors and have a low Fuhrman grade 1 or 2 [22]. The tumors have little or no malignant potential in their pure form but the presence of mesothelial sarcomatoid components has been described as leading to a more malignant form of MCRCC, with distant metastases [23]. Eble *et al*. have suggested three diagnostic criteria for MCRCC: (1) an expansile mass surrounded by a thick fibrous capsule; (2) the interior of the mass is entirely composed of cysts and septa with no expansile solid nodule; (3) the septa contain aggregates of epithelial neoplastic clear cells with clear cytoplasm, grade 1 nuclear features, and little or no mitotic activity [24].

Macroscopically MCRCCs are well-demarcated multicystic lesions with densely fibrotic cystic walls. The cysts are filled with gelatinous, hemorrhagic fluid and the solid components are yellowish, characteristic of CCRCC. The solid components constitute less than 10% of the entire lesion. Microscopically, the cyst walls are often devoid of epithelium. The imaging features mimic the described macroscopic appearances of the tumor. On ultrasound, they appear well defined, multilocular, septate cystic masses without solid nodules (Figures 7.6a and b). The fluid may be anechoic or contain hyperechoic debris [20]. On unenhanced CT, the cystic portions are mainly hypodense but a minority of the locules may contain hyperdense hemorrhagic fluid. Calcification may be present in the septa. On contrast-enhanced CT, the solid components demonstrate low-grade enhancement with an average increase in CT attenuation of 12–28 HU. MRI appearances also reflect the cystic composition of the tumor and on T1-weighted images the cystic fluid may have intermediate to high signal intensity, in keeping with proteinaceous and hemorrhagic cystic fluid [25].

The preoperative recognition of MCRCC has been shown to be possible using strict criteria of no expanding solid enhancing mural nodules > 5 mm in thickness within a multicystic tumor with thin regular cyst walls and septa. When these criteria are adopted the imaging accuracy for the diagnosis of MCRCC is 92% [25]. However the distinction between MCRCC, cystic RCC, multicystic nephroma, and

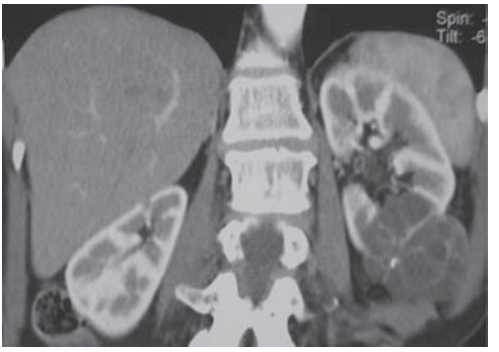

(a)

Figure 7.6a Contrast-enhanced CT reformatted in the coronal plane. This shows a left-sided multilocular cystic RCC with multiple cystic locules, smooth septa and a small area of calcification. Note there are no areas of enhancing solid components within the mass.

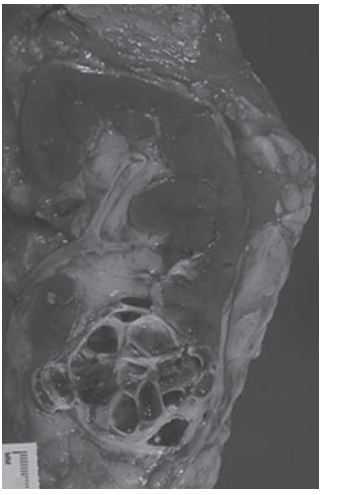

(b)

Figure 7.6b The histological specimen showing the macroscopic appearances of the multilocular cystic RCC (see also color plate section).

infective or hemorrhagic cysts can be difficult to establish on imaging criteria and even on frozen-section analysis.

Summary of imaging characteristics of common renal cell cancer subtypes

Although there is an overlap in the imaging appearances of the different RCC subtypes, certain combinations are helpful in predicting specific subtypes. For instance, large (>7 cm) homogenous solid tumors with calcification and poor contrast medium enhancement are strongly suggestive of a CHRCC. Heterogeneous tumors with small amounts of calcification and weak enhancement are typical of PRCC. Heterogeneous tumors of any size with peripheral avid contrast enhancement indicate clear cell or collecting duct carcinomas. Thus, the degree and patterns of contrast enhancement are the most useful imaging characteristics in predicting the RCC subtype, which may influence the appropriate extent of surgery (nephrectomy versus partial nephrectomy or localized versus wide resection) and assist in the selection of patients for nephron-sparing procedures.

Renal cell cancers of non-renal cell origin

Carcinoma of the upper urinary tract and collecting system

Embryologically, the collecting system of the urinary tract develops from the mesonephros. Tumors of the collecting system are classified according to their mesodermal or epithelial origins. Mesodermal tumors are very rare, arising from smooth muscle, neural tissue, fibrous tissue, and blood vessels. Epithelial tumors include transitional cell carcinomas (TCC), squamous cell carcinomas (SCC), adenocarcinomas, and sarcomas. Primary renal collecting system tumors account for less than 10% of all renal carcinomas and of these 90% are transitional cell carcinomas (TCC).

Transitional cell carcinoma

The renal pelvis is the commonest site of origin of upper tract TCC and tumors arising at the infundibulo-calyceal regions occur less frequently. Upper tract TCC including ureteric tumors account for less than 5% of all urothelial tumors [26,27].

The risk factors for developing upper tract tumors are similar to the risk factors for bladder TCC. These include increasing age over 40 years, smoking, occupational exposure to chemicals containing hydrocarbons (aniline dyes, azo dyes, and rubber), drugs such as cyclophosphamide and its metabolite acrolein, analgesic abuse, and a strong familial history of TCC [28,29]. Upper tract TCCs occur more frequently in men, with a male to female ratio of 3:1, and more frequently in Caucasians with a ratio of 2:1. There is an association with Balkan nephropathy, a degenerative nephropathy that confers a 100–200 times increase in the incidence of upper tract TCC which are generally low grade, multiple, and bilateral. Lynch syndrome II includes upper tract TCC, multiple proximal colonic non-polypoid tumors, and multiple extra-colonic tumors [30,31].

There is an increased incidence of bladder TCC in patients with an upper tract TCC and between 50% and 75% of patients will have a bladder tumor either previously, synchronously, or subsequently. Bilateral upper tract disease occurs in 1%–5% of patients and subsequent ipsilateral tumors occur in 14%–30% of patients presenting with an upper tract TCC [28,32]. This multifocal involvement affects the choice of radiological investigation and treatment for upper tract TCC. Unlike bladder TCC, tumors in the upper tract are usually higher-grade (up to 79%), demonstrate a higher rate of unusual morphological features (including squamous cell carcinoma, sarcomatoid, and glandular differentiation), and metaplasia. Whereas 85% of bladder TCC present as superficial ($<$ T1) tumors, 45% of TCC

Table 7.2. TNM classification of upper tract TCC with correlating imaging features

Stage	Histopathologic findings	Imaging features
Ta	Papillary non-invasive carcinoma	1. Single or multiple filling defects with minimal enhancement on CT, papillary, or flat, irregular surface with "stippled" effect 2. Dilated calyces, stenosis of infundibulum, amputation of calyces, and ureteric strictures 3. PC system mass remains separated from the renal parenchyma by sinus fat, urine, or contrast in the PC system. Secondary dilation of the calyces and/or pelvis is a good criteria for T1–T2 tumor
Tis	Carcinoma *in situ*	
T1	Invasion of subepithelial connective tissue	
T2	Invasion of muscularis mucosa	
T3	Invasion beyond muscularis mucosa into periuretric fat or renal parenchyma	1. Loss of peripelvic fat 2. Areas of abnormal parenchymal enhancement
T4	Invasion of adjacent organs, pelvic or abdominal wall, or through the kidney into perinephric fat	1. Extension into perinephric fat 2. Invasion of adjacent structures and/or renal vein and IVC
N1	Single nodal metastases <2 cm	
N2	Single nodal metastases >2 cm but <5 cm or multiple nodes <5 cm	
N3	Nodal metastases >5 cm	
M1	Distant metastases	

of the renal pelvis present with locally advanced disease ($>$pT2) [28,33,34]. These features emphasize the need for a more aggressive treatment of upper tract TCCs.

Tumors are staged by the TNM classification (Table 7.2). The accepted management for upper tract TCC is a nephroureterectomy with removal of the bladder cuff and mucosa with local lymphadenectomy. This is often performed laproscopically. Lymphadenectomy is particularly beneficial in detecting microscopic lymph node

metastases, which dictate the use of adjuvant chemotherapy [35,36]. In the absence of nodal disease, systemic chemotherapy can be avoided. Lymphadenectomy of macroscopically involved nodes has been shown to have no therapeutic benefit [35,36]. Local excision and minimally invasive surgical techniques can be performed for patients with a solitary kidney, bilateral tumors, low-grade tumors, or for palliation in patients unfit for definitive surgery, with results comparable to definitive surgery [37,38,39]. The 5-year survival rate for non-invasive (pTis-pT1) disease approaches 91%, for pT2 is 43%, whilst for invasive (T3–4) and metastatic disease (N1–3, M1) the survival rate falls dramatically to between 0% and 23% [40,41].

Currently the most widely used radiological technique to detect upper tract TCCs is intravenous urography (IVU) although cross-sectional techniques, particularly CT urography, are increasingly replacing IVU. About 50%–75% of tumors are seen as irregular filling defects, either papillary or flat lesions, within the collecting system. Infundibular tumor growth results in infundibular stenosis causing a localized hydrocalyx or calyceal amputation. At the renal pelvis, tumor growth results in expansion of the renal pelvis and pelvo-calyceal junction obstruction. In 10%–30% of patients, pelvic tumor results in non-visualization of the collecting system on IVU. If the tumor has a flat growth pattern, smooth or irregular pelvic strictures will result in proximal calyceal dilation and/or upstream ureteric dilatation.

The technique of CT urography includes triple phase CT, consisting of an unenhanced scan, nephrographic phase (100–120 seconds) and excretory phase (5–7 minutes) after contrast enhancement. The addition of the cortico-medullary phase (27–70 seconds) aids in the assessment of venous infiltration when the opacification of the IVC is optimal. There are several radiological signs seen on CT. Early stage TCC is seen as a focal mass or focal areas of irregular thickening of the calyceal/pelvic, or ureteral walls. On pre-contrast images TCCs have a soft tissue Hounsfield measurement between 5 and 39 HU and appear hyperattenuating compared to urine in the collecting system. After contrast administration, TCCs demonstrate minimal enhancement with a mean value of 65 HU [42]. Stage T1 or T2 tumors are separated from the renal parenchyma by renal sinus fat or by contrast media in the collecting system (Figures 7.7 and 7.8). Late stage tumors demonstrate invasion of the peripelvic and periureteral fat and renal parenchymal invasion seen as areas of abnormal parenchymal enhancement at the sites of tumor invasion and perirenal stranding. Infiltration into the renal parenchyma is usually infiltrative with enlargement of the renal contour rather than a focal rounded mass lesion as for RCC (Figures 7.9 and 7.10). The reniform configuration of the kidney is typically preserved unlike in RCC. Pitfalls in interpreting T3 tumors occur when

Figure 7.7 Contrast-enhanced CT in the excretory phase with a stage T2 TCC. A flat sheet like mass is seen in the left renal pelvis (arrow). This is limited to the renal pelvis and no invasion of the renal parenchyma is seen in keeping with an early TCC.

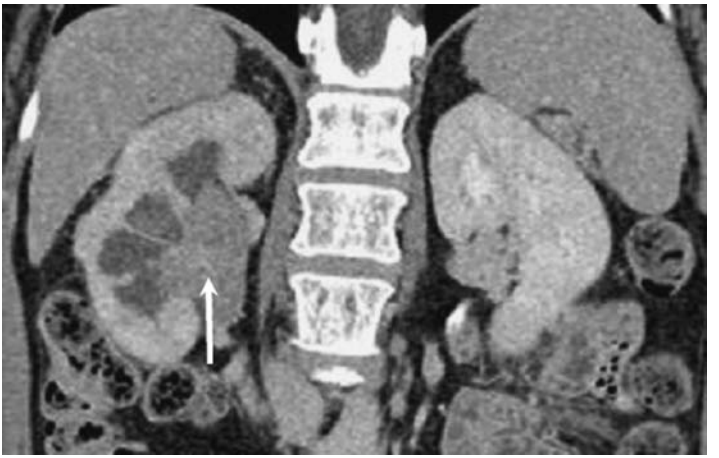

Figure 7.8 Coronal reformatted image of contrast-enhanced CT in the excretory phase. A large TCC is seen expanding and occupying the whole of the right renal pelvis (arrow). There is hydronephrosis and the tumor is surrounded by fluid excluding renal parenchymal invasion.

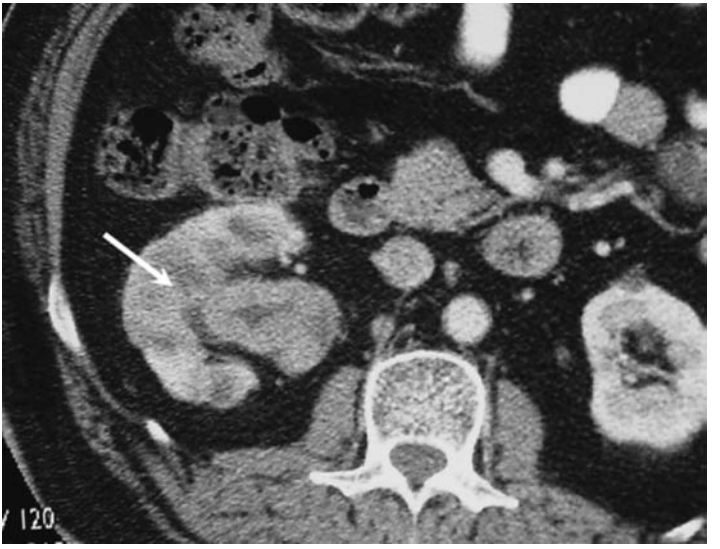

Figure 7.9 Contrast-enhanced CT in the nephrographic phase. There is a large right-sided pelvis mass which invades the surrounding renal parenchyma (arrow) with resultant expansion and heterogeneous enhancement of the renal cortex. The appearances are of a stage T3 TCC.

Figure 7.10 Contrast-enhanced CT in the corticomedullary phase. There is a large right-sided pelvic TCC invading the surrounding posterior renal cortex with resultant poor enhancement of the renal cortex. There are several para-aortic lymph nodes (arrow). The appearances are in keeping with a stage T3, N1 TCC.

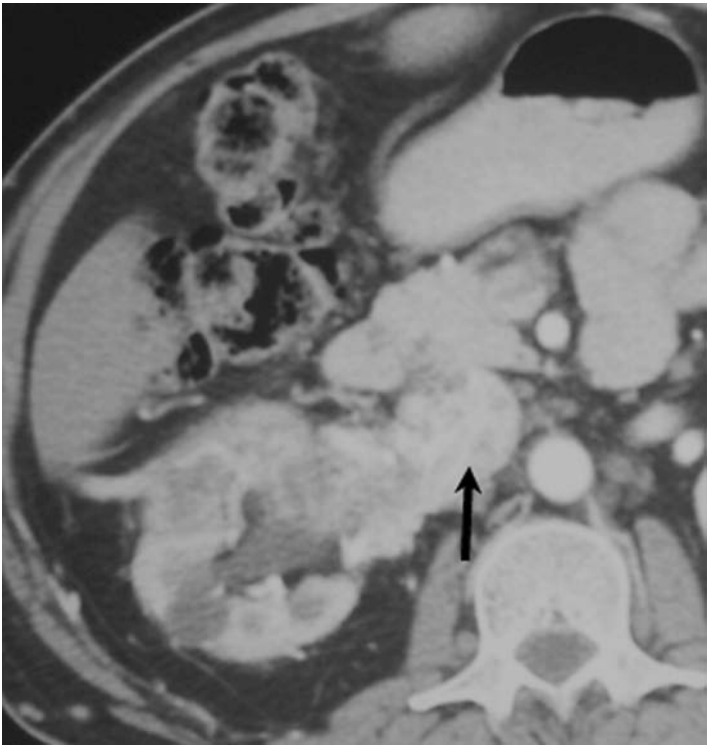

Figure 7.11 Contrast-enhanced CT in the nephrographic phase. There is a large advanced right-sided stage T4 TCC demonstrating invasion of the renal parenchyma, renal vein, IVC (arrow), and the duodenum.

there is compression rather than invasion of the surrounding renal sinus fat and there are areas of abnormal parenchymal enhancement owing to infection, vascular occlusion, or obstruction. More advanced or T4 tumors invade adjacent structures, renal vein, and the IVC (Figure 7.11).

Computed tomography has limited value in staging TCC as it cannot reliably differentiate between low stage pTa and pT2 tumors where it may under- or overstage peripelvic and parenchymal invasion [43,44,45]. The overall staging accuracy for CT is between 50% and 60% and early stage tumors remain undetected on conventional CT in 24%–80% of cases [43,44]. With multidetector CT (MDCT), images collimated down to 1 mm and multiplanar imaging, the detection rate of small TCCs has increased to almost 90% but the staging accuracy and, in particular, the differentiation between stages Ta, T1, and T2 remains poor with significant therapeutic implications [46,47]. Patients with stage Ta-T1 tumors are candidates for nephron-sparing treatment but patients with T2 tumors require nephro-ureterectomy. Tumor stage in various studies has been confirmed as an independent predictor of recurrence and tumors stage T2 and above do not benefit from a conservative approach [48,49,50,51]. The value of CT lies in demonstrating peripelvic or periureteral tumor extension in advanced disease [47,51]. It remains the modality of choice to detect direct parenchymal invasion, extrarenal extension, nodal, and venous involvement. The detection of enlarged lymph nodes is important as it suggests high stage disease and in this group of patients no benefit of routine lymphadenectomy has been shown [35,36].

There are few published data on the use of MRI for detection and staging of upper tract TCC. Small studies have demonstrated that standard T2-weighted and post-contrast-enhanced images, like CT, have limited value in staging early upper tract TCC, as superficial invasion of the renal parenchyma is difficult to detect [52]. Without the use of nanoparticle contrast agents, the detection of microscopic nodal metastases is also poor. With lymph-node-specific contrast agents the sensitivity and negative predictive values improve significantly to 96% and 98% from 76% and 91% respectively [53,54]. More recently, MRI has been advocated as a problem-solving modality in patients with a high risk of upper tract TCC for evaluating hydronephrosis unexplained by standard investigations [55]. Targeted high-resolution T2-weighted images demonstrated ureteral and renal pelvic TCC in a significant number of patients in whom routine investigations with IVU and endoscopic techniques had failed to provide a diagnosis.

Squamous cell carcinoma (SCC)

Squamous cell carcinoma is the commonest non-transitional cell tumor of the upper urinary tract accounting for 75% of the non-transitional cell carcinomas. Up to 50% have associated stone disease and chronic irritation and inflammation are

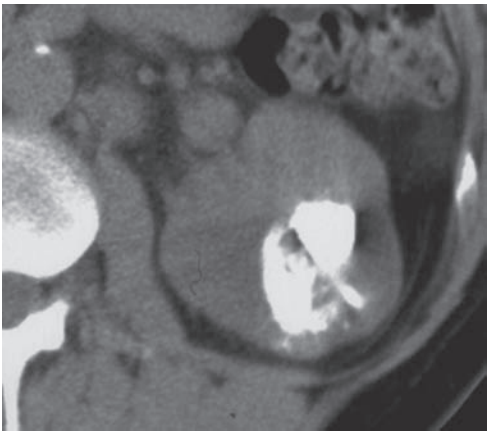

(a)

Figure 7.12a Non-contrast-enhanced CT showing large left-sided renal calculus and a distorted renal contour.

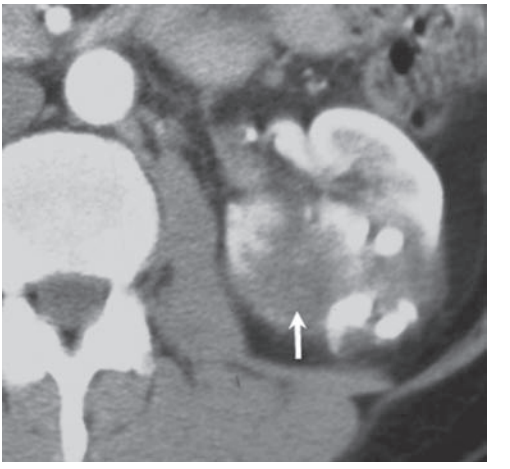

(b)

Figure 7.12b Contrast-enhanced CT in the corticomedullary phase demonstrating an ill-defined squamous cell carcinoma (arrow) around the calculi, involving the collecting system and the renal parenchyma. These features are typical of a squamous cell carcinoma of the collecting system.

postulated causative factors [56]. Other suggested risk factors are horseshoe kidney and long-standing hydronephrosis, but these are speculative. These tumors have a poor prognosis, a combination of locally advanced stage at diagnosis (94% > pT3) and rapid disease progression (mean survival time of 2 years) [56]. The treatment remains nephrectomy or nephro-ureterectomy with platinum-based adjuvant chemotherapy but the response to treatment is usually poor. On imaging, the presence of stones in the renal pelvis or ureters with a long history of urolithiasis combined with a focal mass should alert the reporting radiologist of the possibility of an SCC (Figures 7.12a and b). On CT, the tumors show an equal distribution of endo-luminal and extra-luminal growth patterns [57].

Lymphoma

In autopsy series of patients who have died of lymphoma, up to 40% of patients have microscopic or macroscopic renal involvement [58]. This is usually non-Hodgkins B-cell intermediate and high grade lymphoma, with up to 50%

involving the renal and perirenal space at presentation [59,60]. Despite this high incidence of involvement, cross-sectional imaging, in particular CT, identifies abnormalities in only 3%–10% of the patients with lymphoma [60,61]. When renal abnormalities occur in the context of other disseminated lymphomatous disease, the diagnosis is clear but in $< 1\%$ of lymphomas the kidneys may be the sole or predominant site of disease. Renal parenchyma does not normally contain lymphoid tissue. It is thought that the lymphoma, usually of B cell origin, originates in the lymphatic rich capsule and perirenal fat and invades the parenchyma. Alternatively, lymphocytes within areas of chronic inflammation may be the site of origin [62,63]. Another possible mechanism is for malignant lymphocytes to be deposited in the renal parenchyma after hematogenous spread, which proliferate into multiple renal masses or a more diffuse renal enlargement, retaining the normal reniform configuration. Contrast-enhanced CT, particularly the nephrographic phase, is the most widely used diagnostic modality to detect renal lesions. MRI is used for patients with an iodine contrast allergy or severe renal insufficiency. Combined PET-CT is increasingly used to stage lymphoma and is more sensitive and specific than conventional anatomic imaging in detecting small tumor deposits [64].

Typical CT patterns of renal lymphoma

Multiple masses

This is the commonest manifestation with multiple renal masses of variable sizes between 1 and 7 cm in diameter, usually bilateral, and with little mass effect. On non-contrast images the masses tend to be of a higher attenuation than the surrounding renal parenchyma, but after contrast enhancement they are of lower attenuation than the renal parenchyma as they demonstrate minimal contrast enhancement (Figure 7.13). This pattern is seen in 50%–60% of renal lymphoma [59,65]. In only 50% of adult cases is there associated retroperitoneal lymphadenopathy. A high association (up to 46%) with bone involvement has been reported [59]. In children associated retroperitoneal disease is more common than in adulthood, occurring in 73% [66,67,68].

In the absence of lymphomatous disease elsewhere, patients presenting with multiple renal masses usually require a biopsy as many other conditions including septic emboli, renal infarcts, acute pyelonephritis, abscesses, multiple angiomyolipomas associated with tuberous sclerosis, multiple renal cell carcinomas

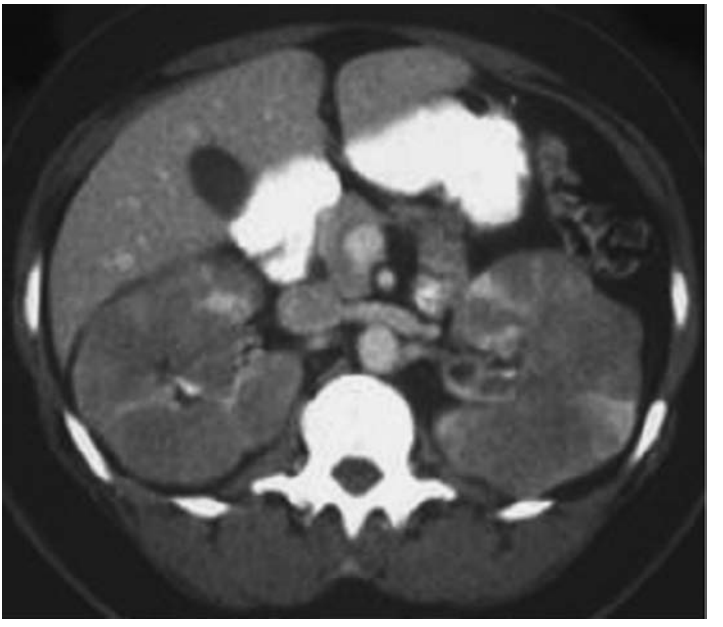

Figure 7.13 Contrast-enhanced CT demonstrating multiple bilateral poorly enhancing renal masses. The normal renal parenchyma is seen as areas of higher attenuation between the low attenuation masses. Also note that despite the multiple masses the kidneys retain a normal reniform configuration typical of lymphomatous renal involvement.

associated with von Hippel–Lindau syndrome, and metastases particularly from melanoma, lung, breast, and gastric cancer may simulate these appearances.

Solitary renal mass

A solitary renal mass is the pattern seen in up to 25% of patients. The lymphomatous mass characteristically demonstrates minimal enhancement which is helpful in differentiating from conventional hyper-enhancing heterogeneous RCC (Figure 7.14) [65]. However, papillary, chromophobe and collecting duct carcinomas, xanthogranulomatous pyelonephritis, and acute pyelonephritis may also appear as poorly enhancing masses.

Diffuse renal enlargement

Diffuse enlargement with preservation of the normal renal contour results from infiltration of the renal interstitium by malignant lymphocytes. This pattern is seen in 20% of renal lymphoma and is almost always bilateral [65]. Detection of this pattern relies on contrast enhancement and imaging in the cortico-medullary and

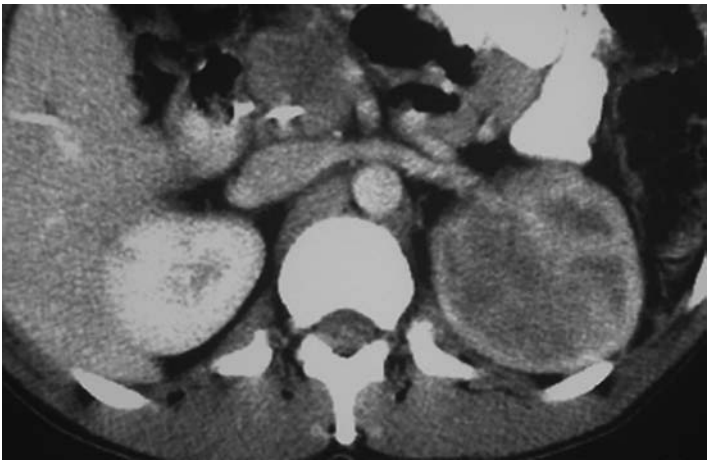

Figure 7.14 Contrast-enhanced CT showing a large solitary mass occupying and expanding the upper pole of left kidney. The mass is poorly enhancing and ill-defined. The expanded kidney retains its normal reniform contour.

nephrographic phases. The kidneys demonstrate heterogeneous enhancement, loss of cortico-medullary differentiation, and infiltration of the sinus fat and renal collecting system. When the infiltration is predominantly within the collecting system, extending into the parenchyma, the appearances are similar to invasive TCC or collecting duct carcinoma. Occasionally a large reniform mass infiltrates and destroys the entire kidney and manifests as a non-functioning kidney with a tumor. If the clinical diagnosis of lymphoma is not available, a renal biopsy may be required.

Perirenal mass

Isolated perirenal masses although less common are characteristic, presenting in up to 10% of renal lymphoma [59]. Contrast-enhanced CT is essential for the detection of the perirenal soft tissue mass which encases but does not destroy the whole or part of the kidney. The underlying kidney enhances normally, showing clear definition of the renal parenchyma whilst the perirenal mass is poorly enhancing (Figure 7.15). This perinephric infiltration may be subtle with thickening of the Gerota's fascia or minor plaque formation. The differential diagnosis of this perinephric thickening includes benign conditions like pancreatitis, retroperitoneal fibrosis, and amyloid. The perinephric masses appear similar to subcapsular hematomas and extramedullary hemopoiesis but the clinical history separates these processes from lymphoma.

Figure 7.15 Contrast-enhanced CT demonstrating a perirenal mass surrounding the lower pole of the left kidney. The underlying renal cortex enhances normally and retains its normal configuration. This pattern of renal involvement is a characteristic appearance of perirenal lymphoma.

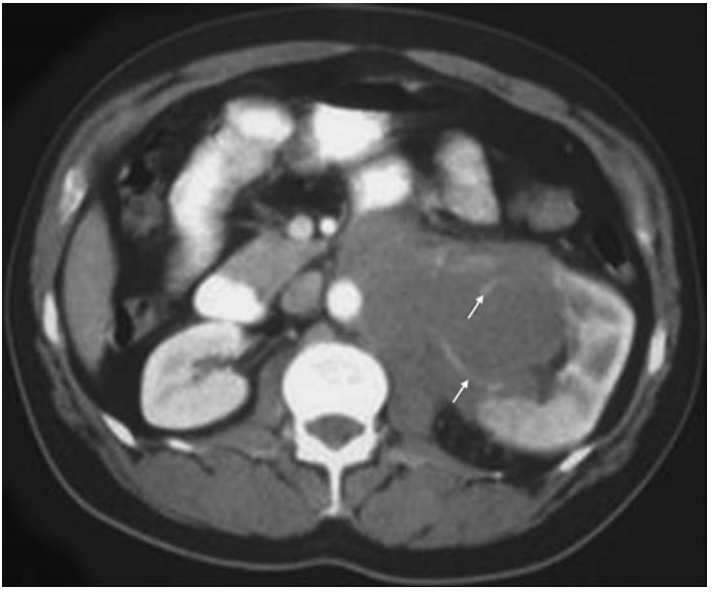

Figure 7.16 Contrast-enhanced CT showing a large left lymphomatous retroperitoneal mass invading the renal hilum, renal parenchyma, and the left psoas muscle. Characteristically the renal vessels are distorted but not invaded and demonstrate contrast enhancement (arrows).

Contiguous retroperitoneal extension

Direct extension of retroperitoneal disease to engulf or involve the kidneys is the second commonest pattern of renal lymphomatous involvement seen in up to 30% of patients [59,61]. Bulky retroperitoneal masses encase the renal vessels, renal hila, renal pelvis, and parenchyma. Despite the encasement of the renal vessels, they

tend to remain patent (Figure 7.16). The involvement of the renal pelvis can result in hydronephrosis.

Renal malignancy in the immunocompromised

Renal tumors after renal transplantation

Several factors have been postulated to play a role in the increased incidence of malignancy in transplant recipients. These include post-transplant viral infections, immunosuppressive and other drugs, and transfer of malignancy from donors. The introduction of azathioprine, corticosteroids, and cyclosporin have all been linked to the increase in the incidence of lymphoma in post-transplant patients [69,70,71,72]. Skin cancer, particularly aggressive squamous cell carcinoma and non-Hodgkin lymphoma are the most common malignancies in renal transplant recipients [73].

Post-transplant lymphoproliferative disorder (PTLD) has an increased incidence in patients treated with increasingly aggressive immunosuppression and particularly cytolytic therapy. This represents a spectrum of abnormal lymphocytic proliferation that ranges from polymorphic hyperplasia to monomorphic lesions indistinguishable from non-Hodgkin's lymphoma. The overall incidence of PTLD is 1% after renal transplantation and 10% after other solid organ transplantation. The pathogenesis of PTLD is related to immunosuppression and EBV-induced B cell proliferation. Non-Hodgkin's lymphoma or monomorphic PTLD accounts for 93% of PTLD and affects extra-nodal sites including both native and transplant kidneys. Allograft involvement has been reported in up to 30% of cases [73]. Mortality rate for this group of patients remains high, between 22% and 39% [74]. Survival is worse in patients older than 55 years, in late-onset PTLD, after azathioprine use and in those with multisite involvement and high Ann Arbor staging [75,76]. Treatment includes reduction or change of immunosuppression (particularly cyclosporin), systemic chemotherapy, and surgical resection, depending on the presentation and site involvement. Allograft involvement usually occurs in association with disseminated multi-organ involvement [73]. It occurs as focal renal masses in normal sized kidneys or diffuse infiltration causing renal enlargement. Focal renal masses mirror appearances of renal non-Hodgkin's lymphoma described previously. There is a noteworthy predilection for renal hilar involvement and encasement of the renal vessels. Ultrasound and MRI are both suitable imaging modalities for surveillance of the allograft, although lesion

(a)

Figure 7.17a Non-enhanced CT demonstrating end-stage kidneys with multiple calcified cysts. A high attenuation solid mass is seen in the posterior cortex with an attenuation value of 39 HU.

(b)

Figure 7.17b Contrast-enhanced CT demonstrating poor enhancement of the solid mass (arrow) to 50 HU. Histologically this was a papillary RCC.

characterization is superior on MRI [77]. Ultrasound has the added advantage of guiding biopsies of detected masses.

Renal cell carcinomas account for 4.6% of post-transplant cancers and less than 10% occur in the allograft kidney [78]. Although probably not related to increased immunosuppression, renal cell carcinoma, particularly papillary RCC, occurs at a higher rate in the native kidneys of transplant recipients than the normal population [78]. The likely reason relates to the presence of acquired cystic disease in the native kidneys, a finding correlated with length of time on dialysis and an increased incidence of carcinomas in end-stage renal disease. The imaging features are similar to papillary RCC in the non-immunocompromised population (Figures 7.17a and b). In a study comparing the biological behavior of renal cancer among transplant patients and those undergoing chronic dialysis, Pope *et al.* showed that RCCs in the transplanted group behaved more aggressively, with a higher rate of metastatic disease (in 53% of patients) at presentation and a higher mortality rate [79]. An increased incidence of urothelial carcinomas has also been reported, and analgesic overuse underlies the association between end-stage renal failure and TCC [71].

Acquired immunodeficiency disorder syndrome (AIDS)

About 30%–50% of patients with AIDS develop a cancer. Kaposi's sarcoma (KS) and AIDS-related lymphoma (ARL) account for the majority of the renal neoplasms. Highly aggressive B-cell, non-Hodgkin's lymphoma is the most common type but Burkitt type and Hodgkin's lymphoma are also seen. Solid organs are more frequently involved than in non-ARL lymphoma, conversely enlarged lymphadenopathy is less frequent. In patients with ARL, imaging shows renal involvement in 3%–11% usually as part of disseminated, asymptomatic disease. The commonest pattern is multifocal bilateral discrete renal masses. Diffuse renal infiltration has not been described in AIDS. Enlarged retroperitoneal nodes may directly invade the kidneys or the ureters leading to obstruction of the collecting system [80,81,82].

Kaposi's sarcoma, which may involve any urogenital organ, is usually part of systemic disease. Renal involvement is present in 11% of patients with evidence of abdominal KS. This is seldom demonstrated on imaging as the involvement is microscopic [80,83]. On abdominal CT the commonest form of renal involvement is secondary to extensive retroperitoneal lymphadenopathy which invades and obstructs the collecting system. The key feature of KS-related retroperitoneal lymphadenopathy is avid enhancement of the nodes after contrast administration. It may also occur in the form of a "sheet" of abnormal tissue occupying the retroperitoneum [82]. CT remains the primary mode of evaluation for diagnosis, biopsy guidance, and to monitor response to chemotherapy.

Conclusion

Renal cancer is a heterogeneous collection of malignancies with overlapping imaging features among the histological subtypes. The variable biological behavior of renal cancers has led to an increasing diversity in their management. In this chapter we have discussed imaging features of some unusual tumors that may aid preoperative identification. These include some papillary, chromophobe and collecting duct carcinomas, lymphoma, and upper tract TCC. Preoperative information of the likely tumor type allows more appropriate treatment selection. The increasing use of radiologically led ablation techniques, which are more suitable for small, less aggressive tumors, requires the radiologist to distinguish between histological subtypes based on the imaging features or from imaging guided biopsy.

REFERENCES

1. J. A. Leslie, T. Prihoda, and I. M. Thompson, Serendipitous renal cell carcinoma in the post-CT era: continued evidence in improved outcomes. *Urol Oncol*, **21** (2003), 39–44.
2. W. Y. Siow, S. K. Yip, L. G. Ng *et al.*, Renal cell carcinoma: incidental detection and pathological staging. *J R Coll Surg Edin*, **45** (2000), 291–5.
3. D. A. Barocas, S. M. Rohan, J. Kao *et al.*, Diagnosis of renal tumors on needle biopsy specimens by histological and molecular analysis. *J Urol*, **176**:5 (2006), 1957–62.
4. B. K. Somani, G. Nabi, P. Thorpe *et al.*, Aberdeen academic and clinical urological surgeons (ABACUS) group. Image-guided biopsy-diagnosed renal cell carcinoma: critical appraisal of technique and long-term follow-up. *Eur Urol*, **51**:5 (2007, May), 1289–95.
5. A. Lopez-Beltran, M. Scarpelli, R. Montironi *et al.*, 2004 WHO classification of the renal tumors of the adults. *Eur Urol*, **49**:5 (2006), 798–805.
6. K. A. Furge, K. A. Lucas KA, M. Takahashi *et al.*, Robust classification of renal cell carcinoma based on gene expression data and predicted cytogenetic profiles. *Cancer Res*, **64**:12 (2004), 4117–21.
7. M. B. Amin, C. L. Corless, A. A. Renshaw *et al.*, Papillary (chromophil) renal cell carcinoma: histomorphologic characteristics and evaluation of conventional pathologic prognostic parameters in 62 cases. *Am J Surg Pathol*, **21**:6 (1997), 621–35.
8. E. A. Ronnen, G. V. Kondagunta, N. Ishill *et al.*, Treatment outcome for metastatic papillary renal cell carcinoma patients. *Cancer*, **107**:11 (2006), 2617–21.
9. B. R. Herts, D. M. Coll, A. C. Novick *et al.*, Enhancement characteristics of papillary renal neoplasms revealed on triphasic helical CT of the kidneys. *AJR Am J Roentgenol*, **178**:2 (2002), 367–72.
10. J. K. Kim, T. K. Kim, H. J. Ahn *et al.*, Differentiation of subtypes of renal cell carcinoma on helical CT scans. *AJR Am J Roentgenol*, **178**:6 (2002), 1499–506.
11. H. Fujimoto, F. Wakao, N. Moriyama *et al.*, Alveolar architecture of clear cell renal carcinomas ($<$ or $=$ 5.0 cm) show high attenuation on dynamic CT scanning. *Jpn J Clin Oncol*, **29**:4 (1999), 198–203.
12. T. G. Schuster, M. R. Ferguson, D. E. Baker *et al.*, Papillary renal cell carcinoma containing fat without calcification mimicking angiomyolipoma on CT. *AJR Am J Roentgenol*, **183**:5 (2004), 1402–4.
13. C. Roy, B. Sauer, V. Lindner *et al.*, MR imaging of papillary renal neoplasms: potential application for characterization of small renal masses. *Eur Radiol*, **17**:1 (2007, January), 193–200.
14. K. Tsuda, T. Kinouchi, G. Tanikawa *et al.*, Imaging characteristics of papillary renal cell carcinoma by computed tomography scan and magnetic resonance imaging. *Int J Urol*, **12**:9 (2005), 795–800.
15. K. T. Mai, P. Dhamanaskar, E. Belanger *et al.*, Hybrid chromophobe renal cell neoplasm. *Pathol Res Pract*, **201**:5 (2005), 385–9.

16. M. Akhtar, H. Kardar, T. Linjawi *et al.*, Chromophobe cell carcinoma of the kidney. A clinicopathologic study of 21 cases. *Am J Surg Pathol*, **19**:11 (1995), 1245–56.
17. P. Soyer, A. Dufresne, I. Klein *et al.*, Renal cell carcinoma of clear type: correlation of CT features with tumor size, architectural patterns, and pathologic staging. *Eur Radiol*, **7**:2 (1997), 224–9.
18. K. Yoshimitsu, H. Irie, T. Tajima *et al.*, Iimaging of renal cell carcinoma: its role in determining cell type. *Radiat Med*, **22**:6 (2004), 371–6.
19. N. Tokuda, S. Naito, O. Matsuzaki *et al.*, Japanese Society of Renal Cancer. Collecting duct (Bellini duct) renal cell carcinoma: a nationwide survey in Japan. *J Urol*, **76**:1 (2006), 40–3; discussion 43.
20. P. Levy, O. Helenon, S. Merran *et al.*, Cystic tumors of the kidney in adults: radio-histopathologic correlations. *J Radiol*, **80**:2 (1999), 121–33.
21. J. C. Kim, K. H. Kim, and J. W. Lee, CT and US findings of multilocular cystic renal cell carcinoma. *Korean J Radiol*, **1**:2 (2000), 104–9.
22. K. R. Han, N. K. Janzen, V. C. McWhorter *et al.*, Cystic renal cell carcinoma: biology and clinical behaviour. *Urol Oncol*, **22**:5 (2004), 410–4.
23. D. S. Hartman, C. J. Davis, Jr., T. Johns *et al.*, Cystic renal cell carcinoma. *Urology*, **28**:2 (1986), 145–53.
24. J. N. Eble and S. M. Bonsib, Extensively cystic renal neoplasms: cystic nephroma, cystic partially differentiated nephroblastoma, multilocular cystic renal cell carcinoma, and cystic hamartoma of renal pelvis. *Semin Diagn Pathol*, **15**:1 (1998), 2–20.
25. S. Aubert, L. Zini, J. Delomez *et al.*, Cystic renal cell carcinomas in adults. Is preoperative recognition of multilocular cystic renal cell carcinoma possible? *J Urol*, **174**:6 (2005), 2115–19.
26. E. M. Genega and C. R. Porter, Urothelial neoplasms of the kidney and ureter. An epidemiologic, pathologic, and clinical review. *Am J Clin Pathol*, **117**:Suppl (2002), S36–48.
27. E. M. Genega, M. Kapali, M. Torres-Quinones *et al.*, Impact of the 1998 World Health Organization/International Society of Urological Pathology classification system for urothelial neoplasms of the kidney. *Mod Pathol*, **18**:1 (2005), 11–18.
28. S. Olgac, M. Mazumdar, G. Dalbagni *et al.*, Urothelial carcinoma of the renal pelvis: a clinicopathologic study of 130 cases. *Am J Surg Pathol*, **28**:12 (2004), 1545–52.
29. O. M. Jensen, J. B. Knudsen, J. K. McLaughlin *et al.*, The Copenhagen case-control study of renal pelvis and ureter cancer: role of smoking and occupational exposures. *Int J Cancer*, **41**:4 (1988), 557–61.
30. J. E. Greenland, P. M. Weston, and D. M. Wallace, Familial transitional cell carcinoma and the Lynch syndrome II. *Br J Urol*, **72**:2 (1993), 177–80.
31. V. Stefanovic, D. Toncheva, S. Atanasova *et al.*, Etiology of Balkan endemic nephropathy and associated urothelial cancer. *Am J Nephrol*, **26** (2006), 1–11.
32. B. N. Nocks, N. M. Heney, J. J. Daly *et al.*, Transitional cell carcinoma of renal pelvis. *Urology*, **19**:5 (1982), 472–7.
33. G. D. Stewart, S. V. Bariol, K. M. Grigor *et al.*, A comparison of the pathology of transitional cell carcinoma of the bladder and upper urinary tract. *BJU Int*, **95**:6 (2005), 791–3.

34. D. Perez-Montiel, P. E. Wakely, O. Hes *et al.*, High-grade urothelial carcinoma of the renal pelvis: clinicopathologic study of 108 cases with emphasis on unusual morphologic variants. *Mod Pathol*, **19**:4 (2006), 494–503.
35. H. Miyake, I. Hara, K. Gohji *et al.*, The significance of lymphadenectomy in transitional cell carcinoma of the upper urinary tract. *Br J Urol*, **82**:4 (1998), 494–8.
36. N. Miyao, N. Masumori, A. Takahashi *et al.*, Lymph node metastasis in patients with carcinomas of the renal pelvis and ureter. *Eur Urol*, **33**:2 (1998), 180–5.
37. D. S. Elliott, J. W. Segura, D. Lightner *et al.*, Is nephroureterectomy necessary in all cases of upper tract transitional cell carcinoma? Long-term results of conservative endourologic management of upper tract TCC in individuals with a normal contralateral kidney. *Urology*, **58**:2 (2001), 174–8.
38. G. L. Chen and D. H. Bagley, Ureteroscopic management of upper tract transitional cell carcinoma in patients with normal contralateral kidneys. *J Urol*, **164** (2000), 1173–6.
39. F. X. Keeley, Jr., M. Bibbo, and D. H. Bagley, Ureteroscopic treatment and surveillance of upper urinary tract transitional cell carcinoma. *J Urol*, **157**:5 (1997), 1560–5.
40. S. Razdan, J. Johannes, M. Cox *et al.*, Current practice patterns in urologic management of upper-tract transitional-cell carcinoma. *J Endourol*, **19**:3 (2005), 366–71.
41. E. K. Seaman, K. M. Slawin, and M. C. Benson, Treatment options for upper tract transitional-cell carcinoma. *Urol Clin North Am*, **20**:2 (1993), 349–54.
42. E. K. Lang, R. Thomas, R. Davis *et al.*, Multiphasic helical computerized tomography for the assessment of microscopic hematuria: a prospective study. *J Urol*, **171** (2004), 237–43.
43. M. J. Scolieri, M. L. Paik, S. L. Brown *et al.*, Limitations of computed tomography in the preoperative staging of upper tract urothelial carcinoma. *Urology*, **56**:6 (2000), 930–4.
44. J. A. Buckley, B. A. Urban, P. Soyer *et al.*, Transitional cell carcinoma of the renal pelvis: a retrospective look at CT staging with pathologic correlation. *Radiology*, **201**:1 (1996), 194–8.
45. J. G. McCoy, H. Honda, M. Reznicek *et al.*, Computerized tomography for detection and staging of localized and pathologically defined upper tract urothelial tumors. *J Urol*, **146**:6 (1991), 1500–3.
46. E. M. Caoili, R. H. Cohan, P. Inampudi *et al.*, MDCT urography of upper tract urothelial neoplasms. *AJR Am J Roentgenol*, **184**:6 (2005), 1873–81.
47. G. A. Fritz, H. Schoellnast, H. A. Deutschmann *et al.*, Multiphasic multidetector-row CT (MDCT) in detection and staging of transitional cell carcinomas of the upper urinary tract. *Eur Radiol*, **16**:6 (2006), 1244–52.
48. M. C. Goel, V. Mahendran, and J. G. Roberts,. Percutaneous management of renal urothelial tumours: long-term follow-up. *J Urol*, **169**:3 (2003), 925–9.
49. E. Deligne, M. Colombel, L. Badet *et al.*, Conservative management of upper urinary tract tumors. *Eur Urol*, **42** (2002), 43–8.
50. T. R. Hatch, T. R. Hefty, and J. M. Barry, Time-related recurrence rates in patients with upper tract transitional cell carcinoma. *J Urol*, **140**:1 (1988), 40–1.
51. P. Hallscheidt, N. Wagener, F. Gholipour *et al.*, Multislice computed tomography in planning nephron-sparing surgery in a prospective study with 76 patients: comparison of radiological and

histopathological findings in the infiltration of renal structures. *J Comput Assist Tomogr*, **30**:6 (2006), 869–74.

52. S. M. Weeks, E. D. Brown, J. J. Brown *et al.*, Transitional cell carcinoma of the upper urinary tract: staging by MRI. *Abdom Imaging*, **20**:4 (1995), 365–7.
53. W. M. Deserno, M. G. Harisinghani, M. Taupitz *et al.*, Urinary bladder cancer: preoperative nodal staging with ferumoxtran-10-enhanced MR imaging. *Radiology*, **233**:2 (2004), 449–56.
54. J. E. Montie, Urinary bladder cancer: preoperative nodal staging with ferumoxtran-10-enhanced MR imaging. *J Urol*, **174**:3 (2005), 870–1.
55. R. Chahal, K. Taylor, I. Eardley *et al.*, Patients at high risk for upper tract urothelial cancer: evaluation of hydronephrosis using high resolution magnetic resonance urography. *J Urol*, **174**:2 (2005), 478–82.
56. J. E. Busby, G. A. Brown, P. Tamboli P *et al.*, Upper urinary tract tumors with nontransitional histology: a single-centre experience. *Urology*, **67**:3 (2006), 518–23.
57. Y. Narumi, T. Sato, S. Hori *et al.*, Squamous cell carcinoma of the uroepithelium: CT evaluation. *Radiology*, **173**:3 (1989), 853–6.
58. O. Miyake, M. Namiki, T. Sonoda *et al.*, Secondary involvement of genitourinary organs in malignant lymphoma. *Urol Int*, **42**:5 (1987), 360–2.
59. M. A. Richards, I. Mootoosamy, R. H. Reznek *et al.*, Renal involvement in patients with non-Hodgkin's lymphoma: clinical and pathological features in 23 cases. *Hematol Oncol*, **8**:2 (1990), 105–10.
60. R. H. Reznek, I. Mootoosamy, J. A. Webb *et al.*, CT in renal and perirenal lymphoma: a further look. *Clin Radiol*, **42**:4 (1990), 233–8. Erratum in: *Clin Radiol*, **43**:4 (1991), 289.
61. R. H. Cohan, N. R. Dunnick, R. A. Leder *et al.*, Computed tomography of renal lymphoma. *J Comput Assist Tomogr*, **14**:6 (1990), 933–8.
62. G. Stallone, B. Infante, C. Manno *et al.*, Primary renal lymphoma does exist: case report and review of the literature. *J Nephrol*, **13**:5 (2000), 367–72.
63. A. Cupisti, R. Riccioni, G. Carulli *et al.*, Bilateral primary renal lymphoma treated by surgery and chemotherapy. *Nephrol Dial Transplant*, **19**:6 (2004), 1629–33.
64. F. Moog, M. Bangerter, C. G. Diederichs *et al.*, Extranodal malignant lymphoma: detection with FDG PET versus CT. *Radiology*, **206**:2 (1998), 475–81.
65. B. A. Urban and E. K. Fishman, Renal lymphoma: CT patterns with emphasis on helical CT. *Radiographics*, **20**:1 (2000), 197–212.
66. N. B. Chepuri, P. J. Strouse, and G. A. Yanik, CT of renal lymphoma in children. *AJR Am J Roentgenol*, **180**:2 (2003), 429–31.
67. N. B. Chepuri, P. J. Strouse, and G. A. Yanik, CT of renal lymphoma in children. Imaging of renal lymphoma: patterns of disease with pathologic correlation. *Radiographics*, **26** (2006), 1151–68.
68. S. R. Sheeran and S. K. Sussman, Renal lymphoma: spectrum of CT findings and potential mimics. *AJR Am J Roentgenol*, **171** (1998), 1067–72.

69. B. Jamil, K. Nicholls, G. J. Becker *et al.*, Impact of acute rejection therapy on infections and malignancies in renal transplant recipients. *Transplantation*, **68**:10 (1999), 1597–603.
70. J. Dantal, M. Hourmant, D. Cantarovich *et al.*, Effect of long-term immunosuppression in kidney-graft recipients on cancer incidence: randomised comparison of two cyclosporin regimens. *Lancet*, **351**:9103 (1998), 623–8.
71. V. Kliem, M. Kolditz, M. Behrend *et al.*, Risk of renal cell carcinoma after kidney transplantation. *Clin Transplant*, **11**:4 (1997), 255–8.
72. M. A. Martin-Gomez, M. Pena, M. Cabello *et al.*, Post transplant lymphoproliferative disease: a series of 23 cases. *Transplant Proc*, **38**:8 (2006), 2448–50.
73. P. J. Pickhardt and M. J. Siegel, Abdominal manifestations of post transplantation lymphoproliferative disorder. *AJR Am J Roentgenol*, **171**:4 (1998), 1007–13.
74. S. Caillard, C. Lelong, F. Pessione *et al.*, Working group. Post-transplant lymphoproliferative disorders occurring after renal transplantation in adults: report of 230 cases from the French Registry. *Am J Transplant*, **6**:11 (2006), 2735–42.
75. K. Burney, M. Bradley, A. Buckley *et al.*, Post transplant lymphoproliferative disorder: A pictorial review. *Australas Radiol*, **50**:5 (2006), 412–18.
76. M. J. Soler, J. M. Puig, M. Mir *et al.*, Posttransplant lymphoproliferative disease: treatment and outcome in renal transplant recipients. *Transplant Pro*, **35**:5 (2003), 1709–13.
77. M. G. Ali, F. V. Coakley, H. Hricak *et al.*, Complex post transplantation abnormalities of renal allografts: evaluation with MR imaging. *Radiology*, **211**:1 (1999), 95–100.
78. S. K. Tickoo, M. N. dePeralta-Venturina, L. R. Harik *et al.*, Spectrum of epithelial neoplasms in end-stage renal disease: an experience from 66 tumor-bearing kidneys with emphasis on histologic patterns distinct from those in sporadic adult renal neoplasia. *Am J Surg Pathol*, **30**:2 (2006), 141–53.
79. J. C. Pope, M. O. Koch, and R. F. Bluth, Renal cell carcinoma in patients with end-stage renal disease: a comparison of clinical significance in patients receiving hemodialysis and those with renal transplants. *Urology*, **44**:4 (1994), 497–501.
80. C. F. Heyns and M. Fisher, The urological management of the patient with acquired immunodeficiency syndrome. *BJU Int*, **95**:5 (2005), 709–16.
81. D. R. Radin, J. A. Esplin, A. M. Levine *et al.*, AIDS-related non-Hodgkin's lymphoma: abdominal CT findings in 112 patients. *AJR Am J Roentgenol*, **160**:5 (1993), 1133–9.
82. D. A. Nyberg, R. B. Jeffrey, Jr., M. P. Federle *et al.*, AIDS-related lymphomas: evaluation by abdominal CT. *Radiology*, **159**:1 (1986), 59–63.
83. J. E. Kuhlman, D. Browne, M. Shermak *et al.*, Retroperitoneal and pelvic CT of patients with AIDS: primary and secondary involvement of the genitourinary tract. *Radiographics*, **11**:3 (1991), 473–83.

8

Surgery for renal cancer: current status

Ravi Barod and Tim O'Brien

Introduction

Currently, surgery offers the only well-recognized chance of cure from kidney cancer. The principal developments in renal cancer surgery in recent years relate to the use of laparoscopy and it is likely that the scope of minimal access surgery will continue to increase in the future. In this chapter, we give an overview of the indications and current status of both open and laparoscopic techniques of radical and partial nephrectomy, as well as surgery for metastatic disease.

Radical nephrectomy (RN)

Surgery has been the mainstay of treatment of renal cell carcinoma (RCC) for over 35 years and remains the only curative therapeutic approach. In 1969, Robson *et al.* described their results from radical nephrectomy in a series of 88 patients with RCC [1]. The original operation involved early ligation of renal vessels to avoid tumor embolization, adrenalectomy, removal of perirenal fat, and extensive lymph node dissection from the crus of the diaphragm to the bifurcation of the aorta. This approach was described in a time when diagnosis was often made on the basis of intravenous urography (IVU) or angiography. Accurate preoperative anatomical definition was not possible and the tumor was often of an advanced stage at operation. Recently, with the increased sensitivity of imaging and high resolution computerized tomography (CT) scans the exact anatomy of the tumor can be confidently mapped prior to surgery. This has called into question several of the individual components of the original operation, such as the necessity for extensive lymphadenectomy, adrenalectomy, and excision of the entire kidney. Preoperative evaluation is now non-invasive in the majority of patients and involves ultrasonography (US), computerized tomography, or magnetic resonance imaging (MRI).

Carcinoma of the Kidney, ed. Uday Patel. Published by Cambridge University Press.

All patients should undergo metastatic evaluation with abdominal CT [2] and at least chest radiography, but those with large primary tumors should also have a chest CT. If the patient has bone pain or an elevated alkaline phosphatase, a bone scan is indicated. If the vena cava is involved, the distal limit of caval involvement must be determined prior to surgery and MRI and transoesophageal echocardiography may be of benefit to further assess the supra-diaphragmatic cava and the right atrium. Complications occur in approximately 20% of patients after open radical nephrectomy and the operative mortality rate is 2% [3]. Specific complications after renal surgery include: gastrointestinal injury, pancreatic fistula with possible development of pseudocyst and abscess, and pneumothorax. Liver and splenic lacerations are also recognized.

Lymphadenectomy

The risk of developing lymph node metastases in RCC is around 20% [4] and although the prognostic value of lymphadenectomy is undoubted (the 5-year survival in those with lymph node involvement is 5%–30%), its therapeutic value in the routine treatment of RCC is controversial [5]. The benefits include accurate staging, theoretical lower risk of local recurrence owing to more extensive renal bed dissection, and potential cure in patients with isolated ipsilateral node involvement. The disadvantages include increased operation time and blood loss, leading to greater morbidity. Retrospective studies have given conflicting advice on the benefits of lymphadenectomy. Data from a prospective European Organization for Research and Treatment of Cancer study (EORTC 30881) comparing RN with or without lymphadenectomy, failed to demonstrate a difference in survival between the 2 groups after a median 5-year follow-up [6]. Longer follow-up may be required to demonstrate any possible survival differences.

Increased sensitivity of preoperative imaging, with its high negative predictive value when nodes are of a normal size on CT or MRI, means that staging accuracy is no longer likely to be significantly improved by lymphadenectomy if the imaging is negative. However, the positive predictive value of CT and MRI for abnormal nodes on imaging criteria is more modest (as discussed in Chapter 5, the false positive rate may be up to 50%) and lymphadenectomy may be useful for staging when the nodes are enlarged preoperatively [7]. Lymphadenectomy in patients with retroperitoneal node involvement has been shown to improve outcome of metastatic disease when treated with IL-2 [8]. In this context, resection of the involved nodes may give the best chance of a complete response.

Adrenalectomy

The incidence of adrenal metastases at RN is estimated at 2%–10%, but is now at the lower end of the range with the downward-stage migration of the disease at presentation. Provided the preoperative staging imaging is negative (the negative predictive value of a normal-sized adrenal on CT/MRI is almost 99%, see Chapter 5 for further details) routine adrenalectomy is now felt to be generally unnecessary during the surgical treatment of RCC. Studies have shown no difference in cancer-specific survival between patients who have or have not had adrenalectomy [9,10]. Additionally, if the ipsilateral adrenal is routinely removed and the patient develops contralateral adrenal masses, they may develop adrenal insufficiency. This is an issue, as they may become steroid-dependent, which could negatively impact on the effect of immunotherapy to treat their metastatic disease. However, tumors greater than 7 cm in diameter are associated with an increased risk of adrenal metastases and approximately half of all adrenal metastases develop from upper pole tumors. Therefore, adrenalectomy is recommended in the presence of large upper pole tumors.

Laparoscopic radical nephrectomy

Clayman *et al.* first described this procedure in 1991 as an alternative to open surgery in the management of localized disease [11]. The procedure has a long learning curve, during which time the complication rate is relatively high. However, with adequate laparoscopic training and patient selection, oncological outcome and complication rates are equivalent to open RN, with decreased morbidity and improved cosmesis [12,13]. It may be regarded as standard treatment for organ-confined T1 and T2 disease when performed by experienced surgeons. Some specialist centers have also reported success in T3a disease, but a greater level of technical expertise is required to perform the operation in this group of patients. Laparoscopic RN is contraindicated in patients with tumors involving the renal vein or IVC (Figures 8.1, 8.2, and 8.3).

There are two main approaches: transperitoneal and retroperitoneal (via a flank incision). A hand-assisted laparoscopic RN may be used by novice laparoscopic surgeons for large tumors. The main long-term adverse effect is the risk of port site metastases and tumor spillage, which is reported to occur in 0%–6.25% of patients undergoing the procedure. This is minimized by adhering to the basic principles of cancer surgery, including: minimal violation and direct handling of the tumor, collection of all potentially cancerous material in an impermeable sack, removal of

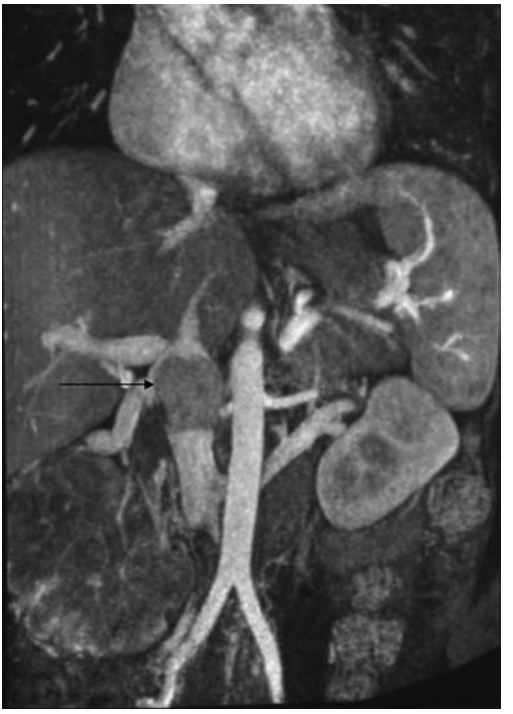

Figure 8.1 Right-sided kidney tumor with thrombus occluding the IVC (arrow).

Figure 8.2 Left-sided renal tumor with thrombus filling the retro-aortic renal vein (arrow) and extending into the IVC.

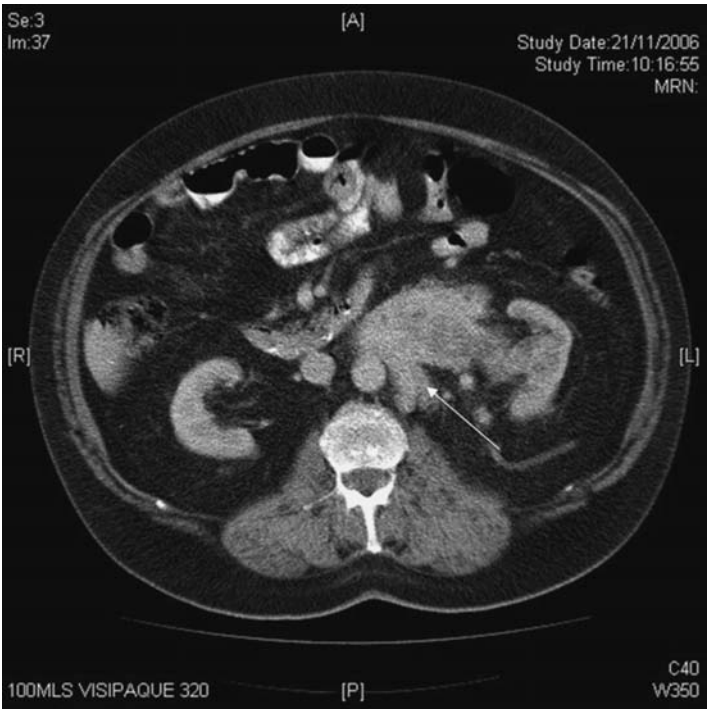

Figure 8.3 Left-sided tumor with massive distension of the left renal vein and extension of tumor into left lumbar veins (arrowed).

contaminated instruments from the operative field, and draping the operative field before morcellation or extraction of the tumor.

Nephron-sparing surgery

Open partial nephrectomy

Smaller tumors may be treated with partial nephrectomy with the benefit of renal parenchymal sparing. Recent studies show equivalent cancer-specific survival rates, hospital stay, blood loss, and complication rates as open RN [14,15,16]. The indications may be classified as: absolute (tumor in an anatomical or functional solitary kidney), relative (tumor in a kidney of a patient with a condition that may impair renal function in the future), or elective (tumor in one kidney with a healthy contralateral kidney). Figures 8.4, 8.5, and 8.6 illustrate examples of various tumors suitable for partial nephrectomy and the indications are listed in Table 8.1.

Preoperative evaluation is the same as for radical nephrectomy, but split renal function should be obtained by functional isotope scan prior to surgery. Complete delineation of the renal blood supply is mandatory for central tumors and can be

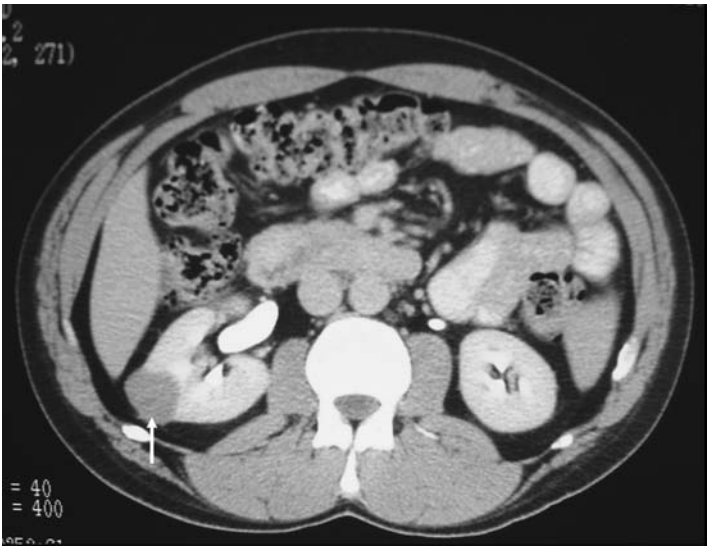

Figure 8.4 Indications for partial nephrectomy. This image shows a 3 cm right kidney tumor (arrowed) with normal contralateral kidney. The tumor is small and peripherally located and so suitable for partial nephrectomy but this is an elective indication for partial resection.

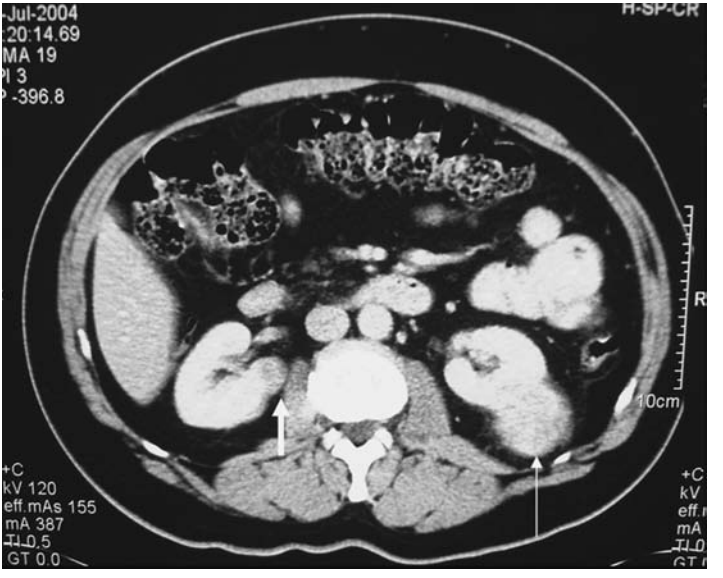

Figure 8.5 This is an example of an imperative indication for partial nephrectomy as the patient has bilateral renal tumors. There is a 5 cm left-sided kidney tumor (thin arrow and only the upper extent of the tumor seen) and a 1.5 cm medial based right-sided tumor (thick, short arrow). Although the left renal tumor is relatively large, being $>$ 4 cm, it is favorably located for partial nephrectomy, being exophytic.

performed by 3D CT scanning (see Chapter 11). Cancer-specific survival rates are better in patients with smaller (pT1a) tumors who have had a PN than those with larger ones (pT2 and above). Generally, the upper limit for elective PN is approximately 4.5 cm but there is now emerging evidence that larger tumors (up to 7 cm) may be treated in this way if surgically amenable, and if adequate margins can be safely

Table 8.1. Indications for partial or nephron-sparing surgery

Indication	Examples
Absolute	RCC in a solitary kidney
	Bilateral RCC
	RCC with a poorly functional contralateral kidney
Relative	Unilateral RCC in patients with diabetes mellitus, hypertension, renovascular, or connective tissue disease
	Renal dysfunction
	Hereditary or familial RCC
Elective	RCC < 4.5 cm diameter
	Bosniak type 3 or indeterminate cyst

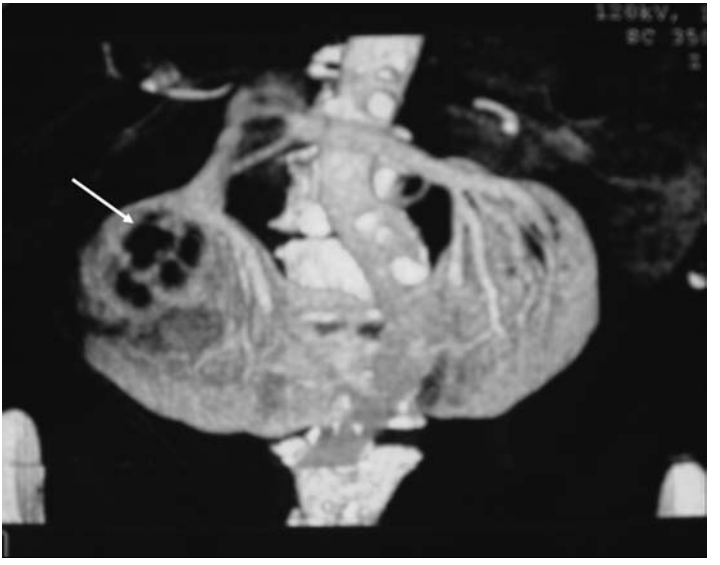

Figure 8.6 Another imperative indication for partial nephrectomy. There is a 6 cm tumor in the right wing of a horseshoe kidney (arrowed) as seen on this volume rendered CT image.

obtained. Complications include hemorrhage, infection, renal insufficiency, ureteric obstruction, and urinary fistula formation. Urinary leaks are common and usually resolve as the collecting system heals, provided there is adequate drainage. If the leak is persistent, a ureteric stent should be placed and if this is not possible, a percutaneous nephrostomy should be inserted. Operative intervention is rarely required.

A major risk in this operation is that of local recurrence in the remaining part of the kidney caused by incomplete excision or undetected microscopic RCC in the renal remnant. This is observed in 4%–6% of patients [17,18] and examination of

frozen sections from the resection margins at the time of surgery should be performed to reduce this risk. The operation is associated with a higher risk of local recurrence and complications when performed for absolute indications compared with elective indications [19,20]. This is probably because of larger tumor size and, for this reason, these patients should have more intensive follow-up (follow-up strategies and findings are discussed in Chapter 10).

As long as the tumor is completely excised, the thickness of the margin does not affect the rate of local recurrence. Figures 8.7a, b, c, d, and e is a montage illustrating the surgical steps during an open partial nephrectomy. In many

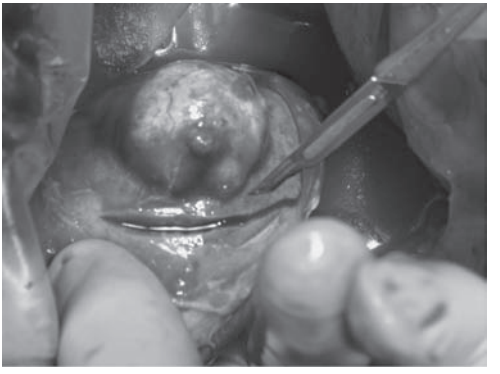

(a)

Figure 8.7a Sequence of images demonstrating a partial nephrectomy being undertaken for a 2 cm renal tumor. This image shows the tumor being excised with a margin of normal tissue (see also color plate section).

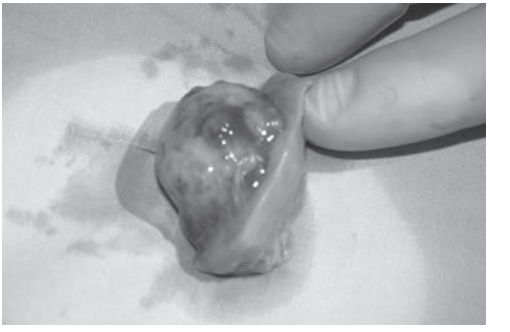

(b)

Figure 8.7b The resected tumor seen on a bed of normal tissue (see also color plate section).

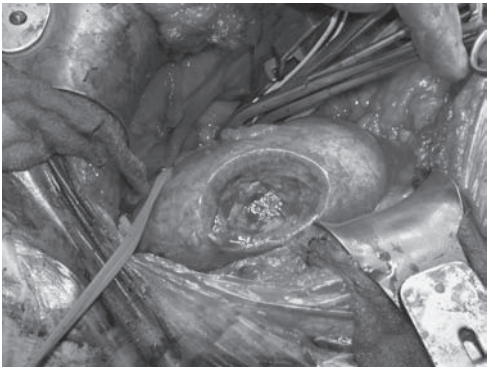

(c)

Figure 8.7c Typical renal defect post-partial nephrectomy (see also color plate section).

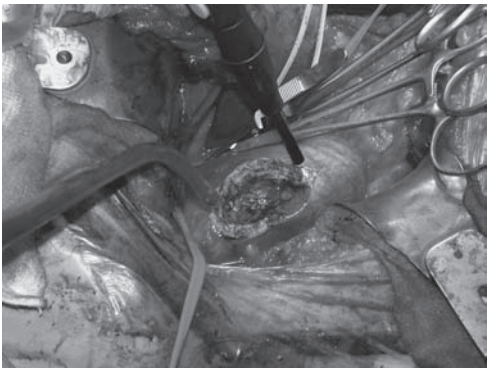

(d)

Figure 8.7d Argon beam coagulator used to seal surface vessels (see also color plate section).

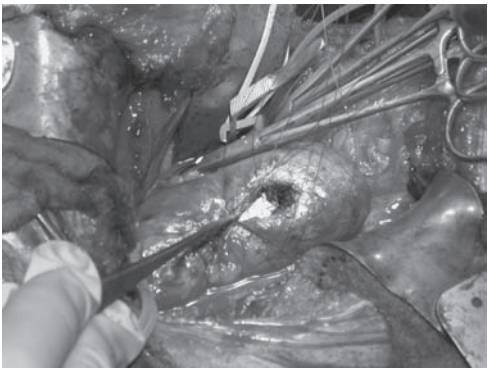

(e)

Figure 8.7e Interrupted sutures to close the renal defect tightly over a hemostatic gauze bolster (see also color plate section).

(a)

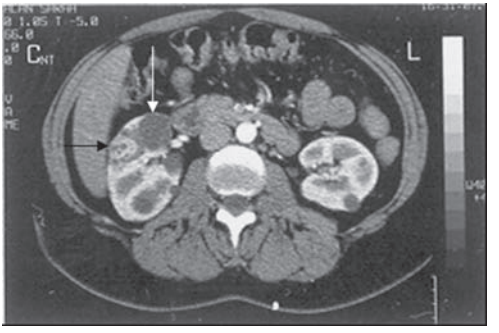

(b)

Figure 8.8a and b Typical renal appearances in von Hippel–Lindau syndrome. The first image is an orthogonal reformatted image showing a complex cyst arising from the lower pole of the left kidney. The second image is an axial image showing cysts in both kidneys (white arrow; right kidney) and a solid tumor also in the right kidney (black arrow).

patients, tumors may be treated either by laparoscopic RN or open PN and the choice must be carefully made. Laparoscopic RN generally involves a shorter hospital stay and less morbidity, whereas open PN offers renal parenchymal sparing and therefore better long-term renal function (Figures 8.8a, b, and c).

Laparoscopic partial nephrectomy

Laparoscopic PN is technically demanding, but it may act as an alternative to open nephron-sparing surgery when performed on a very select patient group by an

Figure 8.8c Operative appearances of the left kidney from the same patient. Note the exophytic lower pole tumor and the multiple cysts (see also color plate section).

(c)

experienced surgeon. Several specialist centers have published intermediate term survival data from this operation which appears to be equivalent to open PN [21,22,23,24]. Relatively small and peripherally placed tumors are ideally suited for this procedure. Operative difficulties include renal hypothermia, parenchymal hemostasis, pelvicalyceal reconstruction, and parenchymal renorraphy. Improvements in hemostasis have been achieved by using electrocautery, ultrasonic energy, argon beam coagulation, and microwave thermotherapy. Closure of the collecting system may be achieved by the use of topical sealants. Currently, open PN is the standard treatment for these tumors, but laparoscopic PN is feasible when performed in experienced centers.

Surgery for metastatic disease

Approximately one-third of patients still present with metastatic renal cancer and 20%–40% of those undergoing nephrectomy for localized disease will eventually develop metastases [4]. Nephrectomy is only curative if all tumor deposits are removed by surgery. The majority of patients with metastatic disease will require systemic treatments for optimal cancer control. Retrospective studies have shown that a small minority of patients show spontaneous regression of their metastases following nephrectomy [25,26]. Standard chemotherapy and radiotherapy are

ineffective in the treatment of metastatic RCC and immunotherapy with interferon gamma (IFN) and interleukin-2 may provide a small but significant effect in 5%–20% of patients.

The role of cytoreductive nephrectomy has been examined prospectively and has been shown to be of benefit in two large trials [27,28]. Patients who had nephrectomy followed by adjuvant IFN had a longer median survival than those treated with IFN alone. Nephrectomy is therefore indicated in patients with metastatic disease who have a good performance status. Cytoreductive nephrectomy is also indicated in patients for symptom control. Examples of such indications include pain caused by tumor mass, intractable hematuria, erythrocytosis, uncontrollable hypertension, and hypercalcemia which is refractory to pharmacological agents. Newer treatments for metastatic RCC include the receptor tyrosine kinase inhibitors Sorafenib and Sunitinib, and the anti-VEGF antibody Bevacizumab (discussed in Chapter 1). Use of these drugs in combination with adjuvant surgery is currently being evaluated.

Metastasectomy

Complete removal of metastatic deposits is associated with improved clinical prognosis. Metastasectomy is therefore indicated in locally recurrent disease, surgically amenable solitary metastases, residual masses post-immunotherapy, and for palliation. Best results are obtained if metastases are pulmonary, solitary, and metachronous with a long disease-free interval [29,30].

Conclusion

The role of surgery for the treatment of renal cell cancer has changed substantially since Robson's pioneering study [1]. The downward-stage migration of the disease at presentation means that many are now treated by radical or partial nephrectomy, either as an open or laparoscopic procedure, with good cure rates. The role of surgery has further expanded to those considered high risk in the past, such as patients with single kidneys; but in other areas the place of surgery has diminished. The thermal ablative therapies (discussed in Chapter 9) may further modify the surgical indications; and adrenalectomy or lymphadenectomy are now only performed in selected cases. Debulking nephrectomy and metastectomy still have a role and this may increase with the advent of targeted therapies for advanced and metastatic disease.

REFERENCES

1. C. J. Robson, B. M. Churchill, and W. Anderson, The results of radical nephrectomy for renal cell carcinoma. *J Urol*, **101**:3 (1969), 297–301.
2. A. Heidenreich and V. Ravery, Preoperative imaging in renal cell cancer. *World J Urol*, **22**:5 (2004), 307–15.
3. D. A. Swanson and P. M. Borges, Complications of transabdominal radical nephrectomy for renal cell carcinoma. *J Urol*, **129**:4 (1983), 704–7.
4. J. S. Lam, O. Shvarts, J. T. Leppart *et al.*, Renal cell carcinoma 2005: new frontiers in staging, prognostication and targeted molecular therapy. *J Urol*, **173**:6 (2005), 1853–62.
5. A. J. Pantuck, A. Zisman, F. Dorey *et al.*, Renal cell carcinoma with retroperitoneal lymph nodes: role of lymph node dissection. *J Urol*, **169**:6 (2003), 2076–83.
6. J. H. Blom, H. van Poppel, J. M. Marechal *et al.*, Radical nephrectomy with and without lymph node dissection: preliminary results of the EORTC randomized phase III protocol 30881. EORTC Genitourinary Group. *Eur Urol*, **36**:6 (1999), 570–5.
7. J. S. Lam, J. S. Belldegrun, and A. J. Pantuck, Long-term outcomes of the surgical management of renal cell carcinoma. *World J Urol*, **24**:3 (2006), 255–66.
8. J. R. Vasselli, J. C. Yang, W. M. Linehan *et al.*, Lack of retroperitoneal lymphadenopathy predicts survival of patients with metastatic renal cell carcinoma. *J Urol*, **166**:1 (2001), 68–72.
9. S. Siemer, J. Lehmann, J. Kamradt *et al.*, Adrenal metastases in 1635 patients with renal cell carcinoma: outcome and indication for adrenalectomy. *J Urol*, **171**:6 (Pt 1) (2004), 2155–9; discussion 2159.
10. K. H. Tsui, O. Shvarts, R. B. Smith *et al.*, Prognostic indicators for renal cell carcinoma: a multivariate analysis of 643 patients using the revised 1997 TNM staging criteria. *J Urol*, **163**:4 (2000), 1090–5; quiz 1295.
11. R. V. Clayman, L. R. Kavoussi, N. J. Soper *et al.*, Laparoscopic nephrectomy. *N Engl J Med*, **324**:19 (1991), 1370–1.
12. M. D. Dunn, A. J. Portis, A. L. Shalhav *et al.*, Laparoscopic versus open radical nephrectomy: a 9-year experience. *J Urol*, **164**:4 (2000), 1153–9.
13. I. S. Gill, D. Schweizer, M. G. Hobart *et al.*, Retroperitoneal laparoscopic radical nephrectomy: the Cleveland clinic experience. *J Urol*, **163**:6 (2000), 1665–70.
14. C. T. Lee, J. Katz, W. Shi *et al.*, Surgical management of renal tumors 4 cm or less in a contemporary cohort. *J Urol*, **163**:3 (2000), 730–6.
15. R. G. Uzzo and A. C. Novick, Nephron sparing surgery for renal tumors: indications, techniques and outcomes. *J Urol*, **166**:1 (2001), 6–18.
16. D. Delakas, I. Karyotis, G. Daskalopoulos *et al.*, Nephron-sparing surgery for localized renal cell carcinoma with a normal contralateral kidney: a European three-center experience. *Urology*, **60**:6 (2002), 998–1002.

17. M. R. Licht, A. C. Novick, and M. Goormastic, Nephron sparing surgery in incidental versus suspected renal cell carcinoma. *J Urol*, **152**:1 (1994), 39–42.
18. F. Steinbach, M. Stockle, S. C. Muller *et al.*, Conservative surgery of renal cell tumors in 140 patients: 21 years of experience. *J Urol*, **148**:1 (1992), 24–9; discussion 29–30.
19. A. R. Kural, O. Demirkesen, B. Onal *et al.*, Outcome of nephron-sparing surgery: elective versus imperative indications. *Urol Int*, **71**:2 (2003), 190–6.
20. K. S. Hafez, A. F. Fergany, and A. C. Novick, Nephron sparing surgery for localized renal cell carcinoma: impact of tumor size on patient survival, tumor recurrence and TNM staging. *J Urol*, **162**:6 (1999), 1930–3.
21. I. S. Gill, S. F. Matin, M. M. Desai *et al.*, Comparative analysis of laparoscopic versus open partial nephrectomy for renal tumors in 200 patients. *J Urol*, **170**:1 (2003), 64–8.
22. R. E. Link, S. B. Bhayani, M. E. Allaf *et al.*, Exploring the learning curve, pathological outcomes and perioperative morbidity of laparoscopic partial nephrectomy performed for renal mass. *J Urol*, **173**:5 (2005), 1690–4.
23. J. J. Rassweiler, C. Abbou, G. Janetschek *et al.*, Laparoscopic partial nephrectomy. The European experience. *Urol Clin North Am*, **27**:4 (2000), 721–36.
24. A. C. Novick, Laparoscopic and partial nephrectomy. *Clin Cancer Res*, **10**:18 (Pt 2) (2004), 6322S–7S.
25. S. G. Marcus, P. L. Choyke, R. Reiter *et al.*, Regression of metastatic renal cell carcinoma after cytoreductive nephrectomy. *J Urol*, **150**:2 (Pt 1) (1993), 463–6.
26. J. E. Montie, B. H. Stewart, R. A. Straffon *et al.*, The role of adjunctive nephrectomy in patients with metastatic renal cell carcinoma. *J Urol*, **117**:3 (1977), 272–5.
27. R. C. Flanigan, S. E. Salmon, B. A. Blumenstein *et al.*, Nephrectomy followed by interferon alfa-2b compared with interferon alfa-2b alone for metastatic renal-cell cancer. *N Engl J Med*, **345**:23 (2001), 1655–9.
28. G. H. Mickisch, A. Garin, H. van Poppel *et al.*, Radical nephrectomy plus interferon-alfa-based immunotherapy compared with interferon alfa alone in metastatic renal-cell carcinoma: a randomized trial. *Lancet*, **358**:9286 (2001), 966–70.
29. H. S. Hofmann, H. Neef, K. Krohe *et al.*, Prognostic factors and survival after pulmonary resection of metastatic renal cell carcinoma. *Eur Urol*, **48**:1 (2005), 77–81; discussion 81–2.
30. H. G. van der Poel, J. A. Roukema, S. Horenblas *et al.*, Metastasectomy in renal cell carcinoma: A multicenter retrospective analysis. *Eur Urol*, **35**:3 (1999), 197–203.

9

Ablation of renal cancer

Elizabeth E. Rutherford and David J. Breen

Introduction

Image-guided ablation is playing an increasingly important role in the management of small renal tumors. The potential benefits of image-guided ablation over traditional surgery include decreased morbidity and inpatient stay, decreased costs and the potential to treat patients who are poor surgical candidates by a minimally invasive approach. All available ablation techniques are based around the principle of utilizing thermal energy (whether it be hot or cold) to destroy tumor tissue. The aim of all ablation methods is to destroy malignant cells by invoking and maintaining cytotoxic temperatures within a tumor, including an adequate margin of surrounding normal tissue.

Cryotherapy

Cryotherapy has been used for many decades but only recently has there been a resurgence of interest in this technique as a result of the introduction of narrow gauge Argon probes (rather than the historical larger nitrogen probes) enabling treatment via a percutaneous approach [1,2,3]. Multiple probes are inserted into the target lesion (either under imaging guidance or direct vision as an open surgical or laparoscopic procedure) and during the freeze cycle, an ice ball develops over approximately 15 minutes. Cryoablation uses multiple freeze–thaw cycles and requires temperatures of at least –20 to –30 °C to induce lasting tissue damage. There are several theories as to the mechanism of tissue destruction [4]. These include protein damage as the cell dehydrates in response to freezing, damaging the cell membrane and intracellular enzymes. The formation of ice crystals within a cell also damages the intracellular organelles and cell membrane. Vascular injury is also

Carcinoma of the Kidney, ed. Uday Patel. Published by Cambridge University Press.

thought to have a role and another theory involves host immuno-sensitization to the tissue treated by cryosurgery, resulting in immune destruction of any undamaged or sub-therapeutically ablated tumor. Cryoablation may achieve a better-defined treatment margin in comparison to radiofrequency ablation (RFA) and the ablated lesion is well visualized at periprocedural CT, ultrasound, or magnetic resonance (MR) imaging; however the expense of the multiple probes is prohibitive at present.

Laser photocoagulation and high intensity focused ultrasound

Interstitial laser photocoagulation was developed in the 1980s and its use has been reported in liver tumors [5] but it too has the disadvantage of having to place multiple fibres to create even modestly sized treatment areas. High intensity focused ultrasound (HIFU) uses ultrasound in the frequency range 0.8 to 3.5 MHz to produce localized tissue necrosis and has been used to treat renal tumors [6,7] with the advantage of being completely non-invasive. The procedure has the disadvantage of being time-intensive as individual HIFU "lesions" are small and have to be "stacked" together to achieve a reasonably sized treatment zone. Microwave ablation is still evolving as a therapeutic technique that works by causing water molecules to oscillate inefficiently, thereby creating heat and thermal damage. It results in higher treatment temperatures than other methods of ablation (typically 120–150 °C) and so treatment times may be quicker but there is an associated increased risk of collateral injury and a fully effective clinical device is still in evolution.

Radiofrequency ablation

Radiofrequency ablation is the most popular technique for the percutaneous treatment of renal tumors due to its ability to safely create a 3–5 cm sphere of treated tissue within a practical time frame and as a minimally invasive procedure. Monopolar RFA is the application of high frequency (460–500 kHz) alternating current to a targeted tissue by means of catheter electrodes with induction of a sphere of thermal energy around the uninsulated catheter tips. This occurs as a result of ion agitation, which causes frictional heating [8]. A large dispersive electrode (grounding pad) is attached to the patient's skin and the concentration of current flux around the much smaller probe tip induces irreversible cell damage (coagulative necrosis) at temperatures of between 55 and 110 °C [9].

Coagulative tissue necrosis can occur at temperatures as low as 46 °C but only if maintained for 60 minutes. Small increases in temperature above this markedly reduce the time required to induce cell death, whilst at temperatures between 60 and 100 °C, near instantaneous cell death occurs [10]. Temperatures in excess of 105 °C can be counterproductive as they induce tissue boiling, vaporization, and carbonization, all of which impair heat transmission from the probe tip to the periphery of the lesion. The goal therefore is to maintain a temperature of between 60 and 100 °C throughout the entire target volume in order to ensure cell death.

Technique of radiofrequency ablation of renal tumors

At our institution, patients are selected for image-guided ablation following multidisciplinary team discussion. After disease staging, the patients are pre-assessed to determine the optimum imaging modality and approach for ablation and their suitability for general anesthesia or conscious sedation. Ablation of renal tumors may be performed under CT, ultrasound, or MR guidance or a combination of imaging modalities depending on operator preference and available resources. It may be performed under general anesthesia or conscious sedation. Several RFA probes are currently available. (Figures 9.1a and 9.1b). Some systems comprise multiple expandable tines, projecting from the tip of a 14- or 15-gauge catheter. The tines can be extended into the target lesion at 1 cm increments to suit the desired treatment volume. Other probes consist of either a 17-gauge needle or a

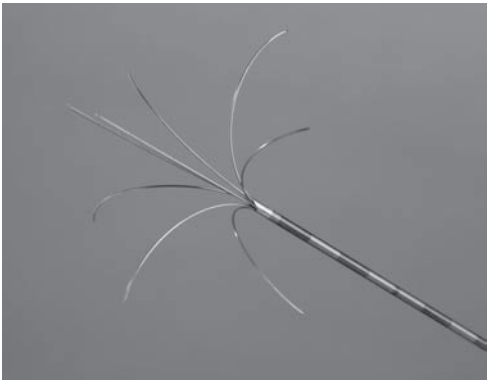

(a)

Figure 9.1a Radiofrequency ablation probe consisting of multiple expandable tines on a 15-gauge catheter.

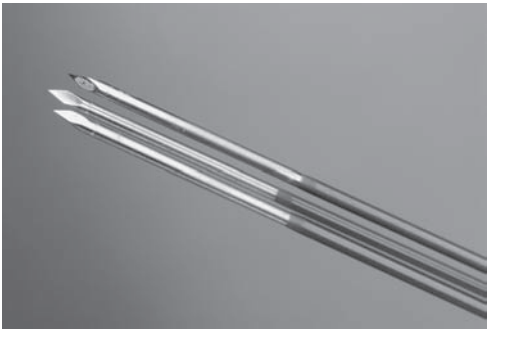

(b)

Figure 9.1b Radiofrequency ablation probe consisting of a cluster of 3 needles in a triangular configuration.

cluster of three needles in a triangular configuration or by "switching" of multiple, separately placed tines.

No absolute indications for the use of RFA in the treatment of renal tumors are currently available. The first line treatment remains partial or radical nephrectomy. There is however a group of patients in whom RFA appears well suited. This includes patients for whom open surgery would pose considerable risk due to comorbidity or who refuse surgery; those with marginal renal reserve where preservation of functioning renal tissue is paramount; and patients at risk of developing further tumors in the future, for example in von Hippel–Lindau disease. Thus the indications overlap with those for partial or nephron-sparing surgery (as discussed in Chapter 8 and listed in Table 8.1). Dependent on accruing experience, the indications may well broaden to include a large proportion of small volume disease.

To perform RFA, the probe is placed within the target tumor under imaging guidance and an appropriate treatment cycle is commenced. The treatment cycles are either impedance regulated or time and temperature regulated, depending on the probe type being used. An average treatment time for a 3 cm tumor would be 20 minutes. Treatment is aimed at achieving a mean target temperature of 105 °C throughout the tumor volume. Most operators would advocate performing thermal "track ablation" at the end of the procedure to reduce the potential risk of track seeding [11]. For all ablation procedures regular imaging follow-up is mandatory. Initial imaging within the first 2 weeks should be performed to assess treatment adequacy. Further regular follow-up should be carried out to confirm adequate treatment and to monitor for local recurrence or metastatic disease (Figures 9.2a, b, and c). CT is the most commonly used modality for follow-up imaging but in cases where intravenous contrast cannot be given, follow-up with MR or contrast-enhanced ultrasound is useful. There is as yet no consensus about the optimum frequency and duration of surveillance, and the complexities regarding the identification of residual or recurrent disease post-thermal ablation are discussed in Chapter 10.

Trouble-shooting during RFA

The most technically demanding part of any ablation procedure is "lesion targeting". This can be made complicated by the presence of hematoma, which distorts local anatomy, so if biopsy of the lesion is to be performed at the time of treatment, this should be performed after the treatment probe has been accurately positioned

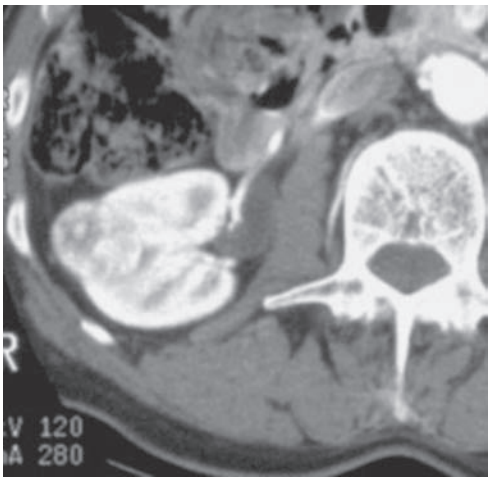

(a)

Figure 9.2a Late arterial phase axial CT image showing a typical 2.5 cm exophytic renal tumor prior to radiofrequency ablation.

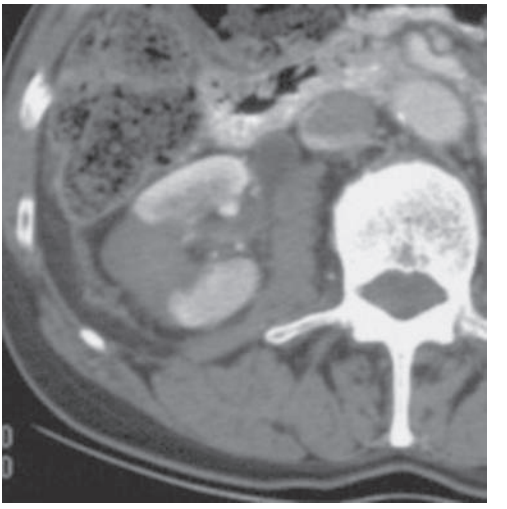

(b)

Figure 9.2b Five days post-radiofrequency ablation. The treated lesion has clearly demarcated margins and demonstrated no contrast enhancement, indicating complete ablation.

(c)

Figure 9.2c Two years post-radiofrequency ablation. Some involution of the ablated lesion has occurred without any enhancement. There is no evidence of disease recurrence.

(Figure 9.3). The perinephric fat generally provides good insulation around target renal lesions but occasionally anterior tumors lie in close proximity to adjacent structures such as the colon or the pancreas. In these cases "hydrodissection" may be employed to displace the adjacent organ and hence reduce risk of thermal injury. This is performed by puncture of the retroperitoneal space with an

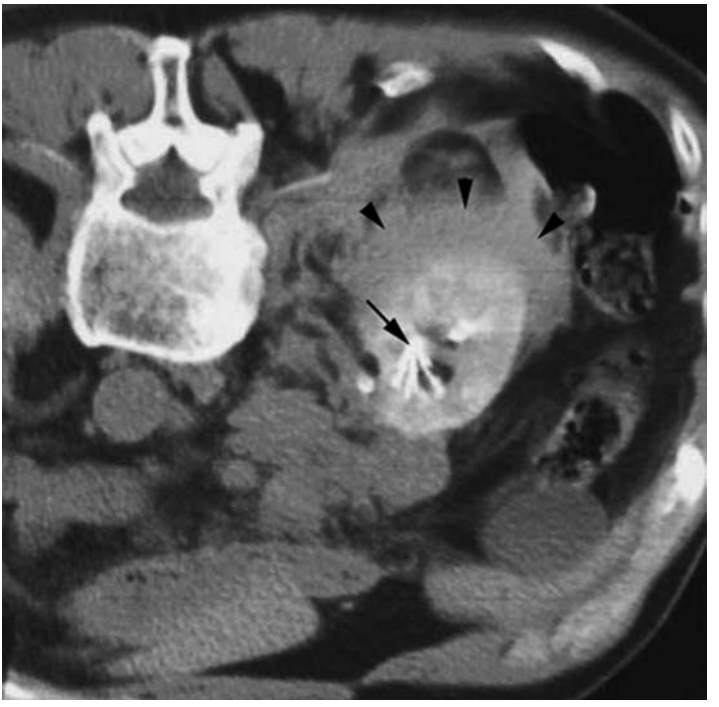

Figure 9.3 Perirenal hematoma (arrowheads) occurring as a result of pre-procedural biopsy hinders subsequent positioning of the radiofrequency ablation probe (arrow) within the target lesion.

18-gauge sheathed needle and instillation of 250 to 750 ml of 5% dextrose ± air to create a safety margin around the tumor.(Figures 9.4a, b, and c). Saline should be avoided, being an ionic conductor.

It can be problematic to obtain reliable, steady, and predictable cytotoxic temperatures within a tumor in vivo. In the clinical situation, there are a number of variables that combine to cause uneven thermal energy deposition. These have been best outlined by Goldberg's modification of Pennes' Bioheat equation [10]. This states that coagulation necrosis is determined by the energy deposited multiplied by local tissue interactions minus heat loss. These local tissue effects may be caused by tumor heterogeneity, and factors such as fibrosis or areas of altered electrical conductivity [12].

Recent results

Radiofrequency ablation. Zlotta *et al.* [13] first reported the treatment of a renal tumor with RFA in 1997. More recently, several large series have been published. These include Gervais *et al.* [14] who have treated 100 tumors in 85 patients over a

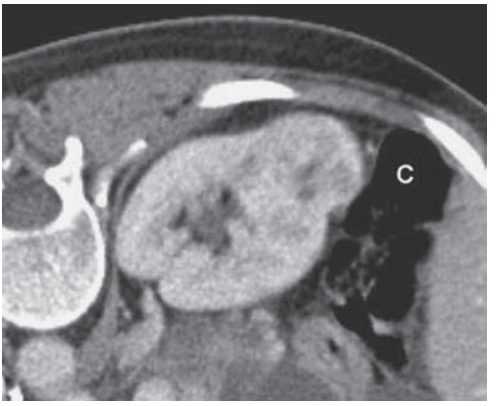

(a)

Figure 9.4a Hydrodissection of a 3 cm exophytic renal tumor seen lying immediately adjacent to colon (C). There is a risk of thermal injury to the colon.

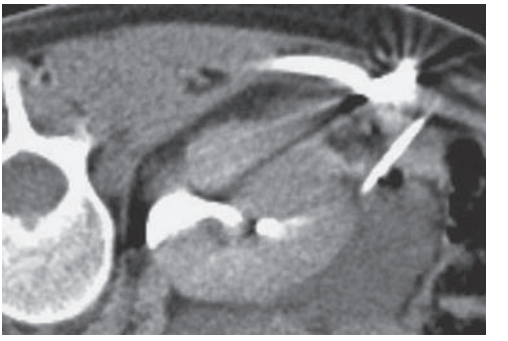

(b)

Figure 9.4b A needle is introduced into the perirenal space and 5% dextrose solution is instilled to dissect and move the colon away from the renal mass.

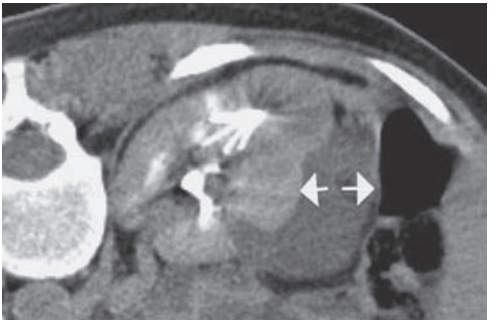

(c)

Figure 9.4c The 5% dextrose has created a "safety margin" (arrows) between the tumor and adjacent colon. An expandable radiofrequency ablation probe has been inserted into the tumor.

6-year period, with 90% of tumors being ablated after a single RFA treatment session. The combined experience of three large urological centers in the United States was reported by Matsumoto *et al.* [15]. In this series, 109 renal tumors were treated via a percutaneous or laparoscopic approach with a 98% rate of successful initial ablation, and one local recurrence over a mean follow-up period of 19.4 months. Two tumors that were initially incompletely ablated were successfully re-treated. In our own experience (up to March 2006) of treating 105 renal tumors in 97 patients via a percutaneous approach (mean tumor size = 32 mm), the overall technical success rate was 90.5% and no local recurrences have occurred. Follow-up has confirmed steady involution of treated lesions (mean follow-up = 16.7 months, range in

surviving patients = 1–76 months) and no revascularization of treated tumors has been noted.

Lesion location appears to be an important determinant of treatment success. Fat serves as an effective heat and current insulator hence exophytic (non-central) tumor location is a predictor of successful tissue necrosis [16]. Central tumors also lie in closer proximity to large vessels which can act as "heat sinks", conducting heat away from them. This reduces the temperature achieved in the target lesion and hence the chance of adequate ablation. It may be that strategies to reduce blood flow during RFA will reduce this problem.

Cryoablation. Several series of patients treated with cryoablation have also been published. Shingleton *et al.* reported the percutaneous treatment of 15 renal tumors under MR guidance with a mean follow-up of 17 months. After initial treatment, four patients had residual enhancing tumor [1]. Subsequently, a cohort of 23 patients with 26 renal tumors treated by MR-guided percutaneous cryoablation were reported by Silverman *et al.* [2]. In a series of 85 patients (in which 70 procedures were laparoscopic), with a mean follow-up of 10 months, two patients had incompletely treated tumors on imaging follow-up [17]. Gupta *et al.* reported the CT-guided percutaneous cryoablation of 27 tumors with promising early results [3]. Of all the ablation techniques, cryotherapy has the longest reported outcomes to date [18,19] – in the longest reported series the 5-year cancer-free survival rate was 87.5% after a single cryoablation procedure and 97.5% after repeat cryoablation [19].

New challenges

Probe development and adjunctive interventions

At present, one of the main limitations of RFA is the relatively restricted maximum size of ablation volume that can be achieved in a single treatment session. Research is currently aimed at improving technology and enabling faster large-volume treatments. Probe design has already evolved to employ features such as electrode cooling by perfusion systems and pulsed energy delivery to increase ablation volume. Multitined "switched probes" also serve to increase speed of treatment and the size of target lesion. It appears that with the current technology, tumors less than 4 cm in size can be successfully ablated during a single RFA session with most series quoting figures close to 100% regardless of tumor location [14,20,21,22]. Larger lesions can still be treated by using several overlapping ablation spheres [23].

The scope of image-guided ablation may increase further with the use of adjunctive pre-procedural embolization, which aims to diminish tumor perfusion and thereby increase the efficacy of thermal ablation. This has been observed experimentally in studies on swine kidneys, where tumor perfusion reduction with either renal artery balloon occlusion or selective tumor embolization with particles prior to RFA results in a 60% increase in the maximum diameter of ablation [24]. Research may also lead to the introduction of strategies combining RFA with other adjunctive treatments such as targeted chemotherapy to improve treatment outcomes.

Reducing thermal injury to adjacent or critical structures

Potential complications from renal RFA include perinephric hematoma [25], hematuria [14], pelvicalyceal system injury [26], and thermal injury to the adjacent bowel [25]. Active cooling of the pelvicalyceal system via a retrogradely placed ureteric catheter has been advocated [27] to protect the collecting system from thermal injury whilst thorough ablation can be performed including the deep aspect of central tumors. As described above, the technique of hydrodissection is used to protect adjacent structures such as the colon and pancreas from injury during the treatment of anterior renal tumors (see Figure 9.4).

Improved image-guidance and tumor targeting

Fundamentally, ablation and other *in situ* techniques require optimal image-guidance and periprocedural assessment. Complete visualization of the tumor volume is required for accurate probe placement and in order to optimize procedural outcome. Whilst renal RFA can be performed laparoscopically, it is crucial to be able to accurately target probe placement in all three dimensions and the deep aspect of the tumor is generally not appreciated at operative exposure. For radiologically guided procedures, a combination of CT and ultrasound guidance is often helpful for accurate lesion targeting and the use of contrast-enhanced ultrasound may further aid probe placement. Magnetic resonance has been used to guide renal RFA procedures [28], but the reduced image quality in the currently available low field strength interventional scanners has made CT guidance more popular. The development of wide bore, high field MR scanners will facilitate MR-guided ablation procedures in the future.

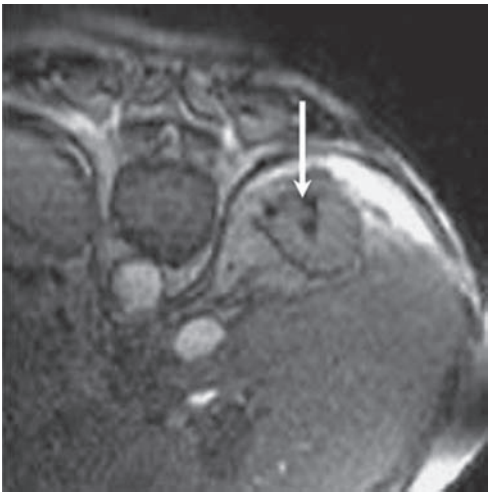

(a)

Figure 9.5a Magnetic resonance image of a renal tumor prior to cryoablation.

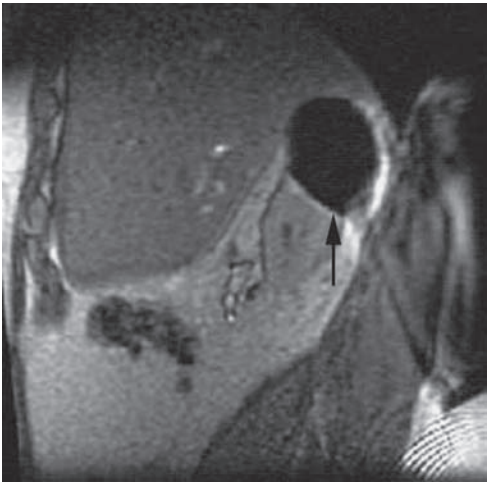

(b)

Figure 9.5b Magnetic resonance image post-cryoablation. Note the well-demarcated treatment margin (arrow) (*Images courtesy of Dr SG Silverman, Brigham and Women's Hospital, Boston, USA*).

Radiofrequency ablation causes vaporization and bubble formation and significantly impairs lesion appreciation by ultrasound at the time of the procedure. Use of microbubble contrast-enhanced ultrasound imaging during the procedure may help in this regard. Some companies are developing innovative imaging techniques such as the co-registration of ultrasound with CT datasets in order to improve small-volume tumor targeting. At present, however, true, robust, real-time imaging guidance for RFA remains to be achieved. Real-time treatment monitoring is less problematic during cryoablation, where magnetic resonance imaging can be used during the procedure to confirm extension of the ice ball beyond the margins of the target lesion [29] (Figures 9.5a and b). Real-time monitoring of HIFU procedures is only reliable if tumor cavitation occurs during treatment.

How to identify and rectify inadequate treatment

Unlike surgical treatment with extirpative histology, all image-guided ablation techniques leave the treated lesion *in situ* and hence determination of treatment adequacy is a challenge. In most series to date, treatment adequacy has been determined by the absence of contrast enhancement within the lesion on post-procedural imaging studies. Lack of enhancement is a useful surrogate determinant

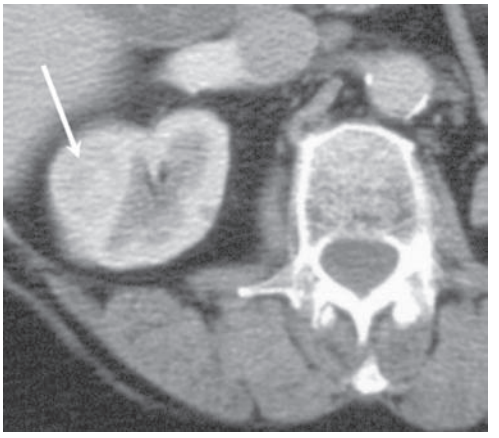

(a)

Figure 9.6a Small renal tumor prior to radiofrequency ablation.

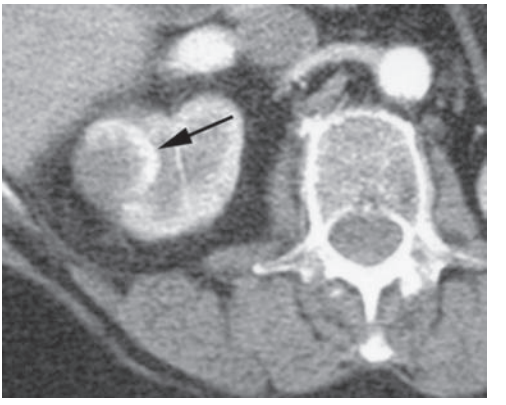

(b)

Figure 9.6b Late arterial phase CT image 5 days after radiofrequency ablation. Note that a crescent of enhancing tumor tissue (arrow) can be clearly appreciated, indicating incomplete ablation.

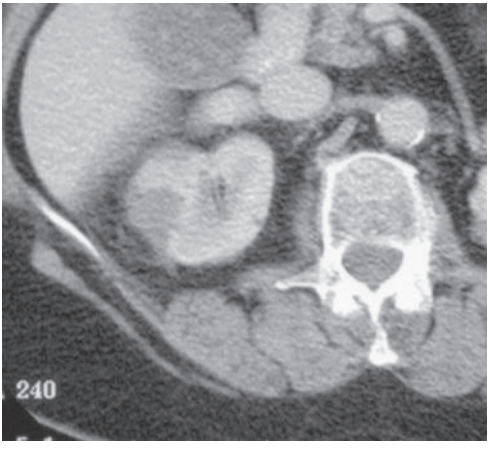

(c)

Figure 9.6c A later phase image from the same study illustrates the value of dual phase imaging. Note how the residual tumor crescent is poorly visualized and could be mistaken for a completely ablated lesion.

of tumor viability provided that post-procedural imaging is performed in the same phase as the diagnostic imaging. Some renal tumors are best visualised in arterial phase studies (Figures 9.6a, b, and c) and hence it is our policy to perform both late arterial phase and portal venous phase follow-up CT imaging. The absence of tumor growth over time and gradual lesion involution are also indicators of successful treatment. In our experience, the zone of absolute tissue death is often best defined at 1 week post-procedure and we therefore perform an

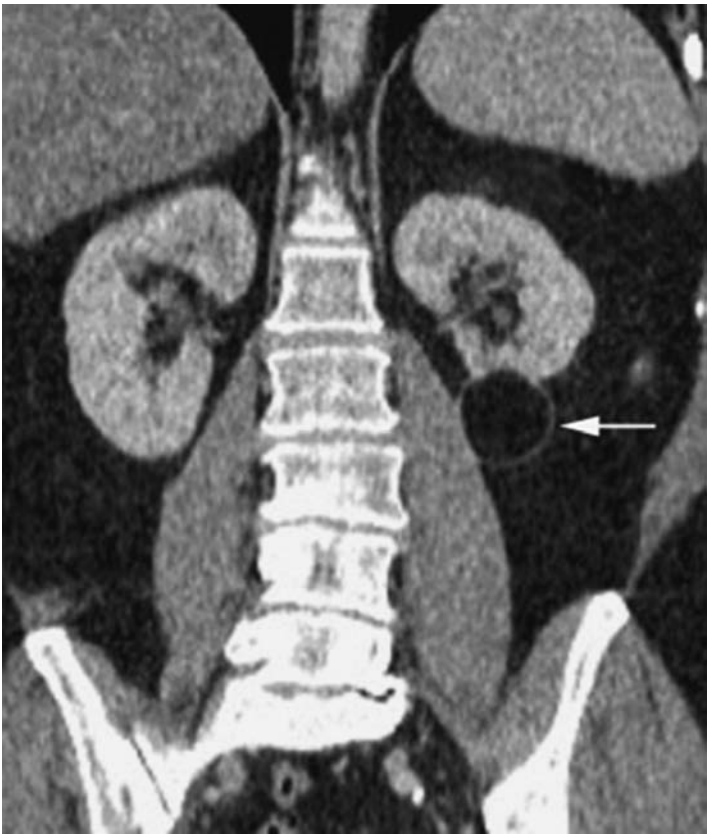

Figure 9.7 Coronal reformatted views of a contrast-enhanced CT study approximately 3 years following radiofrequency ablation of a lower pole renal tumor. A thin "halo" is seen within the perinephric fat at the treatment site (arrow).

outpatient contrast-enhanced CT or MR at this stage. On CT follow-up, a successfully ablated lesion will be of uniformly low attenuation on unenhanced images. At follow-up CT, an ablation "halo" is often noted in the perinephric fat (Figure 9.7). Under follow-up of over 5 years, we have found that lesions may either completely resolve leaving only a small cortical scar, or reduce to a small volume of non-enhancing tissue (Figures 9.8a, b, c, and d). It is important that radiologists reporting follow-up imaging studies are aware of the spectrum of appearances of ablated lesions (discussed in Chapter 9).

At MR follow-up, RFA lesions demonstrate variable appearances that evolve over time. Immediately post-RFA, the ablation zone can be hypo-, iso- or hyperintense on unenhanced T1-weighted imaging. On T2-weighted images, the treated lesion is usually hypointense with a faintly hyperintense surrounding rim. Following contrast administration, a thin rim of enhancement is noted around the ablation zone and appears to correspond to a penumbral inflammatory

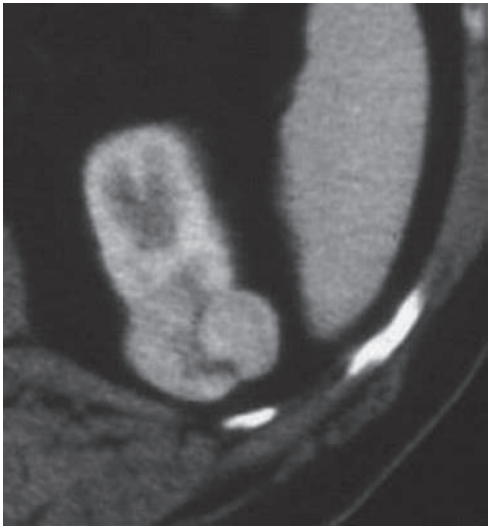

(a)

Figure 9.8a Long-term involution over a 5-year period, of a small exophytic posterior renal tumor, seen prior to radiofrequency ablation on this image.

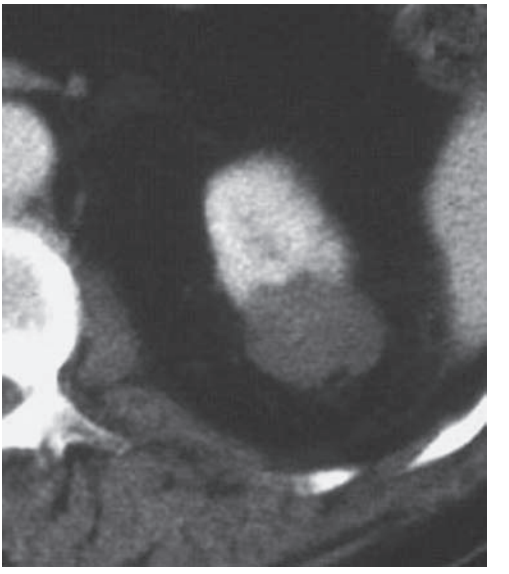

(b)

Figure 9.8b One week after radiofrequency ablation the tumor shows no enhancement in keeping with coagulative necrosis and successful treatment.

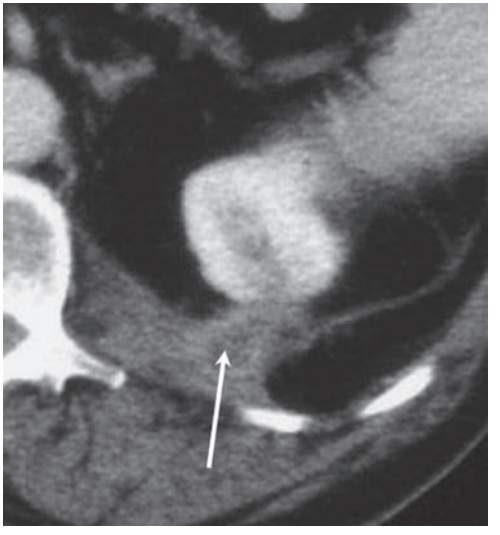

(c)

Figure 9.8c After 2 years, the ablated lesion has involuted and is beginning to "disperse" into the perirenal fat (arrow).

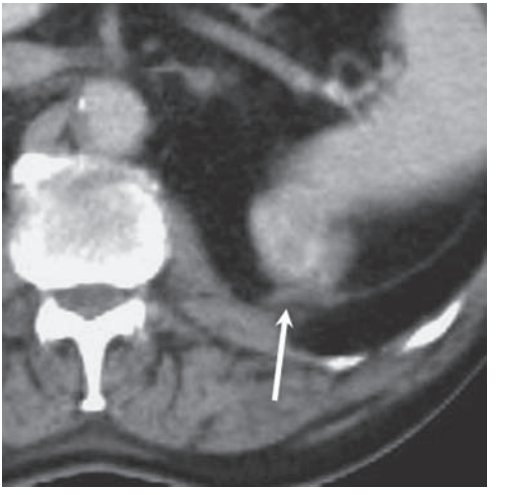

(d)

Figure 9.8d Five years after radiofrequency ablation, CT shows a small residual volume of non-enhancing tissue adjacent to the site of original tumor (arrow).

reaction that has been noted on extirpative histology [30]. This marginal inflammatory response resolves gradually over a couple of months and should not be mistaken for residual tumor. At 3 months post-RFA, the ablated lesion remains hypointense on T2-weighted imaging and 67% of treated tumors will be hyperintense on T1 gradient echo images [31]. MR perfusion imaging has been advocated as a more reliable method for excluding residual tumor [32] and the use of non-contrast perfusion sequences is particularly useful in this patient group who may be at increased risk of nephrotoxicity from CT or MR contrast agents. Availability of MR scanning time and long acquisitions may be limiting factors in the adoption of this technique as a routine follow-up modality.

Importantly, post-procedural biopsy has been found to be a very poor determinant of treatment adequacy, as the dead tumor cells often appear structurally intact but are in fact not viable when examined using vital stains [33]. PET has a sensitivity of only 60% for renal cell carcinoma [34] and so is unreliable as a follow-up imaging modality, particularly for small or low-grade tumors. Reliable periprocedural determination of treatment completion remains the subject of a number of studies, which are investigating the use of contrast-enhanced ultrasound [35] and MR thermometry [36] amongst other techniques.

Conclusion

Long-term follow-up is necessary to establish the oncological efficacy of renal RFA, and all other ablation methods. A lack of large randomized multicenter trials makes it difficult to compare outcomes of different ablation techniques with surgical treatment options. Careful follow-up imaging strategies are of crucial importance in monitoring the success of any ablation technique. Whilst oncological efficacy has yet to be proven, the published series to date suggest that both RFA and cryoablation represent safe and effective treatment methods for small renal tumors.

REFERENCES

1. W. B. Shingleton and P. E. Sewell, Jr., Cryoablation of renal tumours in patients with solitary kidneys. *BJU Int*, **92** (2003), 237–9.
2. S. G. Silverman, K. Tuncali, E. vanSonnenberg *et al.*, To evaluate the initial clinical experience of magnetic resonance (MR) imaging-guided percutaneous cryotherapy of renal tumors. *Radiology*, **236**:2 (2005), 716–24.

3. A. Gupta, M. E. Allaf, L. R. Kavoussi *et al.*, Computerized tomography guided percutaneous renal cryoablation with the patient under conscious sedation: initial clinical experience. *J Urol*, **175**:2 (2006), 447–52.
4. N. E. Hoffmann and J. C. Bischof, The cryobiology of cryosurgical injury. *Urology*, **60**:2A Suppl (2002), 40–9.
5. T. J. Vogl, R. Straub, K. Eichler *et al.*, Colorectal carcinoma metastases in liver: laser-induced interstitial thermotherapy: local tumor control rate and survival data. *Radiology*, **230** (2003), 450–8.
6. F. Wu, Z. B. Wang, W. Z. Chen *et al.*, Preliminary experience using high intensity focused ultrasound for the treatment of patients with advanced stage renal malignancy. *J Urol*, **170** (2003), 2237–40.
7. K. U. Kohmann, M.S Michel, J. Gaa *et al.*, High intensity focused ultrasound as non-invasive therapy for multilocal renal cell carcinoma: case study and review of the literature. *J Urol*, **167** (2002), 2397–403.
8. G. S. Gazelle, S. N. Goldberg, L. Solbiati *et al.*, Tumor ablation with radio-frequency energy. *Radiology*, **217** (2000), 633–46.
9. T. H. Hsu, M. E. Fidler, and I. S. Gill, Radiofrequency ablation of the kidney: acute and chronic histology in porcine model. *Urology*, **56** (2000), 872–5.
10. S. N. Goldberg, G. S. Gazelle, and P. R. Mueller, Thermal ablation therapy for focal malignancy: a unified approach to underlying principles, techniques and diagnostic imaging guidance. *AJR Am J Roentgenol*, **174** (2000), 323–31.
11. W. W. Mayo-Smith, D. E. Dupuy, P. M. Parikh, J. A. Pezullo, and J. J. Cronan, Imaging-guided percutaneous radiofrequency ablation of solid renal masses: technique and outcomes of 38 treatment sessions in 32 consecutive patients. *AJR Am J Roentgenol*, **180** (2003), 1503–8.
12. M. Ahmed, Z. Liu, K. S. Afzal *et al.*, Radiofrequency ablation: effect of surrounding tissue composition on coagulation necrosis in a canine tumor model. *Radiology*, **230**:3 (2004), 761–7.
13. A. R. Zlotta, T. Wilsschutz, G. Raviv *et al.*, Radiofrequency interstitial tumor ablation (RITA) is a possible new modality for treatment of renal cancer: ex vivo and in vivo experience. *J Endourol* **11**:4 (1997), 251–8.
14. D. A. Gervais, F. J. McGovern, R. S. Arellano *et al.*, Radiofrequency ablation of renal cell carcinoma: Part 1, indications, results and role in patient management over a 6-year period and ablation of 100 tumors. *AJR Am J Roentgenol*, **185** (2005), 64–71.
15. E. D. Matsumoto, D. B. Johnson, and K. Ogan, Short-term efficacy of temperature-based radiofrequency ablation of small renal tumors. *Urology*, **65**:5 (2005), 877–81.
16. D. A. Gervais, R. S. Arellano, F. J. McGovern *et al.*, Radiofrequency ablation of renal cell carcinoma: part 2, Lessons learned with ablation of 100 tumors. *AJR Am J Roentgenol*, **185**:1 (2005), 72–80.
17. B. F. Schwartz, J. C. Rewcastle, T. Powell *et al.*, Cryoablation of small peripheral renal masses: a retrospective analysis. *Urology*, **68**:1 Suppl (2006), 14–18.

18. I. S. Gill, E. M. Remer, W. A. Hasan *et al.*, Renal cryoablation: outcome at 3 years. *J Urol*, **173**:6 (2005), 1907.
19. P. E. Davol, B. R. Fulmer, and D. B. Rukstalis, Long-term results of cryoablation for renal cancer and complex renal masses. *Urology*, **68**:1 Suppl 2006, 2–6.
20. L. M. Su, T. W. Jarrett, D. Y. Chan *et al.*, Percutaneous computed tomography-guided radiofrequency ablation of renal masses in high surgical risk patients: preliminary results. *Urology*, **61** (2003), 26–33.
21. R. J. Zagoria, A. D. Hawkins, P. E. Clark *et al.*, Percutaneous CT-guided radiofrequency ablation of renal neoplasms: factors influencing success. *AJR Am J Roentgenol*, **183**:1 (2004), 201–7.
22. J. J. Hwang, M. M. Walther, S. E. Pautler *et al.*, Radiofrequency ablation of small renal tumours: intermediate results. *J Urol*, **171**:5 (2004), 1814–18.
23. D. A. Gervais, F. J. McGovern, R. S. Arellano *et al.*, Renal cell carcinoma: clinical experience and technical success with radio-frequency ablation of 42 tumors. *Radiology*, **226** (2003), 417–24.
24. I. Chang, I. Mikityansky, D. Wray-Cahen *et al.*, Effects of perfusion on radiofrequency ablation in swine kidneys. *Radiology*, **231** (2004), 500–5.
25. A. Z. Weizer, G. V. Raj, M. O'Connell *et al.*, Complications after percutaneous radiofrequency ablation of renal tumors. *Urology*, **66**:6 (2005), 1176–80.
26. M. A. Farrell, W. J. Charboneau, D. S. DiMarco *et al.*, Imaging-guided radiofrequency ablation of solid renal tumors. *AJR Am J Roentgenol*, **180** (2003), 1509–13.
27. V. Margulis, E. D. Matsumoto, G. Taylor *et al.*, Retrograde renal cooling during radiofrequency ablation to protect from renal collecting system injury. *J Urol*, **174** (2005), 350–2.
28. J. S. Lewin, S. G. Nour, C. F. Connell *et al.*, Phase II clinical trial of interactive MR imaging-guided interstitial radiofrequency thermal ablation of primary kidney tumors: initial experience. *Radiology*, **232** (2004), 835–45.
29. M. M. Desai and I. S. Gill, Current status of cryoablation and radiofrequency ablation in the management of renal tumors. *Curr Opin Urol*, **12** (2002), 387–93.
30. S. N. Goldberg, G. S. Gazelle, C. C. Compton *et al.*, Treatment of intrahepatic malignancy with radiofrequency ablation. Radiologic-Pathologic Correlation. *Cancer*, **88**:11 (2000), 2452–63.
31. E. M. Merkle, S. G. Nour, and J. S. Lewin, MR imaging follow-up after percutaneous radiofrequency ablation of renal cell carcinoma: findings in 18 patients during first 6 months. *Radiology*, **235** (2005), 1065–71.
32. A. Boss, P. Martirosian, C. Schraml *et al.*, Morphological, contrast-enhanced and spin labelling perfusion imaging for monitoring of relapse after RF ablation of renal cell carcinomas. *Eur Radiol*, **16** (2006), 1226–36.
33. R. Marcovich, J. P. A. Aldana, N. Morgenstern *et al.*, Optimal lesion assessment following acute radiofrequency ablation of porcine kidney: cellular viability or histopathology? *J Urol*, **170** (2003), 1370–4.
34. D. E. Kang, R. L. White, Jr., J. H. Zuger *et al.*, Clinical use of fluorodeoxyglucose F 18 positron emission tomography for detection of renal cell carcinoma. *J Urol*, **171**:5 (2004), 1806–9.

35. D. B. Johnson, D. A. Duchene, G. D. Taylor *et al.*, Contrast-enhanced ultrasound monitoring of radiofrequency ablation. *J Urol*, **171**:Suppl (2004), 509:A1929.
36. R. M. Botnar, P. Steiner, B. Dubno *et al.*, Temperature quantification using the proton frequency shift technique: in vitro and in vivo validation in an open 0.5 Tesla interventional MR scanner during RF ablation. *J Magn Reson Imaging*, **13** (2001), 437–44.

10

Post-treatment surveillance of renal cancer

Parvati Ramchandani

Introduction

If salvage surgery or immunotherapy is to be offered in a timely fashion for recurrent renal cancer, surveillance after treatment is important to ensure early detection of recurrence, although improved survival with such an approach has yet to be proven. Suggested surveillance protocols have been published [1,2,3,4] to follow patients with treated renal cell carcinoma (RCC). However, in practice, there is little consensus on appropriate surveillance protocols amongst practicing urologists and a recent study documented that published guidelines are often not used with any consistency [5,6]. This chapter is a review of the clinical features of recurrent disease and how they influence chosen surveillance methods and protocols.

Likelihood of recurrent renal cancer

Approximately a third of the patients who present with localized RCC will develop a local or distant recurrence after therapy [4,7]. Higher T-stage tumors are associated with increased risk of tumor recurrence. Lam *et al*. recently reported that overall distant recurrence rate at 5 years after surgical resection was 27.6% for localized disease and 64% for node positive disease [7]. Five-year recurrence-free rate after nephrectomy in patients stratified into a low risk group was 90.4%, intermediate risk group was 61.8%, and high risk group was 41.9%. Median time to recurrence was 28.9 months, 17.8 months, and 9.5 months in the low risk, intermediate risk, and high risk groups respectively. Similar results were reported by Stephenson *et al*. [8]. In their multi-institutional series, 5-year relapse-free survival rates were 93% for T1 disease, 81% for T2 disease, 67% for T3A disease, and 57% for T3B disease. Recurrence was seen in 13.5% of patients overall, with

Carcinoma of the Kidney, ed. Uday Patel. Published by Cambridge University Press.

earlier relapse at 12 months for T3 tumors versus relapse at 26 months for T1/T2 tumors.

High risk factors

Multivariate analysis in patients with clear cell carcinoma has shown that the features associated with progression to metastases include tumor stage, regional lymph node status, tumor size, nuclear grade, and histological tumor necrosis [9,10,11], and thus surveillance protocols are tailored dependent on the pathologic stage and tumor size. The influence of the pathologic subtype of RCC on post-treatment recurrence remains a subject of study; metastatic potential and survival appear to be poorer in patients with collecting duct carcinoma, medullary carcinoma, and tumors with sarcomatoid differentiation, while chromophobe RCC may have a better prognosis than conventional RCC [11,12]. To date, the pathologic subtype of the tumor has not been used as a criterion for a surveillance protocol although a prognostic nomogram has been proposed to predict recurrence in patients with renal clear cell carcinoma [13].

There is an increasing trend toward nephron-sparing surgery for smaller, incidentally discovered tumors. These smaller tumors are believed to have a low metastatic potential. Here too, the pathologic stage appears to be the most important factor in determining tumor prognosis, and suggested surveillance protocols are determined by the initial pathologic tumor stage and tumor size [14].

Sites of tumor recurrence

The most common sites of recurrence are the lung, liver, bone, and brain. A recent imaging-based report [15] indicated that recurrent disease occurred in 21% of patients within the first 2 years, with the commonest sites being lung (70%), bone (31%), and the nephrectomy bed (17%). Of these, 52%–84% of recurrences are asymptomatic and discovered only on routine surveillance laboratory or radiographic testing [16]. Lam *et al.* [7] reported that the chest and abdomen were the sites of recurrence in 75% and 37.5% of their low risk patients, 77.4% and 58.1% of intermediate risk patients, and 45.5% and 68.2% of high risk patients respectively. Resection of solitary metastases, particularly in those with disease-free interval greater than 12 months, may improve survival, with solitary lung metastases demonstrating a more favorable outcome than brain metastases. Furthermore, survival after resection of a second and third solitary metastasis is no different compared with initial metastatectomy [17].

Figure 10.1 An axial CT section showing bilateral lung metastasis (some are arrowed).

Lung

Lung metastases are the most common recurrence and develop in 3%–16% of patients [16], but pulmonary recurrence is even more common in those with other evidence of metastatic disease (frequency 29%–75%) [7,15,16] (Figure 10.1). Although computed tomography (CT) of the chest is a more sensitive imaging modality than chest radiography to identify early pulmonary metastatic disease, its role and application in RCC surveillance is still unclear. Lam *et al.* [7] recommend yearly chest CT for low risk patients and chest CT every 6 months for intermediate risk and high risk patients. As the lung is the most common site for RCC metastases, and solitary recurrences can be surgically treated (see Chapter 8) with good long-term outcome (as discussed above), surveillance for pulmonary recurrence is very important. Most patients with pulmonary metastases are asymptomatic, and the recurrence is detected only on follow-up imaging [3,18].

Bone

Bone metastases occur in 2%–8% of all patients, while bony recurrence is present in 16%–27% of those with recurrent disease [2,3,16,18] (Figure 10.2). Bone secondaries are usually symptomatic. Patients present with pain and the diagnosis is confirmed by plain radiographs and bone scintigraphy. All patients with bone metastases in Lam's series [7] also had extraosseous metastases at presentation, but

Figure 10.2 An axial CT showing a destructive soft tissue mass in the sacrum.

in Chae's series [15] 15% of patients had a solitary bony recurrence at the first diagnosis of tumor recurrence. Palliative treatment is the only option for such patients, and therefore routine surveillance screening for bony disease, using nuclear scintigraphy or plain radiography, is not recommended by some [4]. In contrast, Chae *et al.* [15] reported that 62% of bone metastases occurred within 1 year and 77% within 2 years, and thus felt that bone scanning during the early postoperative period was worthwhile.

Liver

Liver metastases occur in 1% to 7% of cases and carry a poor prognosis [3,16,18], although there are reports of long-term survival after resection of liver metastases [3,16,18,19]. Abdominal CT or magnetic resonance imaging scans (MRI) used for post-therapy surveillance routinely include the liver and will detect recurrent disease.

Contralateral kidney

Tumors may develop in the contralateral kidney after partial or radical nephrectomy (Figure 10.3), and it is unclear whether these new tumors represent a tumor metastasis or an entirely *de novo* tumor [20]. Contralateral tumor development has been reported

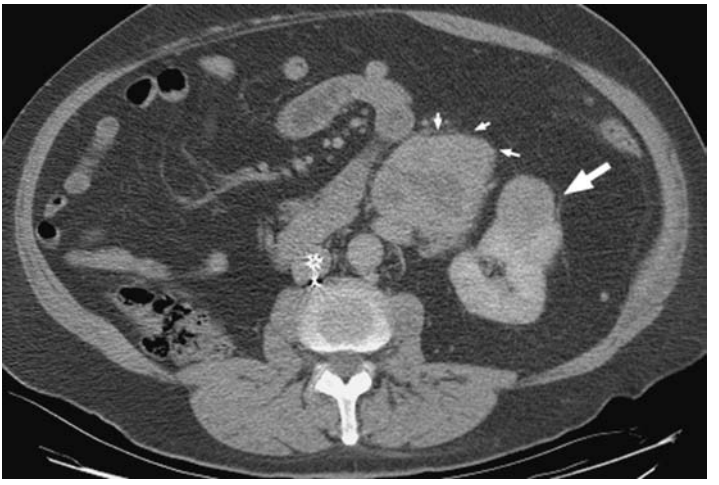

Figure 10.3 An enhanced axial CT scan showing a poorly enhancing mass arising from the lower pole of the left kidney representing a contralateral renal secondary tumor. The small arrows point to a large lymph node metastasis.

in 1%–2% of treated cases [20]. Interestingly, in Lam's series [7], contralateral recurrence was not noted in the low risk or high risk group of patients (196 patients and 72 patients in these groups respectively), but was seen in 6.6% of 251 intermediate risk patients. Abdominal CT or MRI scans are ideally suited to monitor the contralateral kidney for tumor development in patients who have undergone treatment.

Local recurrence

Recurrence of tumor locally in the surgical bed is unusual after radical nephrectomy in the absence of lymph node positive disease or locally advanced disease (Figure 10. 4). In one series [21], only 1.8% of 1737 patients with T3 N0 M0 disease had local recurrence at 5 years. Yet in Lam's series [7], recurrence in the renal fossa bed was seen in 25.8% of high risk patients, 14.5% of intermediate risk patients, and in an unspecified number of low risk patients. Nephron-sparing surgery provides effective long-term therapy for localized RCC. Lam *et al.* [7] reported a 5-year recurrence rate of 5.2% in this group of patient compared to 27.6% in the radical nephrectomy group, probably reflecting the treatment of larger and more advanced tumors by radical nephrectomy. Recurrence in the kidney that was operated on is likely due to microscopic multifocal RCC in the renal remnant that was not detected preoperatively (Figure 10. 5). The incidence of renal recurrence in other large partial nephrectomy series is 3.2% or less [22,23]. Recommendations for postoperative surveillance after nephron-sparing surgery are based on the initial pathologic tumor stage [14]. No postoperative imaging is recommended

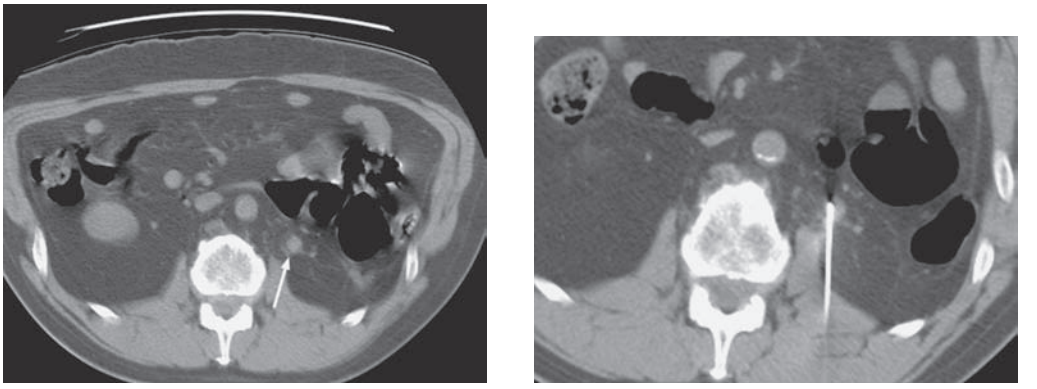

(a) (b)

Figure 10.4 (a) A small nodule seen in the left renal bed post nephrectomy. This would be highly suspicious for local recurrence in the renal bed, and (b) the second image shows a needle placed for percutaneous CT-guided biopsy.

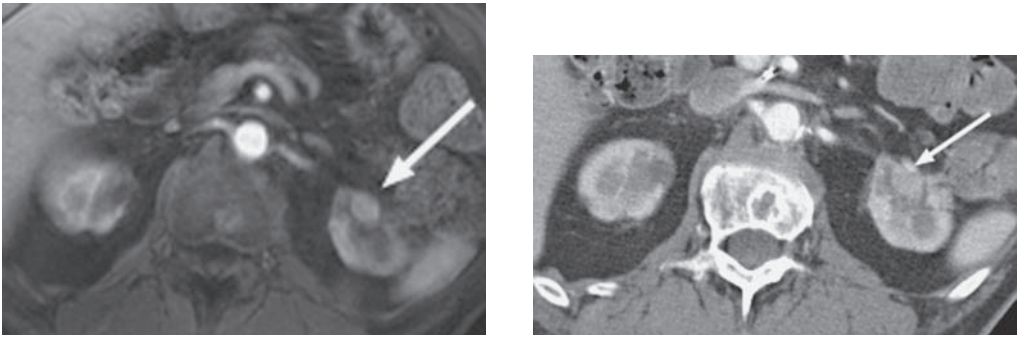

(a) (b)

Figure 10.5 Contrast-enhanced CT and MRI studies showing a small nodule in the left kidney post-partial nephrectomy, representing a local intrarenal recurrence. These most likely represent missed microscopic multifocal RCC.

for patients with tumors < 2.5 cm; yearly chest radiographs and abdominal CT scans every 2 years are suggested for patients with tumors > 2.5 cm (T2 N0 M0) disease; while in patients with T3 disease, chest radiographs and abdominal CT scanning every 6 months for 3 years, and then imaging every 2 years are suggested.

Radiographic surveillance

Both CT and MR scanning can be used to evaluate the postoperative abdomen for recurrence. Neither is of proven superiority. If renal function is normal, CT

scanning with oral and intravenous contrast to cover the area from the diaphragm to the ischial tuberosity is performed. In patients with compromised renal function, or those who cannot receive intravenous iodinated contrast, MR scanning provides an effective alternative to evaluate the abdomen and the contralateral kidney for recurrence, postoperative complications, and local recurrence of tumor. Ultrasound evaluation is often difficult because of rib artefacts or bowel gas which obscures the renal fossa.

Surveillance post radical nephrectomy

Expected postoperative appearance

Following right radical nephrectomy, the liver, ascending colon, second part of duodenum, pancreatic head, and small bowel may migrate into the renal fossa. On the left side, the pancreatic tail, spleen, large and small bowels migrate into the fossa (Figure 10. 6a). Fluid-filled loops of bowel can also simulate recurrent tumor, and thus good bowel opacification with oral contrast is important for ease of evaluation [24,25,26]. Postoperative scarring in the paraspinal muscles and renal bed may be confused with recurrence, but serial scans will document improvement or no change in the appearance of postoperative fibrosis. Percutaneous biopsy may sometimes become necessary to establish the diagnosis when imaging findings are equivocal.

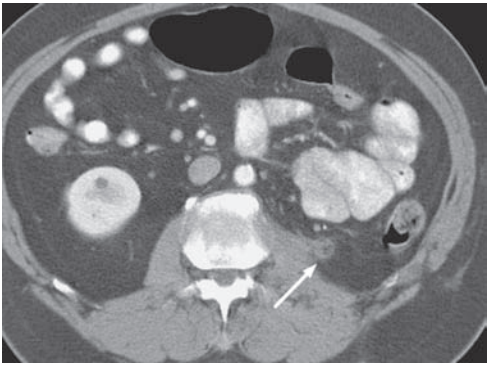

(a)

Figure 10.6a A small nodule (arrowed) is seen in the left renal bed. Note how the large bowel has prolapsed posteriorly to partially occupy the left renal bed. Displaced bowel or organs (particularly the tail of the pancreas) can be mistaken for tumor.

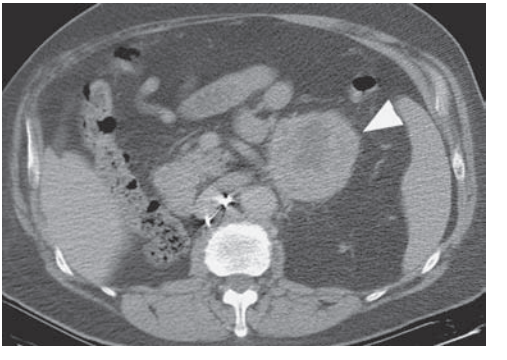

(b)

Figure 10.6b A large lymph node mass is arrowed.

Signs of recurrent or residual tumor

Tumor recurrence in the nephrectomy bed is seen as an enhancing soft tissue mass which may be of any size, depending on when it is discovered (Figure 10.4a). Chae *et al.* [15] reported that all nephrectomy site recurrences in their patients presented as 3–6 cm enhancing solid masses with central necrosis on CT and US examinations. Tumor recurrence may be adherent to the paraspinous muscles, posterior abdominal wall muscles, crus of the diaphragm, aorta, or inferior vena cava. Right renal recurrences may invade the duodenum and present with gastrointestinal bleeding [25,26]. Surgical resection of isolated recurrence improves the survival outcome, compared to medical therapy or observation [21]. Abdominal CT will also demonstrate metastases in the retroperitoneal lymph nodes, liver, adrenal gland, and the opposite kidney (Figures 10.3 and 10.6B) if present.

Lung metastases may be demonstrated on both chest radiographs and on chest CT (Figure 10.1). Sandock *et al.* [19] found that all 19 of their patients with pulmonary metastases had abnormal radiographs. This was of course an early report and, as mentioned previously, chest CT can be anticipated to be a more sensitive study than chest radiographs in detecting lung metastases, but the role of chest CT in the routine surveillance of patients with RCC is not yet well defined.

Bone metastases are usually seen as lytic lesions on conventional radiographs or CT [15] (Figure 10.2). Chae *et al.* reported that in their 13 patients with bony metastases, bone scans demonstrated metastatic foci as cold areas surrounded by increased uptake in six patients (46%), purely cold areas in four patients (31%), and as areas of purely increased uptake in three patients (23%). On MRI, tumor metastases were of heterogeneous intermediate signal intensity on T1- and T2-weighted images and demonstrated enhancement on Gadolinium enhanced T1-weighted images. Contrast-enhanced CT scans showed bone destruction in all patients and solid-enhancing masses in five patients (71%). Cranial CT or MRI demonstrates brain metastases as multiple enhancing nodules with surrounding edema [15].

Suggested surveillance protocols after radical nephrectomy are variable, with institutional and individual bias. Many examples have been published [2,3,4,5,6,13,14] but in general CT based, TNM-stage governed surveillance of the chest and abdomen appears to be favored, [5,6] with no individual protocol (frequency and/or duration) being of proven superiority.

Surveillance post nephron-sparing surgery

Open surgical partial nephrectomy for localized RCC involves complete local resection of a renal tumor while leaving the largest amount of functioning normal parenchyma behind. The procedure is further described in Chapter 8. Initially utilized for RCC in patients with specific indications such as a solitary kidney or preexisting renal insufficiency, the technique is rapidly becoming the procedure of choice for small localized tumors in all patients. Minimally invasive approaches such as laparoscopy are also being increasingly utilized. Nephron-sparing surgery by any technique is technically more complex than traditional radical nephrectomy. Possible complications include infection, injury to vascular structures or the collecting system, and local tumor recurrence. A 1 cm perimeter of parenchyma is usually excised around the tumor to ensure negative surgical margins, although smaller margins may be sufficient [27]. Specimens from the resection margin are sent for histopathological frozen section analysis during the surgery to be certain that the margins are negative, although some reports indicate that this may be an unnecessary maneuver that serves to increase the expense of the procedure without adding meaningful information or improving outcome [28].

Reports indicate an overall complication rate of 23% for laparoscopic partial nephrectomy [29] and a 10% rate of major complications [30]. Laparoscopic techniques are also associated with more major complications than are open techniques for partial nephrectomy, 5% versus 0% [31], although the global rate of postoperative complications is not significantly different between the two techniques.

Expected postoperative appearances

The appearance is dictated in large part by the size and location of the tumor that was resected (Figures 10.7 and 10.8) [32]. Wedge-shaped defects in the renal parenchyma are seen after resection of peripheral tumors (Figure 10.7 and compare with Figure 8.7). Fat may be packed into the perinephric bed, and may simulate a fat-containing tumor, such as an angiomyolipoma (Figure 10.8). Hemostatic sponge may be placed at the resection site, and bubbles trapped within the material may simulate an abscess [32] – gas bubbles within the hemostatic agent usually get absorbed within a week, although they may persist for a month or more after surgery [33]. After open surgery, the kidney may be located more posteriorly in the retroperitoneum, and abut or adhere to the posterior abdominal wall [32] (Figure 10.8).

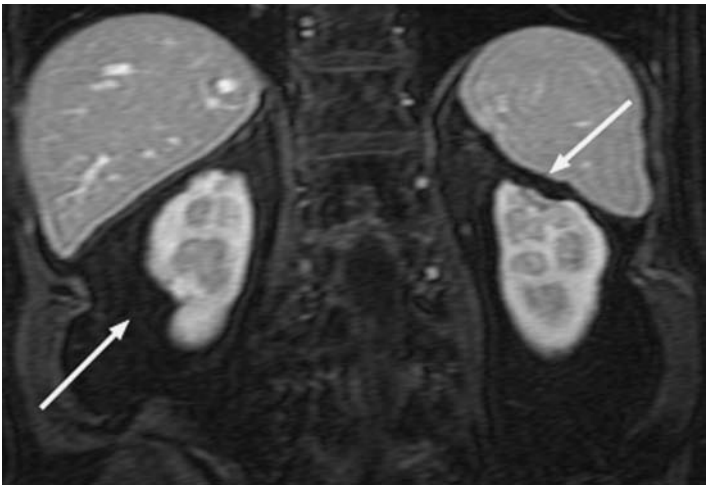

Figure 10.7 A coronal MRI scan showing wedge-shaped renal defects (arrowed) post-bilateral partial nephrectomy.

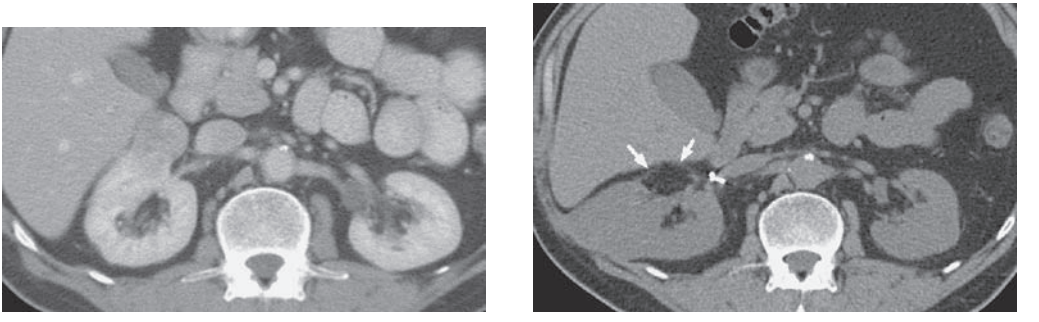

(a) (b)

Figure 10.8 These are axial CT images taken (a) before and (b) after partial nephrectomy. On the first image there is an enhancing right sided, anteriorly located renal tumor. The second image shows the fat (arrow-head) placed at the resection site. Also note how the kidney closely abuts the lateral abdominal wall. This is an unenhanced image (shown to demonstrate the fat) and not sufficient to exclude recurrent or residual tumor, for which an enhanced CT or MRI study is essential.

Signs of recurrent or residual tumor post-partial nephrectomy

Recurrent tumors are seen as enhancing lesions on contrast-enhanced CT or MR imaging. Careful comparison with preoperative images is often required to determine if the lesion represents a new tumor, particularly if there was more than one suspicious mass. There are no generally agreed or recommended surveillance protocols for follow-up after partial nephrectomy. Clearly a good quality enhanced renal protocol CT or MRI is crucial, but the frequency of studies is undetermined.

One policy is to image every 6 months for 2 years and then annually for the 3 years after.

Surveillance after thermal ablation of renal tumors

Radiofrequency ablation (RFA) and cryoablation of small RCCs are an alternative to nephron-sparing surgery [34,35,36] (Figure 10.9). These tumor ablation techniques are usually used to treat small renal tumors in patients who are poor surgical candidates, but may also be requested by otherwise healthy patients [35]. The ablation can be performed percutaneously with image guidance (CT, US, or MRI) [35,36], or intraoperatively with direct visualization during laparoscopic or open surgery, or with intraoperative ultrasonography – RFA is more commonly performed with percutaneous techniques, while cryoablation is more likely to be performed during open surgery or laparoscopically. However, the increasing availability of smaller cryoprobes is expanding the percutaneous options for cryoablation as well [35,36]. With both RFA and cryoablation, treatment is aimed at creating a 5–10 mm tumor-free margin. The long-term results with thermal ablation of renal tumors are not yet known but appear promising with a low complication rate [37].

With percutaneous RFA, local tumor control at 2.3–4.6 years is reportedly 90%–95% [38,39,40]. Local tumor recurrence after cryoablation was seen in 0% [35] and 4.2% of patients [36] treated percutaneously and 3.6% of patients treated laparoscopically [41]. Patients were followed for a mean of 8 months [35] to 3 years [41] in these published reports. Either CT or MRI is the primary imaging technique used to follow patients treated with these techniques. Evaluation is aimed at

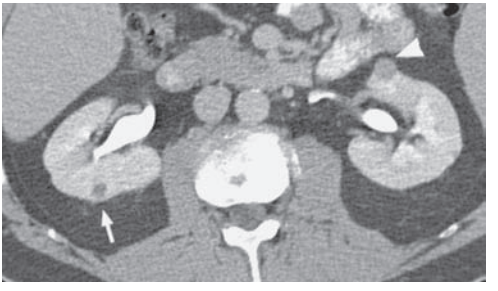

(a)

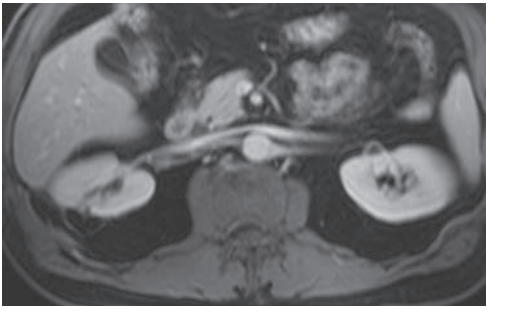

(b)

Figure 10.9 (a) The first study is an axial enhanced CT image showing bilateral small renal tumors (arrow and arrowhead). These are ideally suited for thermal ablation being small and easily accessible. (b) The second study is a post-treatment MRI study.

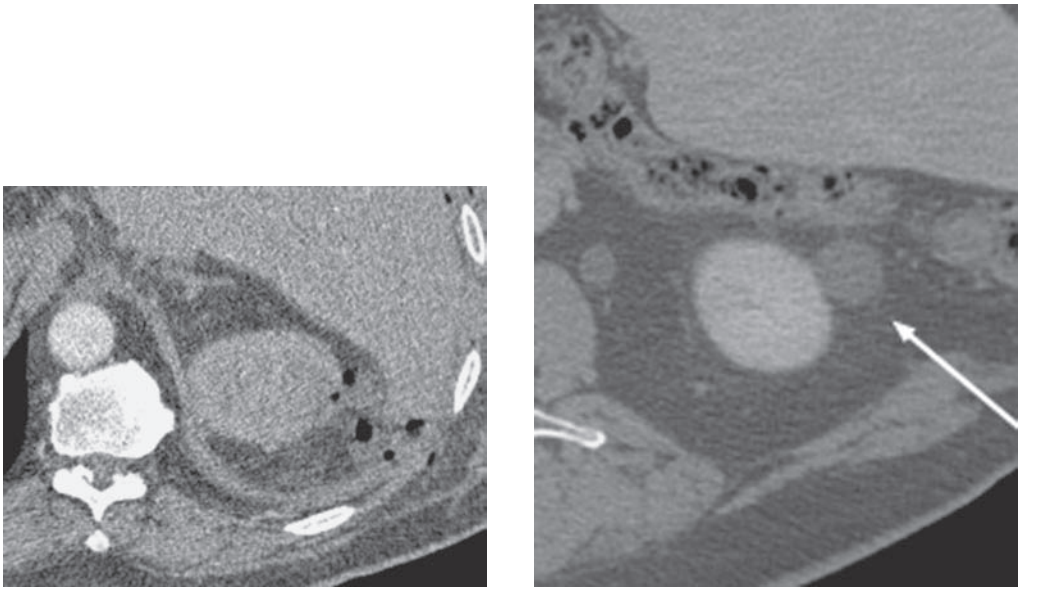

(a) (b)

Figure 10.10 (a) The first image shows locules of gas in the perinephric fat, which is a common phenomenon, immediately post RFA. (b) The second image is another patient showing the typical appearances of a successfully ablated, non-enhancing left renal tumor (arrowed).

assessing the tumor ablation zone, detecting residual or recurrent tumor, identifying metastatic disease, and identifying complications related to the therapy.

Expected appearances post-radiofrequency ablation

During and immediately after RFA, changes seen on imaging include perinephric or subcapsular hemorrhage, stranding in perinephric fat, thickening of paranephric fascia, and locules of gas in the surrounding tissue [37] (Figure 10.10). A completely treated tumor shows no enhancement. There may be a rim of non-enhancing devitalized parenchyma adjacent to the treated tumor zone. Changes in tumor size during ablation may be too subtle to be appreciated [37], or the ablated lesion may look larger than the preablation tumor size due to treatment of a rim of normal parenchyma just peripheral to the tumor [42]. On follow-up imaging, the acute changes of perinephric hemorrhage, perinephric stranding, and gas resolve. The RF ablation zone is clearly demarcated from the adjacent normal parenchyma; peripheral or exophytic lesions may demonstrate a "bull's eye" appearance on the first follow-up scan [37] (Figure 10.11) due to a central avascular tumor zone

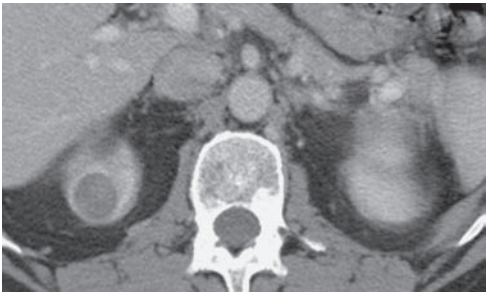

(a)

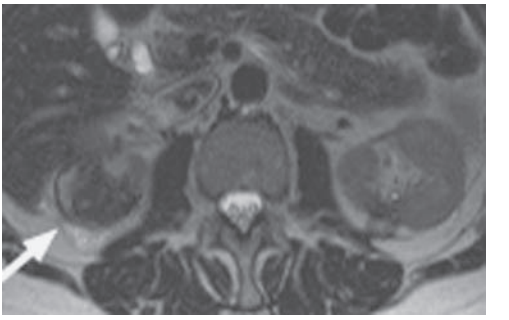

(b)

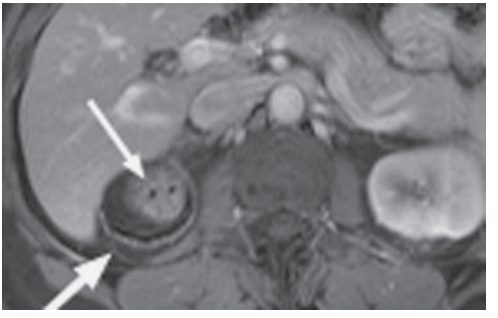

(c)

Figure 10.11 (a) The first image is an enhanced axial CT image showing a successfully ablated right renal tumor. Note how well it is demarcated from adjacent normal parenchyma and that it does not enhance. (b and c) The second two images are MRI studies demonstrating the "bull's eye" appearance (arrowed) that is sometimes seen after RFA (see text for further explanation).

which is surrounded by normal fat, and a thin peripheral peritumoral halo. Wile *et al.* indicate that this peritumoral halo is not seen with lesions ablated with laparoscopic or open surgical guidance [37,43].

On MRI, the ablation zone is mostly bright on T1-weighted images at 1.5 T but mildly heterogeneous [44]. On T2-weighted sequences, the ablated zone is seen as a central mass that is hypointense relative to the normal parenchyma, with a surrounding peritumoral rim of variable signal intensity. T2-weighted sequences without fat suppression are best to delineate the ablation zone. Abnormal Gadolinium enhancement may be difficult to appreciate due to the increased signal intensity seen commonly on T1-weighted images. Subtracting precontrast data set from post-contrast images is often helpful in determining if enhancement is present or not [37]. On follow-up imaging, lesions treated with RFA may remain unchanged in size [43] in contrast to cryoablation where there is rapid shrinkage in tumor size [45]. A persistent mass at the site of ablation is not uncommon, and does not indicate residual tumor as long as it does not enhance [43]. With time, fat may interpose between the normal parenchyma and the treated lesion [37,42,43].

Expected appearances post-cryoablation

During cryoablation, MR scanning demonstrates the ice ball formed with cryoablation as a well-demarcated signal void on T1-weighted images. On T2-weighted imaging, there is a decrease in the signal intensity of the tumor when compared to the baseline pretreatment appearance. [37].On CT, the ablated lesion is seen as a hypoattenuating area which may be slightly larger than the original tumor, as the ice ball extends beyond the margins of the targeted tumor [42]. Follow-up imaging demonstrates the cryoablation zone to be isointense to the renal parenchyma on T1-weighted images, and hypointense on T2-weighted images. The ablation zone, even if it looks larger than the initial tumor immediately after cryoablation, usually involutes dramatically with time. In one series, 32% of 129 tumors were undetectable on follow-up imaging at 2 years after cryoablation, but a detectable mass was present in all patients after RFA [45]. On CT, successfully cryoablated lesions are seen as hypoattenuating areas without focal contrast enhancement [42].

To summarize, renal tumors that are successfully ablated with either RFA or cryoablation are seen as low attenuation masses on contrast-enhanced CT; are hypointense to adjacent renal parenchyma on T2-weighted MRI; and iso- to hyperintense on T1-weighted imaging. The ablated zones demonstrate no enhancement and may decrease in size on follow-up imaging, particularly if treated with cryoablation. Local tumor progression after RFA or cryoablation is diagnosed when there is an increase in tumor size compared to imaging done immediately after ablation, or enhancement of the ablated lesion; the enhancement may be nodular or crescentic in appearance on contrast enhanced CT or MRI [37,42].

Surveillance protocol recommended for patients treated with thermal ablation varies with the institution. Wile *et al.* scan patients after RFA treatment at 1 month, 3 months, and then every 6 months after ablation [37]. Matsumoto *et al.* followed their patients treated with RFA, with contrast-enhanced CT performed at 6 weeks, 3 months, 6 months, 1 year, and every 6 months thereafter [43]. Atwell *et al.* recommended contrast-enhanced CT or MR imaging at 3–6 month intervals [35] in their percutaneously cryoablated patients. However, Atwell also states that the timing of follow-up imaging may be influenced by their confidence in the ablative treatment; small tumors may not be imaged till at least 6 months after treatment and larger, more complex tumors at 3 months [46]. Gill *et al.* obtained serial magnetic resonance imaging after laparoscopic cryoablation treatment at 1 day, 1, 3, 6, 12, 18, and 24 months, and yearly thereafter for 5 years [41]. Computerised

tomography-guided needle biopsy of the cryolesion was performed 6 months postoperatively and repeated if MRI findings were abnormal [41]. Kawamoto *et al.* [42] recommend contrast-enhanced CT or MR imaging at 3, 6, and 12 months after ablation and then at 6–9 months interval.

Signs of residual or recurrent tumor post-thermal ablation

Residual tumor or incomplete treatment is diagnosed when there is focal enhancement in the tumor ablation zone on the first post-procedural imaging study (3 months or earlier, depending on the institutional protocol). Recurrent tumor is diagnosed when there is focal enhancement in the tumor ablation zone which was not present on the first post-procedural imaging study, particularly if it demonstrates growth on serial scans [42,43].

Conclusion

Renal cell carcinoma is being diagnosed at an ever earlier stage and smaller size, and is now treated with a dizzyingly wide array of options, varying from a conventional radical nephrectomy to minimally invasive nephron-sparing surgical techniques, and percutaneous thermal ablative techniques. Imaging is an important component of post-therapy surveillance to detect recurrent disease expeditiously, as patients are generally asymptomatic with early disease recurrence. Contrast-enhanced CT and MRI are the most useful and commonly used imaging modalities in post-therapy surveillance. As yet, there are no firm recommendations or any general agreement on the frequency or duration of necessary CT/MRI surveillance, and a number of examples have been published or advocated as discussed above. Hopefully consensus will emerge with wider experience.

Familiarity with the expected postoperative appearance is important to both detect local recurrence early, and to avoid misdiagnosing changes related to the therapy, as evidence of recurrent or residual disease. Although it is as yet unclear whether early detection can affect long-term outcome, prompt surgical treatment of localized metastatic disease can be beneficial. Furthermore, thermal ablative techniques are becoming a more common technique to treat the patient who is a poor surgical candidate, and novel targeted chemotherapies are undergoing active evaluation (see Chapter 1), which should further increase the treatment options available for the relapsed patient.

REFERENCES

1. G. Mickisch, J. Carballido, and S. Hellsten, European Association of Urology guidelines on renal cell cancer. *Eur Urol*, **40** (2001), 252–5. Uroweb 2002, www.uroweb.org
2. B. Ljungberg, D. C. Hanbury, M. A. Kuczyk *et al.*, Guidelines on renal cell carcinoma. European Association of Urology Update, March 2007. http://berlin.uroweb.org/fileadmin/user_upload/Guidelines/08_Renal Cell Carcinoma 2007.pdf.
3. D. A. Levy, J. W. Slaton, D. A. Sanson *et al.*, Stage specific guidelines for surveillance after radical nephrectomy for local renal cell carcinoma. *J Urol*, **159** (1998), 1163–7.
4. N. K. Janzen, H. L. Kim, R. A. Figlin *et al.*, Surveillance after radical or partial nephrectomy for localized renal cell carcinoma and management of recurrent disease. *Urol Clin North Am*, **30** (2003), 843–52.
5. S. Basu, C. S. Biyani, S. K. Sundaram *et al.*, A survey of follow-up practices of urologists across Britain and Ireland following nephrectomy for renal cell carcinoma. *Clin Rad*, **61** (2006), 854–60.
6. U. Patel and P. Guest, Commentary. A survey of follow-up practices of urologists across Britain and Ireland following nephrectomy for renal cell carcinoma. *Clin Rad*, **61** (2006), 861–2.
7. J. S. Lam, O. Shvarts, J. T. Leppert *et al.*, Postoperative surveillance protocol for patients with localized and locally advanced renal cell carcinoma based on a validated prognostic nomogram and risk group stratification system. *J Urol*, **174** (2005), 466–72.
8. A. J. Stephenson, M. P. Chetner, K. Rourke *et al.*, Guidelines for the surveillance of localized renal cell carcinoma based on the patterns of relapse after nephrectomy. *J Urol*, **172** (2004), 58–62.
9. B. C. Leibovich, M. L. Blute, J. C. Cheville *et al.*, Prediction of progression after radical nephrectomy for patients with clear cell renal cell carcinoma: a stratification tool for prospective clinical trials. *Cancer*, **97**:7 (2003). 1663–71.
10. F. F Marhall, Nomograms for renal cell carcinoma. *BJU Int*, **95**:2 Suppl (2005), 14–15.
11. S. C. Campbell, A. C. Novick, and R. M. Bukowski, Renal tumours. In: A. J. Wein, L. R. Kavoussi, A. C. Novick, A. W. Partin, C. A. Peters, eds., *Campbell-Walsh Urology*, 9th edn (Philadelphia, Saunders: Elsevier, 2007), pp. 1604–6.
12. S. C. Campbell, A. C. Novick, and R. M. Bukowski, Renal tumours. In: A. J. Wein, L. R. Kavoussi, A. C. Novick, A. W. Partin, C. A. Peters, eds., *Campbell-Walsh Urology*, 9th edn (Philadelphia, Saunders: Elsevier, 2007), pp. 1595–7.
13. M. Sorbellini, M. W. Kattan, M. E. Snyder *et al.*, A postoperative prognostic nomogram predicting recurrence for patients with conventional clear cell renal cell carcinoma. *J Urol*, **173**:1 (2005), 48–51.
14. S. C. Campbell, A. C. Novick, and R. M. Bukowski. Renal tumours. In: A. J. Wein, L. R. Kavoussi, A. C. Novick, A. W. Partin, C. A. Peters, eds., *Campbell-Walsh Urology*, 9th edn (Philadelphia, Saunders Elsevier, 2007), pp. 1611–13.
15. E. J. Chae, A. K. Kim, S. H. Ki *et al.*, Renal cell carcinoma: analysis of postoperative recurrence patterns. *Radiology*, **234** (2005), 189–96.

16. K. S. Hafez, A. C. Novick, and S. C. Campbell, Patterns of tumour recurrence and guidelines for follow up after nephron sparing surgery for sporadic renal cell carcinoma. *J Urol*, **157** (1997), 2067–70.
17. J. P. Kavolius, D. P. Mastorakos, C. Pavlovich *et al*., Resection of metastatic renal cell carcinoma.. *J Clinical Oncology*, **16**:6 (1998), 2261–6.
18. B. Ljungberg, F. I. Alamdari, T. Rasmuson *et al*., Follow-up guidelines for nonmetastatic renal cell carcinoma based on the occurrence of metastases after radical nephrectomy. *BJU Int*, **84** (1999), 405–11.
19. D. S. Sandock, A. D. Seftel, M. I. Resnick, A new protocol for the followup of renal cell carcinoma based on pathologic stage. *J Urol*, **154** (1995), 28–31.
20. B. F. Banner, L. Brancazio, R. R. Bahnson *et al*., DNA analysis of multiple synchronous renal cell carcinomas. *Cancer*, **66** (1990), 2180–5.
21. N. B. Itano, M. L. Blute, B. Spotts *et al*., Outcome of isolated renal cell carcinoma fossa recurrence after nephrectomy. *J Urol*, **164** (2000), 322–5.
22. K. S. Hafez, A. F. Fergany, A. C. Novick, Nephron sparing surgery for localized renal cell carcinoma: impact of tumour size on patient survival, tumour recurrence and TNM staging. *J Urol*, **162**:6 (1999), 1930–3.
23. H. W. Herr, Partial nephrectomy for unilateral renal carcinoma and a normal contralateral kidney: 10-year followup. *J Urol.*, **161**:(1) (1999), 33–4; discussion 34–5.
24. P. Ramchandani, B. G. Coleman, H. M. Pollack *et al*., CT evaluation after radical nephrectomy for renal cell cancer. *Radiology*, **181** (1991), 125.
25. A. J. Alter, D. T. Uehling, W. J. Zwiebel, Computed tomography of the retroperitoneum following nephrectomy. *Radiology*, **133** (1979), 663–8.
26. M. E. Bernardino, L. A. deSantos, D. E. Johnson *et al*., Computed tomography in the evaluation of post-nephrectomy patients. *Radiology*, **130** (1979), 183–7.
27. S. E. Sutherland, M. I. Resnick, Maclennan *et al*., Does the size of the surgical margin in partial nephrectomy for renal cell cancer really matter. *J Urol*, **167** (2002), 61–4.
28. D. J. Kubinski, P. E. Clark, D. G. Assimos *et al*., Utility of frozen section analysis of resection margins during partial nephrectomy. *Urology*, **64** (2004) 31–4.
29. J. J. Rassweiler, C. Abbou, G. Janetschek *et al*., Laparoscopic partial nephrectomy: the European experience. *Urol Clin North Am*, **27** (2000), 721–36.
30. I. S. Gill, M. M. Desai, J. H. Kaouk *et al*., Laparoscopic partial nephrectomy for renal tumour: duplicating open surgical techniques. *J Urol*, **167** (2002), 469–75.
31. I. S. Gill, S. F. Matin, M. M. Desai, *et al*., Comparative analysis of laparoscopic versus open partial nephrectomy for renal tumours in 200 patients. *J Urol*, **170**:1 (2003), 64–8.
32. G. M. Israel, E. Hecht, and M. A. Bosniak, CT and MR imaging of complications of partial nephrectomy. *Radiographics*, **26** (2006), 1419.
33. K. Sandrasegaran, C. Lall, A. Rajesh *et al*., Distinguishing Gelatin Bioabsorbable Sponge and Postoperative Abdominal Abscess on CT. *AJR Am J Roentegenol*, **184** (2005), 475–80.

34. D. A. Gervais, F. J. McGovern, R. S. Arellano *et al.*, Renal Cell Carcinoma: Clinical Experience and Technical Success with Radio-frequency Ablation of 42 Tumours. *Radiology*, **226** (2003), 417–24.
35. T. D. Atwell, M. A. Farrell, M. R. Callstrom *et al.*, Percutaneous Cryoablation of 40 Solid Renal Tumours with US Guidance and CT Monitoring: Initial Experience. *Radiology*, **243** (2007), 276–83.
36. S. G. Silverman, K. Tuncali, E. vanSonnenberg *et al.*, Renal Tumours: MR Imaging-guided Percutaneous Cryotherapy – Initial Experience in 23 Patients. *Radiology*, **236** (2005), 716–24.
37. G. E. Wile, J. R. Leyendecker, K. A. Krehbiel *et al.*, CT and MR Imaging after Imaging-guided Thermal Ablation of Renal Neoplasms. *Radiographics*, **27** (2007), 325–39.
38. W. S. McDougal, D. A. Gervais, F. J. McGovern *et al.*, Long-term followup of patients with renal cell carcinoma treated with radio frequency ablation with curative intent. *J Urol*, **174** (2005), 61–3.
39. I. M. Varkarakis, M. E. Allaf, T. Inagaki *et al.*, Radiofrequency ablation of renal masses: results at a 2-year mean followup. *J Urol*, **174**:2 (2005), 456–60; discussion 460.
40. D. A. Gervais, F. J. McGovern, R. S. Arellano *et al.*, Radiofrequency ablation of renal cell carcinoma: Part 1. Indications, results, and role in patient management over a 6-year period and ablation of 100 tumours. *AJR Am J Roentgenol*, **185** (2005), 64–71.
41. I. S. Gill, E. M. Remer, W. A. Hasan *et al.*, Renal cryoablation: outcome at 3 years. *J Urol*, **173** (2005), 1903–7.
42. S. Kawamoto, S. Permpongkosol, D. A. Bluemke *et al.*, Sequential changes after radiofrequency ablation and cryoablation of renal neoplasms: role of CT and MR imaging. *Radiographics*, **27** (2007), 343–55.
43. E. D. Matsumoto, L. Watumumull, D. B. Johnson *et al.*, The radiographic evolution of radiofrequency ablated renal tumours. *J Urol*, **172** (2004), 45–8.
44. E. M. Merkle, S. G. Nour, and J. S. Lewin, MR imaging follow-up after percutaneous radiofrequency ablation of renal cell carcinoma: findings in 18 patients during first 6 months. *Radiology*, **235** (2005), 1065–71.
45. N. J. Hegarty, I. S. Gill, M. M. Desai *et al.*, Probe-ablative nephron-sparing surgery: cryoablation versus radiofrequency ablation. *Urology*, **68**:1 Suppl (2006), 7–13.
46. T. D. Atwell, Invited commentary. *Radiographics*, **27** (2007), 339–41.

11

Imaging for nephron-sparing procedures

Brian R. Herts and Erick M. Remer

Introduction

The classic role of computed tomography (CT) and magnetic resonance (MR) in the imaging of a patient with a renal neoplasm is to characterize the lesion and stage malignant disease: assessing for adenopathy, renal vein tumor extension, adrenal involvement, and metastatic disease. Both CT and MR have a high degree of accuracy for lesion detection and characterization, but CT is the gold standard for detection, diagnosis, and staging of renal cell carcinoma because of high spatial resolution and widespread availability [1,2,3,4,5]. Despite the fact that MR is more sensitive to contrast enhancement and different tissue types than CT, MR is often reserved for patients with a history of severe allergy to iodinated contrast and mild renal insufficiency [6,7,8,9,10]. CT and MR are also frequently used to characterize simple and complex cystic renal masses and the criteria developed by Dr. Morton Bosniak have proved useful in stratifying their malignant potential [11,12,13]. This stratification of risk based on CT or MR appearance serves as a guideline for management used by many clinicians.

The success of nephron-sparing surgery (NSS) in patients with the classic indications for partial nephrectomy such as a tumor in a patient who has undergone prior nephrectomy, or a patient with bilateral renal tumors or underlying renal parenchymal disease, has led to the expanded use of NSS to include elective indications such as renal masses less than 4 cm in patients without risk factors for renal insufficiency [14,15,16]. A small, asymptomatic, renal mass identified as an incidental finding on cross-sectional imaging is now the most common presentation of a renal neoplasm [17]. NSS can be performed using an open or laparoscopic surgical approach but ablative therapies including cryoablation and radiofrequency ablation, both intraoperatively and percutaneously, are now being used with success [18,19,20,21,22,23,24,25].

Carcinoma of the Kidney, ed. Uday Patel. Published by Cambridge University Press.

Nephron-sparing surgery, or any other nephron-sparing procedure, requires the treating physician to have an accurate understanding of the tumor location with respect to the normal renal parenchyma and vascular structures in order to most effectively preserve the function of the remaining normal renal parenchyma. Further, it is standard practice to ensure that any tumor, whether operated on or ablated, should have a 1 cm surgical or ablative margin without encroaching on any critical adjacent structures. As a result, the role of imaging has been expanded from the diagnosis and staging of renal tumors to include complex displays of renal tumor and parenchymal anatomy that are used for surgical planning [26,27,28,29]. Accurate surgical planning information should minimize postoperative complications such as bleeding, urinary leak, or renal infarction, and as a result maximize preserved renal function. Multidetector CT or 1.5 Tesla MR scanners, in combination with 2D and 3D visualization software, can rapidly and reliably provide anatomic information that was previously only available from invasive procedures, such as angiography and venacavography. A description or demonstration of the arterial and venous anatomy, the tumor location and depth of extension into the parenchyma and central renal sinus are just a few examples of the type of anatomic information that was not previously considered when interpreting renal CT scans. The proximity of the tumor to the major branch vessels and to the pelvicalyceal system, as well as the number and course of the ureters can also be described or demonstrated [27,28,29]. This chapter will discuss the protocols for CT and MR imaging of renal tumors and the goals, interpretation, and methods for using CT and MR as a surgical planning tool for nephron-sparing procedures; and review the use of imaging to plan and monitor treatment during these procedures.

Computed tomography

Computed tomography is an excellent modality for preoperative imaging of renal tumors [2,3,4,5,30,31,32,33]. CT examinations are performed both prior to and following a bolus of intravenous contrast. Oral barium contrast is not given because positive (high density) contrast material interferes with 3D reconstructions.

CT protocol

Three-phase imaging CT protocols are the state-of-the-art for the kidneys and can provide all the information necessary for surgical planning in one patient visit [28,29,34,35] (Figure 11.1). CT scans should be performed using a multidetector

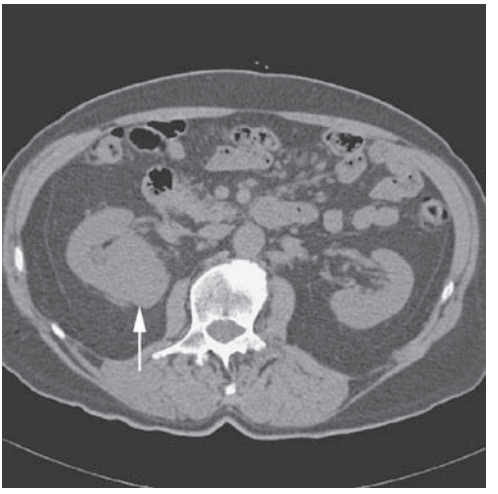

(a)

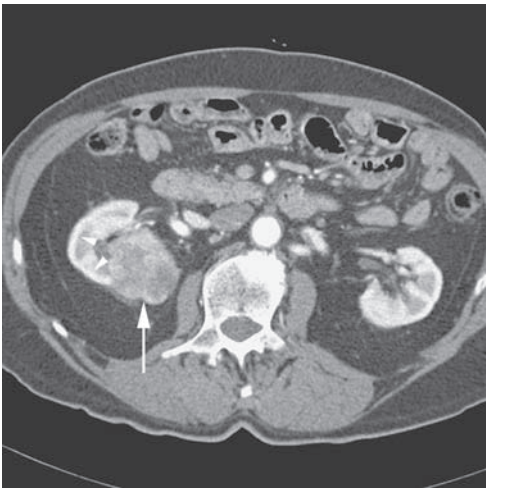

(b)

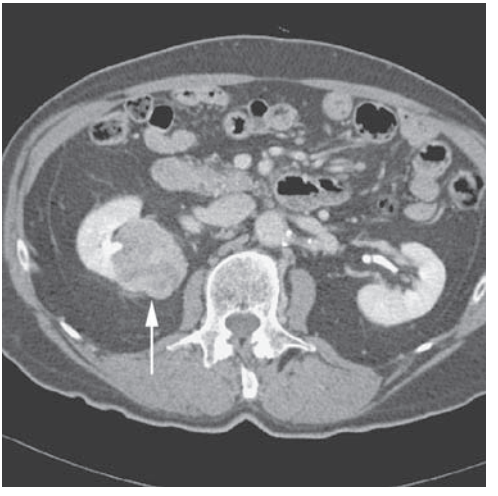

(c)

Figure 11.1 Three-phase CT for the evaluation of renal cell carcinoma. Unenhanced (a), corticomedullary (CMP) or vascular phase (b) and nephrographic (NP) or parenchymal phase (c) CT images show a solid enhancing renal cell carcinoma (arrow). The tumor is isodense to the renal parenchyma on the unenhanced image. On the CMP image, sharp delineation is seen between the dense renal cortex and partially enhanced renal medulla (arrowheads). The NP image (c) is the best image for detecting renal neoplasms.

helical CT (MDCT) scanner; this allows efficient use of contrast and facilitates creating thin-slice datasets for high-quality reconstructions. At our institution, three-phase protocol consists of a non-contrast CT of the adrenal glands and kidneys on a 16- or 64-row MDCT using 0.75 or 0.6 mm collimation respectively. The non-contrast CT is essential both because it is used to plan the contrast study, and because it is necessary to determine the baseline attenuation of renal masses (Figure 11.2). This scan also detects calcifications in the urinary tract and renal masses.

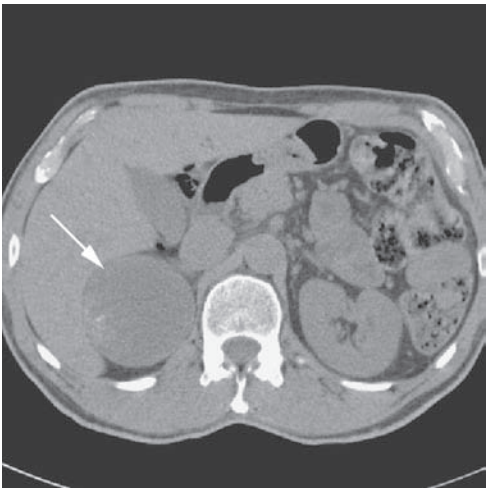

(a)

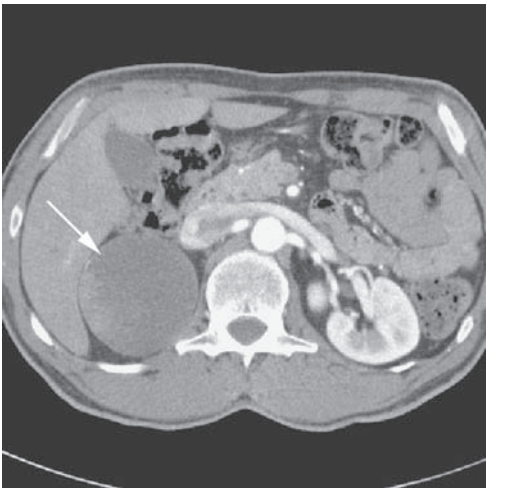

(b)

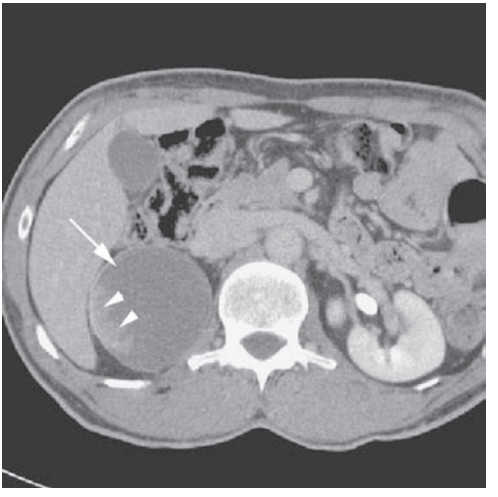

(c)

Figure 11.2 Three-phase CT for the evaluation of cystic renal cell carcinoma. Unenhanced (a), corticomedullary (CMP) or vascular phase (b) and nephrographic (NP) or parenchymal phase (c) CT images show a predominantly cystic, non-enhancing renal mass (arrow). Enhancing soft-tissue masses along the lateral wall (arrowheads) strongly suggest that this would be a cystic renal cell carcinoma, which was proven at pathology.

The second scan phase is a corticomedullary or vascular phase exam, timed for when there is peak contrast concentration in the renal arteries and veins. Automated bolus-tracking techniques are set to trigger off enhancement measured in the upper abdominal aorta, but an extra 5 seconds is added to assure enhancement of the renal veins. The third scan phase is the parenchymal or nephrographic phase exam, timed to occur when there is peak contrast concentration by normal renal parenchyma, typically at 150 s from the initiation of the bolus contrast

injection. The parenchymal and vascular phase scans are performed using the same scan techniques as the unenhanced scan. Scan techniques must be the same for all sequences to allow accurate and consistent characterization of all renal masses. The parenchymal phase is the most sensitive and specific exam phase for detecting renal masses, but the vascular phase scan is also useful when characterizing masses [4,5,35]. We reconstruct 3 mm thick slices without image overlap for diagnostic interpretation on workstations. In addition to the 3 mm slices for

(a)

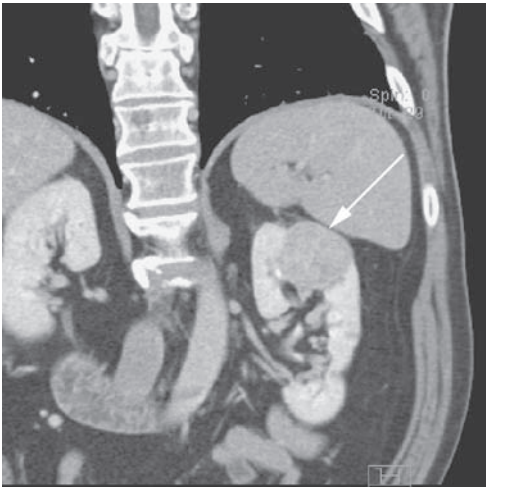

(b)

(c)

Figure 11.3 Multiplanar reformations showing a left upper pole renal cell carcinoma. Axial (a), coronal (b), and sagittal (c) images allow the surgeon to easily localize the tumor (arrow) to the lateral aspect of the upper pole of the left kidney.

diagnostic interpretation, a separate reconstruction set of 1 mm thick slices with 20% overlap (reconstruction interval of 0.8 mm) are created for multiplanar and 3D real-time volume-rendered reformations. Multiplanar reformatted images (MPR) are created through the affected kidney for interpretation and also sent to the referring urologist. True sagittal and coronal oblique images, oriented parallel to the long axis of the kidney, are the most helpful for localizing the tumor within the kidney for the operating room (Figure 11.3). We also create 3 mm thick coronal oblique thin-slab maximum intensity projection images (MIPs) angled parallel to the aorta for visualization of the renal vasculature. These MIP reformations or coronal 3D volume-renderings facilitate measurements of the distance to first renal arterial branches and distances between renal arterial ostia in those patients with multiple renal arteries (Figure 11.4). MPRs and MIP reconstructions can be performed at the CT scanner console by the technologists using the thin-section (1 mm) dataset, or created at advanced reading and computer workstations. Limitations of CT include radiation exposure, especially with three-phase scan protocols, and a risk of contrast nephropathy in patients with pre-existing renal disease. Another limitation is poor demonstration of renal vein tumor extension in small vessels.

Figure 11.4 Anterior coronal view of a patient with a right lower pole tumor (arrow) with two right renal arteries. Reformatted or 3D reconstructed images allow measurement of the distance between the renal artery origins (two-headed arrow).

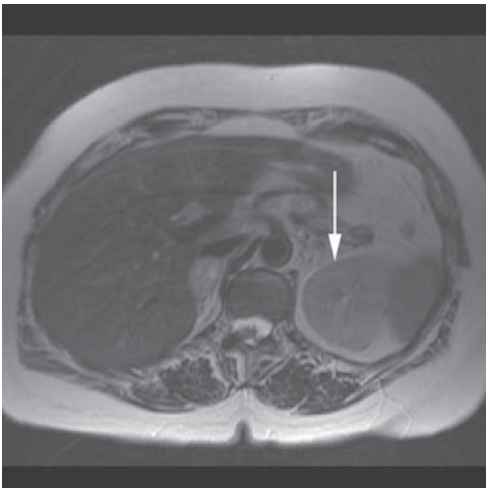

(a)

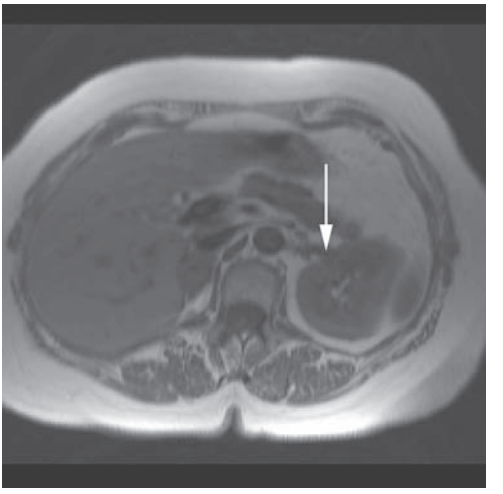

(b)

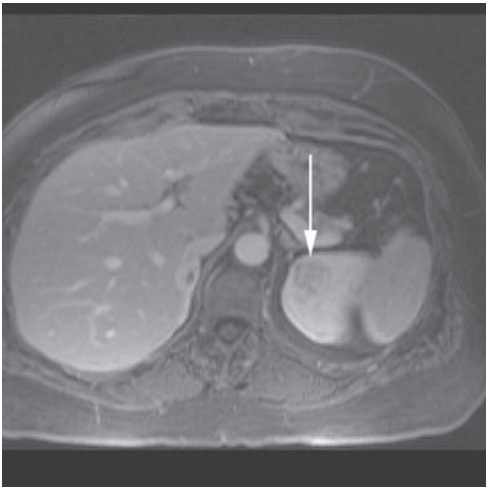

(c)

Figure 11.5 Magnetic resonance images of renal cell carcinoma. Similar to CT, MR is ideally performed without and with IV Gadolinium contrast media. The renal cell carcinoma (arrow) is isointense on the T2-weighted and T1-weighted images (a) and (b), but can be identified as hypointense to the enhanced renal parenchyma on the fat-saturated T1-weighted images after IV contrast (c).

Magnetic resonance imaging

Magnetic resonance is also an excellent modality for imaging renal tumors. As with CT, preoperative evaluation for nephron-sparing surgery with MR also includes both pre- and post-contrast evaluation [36,37,38,39,40,41] (Figure 11.5). The importance of patient preparation and proper scanning techniques cannot be overstated for body MR. A body phased-array surface coil should be used to increase received signal and must be positioned over the kidneys. A second

important factor for improving imaging quality in MR of the abdomen relates to eliminating respiratory motion because motion leads to image artifacts. Breath-hold imaging techniques take advantage of subtraction techniques that allow a qualitative assessment of contrast enhancement [38,42].

MR protocol

Scout images are obtained as localizers to plan the diagnostic sequences. T1-weighted 5–6 mm thick images without overlap are obtained to demonstrate anatomic abnormalities. A combination of both in-phase and out-of-phase T1-weighted sequences are used to detect microscopic fat. A T1-weighted sequence with fat saturation is also employed to identify regions of bulky or macroscopic fat, such as seen in an angiomyolipoma. Next, fast heavily T2-weighted images are obtained; T2-weighted images detect and characterize fluid such as within cystic renal masses and fluid within the collecting system. Slice thickness in the axial plane is again typically 5–6 mm. The kidneys and adrenal glands can thus be covered in a single breath hold, with approximately 20 slices. In the coronal plane, the volume of interest can be scanned with a slice thickness of 4–5 mm.

When studies for NSS surgical planning are performed, it is beneficial to increase the standard IV contrast dose. For most typical contrast-enhanced MR studies, a dose of 0.1 mmol per kilogram is adequate. In order to obtain good venous opacification for surgical planning studies 0.15 mmol/kg (1.5 times the standard dose, typically 30 cc) of Gadolinium chelate intravenous contrast is given utilizing a power injector. Since the intravenous contrast bolus is small (20–30 cc), there is typically only a 10-second window for optimal arterial enhancement. Therefore, the timing of scans obtained during the arterial phase is critical. The use of a timing examination, achieved by injecting 1 cc of contrast followed by a 20 cc saline flush, has proven useful to consistently obtain images during the arterial phase of contrast enhancement. Imaging is performed at fixed intervals (typically 1–2 s) following the start of the injection at the level of the mid kidneys for a period of 60 seconds, defining the time course of contrast administration. Evaluation of these images allows the easy determination of the length of time needed to achieve peak arterial enhancement. Post-contrast imaging is obtained in serial fashion using a 3D T1-weighted gradient echo fat saturated sequence. This is done at 30–60 second intervals from the start of the contrast injection until 3 minutes. This imaging sequence allows a slice resolution of 1.5 mm or less for images in the coronal plane and 2 mm or less for images in the axial plane. Arterial phase [7] and venous phase

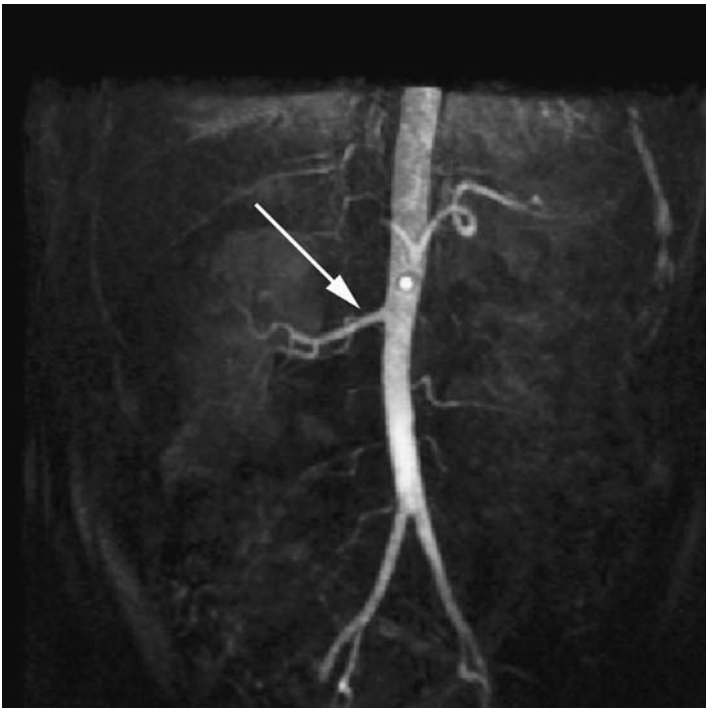

Figure 11.6 Magnetic resonance angiogram showing a single renal artery (arrow) in this patient with a right renal neoplasm in a solitary right kidney following left nephrectomy for a contralateral renal cell carcinoma.

imaging in the coronal plane is obtained using an angiographic pulse sequence that results in some advantageous background tissue signal suppression (Figure 11.6). Then, anatomic imaging is performed in the axial plane during the cortical phase of renal enhancement using a more tissue-sensitive sequence. By combining these techniques, accurate assessment of the vasculature and accurate characterization of specific lesions are possible. Administration of intravenous furosemide during the examination will create diuresis and effectively achieve an MR urogram, distending the calyces to assess the collecting system in patients whose lesions approach the central renal sinus. Coronal MR urogram images are obtained 5–10 minutes after contrast (Figure 11.7).

Contrast and chronic kidney disease

A full discussion of the risks and benefits of the different types of intravenous contrast for CT and MR is well beyond the scope of this chapter but the risks must be acknowledged. In brief, serum creatinine levels alone are no longer recommended to identify chronic kidney disease; instead measured or estimated glomerular

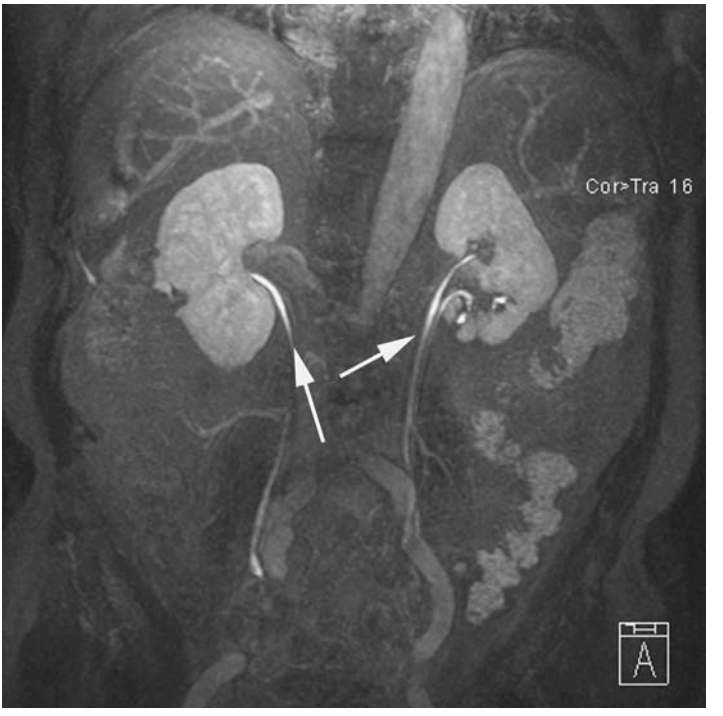

Figure 11.7 Magnetic resonance urogram. Delayed images post IV contrast and IV furosemide are obtained to identify the collecting system and ureters, which is partially duplicated on the left (arrows).

filtration rate (GFR) is thought to be a better indicator. The risk of contrast nephrotoxicity from iodinated contrast media used for CT rises with the severity of the kidney disease and the presence of co-morbid conditions such as diabetes mellitus. Patients with an estimated GFR above 90 ml/min/1.73 m^2 can probably be given a full dose of a low-osmolar non-ionic contrast agent without a significantly elevated risk of contrast nephrotoxicity. However, the literature continues to evolve for patients with mild, moderate, or severe chronic kidney disease. In general, in order to lower the risk of contrast-associated nephropathy due to iodinated contrast agents in CT, patients with mild renal insufficiency (estimated GFR 60–90 ml/min/1.73 m^2) should be well hydrated. Outpatients with estimated GFR less than 60 ml/min/1.73 m^2 can be hydrated intravenously with 250–500 ml of normal saline solution (depending on cardiac function) given over 3 hours before the exam and also instructed to drink fluids after the scan. Inpatients with chronic kidney disease should be hydrated with normal saline solution at 1 ml/min for 12 hours prior to and if possible following the exam. In these patients iso-osmolar contrast agents may be beneficial based on a study showing reduced nephrotoxicity following coronary angiography [43].

Patients with more severe chronic kidney disease (estimated GFR < 30) are usually referred for MRI for contrast studies with Gadolinium chelates and other similar Gadolinium-based contrast agents. However, a rare but debilitating and potentially fatal chronic disease, nephrogenic systemic fibrosis, has been associated with Gadolinium-based contrast agents in patients with severe chronic kidney disease. Therefore, MRI may be relatively contraindicated in patients with the most severe levels of chronic kidney disease or on dialysis. Of note, imaging studies in these patients are limited because when renal function is poor, the enhancement of normal parenchyma needed to detect small tumors does not occur with either CT or MR.

Two-dimensional and three-dimensional reformations for nephron-sparing procedures

When interpreting CT and MR scans, renal lesions detected on CT or MR are reviewed to characterize each lesion, to measure lesion size, and document location [28,29]. Tumors are generally localized to one of the major renal segments as defined by the arterial segmental branches: apical, anterior, posterior, and basilar (Figures 11.8, 11.9, and 11.10). It is also important to recognize whether tumors are

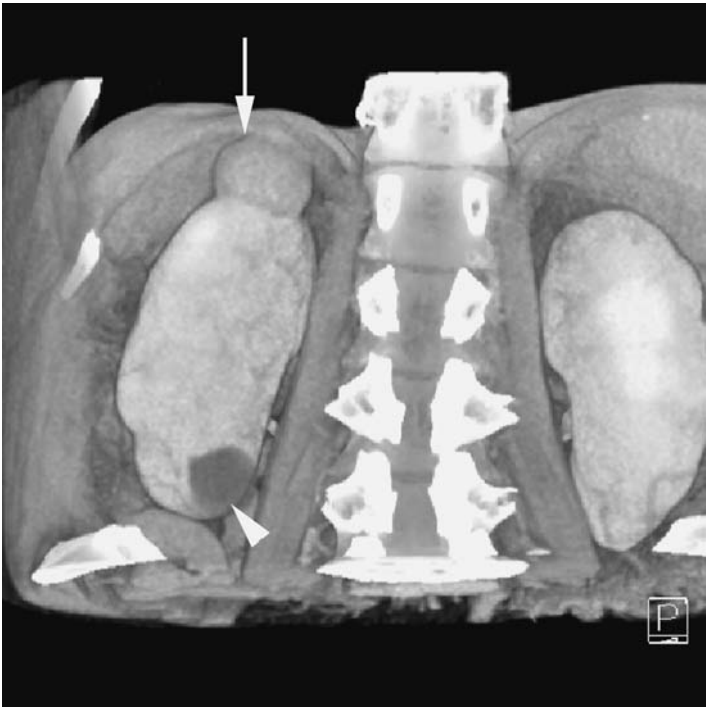

Figure 11.8 Upper pole – apical segment tumor. Three-dimensional volume rendered image from posterior view shows an exophytic left upper pole neoplasm (arrow) as well as a lower pole – basilar segment simple cyst (arrowhead).

(a)

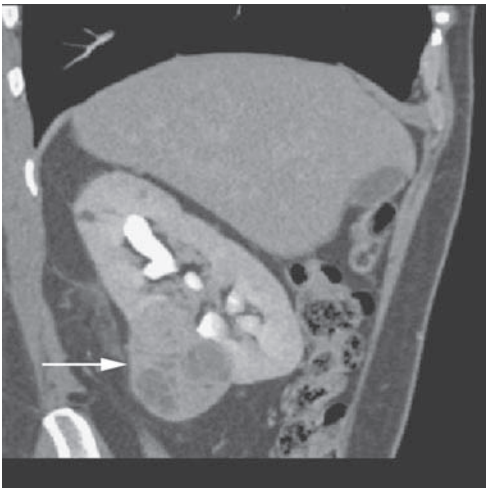

(b)

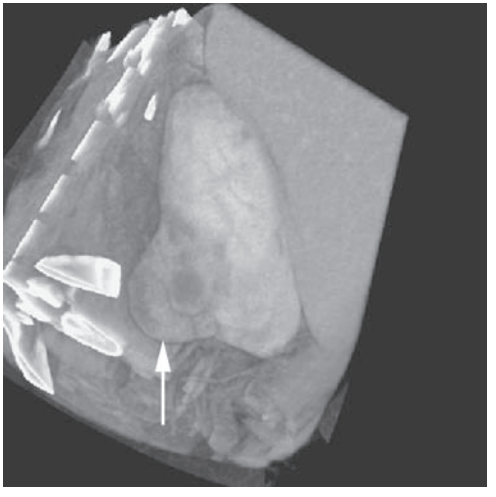

(c)

Figure 11.9 Posterior interpolar right renal cell carcinoma. The axial image (a) shows the renal neoplasm (arrow) projecting posteriorly off what may be the lower pole; however, because of the axis of the kidney, lateral multiplanar reformation (b) and 3D volume rendering (c) demonstrate that this tumor is off the posterior aspect of the mid to lower pole.

in part exophytic and, therefore, likely to be visible on the surface of the kidney, or completely intrarenal (Figure 11.11). The renal vasculature is assessed for number and origin of arteries and veins, and the presence or absence of renal vein and inferior vena cava tumor extension. (Figures 11.12 and 11.13). The retroperitoneum is assessed for local, regional, and distant lymphadenopathy; and the entire exam for local or regional metastatic disease. Table 11.1 lists the anatomical information that can be derived from planning CT (or MRI).

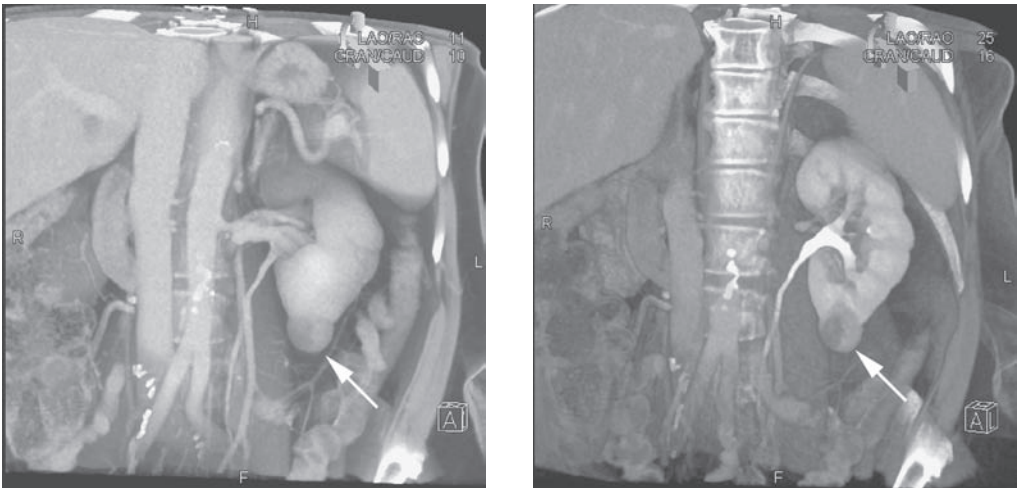

(a) (b)

Figure 11.10 Lower pole – basilar segment tumor. 3D anterior view of the entire kidney (a) and through the anterior kidney (b) show the tumor arising from the basilar segment of the left kidney (arrow).

If the patient is a NSS candidate, a series of 2D and 3D images is created using dedicated post-processing imaging software. We developed our 3D imaging technique in conjunction with a senior urologist highly experienced in performing NSS. We use real-time volume rendering to create 3D images, as well as a series of coronal oblique and sagittal multiplanar reformations (MPR) and maximum intensity projection (MIP) images [28,29,44,45] (Figure 11.14). Multiplanar reconstructions are simple reformations of the axial images into coronal, sagittal, or oblique images that provide an anatomic view more closely simulating what is seen in the operating room. Thick-slab maximum intensity projections (MIP) and surface-shaded displays (SSD) have been used for NSS surgical planning but are limited by the need for intensive image editing which is too time-consuming for most radiologists. Volume rendering typically requires little image editing and preserves the entire dataset [44,45]. When the renal tumor and vascular anatomy is particularly complex such as in patients with a tumor in a horseshoe kidney, 3D images are almost critical to the success of the procedure (Figure 11.15).

Multiplanar reformation and MIP images can be done simply, reliably, and reproducibly by CT and MR technologists. However, because of the complexity of the renal tumor and vascular anatomy, real-time 3D volume rendering may be best performed by the radiologist using a dedicated 3D workstation (e.g. the

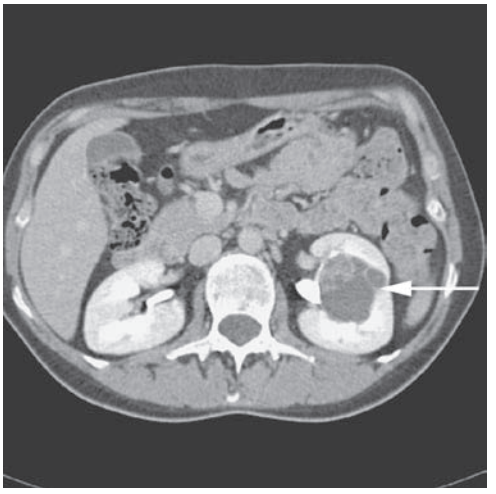

(a)

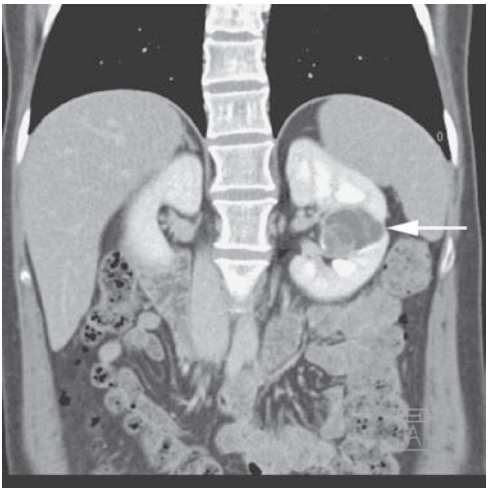

(b)

(c)

Figure 11.11 Intrarenal cystic renal cell carcinoma. Multiplanar reformations in the axial (a), coronal (b), and sagittal (c) planes show this cystic renal cell carcinoma (arrow) to be completely intrarenal. Intrarenal tumors typically benefit from the use of intraoperative ultrasound for localizing the mass during nephron-sparing surgery.

Leonardo™ or Wizard™ workstation, Siemens Medical Solutions, Malvern, PA; and other manufacturers have their own systems). We currently create one or occasionally two MPEG-encoded digital movie files for each case illustrating the critical anatomy for surgical planning. We believe that the movie format takes full advantage of the real-time editing and review capabilities of the 3D workstations. However, simpler more user-friendly alternatives to a movie format include filming of static volume-rendered reconstructions, either on radiographic film, paper, or as digital image files.

Figure 11.12 Renal cell carcinoma with renal vein and inferior vena cava tumor extension. Tumor thrombus (arrowheads) is seen extending from this infiltrating left renal cell carcinoma (arrow).

(a)

(b)

Figure 11.13 Renal cell carcinoma with renal vein tumor thrombus. In the axial (a) and 3D volume-rendered image (b) vascular tumor thrombus is shown enlarging a posterior segmental branch of the left renal vein (arrowheads) and continuing into the main left renal vein (arrow).

Table 11.1. Anatomical information for the planning of nephron-sparing procedures

1. Position of the kidney in relation to the ribs, spine, and organs
2. Number and origin of renal arteries and veins, noting early arterial branches (less than 1 cm away from the ostium). Number and size of lumbar, adrenal, and gonadal veins draining into the renal veins
3. Size and stage of tumor
4. Localize tumor according to the renal arterial segments (apical, posterior, anterior, or basilar – see text)
5. Note whether the tumor is exophytic or completely intrarenal
6. Location, depth of extension, and involvement of the pelvicalyceal system by the tumor. Margin of clearance between the tumor and nearby vessels/calyces (for both surgery and ablation, a 1 cm margin is required for optimal tumor clearance)

Figure 11.14 Multiple renal arteries and veins. Vascular control is important to minimize bleeding when performing nephron-sparing surgical procedures. Some patients will have multiple renal arteries (arrows) and veins (arrowheads) that complicate the dissection needed to gain vascular access.

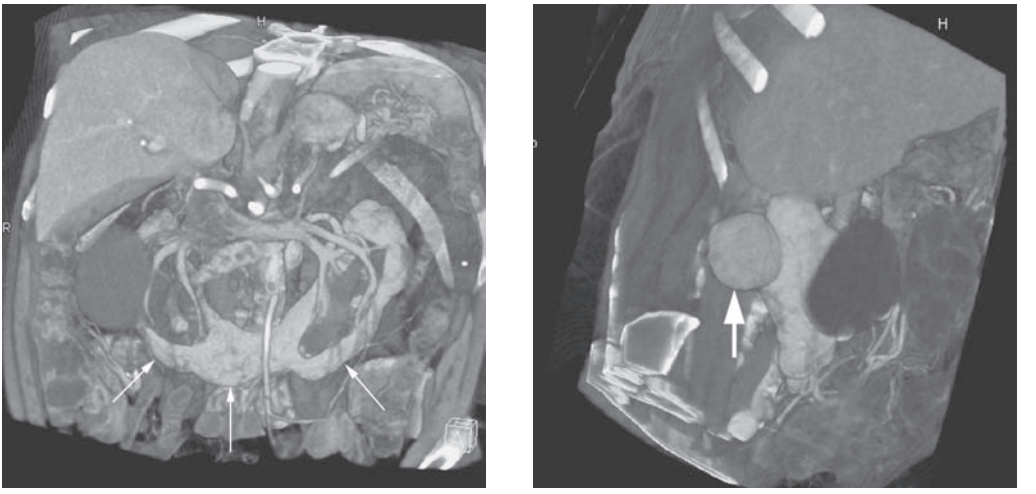

(a) (b)

Figure 11.15 3D volume-rendering is particularly helpful in patients with renal fusion anomalies, such as this patient with an exophytic tumor (thick arrow) from the posterior aspect of the left moiety of a horseshoe kidney (thin arrows).

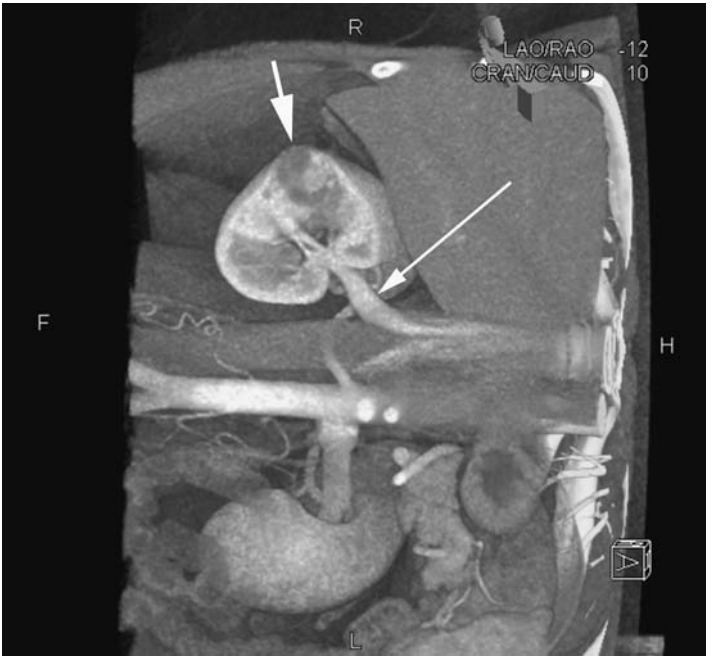

Figure 11.16 Laparoscopic renal surgery places the patient in the contralateral side-down decubitus position. 3D volume-rendered images can easily be oriented to match the surgical position, showing the tumor (short arrow), renal artery coursing behind the IVC, and the right renal vein (long arrow).

Figure 11.17 Early arterial branching. 3D volume-rendering shows the upper pole tumor (arrow) and the multiple branches of the left renal artery (arrowheads).

As the surgical technique necessitates control of the renal vasculature before resection or ablation, we render the renal vasculature first using the images from vascular scan phase (Figure 11.16). The size, origin, and course of all renal arteries, veins and early or other major segmental arterial branches are shown (Figure 11.17). Additional vasculature anatomy includes the lumbar, gonadal, and adrenal veins: the left adrenal vein is almost always seen, but the right adrenal vein is extremely short and usually cannot be identified. Next, the renal parenchymal phase is used to render the position of the kidney with respect to the rib cage, iliac crest, and spine, and the relationship of the renal tumor to the normal renal parenchyma including the location, depth of extension, and any involvement of the pelvicalyceal system (Figures 11.18 and 11.19). We have shown that when tumors have central extension, the surgeon is more likely to enter and need to repair the collecting system [46]. Post-contrast 3D MR datasets can be displayed in the same manner as CT data using a combination of the post-contrast imaging sequences. In addition, the use of image subtraction facilitates data analysis and display. Subtraction of the pre-contrast data from the cortical phase data results in a dataset that can then be used to assess enhancement within renal masses, helping lesion characterization [42] (Figure 11.20).

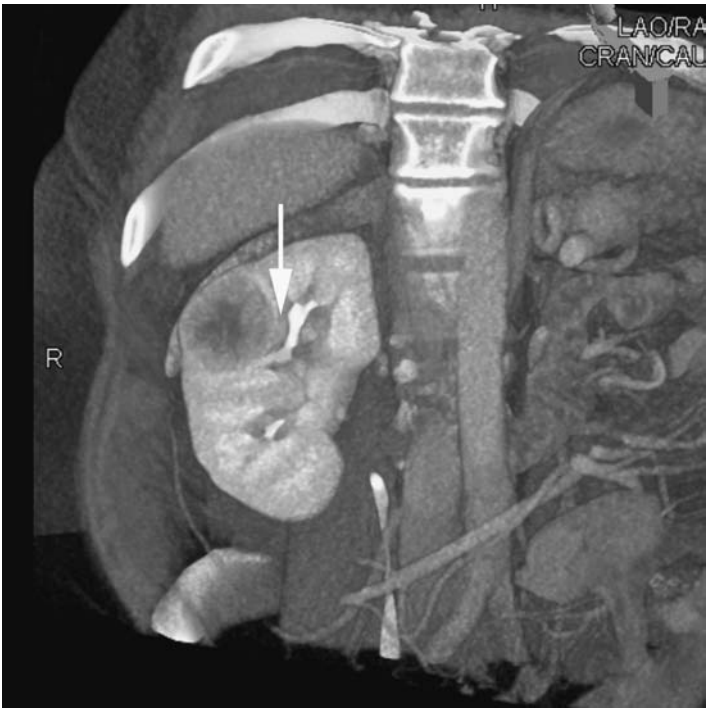

Figure 11.18 Extension of renal cell carcinoma to involve the central sinus. This patient has a lateral mid to upper pole tumor that extends into the central sinus (arrow), displacing the upper pole collecting system slightly medially.

Figure 11.19 Extension of renal cell carcinoma to involve the upper pole calices. This upper pole tumor touches the upper pole calyx (arrow). When resecting a margin of normal parenchyma, the surgeon will often need to enter and repair the calyx when tumors extend into the central sinus.

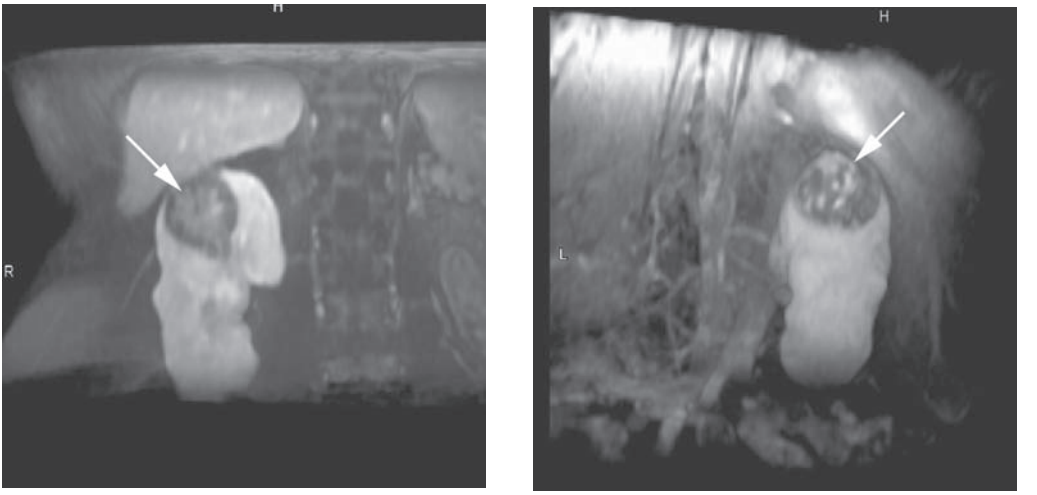

(a) (b)

Figure 11.20 3D volume-rendered MR images. Anterior (a) and posterior (b) views show the right upper pole mass (arrow); these images are reconstructed from thin-section T1-weighted fat-saturated MR images.

Radiological guidance during NSS

Another important role imaging plays for surgical planning in NSS is guidance in the operating room using open or laparoscopic ultrasound for partial nephrectomy, and guidance for laparoscopic and percutaneous ablative therapies [47]. During open or laparoscopic surgery, intraoperative ultrasound is used to identify gross tumor margins. When open partial nephrectomy is performed, the ultrasound transducer can be placed directly on the surface of the kidney. For laparoscopic procedures, the ultrasound transducer used is specifically constructed with the transducer elements on a flexible arm that fits through a 1 cm laparoscopic port (Figure 11.21). During open partial nephrectomy, ultrasound is most helpful for localizing small intrarenal masses and assessing the proximity to the central sinus structures, the pelvicalyceal system and vessels. The margins of the mass are demarcated on the renal surface using ultrasound, and then the kidney surface is scored using electrocautery. Any additional lesions can also be imaged, characterized, and resected if needed. With laparoscopic partial nephrectomy, ultrasound is invaluable for localizing a renal mass because unless a hand-assisted procedure is performed, the tactile cues available during open surgery are absent. Most masses treated laparoscopically are small, thus they

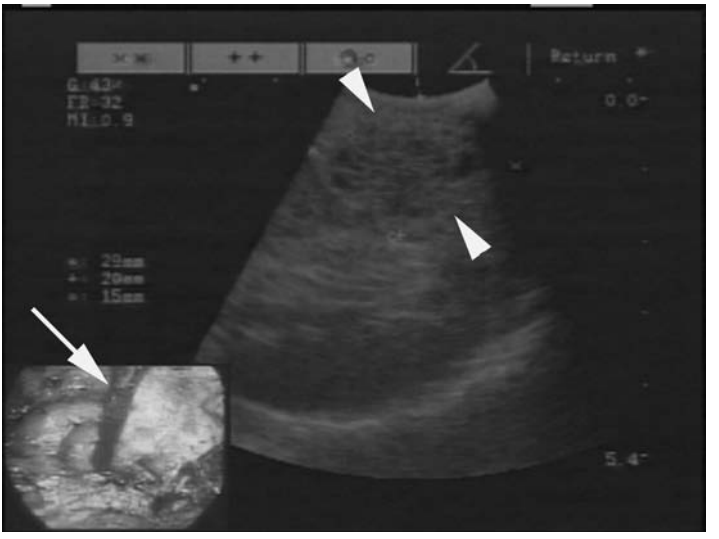

Figure 11.21 Laparoscopic ultrasound during NSS. The laparoscopic ultrasound transducer (arrow) is on the tip of a flexible arm designed to fit through a port. Ultrasound demonstrates a predominantly solid mass (between the arrowheads) with small cystic spaces.

may not be visible on the renal surface; furthermore the depth of extension into the kidney is usually not readily apparent. Ultrasound is used to identify the mass, and the surface of the kidney is scored to demarcate tumor margins as is done during the open procedure. The role for ultrasound is otherwise the same as in open surgery.

Laparoscopic ultrasound is also used to guide ablation of renal masses by cryoablation or radiofrequency. Once the kidney is mobilized and fat excised for pathological analysis, the tumor and remainder of the kidney are imaged with ultrasound. The position of the mass as determined by preoperative CT or MR with 3D imaging and any history of prior retroperitoneal or abdominal surgery determine the laparoscopic approach. Commonly the retroperitoneal approach is used for a posterior or lateral mass, while a transperitoneal approach is used for an anterior or anterolateral mass. The principles described for ultrasound guidance for laparoscopically directed ablative therapies can also be used for percutaneous ablative therapies, although CT and MR are both more commonly used to guide and monitor percutaneous therapy. Tumors amenable for percutaneous treatment must be accessible without traversing the colon, small bowel, blood vessels, pleura, or lung. The percutaneous approach may be best for high surgical risk patients and for patients who have had previous retroperitoneal surgery. The percutaneous approach offers the added benefit of no postoperative recovery time; most patients are discharged the same or the next day.

Conclusion

In the modern era, with multidetector CT and high-field MR scans and minimally invasive surgical techniques, cross-sectional imaging using CT and MR has an increasingly important role for the diagnosis and treatment of patients with renal cell carcinoma. Furthermore, imaging is becoming critical for anatomical demonstration as an aid to treatment planning and performance – monitoring surgical and ablative therapies both before and during these technically demanding procedures. As these newer techniques become more common the role of the radiologist will expand to provide not just diagnosis and characterization of renal masses, but to also provide the necessary anatomical data for procedural planning.

REFERENCES

1. M. A. Bosniak, The small (less than or equal to 3.0 cm) renal parenchymal tumour: detection, diagnosis, and controversies. *Radiology*, **179** (1991), 307–17.
2. R. J. Zagoria and D. B. Dyer, The small renal mass: detection, characterization, and management. *Abdom Imaging*, **23** (1998), 256–65.
3. B. A. Birnbaum, J. E. Jacobs, and P. Ramchandani, Multiphasic renal CT: comparison of renal mass enhancement during the corticomedullary and nephrographic phases. *Radiology*, **200** (1996), 753–8.
4. D. H. Szolar, F. Kammerhuber, S. Altziebler *et al.*, Multiphasic helical CT of the kidney: increased conspicuity for detection and characterization of small (< 3-cm) renal masses. *Radiology*, **202** (1997), 211–17.
5. R. H. Cohan, L. S. Sherman, M. Korobkin *et al.*, Renal masses: assessment of corticomedullary-phase and nephrographic-phase CT scans. *Radiology*, **196** (1995), 445–51.
6. N. M. Rofsky, V. S. Lee, G. Laub, *et al.* Abdominal MR imaging with a volumetric interpolated breath-hold examination. *Radiology*, **212** (1999), 876–84.
7. P. L. Choyke, M. M. Walther, J. R. Wagner *et al.*, Renal cancer: preoperative evaluation with dual-phase three-dimensional MR angiography. *Radiology*, **205** (1997), 767–71.
8. G. M. Israel, N. Hindman, and M. A. Bosniak, Evaluation of cystic renal masses: comparison of CT and MR using the Bosniak classification system. *Radiology*, **231** (2004), 365–71.
9. N. M. Rofsky, J. C. Weinreb, M. A. Bosniak *et al.*, Renal lesion characterization with gadolinium-enhanced MR imaging: efficacy and safety in patients with renal insufficiency. *Radiology*, **180** (1991), 85–9.
10. L. A. Kramer, Magnetic resonance imaging of renal masses. *World J Urol*, **16** (1998), 22–8.
11. M. A. Bosniak, The current radiological approach to renal cysts. *Radiology*, **158** (1986), 1–10.
12. M. A. Bosniak, Diagnosis and management of complicated cystic lesions of the kidneys. *AJR Am J of Roentgenol*, **169** (1997), 819–21.

13. G. M. Israel and M. A. Bosniak, Follow-up CT of moderately complex cystic lesions of the kidney (Bosniak category IIF). *AJR Am J of Roentgenol*, **181** (2003), 627–33.
14. A. C. Novick, Current surgical approaches, nephron-sparing surgery, and the role of surgery in the integrated immunologic approach to renal-cell carcinoma. *Semin Oncol*, **22** (1995), 29–33.
15. A. C. Novick, Nephron-sparing surgery for renal cell carcinoma. *Annu Rev Med*, **53** (2002), 393–407.
16. B. P. Butler, A. C. Novick, D. P. Miller *et al.*, Management of small unilateral renal cell carcinomas: radical versus nephron-sparing surgery. *Urology*, **45** (1995), 34–40; discussion 40–1.
17. M. Jayson and H. Sanders, Increased incidence of serendipitously discovered renal cell carcinoma. *Urology*, **51** (1998), 203–5.
18. I. S. Gill, Minimally invasive nephron-sparing surgery. *Urol Clin of N Amer*, **30** (2003), 551–79.
19. I. S. Gill, S. F. Matin, M. M. Desai *et al.*, Comparative analysis of laparoscopic versus open partial nephrectomy for renal tumours in 200 patients. *J Urol*, **170** (2003), 64–8.
20. S. C. Campbell, V. Krishnamurthi, G. Chow, *et al.*, Renal cryosurgery: experimental evaluation of treatment parameters. *Urology*, **52** (1998), 29–33; discussion 33–4.
21. C. P. Pavlovich, M. M. Walther, P. L. Choyke *et al.*, Percutaneous radiofrequency ablation of small renal tumours: initial results. *J Urol*, **167** (2002), 10–15.
22. W. B. Shingleton and P. E. Sewell, Jr., Percutaneous renal tumour cryoablation with magnetic resonance imaging guidance. *J Urol*, **165** (2001), 773–6.
23. D. P. Murphy and I. S. Gill, Energy-based renal tumour ablation: a review. *Semin in Urol Oncol*, **19** (2001), 133–40.
24. I. S. Gill, E. M. Remer, W. A. Hasan *et al.*, Renal cryoablation: outcome at 3 years. *J Urol*, **173**:6 (2005), 1903–7.
25. N. J. Hegarty, I. S. Gill, M. M. Desai *et al.*, Probe-ablative nephron-sparing surgery: cryoablation versus radiofrequency ablation. *Urology*, **68**:1 Suppl (2006), 7–13.
26. D. M. Chernoff, S. G. Silverman, R. Kikinis *et al.*, Three-dimensional imaging and display of renal tumours using spiral CT: a potential aid to partial nephrectomy. *Urology*, **43** (1994), 125–9.
27. H. Wunderlich, O. Reichelt, R. Schubert *et al.*, Preoperative simulation of partial nephrectomy with three-dimensional computed tomography. *BJU Int*, **86** (2000), 777–81.
28. D. M. Coll, R. G. Uzzo, B. R. Herts *et al.*, 3-dimensional volume rendered computerized tomography for preoperative evaluation and intraoperative treatment of patients undergoing nephron sparing surgery. *J Urol*, **161** (1999), 1097–102.
29. D. M. Coll, B. R. Herts, W. J. Davros *et al.*, Preoperative use of 3D volume rendering to demonstrate renal tumours and renal anatomy. *Radiographics*, **20** (2000), 431–8.
30. N. S. Curry and N. K. Bissada, Radiologic evaluation of small and indeterminant renal masses. *Urol Clin N Amer*, **24** (1997), 493–505.
31. A. J. Davidson, D. S. Hartman, P. L. Choyke *et al.*, Radiologic assessment of renal masses: implications for patient care. *Radiology*, **202** (1997), 297–305.
32. C. A. Jamis-Dow, P. L. Choyke, S. B. Jennings *et al.*, Small ($<$ or $=$ 3-cm) renal masses: detection with CT versus US and pathologic correlation. *Radiology*, **198** (1996), 785–8.

33. S. G. Silverman, B. Y. Lee, S. E. Seltzer *et al.*, Small (< or = 3 cm) renal masses: correlation of spiral CT features and pathologic findings. *AJR Am J Roentgenol*, **163** (1994), 597–605.
34. B. R. Herts, D. M. Coll, M. L. Lieber *et al.*, Triphasic helical CT of the kidneys: contribution of vascular phase scanning in patients before urologic surgery. *AJR Am J Roentgenol*, **173** (1999), 1273–7.
35. M. Garant, V. M. Bonaldi, P. Taourel *et al.*, Enhancement patterns of renal masses during multiphase helical CT acquisitions. *Abdom Imaging*, **23** (1998), 431–6.
36. E. S. Pretorius, E. S. Siegelman, P. Ramchandani *et al.*, Renal neoplasms amenable to partial nephrectomy: MR imaging. *Radiology*, **212** (1999), 28–34.
37. V. S. Lee, N. M. Rofsky, G. A. Krinsky *et al.*, Single-dose breath-hold gadolinium-enhanced three-dimensional MR angiography of the renal arteries. *Radiology*, **211** (1999), 69–78.
38. N. M. Rofsky, V. S. Lee, G. Laub *et al.*, Abdominal MR imaging with a volumetric interpolated breath-hold examination. *Radiology*, **212** (1999), 876–84.
39. V. B. Ho and P. L. Choyke, MR evaluation of solid renal masses. *MRI Clinics of N Amer*, **12** (2004), 413–27.
40. P. J. Hallscheidt, M. Bock, G. Riedasch *et al.*, Diagnostic accuracy of staging renal cell carcinoma using multidetector-row computed tomography and magnetic resonance imaging. *J Comput Assist Tomogr*, **28** (2004), 333–9.
41. E. S. Pretorius, L. Wickstrom, and E. S. Siegelman, MR imaging of renal neoplasms. *MRI Clinics of N Amer*, **8** (2000), 813–36.
42. V. S. Lee, M. A. Flyer, J. C. Weinreb *et al.*, Image subtraction in gadolinium-enhanced MR imaging. *AJR Am J Roentgenol*, **167** (1996), 1427–32.
43. P. Aspelin, P. Aubry, S. G. Fransson *et al.*, Nephrotoxic effects in high-risk patients undergoing angiography. *N Engl J of Med*, **348** (2003), 491–9.
44. P. T. Johnson, D. G. Heath, D. F. Bliss *et al.*, Three-dimensional CT: real-time interactive volume rendering. *AJR Am J of Roentgenol*, **167** (1996), 581–3.
45. P. S. Calhoun, B. S. Kuszyk, D. G. Heath *et al.*, Three-dimensional volume rendering of spiral CT data: theory and method. *Radiographics*, **19** (1999), 745–64.
46. I. H. Derweesh, B. R. Herts, G. A. Motta-Ramirez *et al.*, The predictive value of helical computed tomography for collecting-system entry during nephron-sparing surgery. *BJU Int*, **98** (2006), 963–8.
47. E. M. Remer, J. C. Hale, C. M. O'Malley *et al.*, Sonographic guidance of laparoscopic renal cryoablation. *AJR Am J Roentgenol*, **174** (2000), 1595–6.

Index

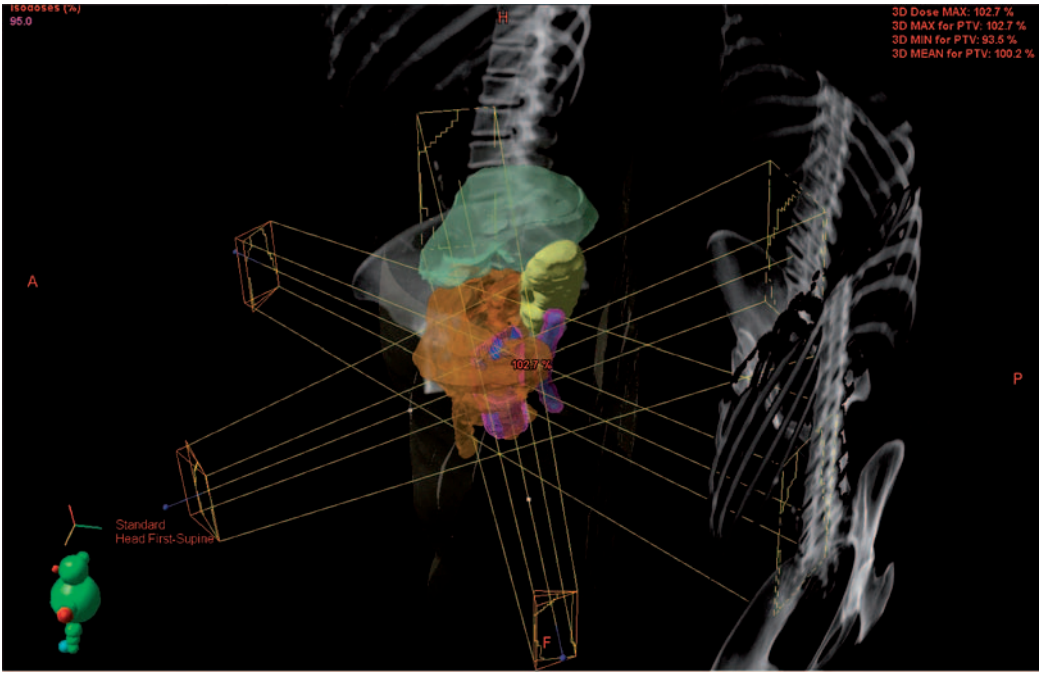

Figure 1.1 Conformal radiotherapy treatment for a postoperative renal bed recurrence. Each treatment beam has been shaped to the profile of the tumor volume within the orientation of the projected treatment beam. This shaped treatment field is then projected onto the outline of the patient's axial skeleton for further illustration of the conformal field shapes. The target volume (near cylindrical shape) is located centrally and is denoted by the pink outline.

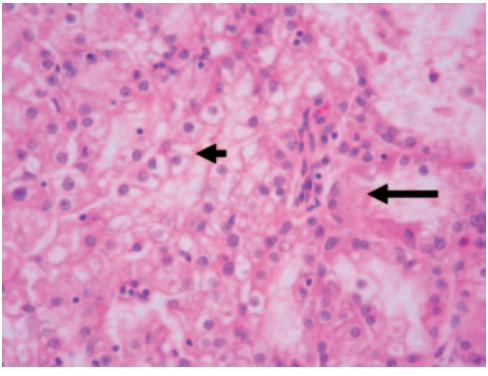

Figure 2.1 Conventional renal carcinoma showing a mixture of clear (short arrow) and granular (long arrow) cells.

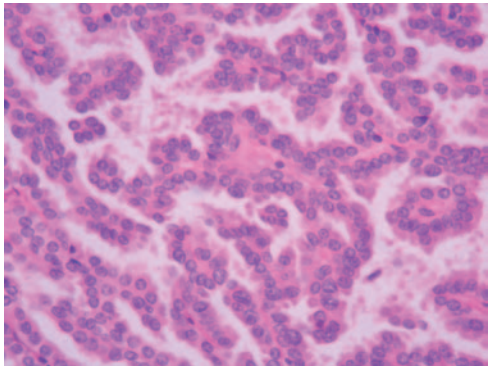

Figure 2.2 Papillary renal carcinoma composed of fibrovascular stalks and fairly uniform cells.

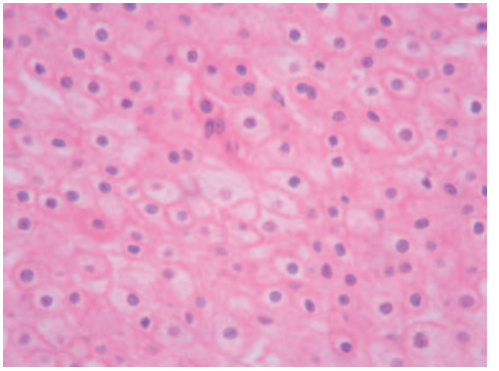

Figure 2.3 Chromophobe renal carcinoma with perinuclear haloes, slightly flocculent cytoplasm and accentuated cell membranes.

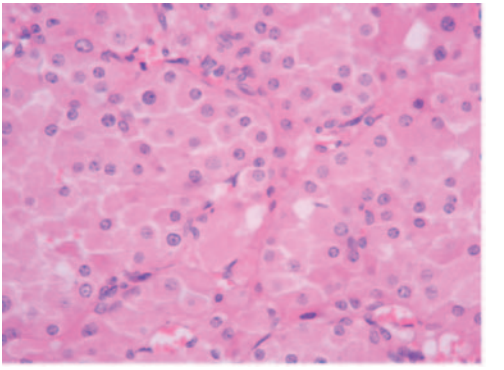

Figure 2.4 Oncocytoma composes of cells with eosinophilic, granular cytoplasm.

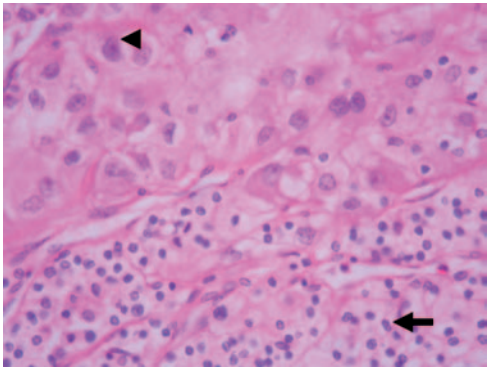

Figure 2.5 Grade heterogeneity within conventional renal carcinoma contrasting Fuhrman grade 3 cells with prominent nucleoli (arrowhead) with small grade 1 cells (arrow).

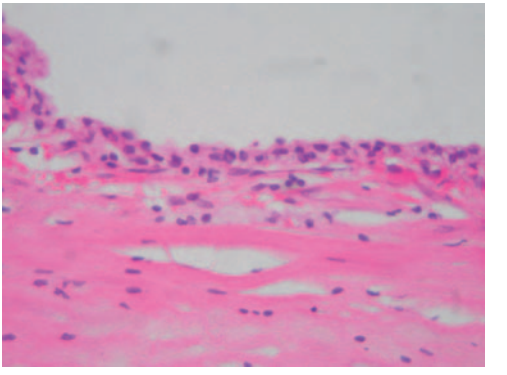

Figure 2.6 Multilocular cystic renal carcinoma with clear cells lining the cysts and a small number of clear cells in the stroma of the septa.

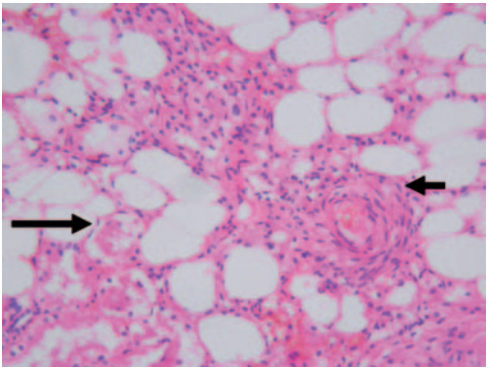

Figure 2.7 Intrarenal angiomyolipoma with abnormal vessels and proliferation of pericytes (short arrow), fat and adjacent normal renal parenchyma (long arrow).

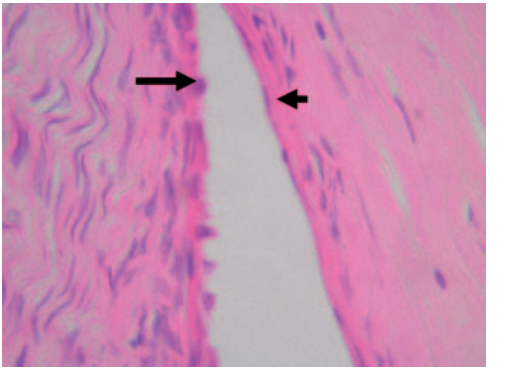

Figure 2.8 Cystic nephroma with cysts lined by hobnail cells with underlying cellular stroma (long arrow) or attenuated cells and paucicellular stroma (short arrow).

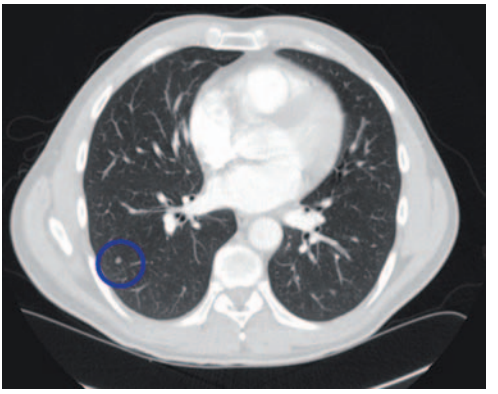

Figure 5.11 Incidental pulmonary nodule (circled) discovered on staging a new renal cancer. This lesion is too small to classify as a definite metastasis and is too small for PET. A follow-up CT chest was performed at 6 months and 1 year post-surgery, and confirmed an absence of growth of the lesion, which was assumed to be benign.

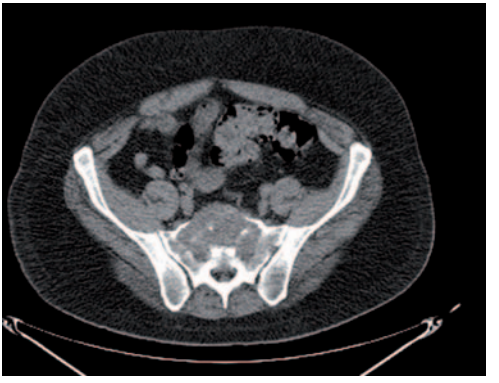

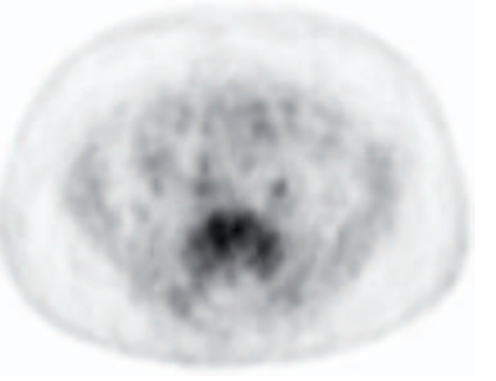

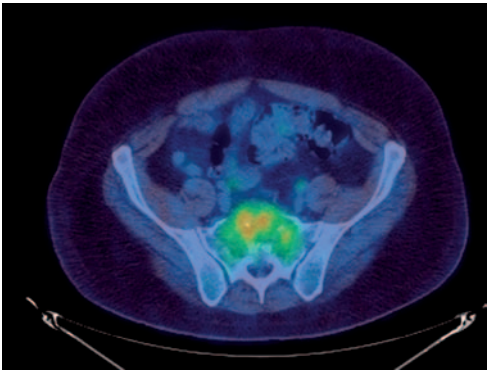

Figure 5.13 25-year-old man presented with back pain. Computed tomography of the abdomen demonstrated a right-sided renal tumor (A) with a large destructive lesion in the sacrum (B, C). CT did not demonstrate any other metastatic disease. A FDG-PET scan was performed (C) prior to palliative sacral surgery for intractable bone pain. FDG-PET did not demonstrate activity in the primary tumor but uptake was demonstrated in the metastatic sacral deposit.

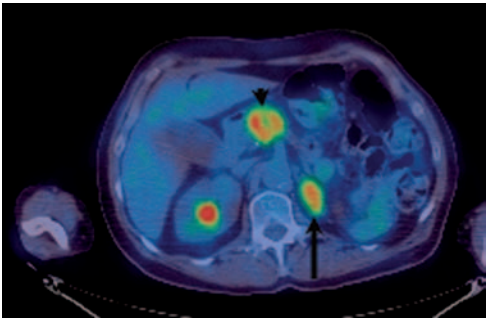

Figure 5.14 FDG-PET scan in a 55-year-old man with a previous history of renal cell cancer demonstrates marked increased uptake in metastatic deposits in the adrenal gland (long arrow) and pancreas (short arrow).

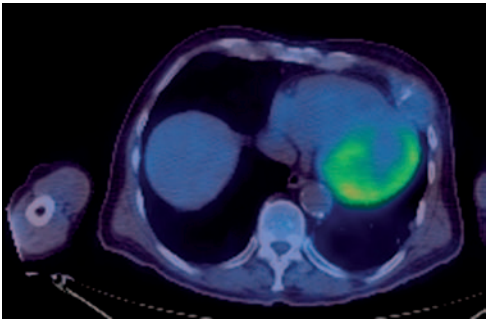

Figure 5.15 This montage demonstrates an expansible lytic lesion in one of the left-sided ribs from metastatic renal cell cancer, clearly seen on thoracic CT. However a FDG-PET shows negative uptake.

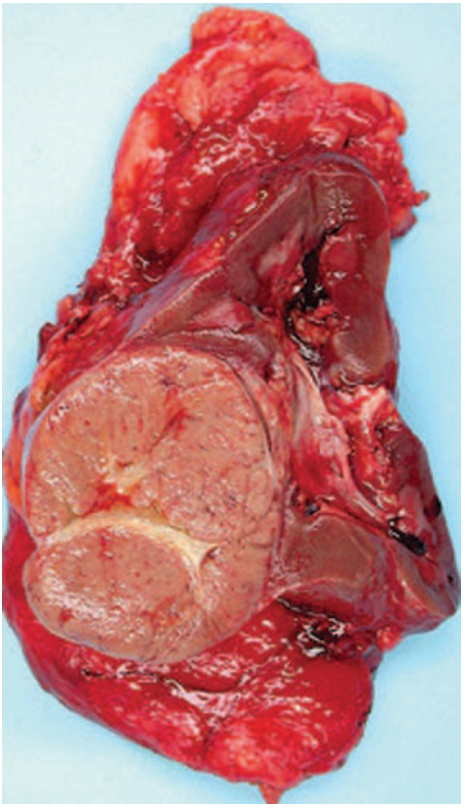

Figure 7.3c The histological specimen showing the macroscopic appearances of the chromophobe RCC as a solid, lobulated brown tumor.

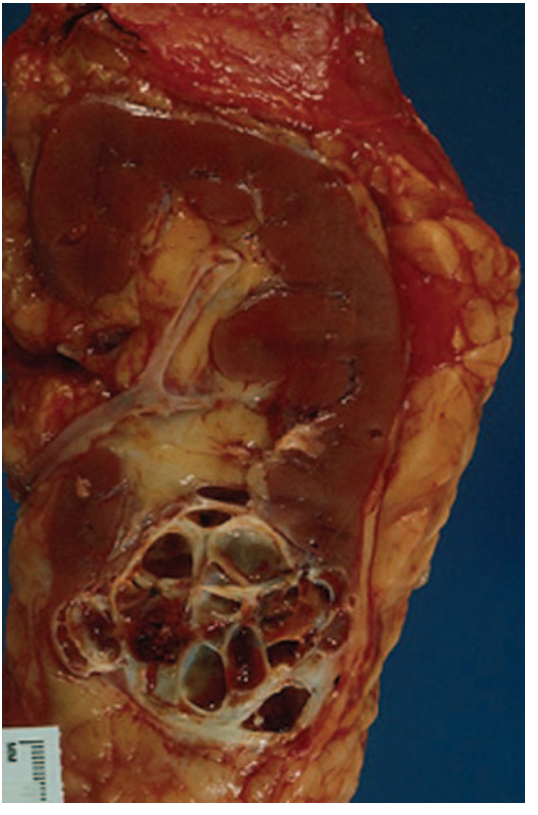

Figure 7.6b The histological specimen showing the macroscopic appearances of the multilocular cystic RCC.

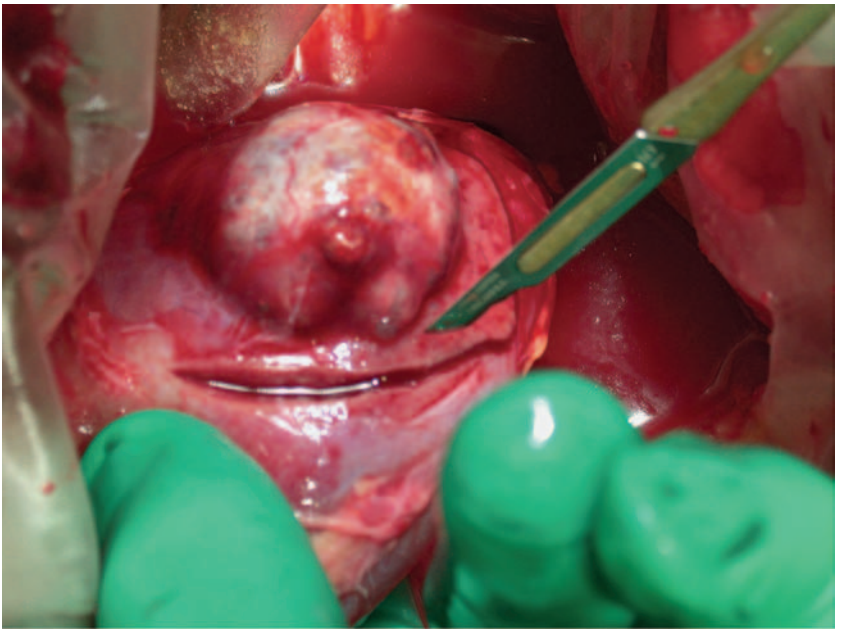

Figure 8.7a Sequence of images demonstrating a partial nephrectomy being undertaken for a 2 cm renal tumor. This image shows the tumor being excised with a margin of normal tissue.

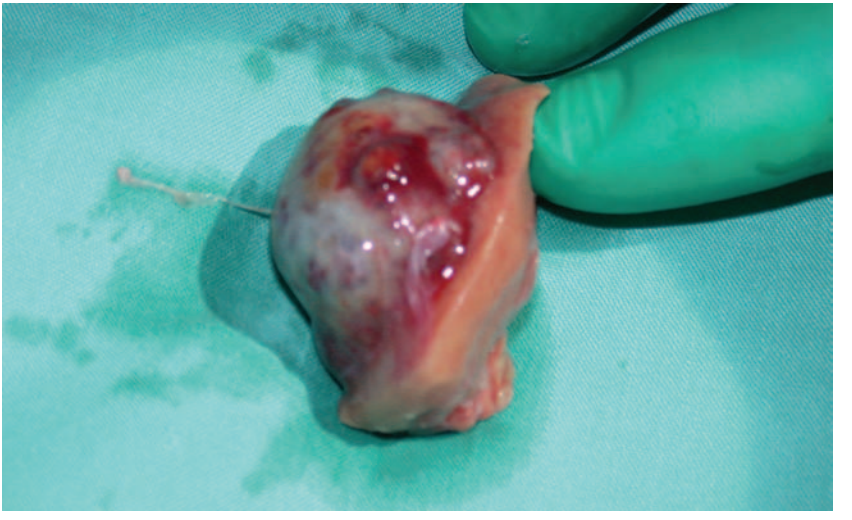

Figure 8.7b The resected tumor seen on a bed of normal tissue.

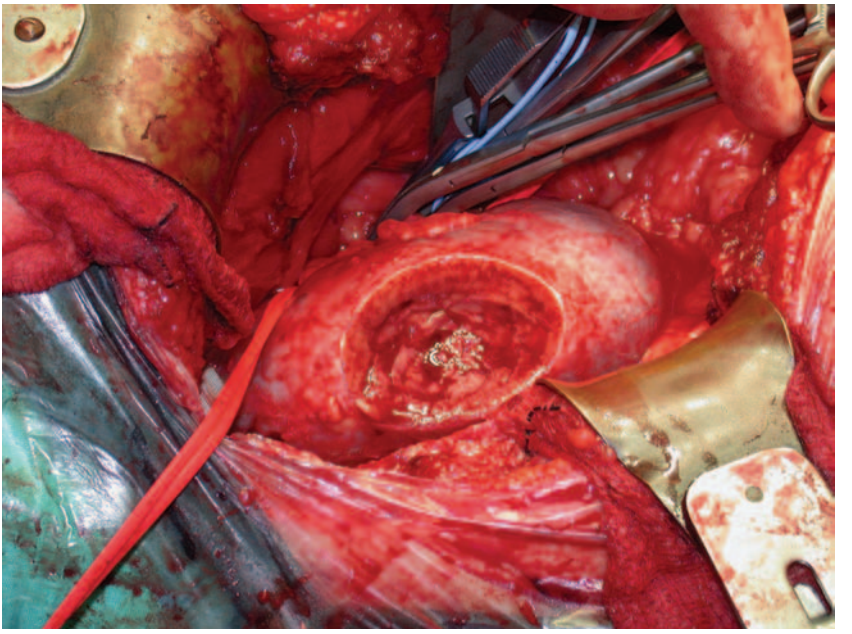

Figure 8.7c Typical renal defect post-partial nephrectomy.

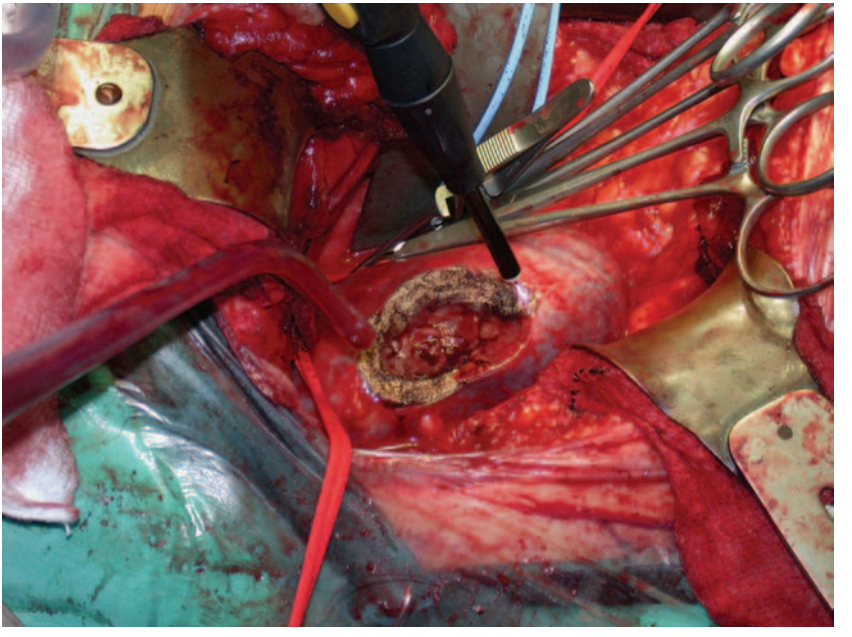

Figure 8.7d Argon beam coagulator used to seal surface vessels.

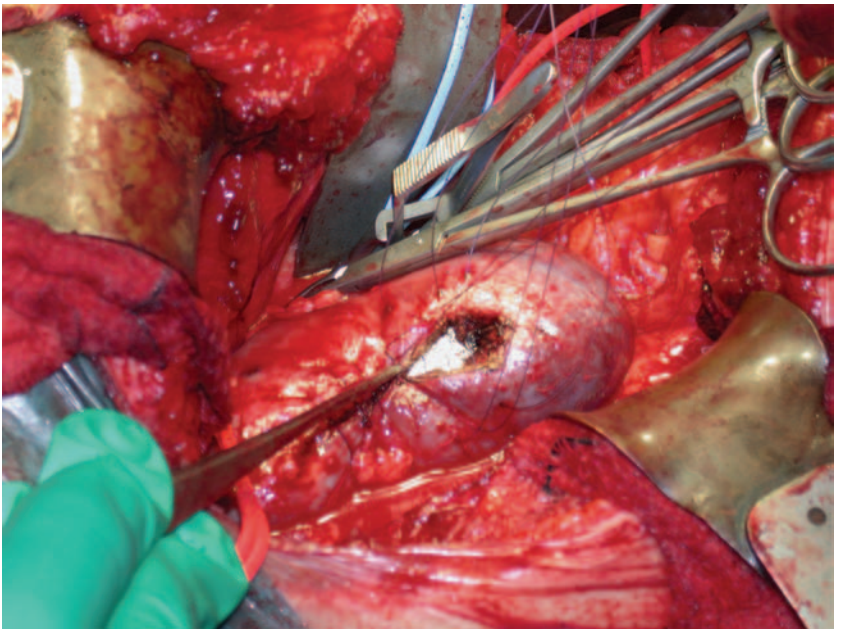

Figure 8.7e Interrupted sutures to close the renal defect tightly over a hemostatic gauze bolster.

Figure 8.8c Operative appearances of the left kidney from the same patient. Note the exophytic lower pole tumor and the multiple cysts.